THE JOURNAL OF

PHYSICAL CHEMISTRY

THE JOURNAL OF
PHYSICAL CHEMISTRY

COMMUNICATIONS TO THE EDITOR

■ Supplementary and/or miniprint material for this paper is available separately, in
photocopy or microfiche form. Ordering information is given in the paper.

* In papers with more than one author, the asterisk indicates the name of the author to
whom inquiries about the paper should be addressed.

AUTHOR INDEX

Ion–Molecule Reactions in Methanol and Hydrogen Sulfide

L. Y. Wei and L. I. Bone*

Department of Chemistry, East Texas State University, Commerce, Texas 75428   (Received June 10, 1974)

Publication costs assisted by the Robert A. Welch Foundation

A photoionization quadrupole mass spectrometer has been used to study the difference in proton affinities for CH_3OH and H_2S. Mixtures of CH_3OH and H_2S are photolyzed in the source of the mass spectrometer with a krypton resonance lamp at 10.63 eV. The only initial reactant ion is H_2S^+. H_2S^+ reacts with H_2S and CH_3OH, under field free conditions, to produce H_3S^+ and $H(CH_3OH)^+$. The rate constants for these two reactions are measured. The following reaction then proceeds toward equilibrium: $H_3S^+ + CH_3OH \rightleftharpoons H_2S + CH_3OH_2^+$. Further clustering of $H(CH_3OH)^+$ is observed in competition with the equilibrium. The standard enthalpy change for the equilibrium is found to be -5.1 ± 0.3 kcal/mol and the standard entropy change is found to be -8.0 ± 0.4 cal/deg mol. By comparing this difference in proton affinities with previously determined literature values, the most consistent proton affinity values are 175 kcal/mol for CH_3OH and 170 kcal/mol for H_2S.

Introduction

A recent paper from this laboratory[1] used a photoionization mass spectrometer to study the relative gas-phase proton affinity of H_2O and H_2S. Proton affinity values of 166 ± 2 kcal/mol for H_2O and 169 ± 2 kcal/mol for H_2S were deduced. In a related study, Chong, Meyers, and Franklin[2] measured the equilibrium constant for the reaction

$$D_3O^+ + D_2S \rightleftharpoons D_3S^+ + D_2O \qquad (1)$$
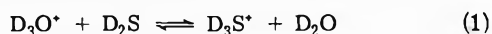
by employing a quadrupole mass spectrometer utilizing electron impact. They determined proton affinity values of 168 ± 3 kcal/mol for water and 170 ± 3 kcal/mol for H_2S.

Beauchamp and Buttrill[3] employed ion-cyclotron single and multiple-resonance spectroscopy to investigate ion-molecule reactions in H_2O and H_2S and obtained proton affinity values of 164 ± 4 kcal/mol for H_2O and 178 ± 2 kcal/mol for H_2S. Haney and Franklin[4] obtained $PA(H_2O) = 165 \pm 3$ kcal/mol and $PA(H_2S) = 170 \pm 3$ kcal/mol by studying appearance potentials from ethanol, ethanethiol, and dimethyl sulfide.

Considering the reported error limits, all these recent proton affinity values for water are in reasonably good agreement. It appears that a major portion of the remaining uncertainty can be attributed to the difference in the proton affinities of H_2S and H_2O and the uncertainty in the proton affinity of H_2S. In view of this uncertainty, it is worthwhile to redetermine the proton affinity of H_2S by

comparing it to another molecule. With this in mind the relative proton affinities of H_2S and CH_3OH have been investigated. The relative proton affinity of H_2S and CH_3OH can be calculated from the enthalpy change of the reaction

$$H_3S^+ + CH_3OH \rightleftharpoons CH_3OH_2^+ + H_2S \qquad (2)$$

A quadrupole photoionization mass spectrometer was used in this study to investigate the rate constants of ion-molecule reaction between H_2S and CH_3OH in a field free ion source. The ionization potentials of H_2S and CH_3OH are 10.46 and 10.85 eV, respectively. The reactant ion H_2S^+ was produced near its ground state by a krypton resonance lamp which emits 10.03- and 10.64-eV lines.

Experimental Section

The instrument used in this study was a Du Pont Instruments Model 21-440 quadrupole residual gas analyzer which has been modified to a photoionization mass spectrometer in this laboratory. This instrument has been described previously.[1,5]

Premixed samples of methanol in hydrogen sulfide at various mole fractions entered the instrument through a Granville-Phillips manually variable leak and a Granville-Phillips automatic pressure controller leak. The manual leak and the automatic leak were connected in series so that the flow of gas from the sample reservoir to the ion source could be controlled by either. The manual leak was

used at the lowest pressures where the automatic controller fluctuates excessively.

The ion source which was used is made of Tobin bronze and is 1 cm³ in volume with two 1 mm thick lithium fluoride windows attached to opposite sides. This design permits photons to pass through the ion source without striking metal and producing photoelectrons. The gas inside the source was ionized by a lamp filled with a low pressure (2 Torr) of krypton gas and is similar to the design of Ausloos and Lias.[6] The lamp emits 10.03- and 10.64-eV lines which are sufficient to ionize H_2S but are insufficient to produce any fragment ions from H_2S, any ions from CH_3OH or any background ions.

The ion source can be heated by radiant heat from a tungsten filament located 2 mm above the ion source. A constant direct current through the filament was maintained during each experiment to keep the source temperature constant. Gas temperatures in the ion source were measured with an iron–constantan thermocouple. The thermocouple emf was measured with a Keithly electrometer, and the temperature was calculated from the emf. The temperature in the source was measured in blank experiments exactly like those where ion abundance measurements were made. However, when data were being collected, the thermocouple was removed since it may affect the actual ion–molecule reactions.

No draw-out or repeller potential was used in the ion source, leaving the reaction region entirely field free. The ion exit hole was covered with a 45/60 mesh screen to prevent electrical field penetration into the source. The positive ions formed in the ion source were accelerated after they diffuse from the source by an ion-focus plate which normally operated from −150 to −200 V. The final ion energy was 18 V. The ion current passing completely through the quadrupole filter was amplified by a 13-stage Cu–Be electron multiplier. This signal was further amplified by a dc amplifier and recorded on a Honeywell Model 906-C oscillograph.

Methanol used in this study was Baker Analyzed Reagent grade, and hydrogen sulfide was Matheson Company CP grade. The mass spectra of these reagents were checked with a Du Pont Instruments Model 21-490 mass spectrometer. No interfering impurities were found. These reagents were used without purification, but were out gased at liquid nitrogen temperature prior to use.

Results and Discussion

Proton Affinities of H_2S and CH_3OH. Experiments have been carried out at three different ion source temperatures (299, 329, and 360°K) and at various mole per cent (based on total pressure) of CH_3OH ranging from 10 to 50%. At a given mole fraction and ion source temperature, mass spectra were taken at a series of pressure increments. The percentage of total ionization for each peak was calculated from the ratio of the individual peak heights to the sum of all peaks heights. The logarithm of per cent ionization was then plotted as a function of the ion source pressure for each series of experiments at the same mole fraction and temperature. Figure 1 is a typical graph of this data. At the low pressure limit the only ion observed is H_2S^+. This was expected since the krypton resonance lamp cannot fragment H_2S or ionize CH_3OH.

As the total pressure in the ion source increases, both H_3S^+ and $CH_3OH_2^+$ concentrations increase. The H_3S^+ concentration increases rapidly until it reaches a maximum
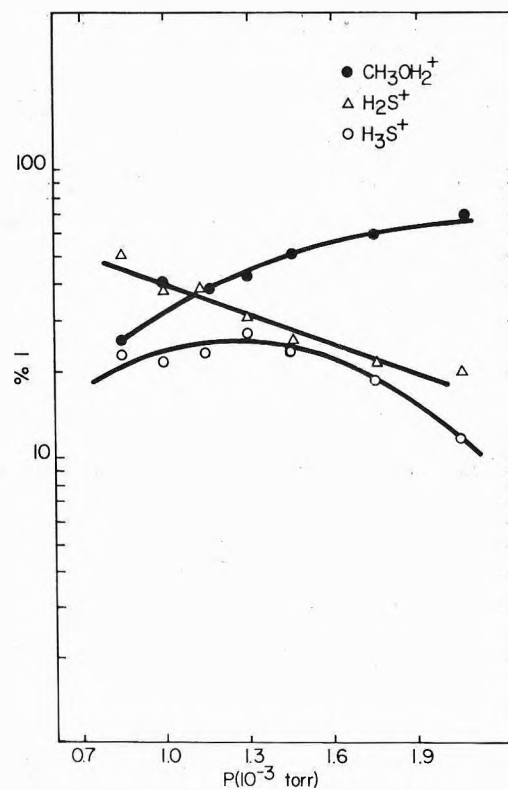
Figure 1. Ion distribution as a function of pressure at $X_{CH_3OH} = 0.15$ and 299°K.

point. As the pressure increases further, the H_3S^+ concentration decreases, and this is compensated by an increase in $CH_3OH_2^+$, $(CH_3OH)_2H^+$, $(CH_3OH)_3H^+$, and $(CH_3OH)_4H^+$. Based upon the above observation, the following mechanism is deduced

$$H_2S^+ + H_2S \xrightarrow{k_3} H_3S^+ + HS \quad (3)$$

$$H_3S^+ + CH_3OH \underset{k_{-4}}{\overset{k_4}{\rightleftharpoons}} H_2S + CH_3OH_2^{\cdot} \quad (4)$$

$$H_2S^+ + CH_3OH \xrightarrow{k_5} HS + CH_3OH_2^+ \quad (5)$$

$$CH_3OH_2^{\cdot} + CH_3OH \xrightarrow{k_6} (CH_3OH)_2H^+ \quad (6)$$

$$(CH_3OH)_nH^+ + CH_3OH \longrightarrow (CH_3OH)_{n+1}H^+ \quad (7)$$
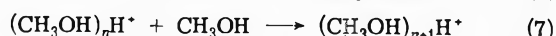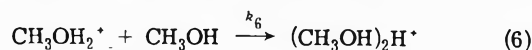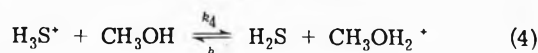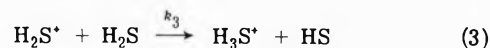
Since H_3S^+ passes through a maximum, a kinetic steady state is assumed to occur at the maximum point. Although a kinetic steady state occurs when the first derivative of concentration of an intermediate relative to time is equal to zero, both time and pressure increase the extent of reaction. Since we have previously shown[7] that the ion residence time is constant up to at least 10^{-2} Torr, where the mean free path is long compared to the source dimensions, a maximum in the concentration *vs.* pressure curve also constitutes a steady state. At the pressure where the steady state applies the following mathematic expression is valid

$$k_3[H_2S^+][H_2S] + k_{-4}[H_2S][CH_3OH_2^{\cdot}] = k_4[H_3S^+][CH_3OH]$$

$$(8)$$

therefore

$$\frac{k_4}{k_{-4}} = \frac{k_3}{k_{-4}} \frac{[H_2S^+][H_2S]}{[H_3S^+][CH_3OH]} + \frac{[CH_3OH_2^{\cdot}][H_2S]}{[H_3S^+][CH_3OH]} \quad (9)$$

or

$$K = (k_3/k_{-4})A + B \qquad (10)$$

where

$$A = [H_2S^+][H_2S] / [H_3S^+][CH_3OH]$$

$$B = [CH_3OH_2^+][H_2S] / [H_3S^+][CH_3OH]$$

This steady-state treatment was applied to the calculation of the equilibrium constant for reaction 4. Plots of B vs. A from eq 10, at all three different temperatures, were observed to be straight lines. Figure 2 contains the plot of B vs. A at 329°K. From the intercept and slope, K and k_3/k_{-4} can be obtained at each temperature. Table I shows the values of K and k_3/k_{-4} at three different temperatures. Both K and k_3/k_{-4} decrease at higher temperatures.

The K values from Table I were plotted as a function of inverse temperature (Figure 3) in a conventional Van't Hoff plot; i.e., $\ln K = (-\Delta H^\circ/RT) + (\Delta S^\circ/R)$. From the slope and intercept, ΔH° and ΔS° were found to be -5.1 ± 0.3 kcal/mol and -8.0 ± 0.4 cal/deg mol. Thus, the proton affinity of CH_3OH is 5.1 ± 0.3 kcal/mol greater than the proton affinity of H_2S and the corresponding entropy difference is 8.0 ± 0.4 cal/deg mol.

There are a few data in the literature for the proton affinity of CH_3OH with which to compare this result. Buttrill and Kriemler[8] have estimated the proton affinity of CH_3OH to be 175 kcal/mol, which is based on the data of Benson,[9] Beauchamp,[10] and Franklin, et al.[11]

Haney and Franklin[12,13] investigated several exothermic ion–molecule reactions of the following type

$$RH^+ + RH \longrightarrow RH_2^+ + R \qquad (11)$$

or

$$CH_3OH^+ + CH_3OH \longrightarrow CH_3OH_2^+ + CH_3O \qquad (12)$$
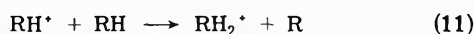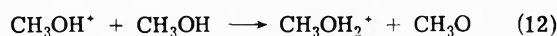
They obtained the proton affinity of CH_3OH, $PA(CH_3OH)$ $= 182 \pm 3$ kcal/mol, from the following relation

$$PA(RH) = \Delta H_f(H^+) + \Delta H_f(R) - \Delta H_f(RH^+) - \Delta H^\circ_{11} \qquad (13)$$

or

$$PA(CH_3OH) = \Delta H_f(H^+) + \Delta H_f(CH_3O) - \Delta H_f(CH_3OH^+) - \Delta H^\circ_{12} \qquad (14)$$

where ΔH°_{11} of eq 13 is the exothermicity (heat of reaction) of reaction 11 and ΔH°_{12} is the heat of reaction 12.

They suggested that the reaction intermediate complexes are very loosely coupled, and if a long-lived complex is formed, a redistribution of the heat of reaction among the various degrees of freedom of the complex might be observed. Figure 4, including the solid line, has been reproduced from the original work[13] and shows the observed relation between exothermicity and translational energy. ΔH°_{12} in eq 14 was calculated by assuming that the ratio of translational energy to exothermicity equals 0.20[13] or

$$T_c = \Delta H^\circ(0.20) \qquad (15)$$

Equation 15 is plotted as a dash line in Figure 4 for comparison. Since the total translational energy of the products in reaction 12 was found to be 3.8 kcal/mol[13] the exothermicity of reaction 12, $\Delta H^\circ = 19$ kcal/mol, was obtained from eq 15 by Haney and Franklin.[13]

Although eq 15 gives a theoretical explanation for zero exothermicity at zero translational energy, other values of exothermicity calculated by eq 15 may be questionable. We have recalculated the value of ΔH°_{12} by directly reading the solid line in Figure 4 and obtained $\Delta H^\circ_{12} = 14$ kcal/mol. By doing so, we estimate the proton affinity of

TABLE I: Values of K and k_3/k_{-4} at 299, 329, and 360°K

Temp, °K	$K = k_4/k_{-4}$	k_3/k_{-4}
299	45.0 ± 2.3	5.13 ± 0.26
329	15.5 ± 0.8	1.20 ± 0.06
360	10.0 ± 0.5	0.50 ± 0.03
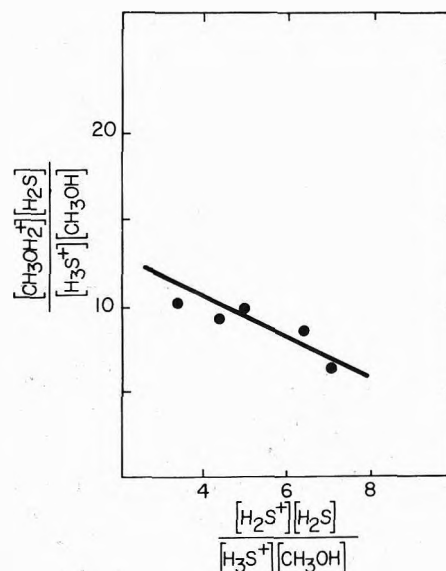
Figure 2. Determination of K at 329°K for $H_3S^+ + CH_3OH \rightleftharpoons H_2S + CH_3OH_2^+$.
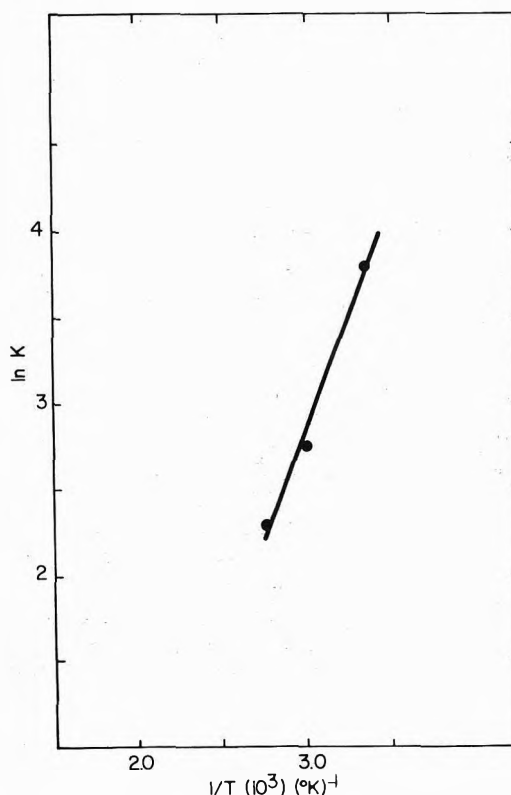
Figure 3. Van't Hoff plot for the reaction $H_3S^+ + CH_3OH \rightleftharpoons H_2S + CH_3OH_2^+$.

CH_3OH to be 177 ± 3 kcal/mol, which is 5 kcal/mol smaller than the original value of 182 ± 3 kcal/mol reported by Haney and Franklin.[13]
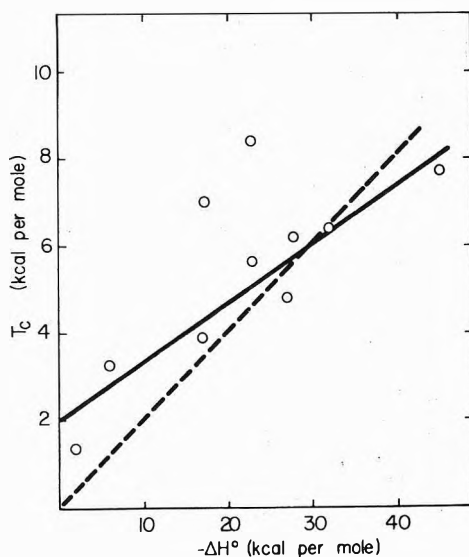
Figure 4. Translational energy of products of hydrogenic transfer reactions vs. exothermicity (from ref 13).

Since this study has determined the proton affinity of CH_3OH is 5.1 ± 0.3 kcal/mol greater than the proton affinity of H_2S, values of 175 kcal/mol for CH_3OH and 170 kcal/mol for H_2S would seem to be most consistent with previously reported values. This value of proton affinity of H_2S is in good agreement with independent measurements by other workers,[2,4] including the value of 169 ± 2 kcal/mol measured in this laboratory.[1]

Rate of Reaction of H_2S^+. In order to calculate rate constants for the disappearance of H_2S^+, the following analysis was made. From reaction 3 and 5, the rate expression for (H_2S^+) is given by

$$-d(H_2S^+)/dt = [k_3(H_2S) + k_5(CH_3OH)](H_2S^+) \quad (16)$$

By integrating this equation, the result is

$$\ln (H_2S^+) = -(k_3X_1 + k_5X_2)P\tau + C \quad (17)$$

where X_1 and X_2 are mole fractions of H_2S and CH_3OH, P represents the total ion source pressure, τ is the residence time of an ion in the ion source, and C is a constant of integration. Equation 17 reveals that the rate constants k_3 and k_5 can be calculated from the slopes of a series of plots of $\ln (H_2S^+)$ vs. pressure at different mole fractions. An IBM 360/40 computer was used in this study to calculate the best least-squares slopes. From the computer calculated slopes, k_3 and k_5 were found to be 5.8×10^{-10} (cc/molecule sec) and 22×10^{-10} (cc/molecule sec), respectively, at $299°K$. It appears that our value of k_3 is quite consistent with the other results.[14,15]

The Production of $(CH_3)_2OH^+$. It is interesting to report a few observations concerning the ion clusters that were observed at higher pressures. As reported in previous

studies from our laboratory,[1,7] we have observed $CH_3OH_2^+$, $(CH_3OH)_2H^+$, $(CH_3OH)_3H^+$, and $(CH_3OH)_4H^+$, but no clusters involving H_2S.

Grimsrud and Kebarle[16] have recently reported an ion cluster study involving CH_3OH, CH_3OCH_3, and H_2O using a pulsed electron beam, high-pressure ion source, mass spectrometer. In their methanol studies, in addition to the expected ions $H(CH_3OH)_n^+$, $H(H_2O)_n^+$, and $H(CH_3OCH_3)_2^+$, they observed $(CH_3)_2OH^+$ at source temperatures above $600°K$. Henis[17] had previously observed this process at room temperature and lower pressure. In this study we observed $(CH_3)_2OH^+$ as well as $(CH_3OH)(CH_3)_2OH^+$. The intensities of these ions increased somewhat at the highest pressures, but were always less than 1% of total ionization.

It would appear that, since we photoionize near threshold of the initial reactant and all reactions take place at room temperature in a field free source, stabilization of the clusters is highly favored over decomposition into $(CH_3)_2OH^+$. We have previously observed clustering reactions rather than reported particle transfer reactions.[18] The small bit of decomposition that we observed may have taken place in the acceleration region just outside the source, which would explain the increase in $(CH_3)_2OH^+$ at higher pressure. It is not clear whether $(CH_3OH)(CH)_2OH^+$ was produced by decomposition of $(CH_3OH)_2H^+$ or further clustering of $(CH_3)_2OH^+$ but if $(CH_3)_2OH^+$ was produced outside of the source, decomposition of $(CH_3OH)_2H^+$ is more likely.

References and Notes

(1) J. M. Hopkins and L. I. Bone, *J. Chem. Phys.*, **58**, 1473 (1973).
(2) S. Chong, R. Meyers, and J. L. Franklin, *J. Chem. Phys.*, **56**, 2427 (1972).
(3) J. L. Beauchamp and S. E. Buttrill, Jr., *J. Chem. Phys.*, **48**, 1783 (1968).
(4) M. A. Haney and J. L. Franklin, *J. Chem. Phys.*, **50**, 2028 (1969).
(5) M. J. McAdams and L. I. Bone, *J. Chem. Phys.*, **57**, 2173 (1972).
(6) P. Ausloos and S. G. Lias, *Radiat. Res. Rev.*, **75**, 107 (1968).
(7) D. L. Turner and L. I. Bone, *J. Phys. Chem.*, **78**, 501 (1974).
(8) P. Kriemler and S. E. Buttrill, Jr., *J. Amer. Chem. Soc.*, **92**, 1123 (1970).
(9) S. W. Benson, *et al.*, *Chem. Rev.*, **69**, 279 (1969).
(10) J. L. Beauchamp, Ph.D. Thesis, Harvard University, Cambridge, Mass., 1967.
(11) J. L. Franklin, *et al.*, *Nat. Stand. Ref Data Ser.*, *Nat. Bur. Stand.*, **No 26** (1969).
(12) J. L. Franklin and M. A. Haney, *J. Phys. Chem.*, **73**, 2857 (1969).
(13) M. A. Haney and J. L. Franklin, *J. Phys. Chem.*, **73**, 4328 (1969).
(14) S. K. Gupta, E. G. Jones, A. G. Harrison, and J. J. Myher, *Can. J. Chem.*, **45**, 3107 (1967).
(15) W. T. Huntress, Jr., and R. F. Pinizzotto, Jr., *J. Chem. Phys.*, in press.
(16) E. P. Grimsrud and P. Kebarle, *J. Amer. Chem. Soc.*, **95**, 7939 (1973).
(17) J. M. S. Henis, *J. Amer. Chem. Soc.*, **90**, 844 (1968).
(18) M. Garrett and L. I. Bone, 22nd Annual Conference on Mass Spectrometry and Allied Topics, Philadelphia, Pa., 19–24 May 1974.

Ring Opening in 1,1-Dimethylcyclopropane by Recoil Tritium Atoms[1]

Y. Y. Su and Y.-N. Tang*

Department of Chemistry, Texas A&M University, College Station, Texas 77843
(Received July 5, 1973; Revised Manuscript Received July 1, 1974)

Publication costs assisted by the Robert A. Welch Foundation

Recoil tritium reactions with 1,1-dimethylcyclopropane in O_2-scavenged, nonscavenged, and H_2S-scavenged systems have been studied. Products from ring-opening processes are distinguished from those of primary substitution and secondary isomerization. The relative efficiency for the three modes of ring opening in this molecule has been found to be approximately 10:1:1 in favor of the mode involving attachment of the tritium atom to the second carbon and cleavage of the C_1-C_2 bond.

Introduction

The three most fundamental reactions of energetic tritium atoms with saturated hydrocarbons are hydrogen abstraction, hydrogen substitution, and alkyl substitution[2,3] as shown in (1) to (3). For a cyclane, the alkyl substitution

$$T^* + RH \longrightarrow HT + R \qquad (1)$$

$$T^* + RH \longrightarrow RT + H \qquad (2)$$

$$T^* + R\text{-}R' \begin{array}{l} \longrightarrow RT + R' \quad (3a) \\ \longrightarrow R + R'T \quad (3b) \end{array}$$
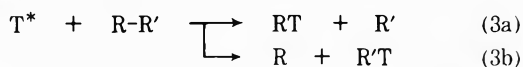
process will open the ring to yield a free radical instead of a stable molecule.[4-7] This type of ring-opening process is illustrated with cyclopropane as shown in (4). Although

$$\dot{T}^* + \begin{array}{c} CH_2 \\ H_2C\text{---}CH_2 \end{array} \longrightarrow CH_2T\text{---}CH_2\text{---}CH_2 \qquad (4)$$
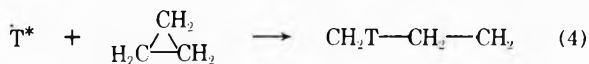
there are indications of a ring-opening process in both cyclopropane[4,5] and cyclobutane[6] systems, the most convincing evidence for its occurrence was obtained in the substituted cyclopropane systems. With molecules such as ethylcyclopropane, *cis*-1,2-dimethylcyclopropane, and *trans*-1,2-dimethylcyclopropane, the resulting tritium-labeled C_5 free radicals have been shown to eliminate either alkyl groups or hydrogen atoms to give olefins.[7]

In the present work, we have studied recoil tritium reactions with 1,1-dimethylcyclopropane (DMC) in O_2-scavenged, nonscavenged, and H_2S-scavenged systems. As illustrated in (5) to (7) there are three different modes of ring-

opening for this molecule. The major purpose of this work is to evaluate the relative probability of each of these three modes of ring opening.
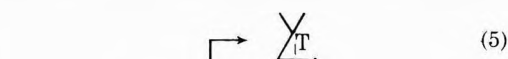
Experimental Section

These experiments were performed using standard techniques employed in studying recoil tritium reactions.[8,9] Gaseous samples, containing ^3He as the tritium source, together with 150–200 Torr of DMC, were prepared using high vacuum techniques and sealed in Pyrex 1720 bulbs. The samples were usually irradiated for 5 min with a neutron flux of 1×10^{13} n cm^{-2} sec^{-1} except for those used in determining tritium position isomers of isopentane-*t*; these were irradiated for 30 min. Either O_2 or H_2S in the amount of 60 Torr was used as a free-radical scavenger. Radio-gas chromatographic methods[9] were employed to analyze tritium-labeled products. Three different columns (dimethylsulfolane, safrole, and propylene carbonate on alumina) were used to separate the wide spectrum of products. Since 3-methyl-1-butene overlapped with DMC in the ordinary separation scheme, additional samples were analyzed with a 20 ft column of $AgNO_3$–ethylene glycol added to the end of the dimethylsulfolane column to effect the separation of these two components.

Proton exchange[10-12] was used to separate tritium position isomers (tritium at primary and tertiary positions) of isopentane-*t*. In order to isolate isopentane-*t* from other tritiated products, the samples were analyzed with the dimethylsulfolane column and isopentane-*t* was trapped down separately at $-196°$. The trapped compound was then apportioned in the following manner. Two thirds of it was transferred to a tube which contained about 5–10 ml of concentrated H_2SO_4. The other third was divided about equally into three aliquots which were analyzed by radio-gas chromatography to determine overall specific activity of isopentane-*t*. The portion in the H_2SO_4 container was shaken for about 10 hr to enhance the exchange process. At this point the vapor phase was removed from the tube. Three small aliquots were withdrawn from the vapor to determine the specific activity of isopentane-*t* after preliminary exchange. The remaining portion of the vapor was again transferred to another tube which contained fresh concentrated H_2SO_4, and the system was shaken for another 10 hr. Finally, the vapor phase was again collected and divided into three aliquots and the specific activity determined. Normally the specific activity obtained after the first exchange was very close to that measured after the second exchange. However, it is the latter value that is quoted in the table of results.

DMC was obtained from the Chemical Sample Co. with less than 0.1% impurity confirmed by gas chromatography. Matheson CP grade H_2S was used as scavenger.

Results and Discussion

Products from Primary Substitution, Secondary Isomerization, and Ring-Opening Processes. A very complicat-

ed product spectrum including products from H abstraction, primary substitution, secondary isomerization, and ring-opening processes is expected from recoil tritium reactions with DMC. The expected primary products include HT from (1); DMC-t from (2); CH_3T and methylcyclopropane-t (MC-t) from (3). If enough excitation energy is deposited on the substitution products,[3] DMC-t* is capable of isomerizing through a biradical mechanism to three different tritium-labeled pentenes:[13] CH_2=$CHCH(CH_3)_2$, $(CH_3)_2C$=$CHCH_3$, and CH_2=$C(CH_3)CH_2CH_3$, while MC-t* is capable of isomerizing to all four kinds of butene-t.[14] All these primary and secondary products are supposedly insensitive to free-radical scavengers such as O_2.

On the other hand, radicals which resulted from ring-opening processes (5)–(7) should be eliminated by O_2. The only possible exceptions are those involving hot radicals which may undergo decomposition by either C–H or C–C bond cleavage before colliding with scavenger molecules. The presence of a small fraction of such hot radicals is evidenced by the previous observation that yields of certain pentene-t molecules expected only from recoil tritium ring-opening processes were quantitatively detected in O_2-scavenged cis- and $trans$-1,2-dimethylcyclopropane systems.[7] In the present case, if ring-opening processes, (5)–(7), give rise to hot C_5 radicals, their direct decomposition products will include the three tritium-labeled pentenes and isobutene-t.

$$\left(\underset{\cdot}{\overset{T}{\diagup\!\!\!\diagdown}}\right)^{*} \longrightarrow \overset{T}{\diagup\!\!\!\diagdown}\diagdown + \text{ H} \qquad (8)$$

$$\left(\underset{T}{\diagup\!\!\!\diagdown}\right)^{*} \longrightarrow \overset{}{\underset{T}{\diagup\!\!\!\diagdown}} + \text{ H} \qquad (9a)$$

$$\longrightarrow \overset{}{\underset{T}{\diagup\!\!\!\diagdown}} + \text{ H} \qquad (9b)$$

$$\left(\underset{T}{\diagup\!\!\!\times\!\!\!\diagdown}\right)^{*} \longrightarrow \diagup\!\!\!=\ + \text{ CH}_3 \qquad (10)$$
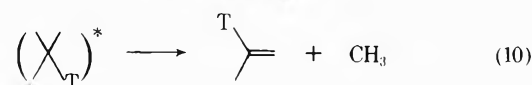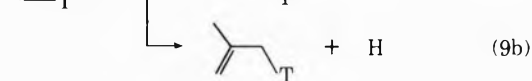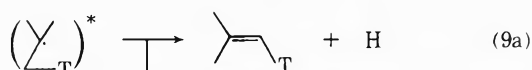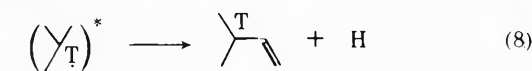
Unfortunately, these four products are also predicted from the secondary decomposition of DMC-t and MC-t.

In the absence of O_2, radicals from ring-opening processes may undergo other reactions such as H abstraction to give a large variety of products. However, besides the three pentenes and isobutene all the other expected ring-opening products are distinctly different from the rest of the secondary decomposition products. Nevertheless, one of the H-abstraction products, CH_3T, can also be obtained through the primary process, (3).

In Table I, the observed product yields from recoil tritium reactions with DMC in O_2-scavenged, nonscavenged, and H_2S-scavenged systems are given. The values given are averages of at least 3, and in some cases as many as 10 samples. The yields are expressed relative to those of DMC-t as 100.

O_2-Scavenged Systems. An examination of the O_2-scavenged results in Table I indicates that essentially only the expected products mentioned in the previous section were observed. The primary products were formed in high yields with the exception of MC-t whose yield was barely detectable. This reflects the low probability of T*-for-R substitution at quaternary carbon sites.[2] The rather high i-C_4H_7T yield is likely to be derived from sources such as (10) instead of the isomerization of MC-t because thermal isomerization of nonlabeled MC is known to give 1-butene as

TABLE I: Average Yields of Tritiated Products from Recoil Tritium Reactions with DMC

Tritiated products	O_2 scavenged[a]	Non-scavenged[b]	H_2S scavenged[c]
HT	141 ± 3	170 ± 5	350 ± 6
CH_3T	9 ± 1	15 ± 1	50 ± 1
C_2H_3T	3 ± 1	5 ± 1	4 ± 1
C_2H_5T	0	12 ± 2	7 ± 1
(structure)	0	7 ± 1	2 ± 1
(structure)	3 ± 1	8 ± 1	7 ± 1
(structure)	0	13 ± 1	7 ± 1
(structure)	0	2 ± 1	1 ± 1
(structure)	NM[d]	1 ± 1	1 ± 1
(structure)	10 ± 1	9 ± 1	22 ± 1
(structure)	0	25 ± 1	117 ± 5
(structure)	2 ± 1	1 ± 1	2 ± 1
(structure)	2 ± 1	3 ± 1	3 ± 1
(structure)	100[e]	100[e]	100[e]
(structure)	3 ± 1	20 ± 1	13 ± 1
(structure)	10 ± 1	14 ± 2	37 ± 1

[a] Sample composition: ^{3}He, 12 Torr; O_2, 60 Torr; DMC, 200 Torr. [b] Sample composition: ^{3}He, 19 Torr; DMC, 150 Torr. [c] Sample composition: ^{3}He, 18 Torr; H_2S, 60 Torr; DMC, 150 Torr. [d] NM = not measured. [e] Assumed standard for relative yields.

the major product and isobutene only in very minor quantities.[14] On the other hand, there is no satisfactory explanation for the lower than anticipated yield of tritium-labeled CH_2=$CHCH(CH_3)_2$.[13]

The observed pentene-t yields indicate that the *isomerization* of DMC-t after T-for-H substitution is about 15%. Moreover, part of this yield may be derived from C–H bond cleavage of hot radicals formed from ring-opening processes. This rather low isomerization/stabilization ratio is likely due to the high activation energy of 62.6 kcal/mol[13] and the complexity of the excited molecule which has many more vibrational modes than simpler molecules such as cyclopropane[4,5] or methyl isocyanide.[15]

It is conceivable that highly excited DMC-t may decompose by the following routes to account for the C_2H_3T, C_3H_7T, and possibly part of the i-C_4H_7T production.[7]

$$\left(\underset{T}{\diagup\!\!\!\times\!\!\!\diagdown}\right)^{**} \Bigg\{ \begin{array}{l} \longrightarrow\ C_2H_3T\ +\ C_3H_6 \qquad (11a) \\ \longrightarrow\ C_2H_4\ +\ C_3H_5T \qquad (11b) \end{array}$$

$$\left(\underset{T}{\diagup\!\!\!\times\!\!\!\diagdown}\right)^{**} \Bigg\{ \begin{array}{l} \longrightarrow\ i\text{-}C_4H_7T\ +\ CH_2 \qquad (12a) \\ \longrightarrow\ i\text{-}C_4H_8\ +\ CHT \qquad (12b) \end{array}$$
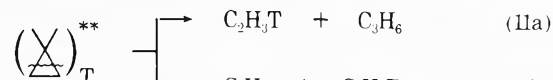
However, even with the inclusion of these high-energy processes, the total yield of unimolecular isomerization and decomposition products relative to that of the stabilized DMC-t is likely to be less than 30%.

Nonscavenged System. In the absence of O_2 as a scavenger, tritiated free radicals derived from ring-opening processes may abstract hydrogen to give easily detectable tritiated hydrocarbons. This is illustrated in (13) with CH_2T

$$\dot{C}H_2T\ +\ \diagup\!\!\!\times\!\!\!\diagdown \longrightarrow\ CH_3T\ +\ \diagup\!\!\!\times\!\!\!\diagdown \qquad (13)$$
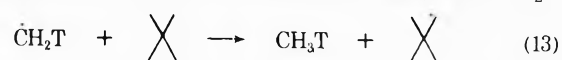
radicals. However, since the C–H bonds in DMC are rather strong and H abstraction should be reasonably slow ($E_a \approx 10.4$ kcal/mol)[16] other competitive reactions such as recombination or disproportionation with free radicals derived from radiation damage should also be significant. Examples include

$$\dot{C}H_2T + \dot{C}H_3 \longrightarrow CH_2TCH_3 \qquad (14)$$

$$(CH_3)_2\dot{C}CH_2CH_2T + (CH_3)_2\dot{C}CH_2CH_3 \longrightarrow$$

$$CH_2{=\!\!=}C(CH_3)CH_2CH_2T + (CH_3)_2CHCH_2CH_3 \quad (15)$$
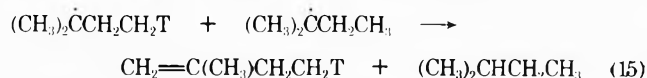
In the third column of Table I, the product spectrum derived from nonscavenged recoil tritium reactions with DMC is shown. Since each radical may undergo a number of possible reactions such as H abstraction, unimolecular decomposition, recombination, or disproportionation, the observed results are definitely not ideal for the evaluation of the original radical yields.

H₂S-Scavenged System. The addition of H_2S to a system provides readily abstractable hydrogen atoms for free radicals.[17-20] With appreciable amounts of H_2S in a system, all free radicals, if not decomposed before collision with this molecule,[21] will undergo H abstraction to give stable hydrocarbons.

In Table I, observed product yields from recoil tritium reactions with H_2S-scavenged DMC systems are listed in column 4. The DMC-t yield is again chosen as a comparison standard. A crude examination of product yields for the H_2S-scavenged system shows tremendous increases in yields for three species: HT, CH_3T, and i-$C_5H_{11}T$. The additional HT comes from direct H abstraction from H_2S by thermalized tritium atoms. The increase in yields of the latter pair stems from the H abstraction of CH_2T and i-$C_5H_{10}T$ radicals.

Three Modes of Ring-Opening Processes. The three modes of ring opening in DMC by recoil tritium atoms have already been shown in (5)–(7). It has been stated that the major purpose of this work is to evaluate the relative probability of these three ring-opening processes.

The observed product yields from H_2S-scavenged DMC systems are alternatively expressed in Table II, where the yields are grouped together according to the three modes of ring-opening processes. For each mode, the resultant C_5 radicals, the simpler radicals derived from the degradation of the C_5 radicals, and the possible stable products either from H abstraction or from unimolecular decomposition of all these radicals, have been worked out and expressed in this table. It can be seen from the list of expected products, that with two exceptions, there is no overlap among the products of these three ring-opening processes. These two exceptions are i-$C_5H_{11}T$ from modes 1 and 2 and CH_3T from modes 2 and 3. Unfortunately, these two products are the ones with the highest yields of all the ring-opening products.

From the product yields of the H_2S-scavenged system as shown in Table II, two major tasks have to be achieved before a complete resolution of products from the three modes of ring opening becomes possible. First the individual contributions of CH_3T and i-$C_5H_{11}T$ yields from overlapping sources must be resolved. Secondly, for products which can be formed by both the ring-opening and the substitution processes, a correction for the latter must be performed in order to evaluate the ring-opening contribution. Of the two, the first evaluation is extremely critical because it concerns about 75% of the total yields of ring-opening

products. However, it is the second correction factor which has to be resolved beforehand.
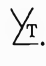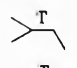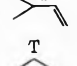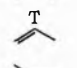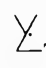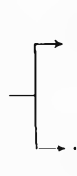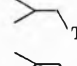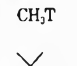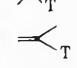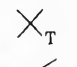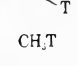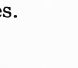
Correction for Contributions from Unimolecular Processes. Before corrections can be applied to the experimental results of the H_2S-scavenged systems, the three sets of data in Table I should be normalized through the normalization of the DMC-t yields which have been employed as the comparison standards of the relative yields. This was done by irradiating a set of six DMC samples (two of each kind) under equivalent neutron flux in a rotisserie. Such experiments are necessary because the DMC-t yields may be quite different under the various scavenging conditions. The results thus obtained which were expressed in terms of the observed DMC-t counts per unit ³He mass peak area per unit DMC mole fraction have indeed shown that the specific activity is the highest in the H_2S-scavenged system. The relative values of the unscavenged and O_2-scavenged systems have averages of 0.89 and 0.77, respectively, if the DMC-t specific activity from the H_2S-scavenged system is assigned as unity. The difference is probably due to the fact that highly excited DMC-t from the hot substitution reactions, in addition to the decomposition modes discussed before, may also undergo C–H bond rupture to give a tritiated radical, which regenerates DMC-t through H abstraction in the presence of H_2S, but is partially or completely removed in the nonscavenged or O_2-scavenged systems. With such background experiments, the yields of various tritiated products of the oxygen-scavenged system in Table I can be normalized to those of the H_2S-scavenged system by multiplying their values by the factor 0.77.

A feasible method for correcting contributions from unimolecular processes due to the five overlapping products (CH_3T, isobutene-t, and the three pentene-t's) as well as C_3H_5T is to subtract off the respective *normalized* yields in the O_2-scavenged systems from those of the H_2S-scavenged systems. The results obtained using such a correction for all overlapping products except isobutene-t are shown in column 6 of Table II. This method should be reasonably accurate for the evaluation of the CH_3T contribution because there are no other expected sources of CH_3T in the presence of O_2. In the case of the three pentene-t's, although the product yields observed in the O_2-scavenged system may not necessarily be completely derived from secondary unimolecular decomposition of substitution products, it is very difficult to evaluate their exact contributions. However, the other possible sources, reactions 8 and 9, are not likely to contribute significantly because of the high activation energies involved in the C–H cleavage processes. Therefore, this correction method should give acceptable results.

For isobutene-t, the contribution from reaction 10 in the O_2-scavenged system may be significant due to the relatively low activation energy for C–C bond cleavage. (The extremely low neo-$C_5H_{11}T$ yield observed in the H_2S-scavenged system indicates that the neopentyl radicals have a very short lifetime.) Since there is no quantitative guideline as to how to separate the two contributions of the observed isobutene-t yield, half of the yield was attributed to each possible source in this O_2-scavenged system.

Any error introduced in the evaluation of such correction factors does not carry much weight into the final analysis. Since the total yield of the products involved in these corrections accounts for only about 20% of the ring-opening products, and since the majority of the yields involved here eventually are added to the ring-opening mode which gives

TABLE II: Relative Yields of the Products Subsequent to Ring-Opening Processes

Ring opening mode no.	T* + △	Free radicals	Possible products	Product yields in H_2S-scavenged system	Product yields *via* ring-opening processes	Evaluated corrected yields	Total yields for each mode
1	(structure)	(structure)	(structure)	(117)[a]	(117)[a]	12	20
			(structure)	3	1	1	
		(structure)	(structure)	2	2	2	
			(structure)	7	5	5	
2	(structure)	(structure)	(structure)	(117)[a]	(117)[a]	105	179
			(structure)	37	29	29	
			(structure)	13	11	11	
		·CH_2T → CH_3T		(50)[a]	(43)[a]	34	
3	(structure)	(structure)	(structure)	1	1	1	28
			(structure)	22	18	18	
		·CH_2T → CH_3T		(50)[a]	(43)[a]	9	

[a] Products come from two different sources.

by far the largest yield, (namely, mode 2), an uncertainty here is not going to significantly affect the overall relative probability of the three ring-opening processes.

Contribution of CH_3T from Mode 2 and Mode 3. For mode 3 of ring opening, the resultant excited neopentyl radical may decompose by two different routes. Reaction 10 can be divided into

$$(X_T)^* \longrightarrow \quad =\!\!<_T \; + \; CH_3 \qquad (10a)$$
$$\longrightarrow \quad \dot{C}H_2T \; + \; =\!\!< \qquad (10b)$$
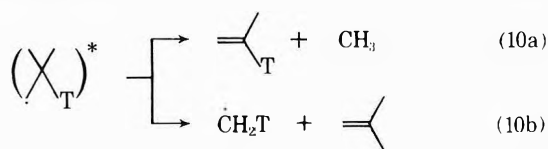
Statistically, barring any tritium isotope effect, (10a) should be twice as likely as (10b). In other words, in the H_2S-scavenged system, the CH_3T derived from mode 3 should be half of the i-C_4H_7T yield formed by the ring-opening process. As a result, the contributions of CH_3T from modes 2 and 3 can be separated.

Proton Exchange Experiments. The i-$C_5H_{10}T$ radicals formed from ring-opening modes 1 and 2 have tritium atoms on different positions of the species. These radicals will abstract H atoms from H_2S to give the corresponding i-$C_5H_{11}T$ as shown in (16) and (17). These two tritium po-

mode 1 → (structure) $>CTCH_2CH_2$ —(+H)→

(structure) $>CTCH_2CH_3$ (16)

mode 2 → (structure) $>\dot{C}CH_2CH_2T$ —(+H)→

(structure) $>CHCH_2CH_2T$ (17)
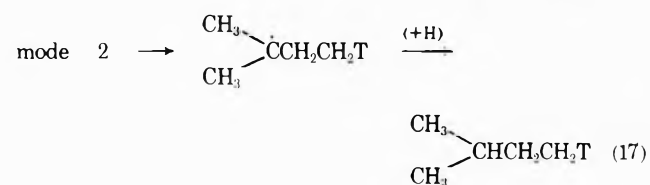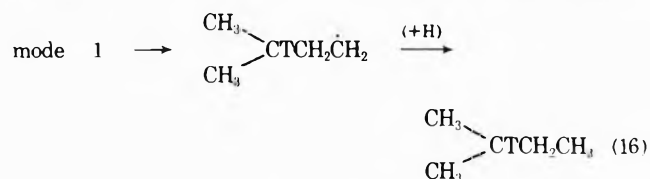
sition isomers of i-$C_5H_{11}T$ may be separated by proton exchange experiments.

It has been well established that the primary hydrogens in isobutane can be quantitatively exchanged with the protons of sulfuric acid through a carbonium ion intermediate.[10] For recoil tritium systems, this method has been successfully applied in earlier studies to separate the two position isomers of i-C_4H_9T.[11,12] It has been shown that tritium at the primary positions exchanged with H_2SO_4 while the tritium at the tertiary positions was retained in i-C_4H_9T.

Here we were interested in separating tertiary tritium at the second carbon and primary tritium at the fourth carbon of i-$C_5H_{11}T$. An uncertainty existed about whether primary tritium at the fourth carbon would be quantitatively exchanged with H_2SO_4 or not. However, in the literature, Stevenson and coworkers have already convincingly demonstrated that in isopentane all the hydrogen atoms but the tertiary ones could be exchanged with the deuterium in D_2SO_4.[22]

Accordingly, proton exchange experiments have been carried out with the isolated i-$C_5H_{11}T$ from recoil tritium reactions with DMC. The results are shown in Table III. The data indicate that the yield of $(CH_3)_2CHCH_2CH_2T$ from mode 2 is about 10 times more than the yield of $(CH_3)_2CTCH_2CH_3$ from mode 1. This ratio was employed to separate the individual contribution of i-$C_5H_{11}T$ from these two modes.

Relative Probabilities of the Three Modes of Ring Opening in DMC. In the seventh column of Table II, the "evaluated corrected yields" of ring-opening products are listed. This means the products from each ring-opening route have been resolved. In the last column of this table, the total yields of products for each of the three modes of ring opening have been tabulated. It can be seen that mode 2 is by far the most predominant ring-opening process. It is approximately 10 times more probable than each of the other two modes which both have about the same probability.

TABLE III: Yields of Tritium Position Isomers of Isopentane-t Separated by the Proton Exchange Method

i-$C_5H_{11}T$ specific activities	$(CH_3)_2$-$CTCH_2CH_3$ specific activities	$(CH_3)_2CH$-CH_2CH_2T specific activities	$(CH_3)_2CH$-$CH_2CH_2T/$ $(CH_3)_2CT$-CH_2CH_3
8.19	0.77	7.42	9.64
3.94	0.39	3.55	9.12
3.81	0.29	3.52	12.20
9.94	0.84	9.10	10.85
		Av	10.45

Mode 2 of the ring-opening processes represents the attack of tritium atoms at the second carbon of DMC and the cleavage of the C_1-C_2 bond. This indicates that the tritium atom will attach itself to a carbon which either possesses a higher electron density, or is less sterically hindered, or both. As expected, it is the weaker C_1-C_2 bond which is preferably broken. The overall picture here is that the ring-opening process, just like other types of recoil interactions, is sensitive to the chemical environment.

References and Notes

(1) Presented in part at the 28th Southwest Regional Meeting of the American Chemical Society, Baton Rouge, La., Dec 1972.
(2) R. Wolfgang, *Progr. React. Kinet.,* **3**, 97 (1965); *Annu. Rev. Phys. Chem.,* **16**, 15 (1965).
(3) F. S. Rowland, "Proceedings of the International School of Physics, 'Enrico Fermi' Course XLIV—Molecular Beam and Reaction Kinetics," Ch. Schlier, Ed., Academic Press, New York, N.Y., 1970.
(4) J. K. Lee, B. Musgrave, and F. S. Rowland, *J. Amer. Chem. Soc.,* **81**, 3803 (1959).
(5) J. K. Lee, B. Musgrave, and F. S. Rowland, *Can. J. Chem.,* **38**, 1756 (1960).
(6) E. K. C. Lee and F. S. Rowland, *J. Amer. Chem. Soc.,* **85**, 897 (1963).
(7) Y.-N. Tang and F. S. Rowland, *J. Phys. Chem.,* **69**, 4297 (1965).
(8) S. H. Daniel, Ph.D. Dissertation, Texas A&M University, 1971.
(9) J. K. Lee, E. K. C. Lee, Y.-N. Tang, J. W. Root, and F. S. Rowland, *Anal. Chem.,* **34**, 741 (1962).
(10) J. W. Otvos, D. P. Stevenson, C. D. Wagner, and O. Beeck, *J. Amer. Chem. Soc.,* **73**, 5741 (1951).
(11) A. Odell, A. Rosenberg, R. Fink, and R. Wolfgang, *J. Chem. Phys.,* **40**, 3730 (1964).
(12) T. Smail and F. S. Rowland, *J. Phys. Chem.,* **74**, 456 (1970).
(13) M. C. Flowers and H. M. Frey, *J. Chem. Soc.,* 3953 (1959); 1157 (1962).
(14) J. P. Chesick, *J. Amer. Chem. Soc.,* **82**, 3277 (1964).
(15) C. T. Ting and F. S. Rowland, *J. Phys. Chem.,* **72**, 763 (1968).
(16) See, for example, J. A. Kerr and A. F. Trotman-Dickenson, *Progr. React. Kinet.,* **1**, 107 (1961).
(17) J. D. Kale and R. B. Timmons, *J. Phys. Chem.,* **72**, 4239 (1968).
(18) N. L. Arthur and T. N. Bell, *Can. J. Chem.,* **44**, 1445 (1966).
(19) P. R. McLean and D. J. McKenney, *Can. J. Chem.,* **48**, 1782 (1970).
(20) P. Gray, A. A. Herod, and L. J. Leyshon, *Can. J. Chem.,* **47**, 689 (1969).
(21) R. Kushner and F. S. Rowland, *J. Phys. Chem.,* **75**, 3771 (1971).
(22) D. P. Stevenson, C. D. Wagner, O. Beeck, and J. W. Otvos, *J. Amer. Chem. Soc.,* **74**, 3269 (1952).

Intramolecular Vibrational Energy Relaxation. Decomposition of a Series of Chemically Activated Fluoroalkyl Cyclopropanes[1]

J. F. Meagher, K. J. Chao, J. R. Barker, and B. S. Rabinovitch*

Department of Chemistry, University of Washington, Seattle, Washington 98195 *(Received June 13, 1974)*

This paper presents the results of a study of the decomposition of the cyclopropane derivatives formed by the addition of singlet methylene-d_2 to perfluoropropene, perfluoropentene, and perfluoroheptene. The decompositions were studied over a wide range of CO bath gas pressures. The rate constants k_a obtained at the lower pressures in each case are essentially independent of pressure. At higher pressures in each range, beginning at 0.25 Torr for pentylcyclopropane and increasing to 650 Torr for methylcyclopropane, the rate constants become pressure dependent and increase with increasing pressure. A reasonable theoretical fit to most of the data has been obtained using a RRKM-type calculation with cognizance of the failure of complete internal energy relaxation at very short times after activation. The data fit the same time constant for the internal relaxation process as was found by us in earlier work, namely, $\tau \sim 10^{-12}$ sec, although this value changes a little under various calculational assumptions. Some collisional deactivation of the nascent methylcyclopropane species, prior to complete intramolecular energy relaxation, occurs at the highest pressure studied, 72 atm.

Introduction

The Rice, Ramsperger, Kassel, and Marcus (RRKM) theory[2] assumes that the internal energy of the reacting species is completely randomized prior to the decomposition event. Much evidence supports the validity of this assumption under conventional experimental conditions.[3] Several recent experimental results have been interpreted[4]

on the basis of the apparent failure of this postulate; unfortunately, in most of these cases (*cf.* ref 4e), the alleged nonequilibration has not been clearly differentiated from other experimental and computational uncertainty involved.

A crucial test of the randomization postulate[5a] and a direct demonstration of its failure was apparently given in a

study of the decomposition of hexafluorobicyclopropyl-d_2 (HBC),[5c] which was formed and simultaneously activated by the addition of a methylene ($^1A_1$) radical to the double bond of perfluorovinylcyclopropane-d_2. This addition is exothermic by ~110 kcal mol^{-1} and the energy input tends to be localized in the new ring of the molecule. The critical threshold for CF_2 elimination, which is the only mode of decomposition[5b,c,6] under these conditions, is below 50 kcal

$$\bigtriangledown_{D_2} \bigtriangledown_{H_2}{}^* \longrightarrow \bigtriangledown_{D_2}\text{—C}{=}CH_2 + CF_2$$

$$\longrightarrow \bigtriangledown_{H_2}\text{—C}{=}CD_2 + CF_2$$
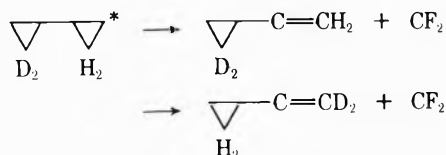
mol^{-1} and is very fast. The short lifetime of the excited adduct is favorable for the observation of the nonequilibrium decomposition. By activating the molecule at either end and measuring the ratio of decomposition of the nascent and adjoining rings as a function of pressure, a nonequilibrium decomposition component was observed. Tang and Su[7] have reported a related demonstration in the recoil-atom activated spiropentane system.

In order to study further the intramolecular energy relaxation process we undertook a new type of approach, the systematic study as a function of pressure of the decomposition of a homologous series of chemically activated molecules—partially fluorinated alkyl cyclopropanes. It was proposed that by substituting progressively larger groups on the cyclopropyl moiety, the variation of the molecular construction would be helpful in clearly distinguishing between the randomized and nonrandomized components of the decomposition. As the side appendages become larger, more of the initial cyclopropane ring excitation will be transferred eventually to the side chain of the molecule and an initial nonrandomized decomposition may be more readily distinguishable from the ensuing random decomposition. We report here the decomposition of the adducts formed by the addition of CD_2 to perfluoropropene, perfluoropentene-1, and perfluoroheptene-1.

Experimental Section

Ketene-d_2 was prepared by the pyrolysis of acetic-d_6 anhydride (99% D, Stohler Isotope Chemicals). It was purified by trap-to-trap distillation and stored at 77°K. Perfluoroheptene-1, obtained from Peninsular ChemResearch, was purified by chromatography. Perfluoropentene-1 was synthesized from perfluorohexanoic acid using the method of Hals, et al.[8] Perfluorohexanoic acid was converted to its sodium salt, which was pyrolyzed to give the desired olefin. The olefin was purified by distillation and by gas chromatography. Its identity was verified by its infrared spectrum and mass spectrometric analysis. The perfluorohexanoic acid was obtained through the kindness of Dr. D. J. La-Zerte of the 3M Company, and was used without further purification. Perfluoropropene (Peninsular ChemResearch), neopentane (Matheson), cycloheptane, and 2,3-dimethylbutane (Aldrich) were each purified by gas chromatography.

Standard fluoroolefin–hydrocarbon mixtures were stored in blackened Pyrex flasks fitted with greaseless stopcocks. The carbon monoxide (CP grade, Matheson) and oxygen (>99%, Airco) were passed through silica gel and a packed trap at 77°K before being mixed (~0.5% O_2 in CO) and stored in a 5-l. Pyrex vessel.

Methylene-d_2 ($^1A_1$) radicals were produced by the photolysis of ketene-d_2 with a high-pressure mercury arc (AH6, PEK Corp.). Methylene-d_2 was used because of its availability and our prejudice[5c] that product yields tended to be higher than with the light species. The lamp was situated in the center of an annular filter arrangement constructed of quartz. The first filter consisted of a 1-cm path filled with Cl_2 gas at 1 atm pressure. The second 1-cm path contained a circulating cobalt sulfate–nickel sulfate solution.[9] The transmitted radiation consisted of a 400-Å wide band centered at 2900 Å. A small amount of O_2 was added in order to scavenge a minor triplet component.

The composition of the reaction mixture was typically, CO:olefin:ketene:hydrocarbon standard:O_2 = ≥200: 10:2:0.2:1; the proportions were varied somewhat, as desirable. Several reactors were used in order to maintain relatively constant dilutions over the wide pressure range investigated. Spherical vessels of 0.75, 69, 570, 2150 and 12,000 ml volumes, constructed of fused silica and fitted with Teflon-Viton O-ring stopcocks, were used for the majority of the experiments. In the propylene system, for the highest pressure runs the reactants were sealed into a small diameter quartz tube (typically 0.15 ml). Most runs were of 2–20 hr duration. During this period, 0.2–2% of the ketene was decomposed, and ~0.05–0.5% of the olefin and ~0.5–5% of the hydrocarbon standard reacted.

Products were analyzed by gas chromatography using a flame ionization detector (fid). A combination column containing 20-ft of C_7 Fluoroalkyl Acrylate MS (Du Pont, 15%) on Chromosorb P followed by 1-ft of Kel F (6%) on Chromosorb P was employed for methylcyclopropane and propylcyclopropane reaction analyses; 2-in. of squalene (5%) on firebrick ahead of this combination was used for pentylcyclopropane reaction analysis. In the later work, the column temperature was reduced to 0° from room temperature since its efficiency deteriorated with use. It was usually necessary to perform at least one preliminary separation in order to achieve adequate resolution of the perfluoroolefin and decomposition product. Calibration checks were made with standard mixtures of these compounds. The gas chromatograph analytical system was equipped with two bypass valves to collect individual peaks as they were eluted. This feature permitted ir and mass spectrometric analysis of some of the products. Ir analysis was performed on a Perkin-Elmer 137 spectrometer and an AEI MS9 was used to obtain high-resolution mass spectra.[10]

Results

CD_2 + $CF_3CF{=}CF_2$ *System.* The processes of interest are

$$CD_2(^1A_1) +$$

$$CF_3CF{=}CF_2 \longrightarrow F_3C\text{—}\underset{D_2}{\bigtriangledown}F_2{}^* \qquad (1)$$

$$CF_3\text{—}\underset{D_2}{\bigtriangledown}F_2{}^* \left.\right\} \xrightarrow{\omega(M)} CF_3\text{—}\underset{D_2}{\bigtriangledown}F_2 \text{ (HMC) (S)} \qquad (2)$$

$$\xrightarrow{k_E} CF_3CF{=}CD_2 + CF_2 \text{ (D) } \qquad (3)$$
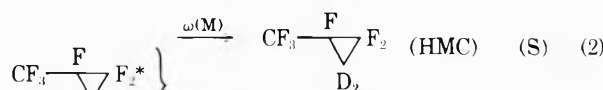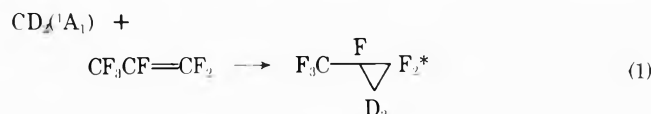
The energetically hot adduct formed in reaction 1 may transfer energy to the bath gas (M) and become stabilized (S), or it can split off a CF_2 and form 2,3,3,3-tetrafluoropropene-d_2 (D).

The stabilization and decomposition products showed

the required pressure dependence and were identified from their mass spectra. Aside from yielding the correct parent masses under low-energy electron impact, their cracking patterns at 70 eV were characteristic of compounds of their respective structures.[5b,10] The most abundant fragment of the decomposition product at 70 eV was m/e 69, corresponding to loss of C_2FD_2. The stabilization product had as its largest fragment the m/e 97 peak, characteristic[10,11] of the cyclopropyl moiety.

Early in the study it became apparent that chromatographic analysis of the stabilization product did not yield quantitative results. This compound was apparently partially destroyed on passage through the chromatographic columns. Consequently, neopentane was adopted as an internal standard in order to eliminate the need for directly measuring the stabilization product. Methylene-d_2 reacts with neopentane to form vibrationally hot 2,2-dimethylbutane (22DMB)

$$CD_2(^1A_1) + C(CH_3)_4 \longrightarrow 22DMB^* \tag{4}$$

$$22DMB^* \xrightarrow{\omega(M)} 22DMB \quad (S') \tag{5}$$

$$\xrightarrow{k_E'} products \quad (D') \tag{6}$$
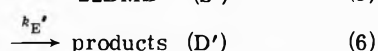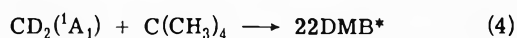
Recent work by Hase, Johnson, and Simons[12] who used diazomethane photolysis at 4358 Å gives an S'/D' of 300 at 10 Torr for this system. In our system, the S'/D' is of similar magnitude at this pressure. By contrast, our preliminary work indicated that the S/D for the HMC* adduct would be about 0.01 at the same pressure.

The amount of 22DMB produced in the photolysis is a measure of the total amount of HMC* formed. In conjunction with the yield of decomposition product, S/D ratios may be determined at pressures above 10 Torr. For D ≫ S

$$R = (D + S)/22DMB = D/22DMB$$

at higher pressures

$$S/D = [(R)(22DMB)/D] - 1$$

The ratio is uncomplicated by any sensitivity correction.

For our mixture composition, the average low pressure value (3.47) for D/22DMB also provides a lower limit to the rate constant ratio, k_1/k_4. With correction for the relative fid sensitivity of the products, it is found that $k_4/k_1 = 6.6$. This corresponds to a C–H insertion vs. C=C addition ratio of 0.55 per bond, as compared with the conventional number for hydrocarbons of 0.125.[13]

The D/22DMB ratios and the average rate constants, $k_a = \langle k_E \rangle$, measured in this study are given in Table I. The k_a values are plotted as a function of the collision frequency ω in Figure 1. Rate constants are plotted for pressures above 100 Torr only. The nature of the expression used to calculate S/D from the D/22DMB ratio leads to an amplification of any uncertainty in the ratio at lower pressures.

As may be seen from Figure 1, k_a is not independent of pressure over the entire range investigated. There is a plateau up to ~650 Torr at an average k_a of 3.6 × 10⁹ sec⁻¹. At higher pressures, the rate constants increase with increasing pressure, with no indication of a leveling trend even at the highest pressures studied. This pressure dependence is several orders of magnitude larger than, and is not to be confused with, the effect expected due to the small range of energies of the adducts formed in reaction 1.[14] It should be pointed out that the rate constants in Table I have been reduced to correct for low pressure rate constant "turn up" [5c]

TABLE I: Experimental k_a for C_3F_6 + CD_2 System (298°K)

Press, Torr	ω, sec⁻¹	R	S/D	$10^{-10} k_a$,[b] sec⁻¹
5	6.90 × 10⁷	3.47		
11	1.35 × 10⁸	3.51		
11	1.35 × 10⁸	3.45		
11	1.35 × 10⁸	3.45		
20	2.53 × 10⁸	3.35	0.036	
32	4.06 × 10⁸	3.23	0.074	
101	1.30 × 10⁸	3.28	0.058 (0.167)[a]	0.780
163	2.10 × 10⁸	3.05	0.138 (0.326)	0.644
202	2.60 × 10⁸	3.00	0.157 (0.351)	0.741
302	3.89 × 10⁸	2.67	0.300 (0.527)	0.738
402	5.16 × 10⁸	2.52	0.377 (0.622)	0.830
411	5.29 × 10⁸	2.50	0.388 (0.632)	0.837
642	8.25 × 10⁸	2.45	0.416 (0.666)	1.24
975	1.25 × 10¹⁰	2.40	0.446 (0.696)	1.80
1163	1.50 × 10¹⁰	2.00	0.735 (1.034)	1.45
1551	2.00 × 10¹⁰	1.98	0.753 (1.043)	1.92
6811	8.73 × 10¹⁰	1.26	1.754 (2.110)	4.14
8402	1.08 × 10¹¹	1.05	2.305 (2.648)	4.08
9913	1.27 × 10¹¹	0.95	2.653 (3.011)	4.22
16479	1.85 × 10¹¹	0.88	2.943 (3.301)	5.60
34596	4.43 × 10¹¹	0.64	4.422 (4.721)	9.38
54622	7.00 × 10¹¹	0.61	4.689 (4.974)	14.1

[a] These numbers have been corrected for low pressure turn up. [b] The strong collider value $k(sc)$ based on the present CO values (assumed as a step-ladder model of collisional transition with $\langle \Delta E \rangle = 4.5$ kcal) are found by dividing all values in the column by 2.
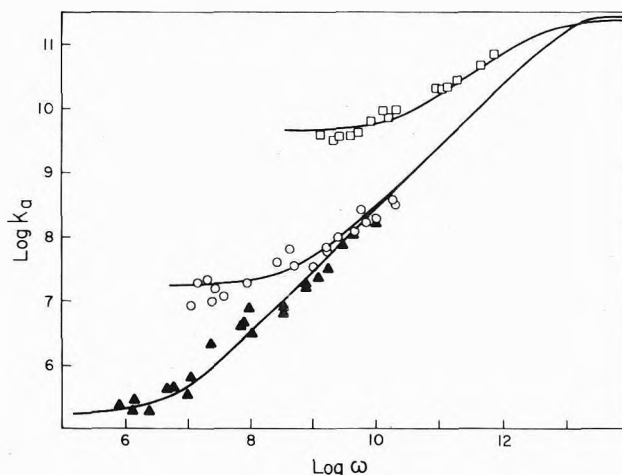
Figure 1. k_a (strong collider) vs. ω for C_3F_6 + CD_2 (□); C_5F_{10} + CD_2 (O); C_7F_{14} + CD_2 (▲); RRKM theoretical values (—).

due to inefficient collisional stabilization by CO, especially at low S/D. The correction was made on the basis of a step-ladder model of collisional transition probabilities with down jumps of 4.5 kcal mol⁻¹. (This is not the preferred model,[5c,11] but "any" correction does the job here.) These corrections affect the values of lower pressure rate constants most. The ratio of weak collider k_a to strong collider k_a equals 2, which was obtained from a stochastic calculation by using a 1600 cm⁻¹ step-ladder model for CO and 4000 cm⁻¹ for reactant. The relationship between k_a and ω will be described later.

CD_2 + n-$C_3F_7CF=CF_2$ System. A set of reactions, analogous to those proposed in the propylene system, apply

J. F. Meagher, K. J. Chao, J. R. Barker, and B. S. Rabinovitch

$$CD_2(^1A_1) + C_3F_7CF{=}CF_2 \longrightarrow C_3F_7{-}\overset{F}{\underset{D_2}{\triangledown}}F_2^* \quad (7)$$

$$C_3F_7{-}\overset{F}{\underset{D_2}{\triangledown}}F_2^* + M \overset{\omega}{\longrightarrow} C_3F_7{-}\overset{F}{\underset{D_2}{\triangledown}}F_2 \text{ (S)} \quad (8)$$

$$\overset{k_{2E}}{\longrightarrow} C_3F_7CF{=}CD_2 + CF_2 \text{ (D)} \quad (9)$$
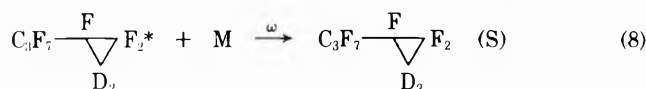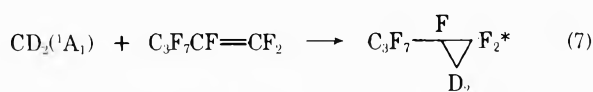
where S and D refer to the stabilized adduct and the products of its unimolecular decomposition, respectively.

Mass spectral analysis showed the major low pressure product to be octafluoropent-1-ene,-*1,1-d*$_2$ (reaction 9). Although an effort was made in high pressure runs, the stabilized adduct from reaction 8 could not be positively identified. Apparently, a mechanism similar to that which complicated the analysis in the propylene system also operated here. Since the same columns were used and the compounds are structurally similar in both systems, it is not surprising that this difficulty manifested itself again.

2,3-Dimethylbutane was employed as an internal standard to provide a measure of the yield of stabilized adduct. Under our conditions, the reactions of interest are

$$CD_2(^1A_1) +$$

$$\overset{H_3C}{\underset{H_3C}{\diagdown}}\overset{H}{\underset{}{C}}{-}\overset{H}{\underset{}{C}}\overset{CH_3}{\underset{CH_3}{\diagup}} \longrightarrow 2,3\text{-dimethylpentane*} \quad (10a)$$
$$\text{(23DMP)}$$

$$\longrightarrow 2,2,3\text{-trimethylbutane*} \quad (10b)$$
$$\text{(223TMB)}$$

$$C_7H_{14}D_2^* \overset{\omega(M)}{\longrightarrow} C_7H_{14}D_2 \quad (11)$$

$$\overset{k_{2E}'}{\longrightarrow} \text{products} \quad (12)$$
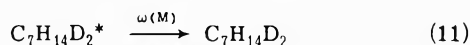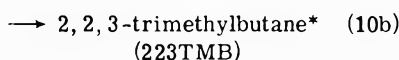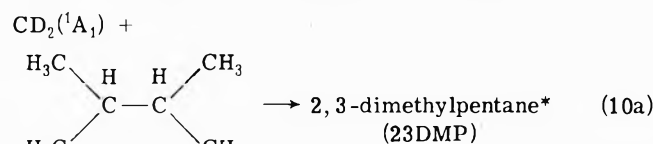
Reaction 10a predominated sixfold over reaction 10b and production of two isomeric insertion products presented no problem.

No kinetic data are available on the decomposition of these chemically activated isomers. However, it is possible to calculate these rates or to estimate them from studies on similar compounds formed at the same level of excitation. Hase, *et al.*,[12] have studied several branched alkanes. From their data we estimate the decomposition rate constants for our compounds to lie in the range 10^4–5×10^4 sec^{-1}. This corresponds to less than 1.5% decomposition at the lowest pressure used so that the insertion product is adequately represented by the stabilization alone; and, indeed, no decomposition products of 23DMP or 223TMB (reaction 12) appeared in the low-pressure products analysis.

An analysis similar to that used in the preceding section yields

$$S/D = [(R)(C_7H_{14}D_2)/D] - 1$$

Since it was not convenient to work in the low-pressure domain where the D/C$_7$H$_{14}$D$_2$ ratio becomes constant, an extrapolation technique was used to obtain R. The best fit to the data was obtained for a limiting low-pressure ratio of 6.50. The rate constant ratio k_{10}/k_7 is then 2.64, and on a per bond basis is 0.19. This value differs from the 0.55 value found in the propylene system more than we had expected, but we believe it to be correct.

The measured rate constants are given in Table II. The constants are plotted as a function of ω in Figure 1. Once again, the lowest pressure rate constants have been correct-

TABLE II: Experimental k_a for C$_5$F$_{10}$ + CD$_2$ System (298°K)

Press, Torr	ω, sec^{-1}	R	S/D	$10^{-7} k_a,^a$ sec^{-1}
0.30		5.62	0.386	
0.70	1.18×10^7	4.53	0.690	1.71
0.90	1.51×10^7	5.56	0.398	3.79
1.3	2.12×10^7	5.04	0.508	4.17
1.5	2.52×10^7	3.19	1.29	1.95
1.7	2.86×10^7	3.95	0.922	3.10
2.3	3.87×10^7	2.79	1.61	2.40
5.4	9.08×10^7	2.07	2.46	3.69
15.8	2.66×10^8	1.56	3.49	7.62
25.6	4.30×10^8	1.48	3.39	12.7
30.3	5.09×10^8	0.790	7.21	7.00
60.6	1.02×10^9	0.390	15.6	6.50
101	1.70×10^9	0.460	13.1	13.0
101	1.70×10^9	0.400	15.2	11.8
151	2.54×10^9	0.450	13.4	19.0
277	4.66×10^9	0.300	20.6	22.6
345	5.80×10^9	0.530	11.3	51.3
411	6.91×10^9	0.290	21.4	32.3
606	1.02×10^{10}	0.220	28.5	35.8
1168	1.96×10^{10}	0.230	27.2	72.1
1248	2.10×10^{10}	0.180	35.1	59.8

^{a} See footnote b, Table I; $k_a(\text{sc}) = k_a(\text{wc})/1.9$.

ed for weak collider effects. These rate constants demonstrate a pressure dependence similar to the one found in the propylene system. However, the rate constants start to increase over their initial plateau value (1.54×10^7 sec^{-1}) at a lower pressure.

$CD_2 + n\text{-}C_5F_{11}CF{=}CF_2$ *System.* The major reactions in this system are

$$CD_2(^1A_1) + C_5F_{11}CF{=}CF_2 \longrightarrow C_5F_{11}{-}\overset{F}{\underset{D_2}{\triangledown}}F_2^* \quad (13)$$

$$C_5F_{11}{-}\overset{F}{\underset{D_2}{\triangledown}}F_2^* \overset{\omega(M)}{\longrightarrow} C_5F_{11}{-}\overset{F}{\underset{D_2}{\triangledown}}F_2 \quad (14)$$

$$\overset{k_{3E}}{\longrightarrow} C_5F_{11}{-}CF{=}CD_2 + CF_2 \quad (15)$$
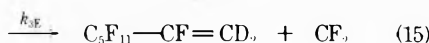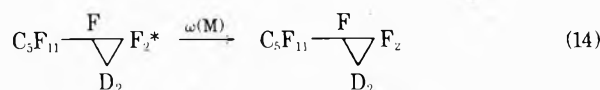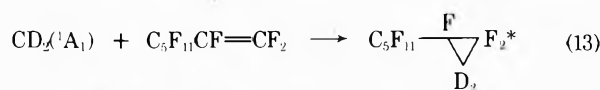
Dodecafluorohept-1-ene-*1,1-d*$_2$ was identified as the decomposition product by mass spectral analysis with use of CBr$_4$ as a mass standard. Cycloheptane (CH) was used as the internal standard. Methyl-*d*$_2$-cycloheptane (MCH) was the sole addition product

$$CD_2(^1A_1) + CH \longrightarrow MCH^* \quad (16)$$

$$MCH^* \overset{\omega(M)}{\longrightarrow} MCH \quad (17)$$
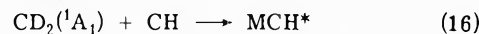
its estimated decomposition rate is $\sim 10^2$ sec^{-1} and the decomposition event is negligible.

Due to the limitations of our apparatus, we could not work in the low-pressure domain where the D/MCH ratio becomes constant. The limiting low-pressure ratio of 2.18 is the value estimated from $k_{16}/k_{13} = 3.92$, which corresponds to a C–H insertion *vs.* C=C addition ratio of $\frac{1}{4} \times 0.55 + \frac{3}{4} \times 0.19 = 0.28$ per bond, weighted under the assumption that the reaction ability of fluoroheptene-1 to methylene relative to hydrocarbon is closer to fluoropentene-1 than fluoropropylene. In the high-pressure range, the D/MCH value reached a plateau, 0.08, due to the fact that D is due almost entirely to a constant amount of nonrandom decomposition; 99.9% of the randomized entity was stabilized. Since the rate of randomized decomposition, $k_{RD} = 1.7 \times 10^5$ sec^{-1} from Figure 1, was relatively low at

all pressures compared to the collision frequency $(3 \times 10^8 - 1 \times 10^{10}$ sec$^{-1})$, most of the randomized molecules were collisionally stabilized at all pressures. However, the rate of nonrandom decomposition is calculated to be $\sim 3 \times 10^{11}$ sec^{-1} (see later) so that in this pressure range collisions play little part in stabilizing the nascent energized cyclopropyl moiety: the magnitude of the constant D value at higher pressures, which is due solely to the nonrandom contribution, is determined by the competition between the intramolecular energy relaxation and nonrandom decomposition.

The measured rate constants are given in Table III. The constants related to strong collision basis are plotted as a function of ω in Figure 1. A low-pressure, weak-collider turn-up correction is not needed in this case because S/D > 1, even at the lowest pressure.

Calculations and Discussion

Decomposition and Stabilization Expressions. In all systems studied, k_a increases at higher pressures by more than an order of magnitude. This behavior is caused by the component of decomposition due to the nascent species which arises from chemical activation and which has a nonrandomized distribution of internal energy initially deposited (in simplest assumption) in the cyclopropyl moiety. To calculate this contribution, we first review the treatment and reaction parameters employed by Rynbrandt and Rabinovitch (RR)[5b,c] for the bicyclopropyl system. Then we will consider some modifications of the calculations.

RR assumed that the energy deposited initially in the nascent moiety, E^0 (assumed randomized within it, of course) declines exponentially with time as

$$E^t = E^0 e^{-\lambda t} \qquad (18)$$

where λ^{-1} is a pragmatic quantity, an effective internal relaxation time. Thus the rate of decomposition of the moiety evolves in time as

$$k_{ND}(t) = k_{ND}(E^t) = k_{ND}(E^0 e^{-\lambda t}) \qquad (19)$$

There is also a time dependence of the rate of whole molecule randomized decomposition, k_{RD}; the nominal form used by RR was

$$k_{RD}(t) = k_{RD}(\infty)(1 - k_{ND}(t)/k_{ND}(0)) \qquad (20)$$

where, $k_{ND}(0)$ and $k_{RD}(\infty)$ are limiting initial $(t = 0)$ and final $(t = \infty)$ values, respectively. The precise form of $k_{RD}(t)$ was unimportant in the work of RR since the amount of randomized decomposition was negligible at very short times and only $k_{RD}(\infty)$ made an appreciable contribution.

Nonrandom and random decomposition compete with collisional stabilization, ω. Relative probabilities of the three events were found by computer integration

$$S = \omega \int_0^\infty N^*(t)\, dt \qquad (21)$$

$$RD = \int_0^\infty N^*(t) k_{RD}(t)\, dt \qquad (22)$$

$$ND = \int_0^\infty N^*(t) k_{ND}(t)\, dt \qquad (23)$$

where $N^*(t)$ is the concentration of active molecules which survive to time t. The naive apparent rate constant is $k_a = \omega(RD + ND)/S$. For bicyclopropyl, the rate of intramolecular energy relaxation was found to be 1.1×10^{12} sec^{-1}, with consideration of the rate of nonrandom decomposition of

TABLE III: Experimental k_a for C$_7$F$_{14}$ + CD$_2$ System (298°K)

Press, Torr	ω, sec^{-1}	R	S/D	$10^{-6} k_a,^a$ sec^{-1}
0.041	8.21×10^5	0.75	1.91	0.43
0.068	1.36×10^6	0.44	3.95	0.34
0.072	1.44×10^6	0.58	2.76	0.52
0.128	2.56×10^6	0.26	7.38	0.35
0.25	5.01×10^6	0.30	6.27	0.80
0.30	6.01×10^6	0.26	7.38	0.81
0.51	1.02×10^7	0.13	15.77	0.65
0.58	1.16×10^7	0.20	9.90	1.17
1.20	2.41×10^7	0.30	6.27	3.84
3.58	7.17×10^7	0.20	9.90	7.24
4.03	8.07×10^7	0.21	9.40	8.60
4.97	9.95×10^7	0.27	7.07	14.1
5.31	1.06×10^8	0.11	18.8	5.63
17.2	3.44×10^8	0.07	30.1	11.4
17.3	3.45×10^8	0.09	23.2	14.9
38.5	7.71×10^8	0.09	23.2	30.9
38.8	7.77×10^8	0.09	23.2	33.5
62.5	1.25×10^9	0.07	30.1	41.5
88.4	1.77×10^9	0.07	30.1	58.7
154	3.07×10^9	0.09	23.2	132
218	4.37×10^9	0.09	23.2	188
514	1.03×10^{10}	0.06	35.3	292

^{a} k_a(sc) is found from these values as k_a(sc) = k(wc)$/1.8$.

the newly formed ring for which $k_{ND}(0)$ was calculated to be 3.5×10^{11} sec^{-1}.

Now, the excess energy of the nascent moiety is $E^0 - E^{rem}$, where E^{rem} is the quasiequilibrium amount of energy remaining in the moiety. An improved expression for E^t is

$$E^t = E^{rem} + (E^0 - E^{rem})e^{-\lambda t} \qquad (24)$$

This more accurate form of E^t is important here only for the CF$_3$ system (E^{rem} = 70 kcal mol^{-1}). The calculations and conclusions of RR are not affected in a substantial way because E^{rem} (55 kcal) is lower and is relatively much closer to E_0 for the R$_F \equiv$ cyclopropyl case.

Equation 23 employs the integration limits 0 to ∞. This is physically incorrect since the RRKM theory does not contemplate decomposition by several subsets of the internal vibrations under conditions of quasiequilibrium. In practice, the exponential decrease with time of the excess energy of the nascent moiety, coupled with a near-exponential decrease in the specific rate constant $k_{ND}(E)$ with energy of the moiety, drastically reduces the value of $k_{ND}(t)$ with time, e.g., $k_{ND}(\lambda^{-1}) = 0.03 k_{ND}(0)$; therefore, it was only necessary to carry the integration for ND from $t = 0$ to $t = 2\lambda^{-1}$.[15a] In this connection, an improvement on the form of eq 20 for $k_{RD}(t)$ was also desirable since $k_{RD}(\infty)$ does not converge properly. We rewrite the expression as $k_{RD}(t) = k_{RD}(\infty)[1 - (E^t - E^{rem})/(E^0 - E^{rem})]$, which takes the correct limiting value, and RD (eq 22) was integrated from $t = 2\lambda^{-1}$ to ∞. The contribution to RD at short times is very small, so that the precise form of $k_{RD}(t)$ is important mainly in principle.

Thermodynamic and Structural Parameters. The levels of activation of the fluoroalkyl cyclopropanes were estimated from the chemistry of the process

$$C_2F_4 + {}^1CH_2 \longrightarrow c\text{-}CF_2CF_2CH_2 \qquad (25)$$
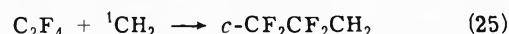
The standard enthalpy of the reaction is 95–101 kcal mol^{-1}, given by

$$\Delta H_f{}^\circ{}_{298}(c\text{-}C_3H_2F_4) - \Delta H_f{}^\circ{}_{298}(CH_2) - \Delta H_f{}^\circ{}_{298}(C_2F_4) \qquad (26)$$

where $\Delta H_f{}^{\circ}{}_{298}(\text{c-C}_3\text{H}_2\text{F}_4)^{15}$ = -155.0 kcal mol^{-1}, $\Delta H_f{}^{\circ}{}_{298}(\text{CH}_2)^{16a} \gtrsim 95.0$ kcal mol^{-1}, $\Delta H_f{}^{\circ}{}_{298}(\text{C}_2\text{F}_4)^{15}$ = -155.0 kcal mol^{-1};[15a] Simons, et al.,[16b] have proposed that $\Delta H_f{}^{\circ}{}_0 \geq 101$ kcal mol^{-1}. There may also be some excess photolysis energy carried by methylene[15,17] from 2900-Å radiation. The internal energy of the ring and alkyl R_F substituents, together with the relative translational energy of the reactants, also contributes approximately 3.0 kcal mol^{-1} to the internal energy of 1,1,2-trifluorocyclopropyl-d_2 moiety, and an additional 1.0, 4.0, and 7.0 kcal mol^{-1} for CF_3, C_3F_7, and C_5F_{11}, respectively.

The thermal decomposition rate of tetrafluorocyclopropane was measured[15] as

$$k_{\infty} = 10^{15.27} \exp(-48,500/RT) \qquad (27)$$

Corresponding to Arrhenius activation energy of 48.5 kcal mol^{-1}, the critical threshold is $E_0 = 46.5$ kcal mol^{-1} for R_F = C_3F_7 and C_5F_{11}. This value was adopted in our initial calculations for all three models. Argument can be made that the value for the methyl compound may be a little higher. A value $E_0 = 47.5$ kcal mol^{-1} fits the data somewhat better and was used.

In our earlier communication[10] we demonstrated that with the arbitrary, but objective, election of the expressions and parameters of RR, a reasonably consistent fit (but not quite as optimal as the present one) of these data can be made. Thus the pragmatic RR value of the total internal energy of hot bicyclopropyl, namely, $\langle E \rangle = 110$ kcal mol^{-1} (which gave a fit for $k_{RD}(\infty)$ but is probably too high (see below)), and the quantity 108 kcal mol^{-1} for the nascent moiety are workable magnitudes. In this work we have followed the same thermochemical pattern simply for consistency, and have retained $E^0 = 108$ kcal mol^{-1} for the moiety; the $\langle E \rangle$ now becomes 109, 112, and 115 kcal mol^{-1}, for the respective alkyl cyclopropanes.

We emphasize that the thermochemistry involved is somewhat uncertain. Thus, Benson and O'Neal[15b] estimate the activation energy for CF_2 elimination as 45.0 kcal mol^{-1}, which lowers E_0 by 3 kcal mol^{-1} and permits somewhat lower (by 5–6 kcal mol^{-1}), and better estimates of $\langle E \rangle$ of the several species, in order to fit $k_{RD}(\infty)$. We have not followed this out because no substantial changes in the deductions from the calculations would result; the experimental values of $k_{RD}(\infty)$ which must be fitted by the theoretical model supply a restraint which prevents any gross aberrations from truth from being introduced by arbitrariness in the thermodynamic and structural parameters. Indeed, the simplified model implied by eq 24 already warns that these calculations can not claim to yield precise values for λ (only sensible ones).

Activated Complex. The frequency assignment for the activated complex was made by fitting the Arrhenius parameter for thermal decomposition of tetrafluorocyclopropane. Two different models were considered by taking one asymmetric ring deformation as the reaction coordinate, by assigning two ring modes as 694 and 1650 cm^{-1}, and either by reducing only C–F frequencies, or both C–F and C–D bending frequencies, to 0.57 or 0.70 of the molecular values, respectively (Appendix I). Both models gave substantially the same results[10] and only the latter is presented here.

F Factor. The F factor correction for centrifugal effects was obtained by using the expression of Waage and Rabinovitch[18]

$$F_W = [1 + (s - 1)(I^+/I - 1)kT/(E_0 + aE_z)]^{-1} \qquad (28)$$
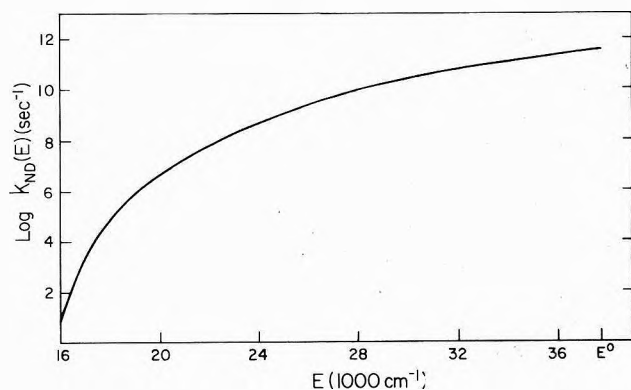
Figure 2. Calculated values of $k_{ND}(E)$ vs. E, where $k_{ND}{}^0$ = 3.0 × 10^{11} sec^{-1}.
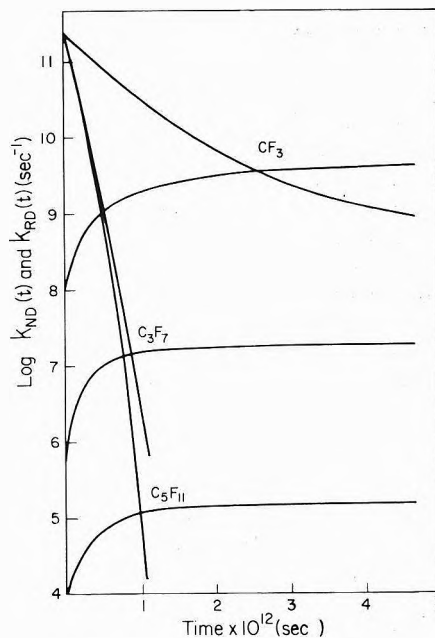
Figure 3. $k_{ND}(t)$ and $k_{RD}(t)$ vs. time for $R_F \equiv CF_3$, C_3F_7, and C_3F_7. The rising and falling curves are for k_{RD} and k_{ND}, respectively.

where I^+/I is the ratio of moments of inertia of the activated complex and molecule (Appendix II), s is the number of active vibrational degrees of freedom, E_z is the zero-point energy of the molecular vibrations, and a is the parameter,[19] $a = 1 - \beta W(E')$, where β is a frequency dispersion parameter and $W(E')$ is a unique function of the reduced energy $E' = E/E_z$. The $F_W{}^{-1}$ factors for methyl-, propyl-, and pentylcyclopropanes are 1.03, 1.02, and 1.02, corresponding to I^+/I ratios of 1.13, 1.07, and 1.05, respectively.[10]

Summary of Calculated and Experimental Results. The Rice–Ramsperger–Kassel–Marcus (RRKM) formulation was used to calculate decomposition rates of the fluoroalkyl cyclopropanes and of the cyclopropyl moiety. It was necessary, also, to make a weak-collider stochastic calculation of the rate constant for decomposition, $k_a(E)$; CO deactivating collisions were represented by a 1600-cm^{-1} step-ladder model, with 4000-cm^{-1} steps for the parent fluoroalkyl cyclopropanes. Although a step-ladder model is not the correct form of the collisional transition probabilities in this case,[20] the average step size was chosen so as to give the correct magnitude for the weak collider effect and the sim-

TABLE IV: Calculated and Experimental Values of $k_{RD}(\infty)$ and $k_{ND}(0)$ (sec^{-1})

	$R_F = CF_3$	C_3F_7	C_5F_{11}	Moiety
	$k_{RD}(\infty)$			$k_{ND}^{(0)}$
$\langle E \rangle$, kcal mol^{-1}	108.5	112	115	108
E^{rem}, kcal mol^{-1a}	70.2	42.9	30.6	
E_0, kcal mol^{-1}	47.5	46.5	46.5	46.5 47.5
RR[b]	6.7(9)[c]	3.2(7)	3.8(5)	2.8(11)
Present[d]	4.2(9)	1.8(7)	1.6(5)	3.0(11) 2.3(11)
Exptl	3.6(9)	1.5(7)	1.7(5)	

[a] Calculated at the "temperature" at which $\langle E \rangle = RT^2(\partial \ln q_{vib}/\partial T)$, which is 2330, 1620, and 1270°K, respectively. [b] Activated complex model of RR with their value $E_0 = 44.5$ kcal mol^{-1} used throughout. [c] (9) represents multiplication by 10^9. [d] With $F_w = 1$.

TABLE V: Calculated and Experimental Values of ND/(ND + RD + S) and of λ

	$R_F = CF_3$	C_3F_7	C_5F_{11}
RR	0.098	0.042	0.032
Present	0.11	0.028	0.028
Exptl	0.12	0.030	0.025
λ, sec^{-1}	6.0×10^{11}	1.6×10^{12}	1.3×10^{12}

ple model was adopted for computational ease and is quite adequate for the purpose. The calculated values are easily converted to a strong collider basis (Tables I–III) and are listed in Table IV. Plots of k_{ND} vs. energy and of $k_{ND}(t)$ and $k_{RD}(t)$ vs. time are shown in Figures 2 and 3. Satisfactory agreement is found between the RRKM theoretical values and the experimental values for each system. In particular, although the fit of the RR quantities to experimental $k_{RD}(\infty)$ values was satisfactory, considering the wide range (a factor of 2×10^4) of the latter, the present agreement is better. In the subsequent theoretical calculations, no further adjustments in k values were made.

Relaxation Rates λ and Low Pressure ND/(S + ND + RD) Values. The naive k_a values and the relative probabilities of three events S, RD, and ND are found by computer integrations of eq 21–23, where the values of λ, the intramolecular energy relaxation rate for successive members in the series, are found to be 6.0×10^{11}, 1.6×10^{12}, and 1.3×10^{12} sec^{-1}, respectively, as obtained from the best fit of calculated results to the experimental data (Figure 1). The corresponding low-pressure ND/(S + ND + RD) values are listed in Table V. The agreement with experiment is satisfactory and the best fit λ values are seen to group around the magnitude 1.1×10^{12} sec^{-1}, which was the value originally transferred from the work of RR and applied to the present systems.[10] The differences between λ values in the three systems may well represent experimental error in the data or inadequacy of the treatment (whether due to error in assigned parameters or to crudeness of the model). If the spread in values between CF_3, on the one hand, and C_3F_7 and C_5F_{11}, on the other, are valid, however, it demonstrates that the coupling in these molecules is stronger for the larger ones. Conflicting arguments may be advanced as to whether this is reasonable. We will await more evidence.

For $R_F = CF_3$, the methyl group is the smallest energy sink, and relaxation of the *total* energy of the cyclopropyl moiety is relatively slowest, so that the percentage of nonrandom decomposition is highest (12%). As R_F become larger, the amount of ND decreases, and for C_3F_7 and C_5F_{11} is almost quasiconstant at a lowest value of ~2.5% (Table V). In the methylcyclopropane system, at sufficiently high pressure (≥ 20 atm) the quantity ND/(ND + RD + S) begins to decrease detectibly due to collisional stabiliza-

tion of nascent nonrandomized entity. This is demonstrated in Figure 1 by the tendency of the experimental points to level off at very high pressure. It is calculated that ~20% of nonrandomized species are collisionally deactivated at the highest pressure (72 atm) in this system.

Experimental Accessibility of Energy Nonrandomization. When may nonrandomized energy effects be experimentally observed by measurement of total rate of reaction? The contribution of ND to total decomposition products depends on the relative magnitudes of $k_{RD}(\infty)$, $k_{RD}(0)$, λ, and ω, and on the magnitude of $(E^0 - E^{rem})$ for the nonrandom moiety. In view of this complexity, it will be sufficient here to examine some approximate relationships. A rule of thumb that is appropriate for many systems is that the low pressure ratio, (ND/(ND + RD + S))$_0$, is proportional to $0.2k_{ND}(0)/\lambda$, where 0.2 is a crude mean adjustment parameter that allows for the decline of $k_{ND}(t)$ with time and energy.

The apparent value of the observed rate constant k_a for unimolecular decomposition reaction is $k_a = \omega D/S$, where $D = ND + RD$, $S = S_N + S_R$, and $D + S = 1$. Here S_N and S_R are collisional stabilization products from nonrandomized and randomized species, respectively. At all pressures such that $\omega \ll \lambda$, the collision deactivation of nonrandomized species is negligible and $S = S_R$. At low pressures where $\omega \ll k_{RD}(\infty)$, $D \gg S$ and k_{a0} becomes ω/S_{R0}. A recognizable turn up in k_a, which depends somewhat upon the experimental accuracy, will occur when the ratio ND/RD starts to increase with increase in pressure. The relationship between the corresponding collision frequency, ω_t, and the reaction parameters is given from $k_a = (1 + x)k_{a0}$, or

$$\omega_t(ND + RD)/S_R = (1 + x)\omega/S_{R0} \qquad (29)$$

where x represents an experimentally detectible fractional change in k_a, corresponding, e.g., to 5–10%. The quantities RD and S_R are given by

$$RD = k_{RD}(\infty)(1 - ND)/(k_{RD}(\infty) + \omega)$$

and

$$S_R = \omega(1 - ND)/(k_{RD}(\infty) + \omega)$$

$$S_{R0} = \omega(1 - ND)/k_{RD}(\infty)$$

Then, eq 29 reduces to

$$\omega_t = xk_{RD}(\infty)/ND \simeq xk_{RD}(\infty)\lambda/0.2k_{ND}(0) \qquad (30)$$

Several cases may be recognized.

Case 1. λ O $k_{ND}(0) \gg k_{RD}(\infty)$. The nonrandom decomposition here is always a significant fraction of the total decomposition. From eq 30, ω_t O $k_{RD}(\infty)$. The present fluorocyclopropane studies correspond to this case. Thus, the percentage ND in the fluoromethylcyclopropane system is 11%. A rise in the k_a value occurs at $\omega \sim 3 \times 10^9$ sec^{-1},

where $k_{RD}(\infty) = 3.6 \times 10^9$ sec^{-1} (Figure 1). Similar considerations apply to the propyl and pentyl systems.

Case 2. $\lambda \gg k_{ND}(0) \gg k_{RD}(\infty)$. The contribution of nonrandom decomposition to decomposition reaction is smaller than that in case 1, *i.e.*, ND $\ll 0.2$. From eq 30 $\omega_t \gg k_{RD}(\infty)$ is predicted.

Fee and Markowitz[21] proposed a test of energy randomization prior to unimolecular decomposition in the cyclohexene-*t* system. Cyclohexene-*t* was produced by the recoil tritium reaction with methylcyclohexene. Their reaction schemes for cyclohexene-*3-t* and cyclohexene-*1-t* are
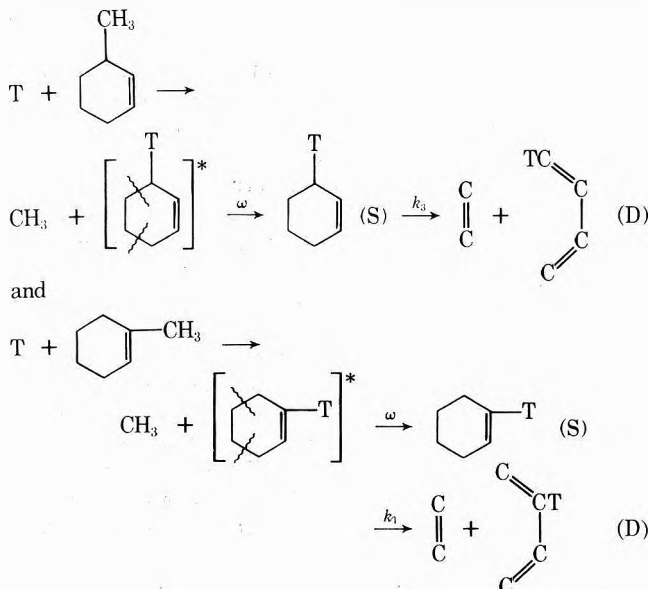
In contrast to cyclohexene-*1-t*, where unimolecular decomposition presumably arises solely from randomized species, both randomized and nonrandomized entities may participate in the decomposition of cyclohexene-*3-t*; four of the six carbons in the ring may be considered as an initially nonrandomized excited moiety, and the value of $k_{ND}(0)$ may be roughly estimated as 20–$50 k_{RD}(\infty)$, where $k_{RD}(\infty)$ was found to be[21] 3×10^6 sec^{-1}. Since $k_{ND}(0)/\lambda \ll 1$, the relative amount of ND is small at ordinary pressures. Then, to a good approximation, $k_a = k_{RD}(\infty)$. Indeed, near equivalence of the unimolecular rate constants k_3 and k_1 was observed. The estimated value of ω_t becomes 4×10^{10}–1×10^{11} sec^{-1} (>6000 Torr), for $x = 0.1$ and a value of λ for hydrocarbons estimated to be somewhat higher than for fluorocarbons, for example, $\lambda = 4 \times 10^{12}$ sec^{-1}. This could explain the absence of nonrandom effects in the range 300–1200 Torr reported by Fee and Markowitz.

Case 3. $\lambda \gg k_{ND}(0)$ O $k_{RD}(\infty)$. The low pressure ratio, (ND/(ND + RD + S))$_0$, is even smaller than in case 2. According to eq 30, a detectable increase in k_a value is expected as ω approaches λ and is well established at ω_t O λ. Under this condition, the collision deactivation of the nonrandomized moiety begins to be a significant process and to compete with decomposition. At even higher pressures, where $\omega > \lambda$, $k_{ND}(t) \rightarrow k_{ND}(0)$, RD ~ 0, and a big increase in k_a is expected.

The decomposition of butyl-2 radicals may be considered as an example of this case[22]

$$H + cis\text{-}CH_3CH{=}CHCH_3 \longrightarrow CH_3\dot{C}HCH_2CH_3{}^* \xrightarrow{\omega}$$
$$CH_3\dot{C}HCH_2CH_3 \xrightarrow{k} CH_3CH{=}CH_2 + CH_3$$
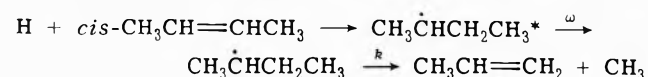
A three-carbon propyl entity may be arbitrarily designated here as the nonrandomized moiety. The value of

$k_{ND}(0)$ calculated from RRKM theory is $k_{ND}(0) = 7.8 \times 10^7$ sec^{-1} $= 4.3 k_{RD}(\infty)$), where the measured value[22] of $k_{RD}(\infty) = 1.8 \times 10^7$ sec^{-1}. Actually, constancy of k_a was observed by Oref, *et al.*, up to a pressure of 200 atm ($\omega \sim 5 \times 10^{12}$ sec^{-1}). Even for λ as big as 5×10^{12} sec^{-1}, some increase in k_a would be expected. That none was found may be interpreted as indicating that no activated moiety is produced *i.e.*, k_{RD} and k_{ND} are essentially degenerate channels. Nonrandomized energy effects would have to be sought in studies of a larger chain radical; but then, unfortunately, new experimental difficulties are introduced.

Appendix I. Frequency Assignments (cm^{-1}) for the Fluoroalkyl Cyclopropanes

A. 1,2,2-Trifluorocyclopropyl-d_2 Moiety $(C_3F_3D_2)$[23]

C–D stretch	2340, 2237
C–F stretch	1285, 1207, 757
C–D bend	1087, 847, 748, 709
CFC, FCC bend	623, 592, 479, 437, 413, 351, 192
C–C stretch	500
Ring def	1518, 982, 823

B. $R_F = CF_3$ Additional Frequencies[24]

C–F stretch	1360, 1281, 1225
CF_3 wag and bend	675, 420, 382, 280, 250, 180
Tors[a]	72

C. $R_F = C_3F_7$ Additional Frequencies[24]

CF_3 stretch	1321, 1179, 1140
CF_2 stretch	1315, 1215, 1155, 725
CF_3 bend	732, 538, 273
CF_2 bend	664(2), 460(2), 351(2), 340(2)
C–C stretch	930, 780
Skel bend	250(2), 125(2)
Tors	65, 57, 43

D. $CF_3 = C_5F_{11}$ Additional Frequencies

CF_3 stretch	1321, 1179, 1140
CF_2 stretch	1315(2), 1215(2), 1155(2), 725(2)
CF_3 bend	732, 538, 273, 149
CF_2 bend	664(4), 460(4), 351(4), 340(4)
C–C stretch	930(2), 780(2)
Skel bend	303(2), 184(2), 70(2)
Tors	65, 57, 43(2), 21

E. Activated Complex Moiety[a]

C–D stretch	2340, 2237
C–F stretch	1285, 1207, 757
C–D bend*	761, 593, 524, 496
CFC, FCC bend	436, 414, 335, 306, 289, 246, 134
C–C stretch	500
Ring def	1650, 694, 0

[a] According to Dorer's[25] assignment for monofluoroalkylcyclopropane, corrected for reduced mass changes.

Appendix II. Effective Hard-Sphere Collision Diameters (Å)[a]

	s	Ref
CO	3.8	5c
O_2	3.6	5c
$C_4F_6D_2$	6.13	b
$C_6F_{10}D_2$	7.70	b
$C_8F_{14}D_2$	8.80	b
$C_3F_3H_2 \cdot C_3F_3D_2$	7.50	5c

[a] For the reaction mixtures used, the following relationships apply at 1 Torr total pressure: $R_F = CF_3$, $\omega = 1.3 \times 10^7$ sec^{-1}; C_3F_7, $\omega = 1.7 \times 10^7$ sec^{-1}; C_5H_{11}, $\omega = 2.0 \times 10^7$ sec^{-1}. [b] Values estimated from ref 26.

References and Notes

(1) This work was supported by the National Science Foundation.
(2) L. Kassel, "Kinetics of Homogenous Gas Reactions," Reinhold, New York, N.Y., 1932; R. A. Marcus and O. K. Rice, J. Phys. Colloid Chem., 55, 894 (1951); for a recent quantum mechanical reinterpretation of the original classical language see O. K. Rice, J. Chem. Phys., 55, 439 (1971).
(3) L. D. Spicer and B. S. Rabinovitch, Advan. Phys. Chem., 21, 349 (1970).
(4) (a) M. A. Haney and J. L. Franklin, J. Chem. Phys., 48, 4993 (1968); J. L. Franklin and M. A. Haney, J. Phys. Chem., 73, 2857 (1969); J. J. DeCorpo, D. A. Bafus, and J. L. Franklin, J. Chem. Phys., 54, 1592 (1971); E. L. Spotz, W. A. Seitz, and J. L. Franklin, ibid., 51, 5142 (1969); (b) R. L. LeRoy, ibid., 53, 846 (1970); 55, 1476 (1971); (c) J. F. Bott and T. A. Jacobs, ibid., 50, 3851 (1969); (d) J. M. Parson and Y. T. Lee, ibid., 56, 4658 (1972), et seq.; (e) A. Lee, R. L. LeRoy, Z. Herman, and R. Wolfgang, Chem. Phys. Lett., 12, 569 (1972).
(5) (a) W. Von E. Doering, J. C. Gilbert, and P. A. Leermakers, Tetrahedron, 24, 6863 (1968); (b) J. O. Rynbrandt and B. S. Rabinovitch, J. Phys. Chem., 74, 4175 (1970); (c) J. D. Rynbrandt and B. S. Rabinovitch, ibid., 75, 2164 (1971).
(6) N. C. Craig, T. Hu, and P. H. Martyn, J. Phys. Chem., 72, 2234 (1968).
(7) Y. N. Tang and Y. Y. Su, J. Chem. Phys., 57, 4048 (1972).
(8) (a) L. J. Hals, T. S. Reid, and G. H. Smith, J. Amer. Chem. Soc., 73, 4054 (1951); (b) T. J. Brice, J. D. LaZerte, L. J. Hals, and W. H. Pearlson, ibid., 75, 2698 (1953); (c) J. D. LaZerte, L. J. Hals, T. S. Reid, and G. H. Smith, ibid., 75, 4525 (1953).
(9) J. G. Calvert and J. N. Pitts, "Photochemistry," Wiley, New York, N.Y., 1966, p 730.
(10) K.-J. Chao, Ph.D. Thesis, University of Washington, 1974; a preliminary account of this work has appeared as B. S. Rabinovitch, J. F. Meagher, K.-J. Chao, and J. R. Barker, J. Chem. Phys., 60, 2932 (1974).
(11) J. D. Rynbrandt, Ph.D. Thesis, University of Washington, 1970.
(12) W. L. Hase, R. L. Johnson, and J. W. Simons, Int. J. Chem. Kinet., 4, 1 (1972).
(13) (a) F. H. Dorer and B. S. Rabinovitch, J. Phys. Chem., 69, 1964 (1965); (b) F. H. Dorer and B. S. Rabinovitch, ibid., 69, 1973 (1965).
(14) B. S. Rabinovitch and R. W. Diesen, J. Chem. Phys., 30, 735 (1959).
(15) (a) A more correct method, in principle, for making the appropriate calculations than that used here, and which would avoid this dilemma, is to consider that the number of active modes of the molecule increase progressively with time from the initial subset, $n(0)$, corresponding to the moiety, to the full set, $n(\infty)$. In the present method, the size of a subset is invariant and its active energy declines with time; in the more correct method, the size of the subset increases to the full set, while the active energy remains constant. Unfortunately, this latter calculational procedure appears to be more intractable and, in practice, might be even more pragmatic than that adopted. However, one may make some qualitative deductions about the nature of the results that would emerge. If the size of the subset increases linearly with time, then the dependence on time of the observed rate constant is of the form $k(t) = k_{RD}(\infty) + (k_{ND}(0) - k_{RD}(\infty))e^{-\lambda' t}$. The apparent relaxation constant λ' is then found to be $\sim 10^{-13}$ sec^{-1}, i.e., an order of magnitude larger than that calculated in the text; these results are detailed in ref 10. If the increase in n were exponential, of the form $n(t) = n(\infty) - (n(\infty) - n(0))e^{-\lambda'' t}$, then the dependence of the nonrandomized rate on time would have a similar functional dependence to that used in the text, and a similar magnitude for λ'' would be expected: in the one case, $\Delta E = E^0 - E^{rem}$ declines exponentially with time and $k_{ND}(t)$ declines pseudoexponentially with decrease of E; in the other, Δn declines exponentially with time and $k(t)$ declines pseudoexponentially with increase of n. (b) S. W. Benson and H. E. O'Neal, Nat. Stand. Ref. Data Ser., Nat. Bur. Stand., No. 21 (1970).
(16) (a) W. A. Chupka, J. Berkowitz, and K. M. A. Refaey, J. Chem. Phys., 50, 1938 (1969); (b) W. L. Hase, R. L. Phillips, and J. W. Simons, Chem. Phys. Lett., 12, 161 (1971); J. W. Simons and G. W. Taylor, J. Phys. Chem., 73, 1274 (1969).
(17) D. W. Setser and B. S. Rabinovitch, Can. J. Chem., 40, 1425 (1962).
(18) E. V. Waage and B. S. Rabinovitch, J. Phys. Chem., 52, 5581 (1970); 53, 3389 (1970).
(19) G. Z. Whitten and B. S. Rabinovitch, J. Chem. Phys., 38, 2466 (1963).
(20) (a) J. D. Rynbrandt and B. S. Rabinovitch, J. Phys. Chem., 74, 1679 (1970); (b) J. H. Georgakakos and B. S. Rabinovitch, J. Chem. Phys., 56, 5921 (1972).
(21) D. C. Fee and S. S. Markowitz, J. Phys. Chem., 28, 354 (1974).
(22) I. Oref, D. Schuetzle, and B. S. Rabinovitch, J. Chem. Phys., 54, 575 (1971).
(23) N. C. Craig, G. J. Anderson, E. Cuellar-Ferreira, J. W. Koepke, and P. H. Martyn, Spectrochim. Acta, Sect. A, 28, 1175 (1972).
(24) E. L. Pace, Spectrochim. Acta, 22, 993 (1966).
(25) F. H. Dorer and B. S. Rabinovitch, J. Phys. Chem., 69, 1973 (1965).
(26) (a) S. C. Chan, J. T. Bryant, L. D. Spicer, and B. S. Rabinovitch, J. Phys. Chem., 74, 2058, 3160 (1970); (b) R. C. Ireton, Ph.D. Thesis, University of Washington, 1974.

Isomerization of Chemically Activated Propenyl Radicals

Toshio Ibuki,* Tetsuo Murata, and Yoshimasa Takezaki

Institute for Chemical Research, Kyoto University, Gokanosho, Uji, Kyoto, Japan (Received November 12, 1973; Revised Manuscript Received September 16, 1974)

The unimolecular rate constant for the isomerization of propenyl to allyl radical via hydrogen atom migration was measured. The propenyl radical was generated by the addition of methyl radical to acetylene, the average excess energy of which when first formed was calculated to be ~ 41 kcal/mol. The average rate constants for isomerization were found to be 4.04×10^7 and 8.38×10^7 sec^{-1} at 129 and 180°, respectively. The experimental data were interpreted using a four-membered, cyclic activated complex model with specific rate constants calculated according to the RRKM formulation of unimolecular reactions. The best agreement between experimental and theoretical results was found when a threshold energy of 34.5 kcal/mol was used.

Introduction

The thermal unimolecular isomerization of radicals via H atom migration has been reported for n-pentyl[1,2] and n-hexyl[3,4] radicals, the rate constants of which have been found to be $1.4 \times 10^7 \exp(-10.8 \times 10^3/RT)$ and $3.3 \times 10^8 \exp(-15.1 \times 10^3/RD)$ for n-pentyl, and $2.07 \times 10^7 \exp(-8.3 \times 10^3/RT)$ and $2.57 \times 10^9 \exp(-11.2 \times 10^3/RT)$

for n-hexyl radicals. Hardwidge, et al.,[5] have concluded that the activation energy for isomerization via H atom migration in a five-membered, cyclic activated complex must be ~ 15 kcal/mol. Recently Watkins, et al., have investigated extensively the unimolecular isomerization of chemically activated n-pentyl,[6,7] 3-methyl-1-buten-1-yl,[8] and 4-penten-1-yl radicals.[9] These vibrationally excited radicals isomerize via five-membered unimolecular reactions and

the activation energies have been found to be in the range 15–21 kcal/mol by using the RRKM calculations as shown in Table I.

Walsh[10] has assumed that for ring closing the activation energies can be fitted to the expression

$E(\text{kcal/mol}) =$

8 + ring strain energy (of acyclic radical) +

stabilization energy, if any (of acyclic radical)

The object of this work is to find the occurrence of isomerization through a four-membered, cyclic activated complex which must have high strain energy ($\sim$30 kcal/mol[11]) and to decide whether the above expression assumed by Walsh can be adopted generally or not.

Experimental Section

The reactions were carried out in a 206-ml cylindrical quartz vessel installed in a coaxial furnace, the temperature of which was maintained within ±1° by means of thermometer-activated relay unit. The cell was illuminated with the output from a 500-W high-pressure mercury lamp, and in the photolysis a Matsuda UV-27 filter was interposed between the arc and cell to cut off the radiation of wavelengths shorter than 2500 Å. In some experiments a wire net coated by soot was interposed to reduce incident light to about 10%.

Acetone for spectroscopy was purchased from E. Merck and acetylene was obtained from Takachiho Co., which contained very small amount of methane as an impurity. Both reactants were purified by bulb-to-bulb distillation *in vacuo*, the purities of which were better than 99.999%.

After irradiation, the mixture of the products and remaining reactants was diluted with nitrogen to prevent acetone from condensing in Töpler pump and analyzed by gas chromatography. For analysis of hydrocarbon products the backflash method[12] was used. The diluted reactant–product mixture was injected into a 10-m column of squalene on C-22 at 50°. When all the light end components up to 1,3-pentadiene had been eluted and their peak areas recorded, the flow of carrier gas was reversed, and the C_6^+ portion was condensed in a U trap immersed in liquid nitrogen. Then the C_6^+ portion was vaporized and analyzed by a 2-m Porapak Q (Waters Associates Inc.,) column with a flame ionization detector. Temperature programming from 170 to 200° was required. Carbon monoxide was analyzed by using a 1.8-m molecular sieves 5A column at 80° with a TC detector. Reaction products were identified by the retention time of authentic substances and also by

means of Shimadzu Model LKB-9000 gas chromatograph–mass spectrometer.

Results

A. Formation of Chemically Excited Propenyl Radicals. Methyl radicals were produced by the photolysis of acetone, the photodecomposition processes of which are well known as following[13]

$$CH_3COCH_3 + h\nu \longrightarrow 2CH_3 + CO \qquad (a)$$

$$CH_3 + CH_3 \longrightarrow C_2H_6 \qquad (1)$$

$$CH_3 + CH_3COCH_3 \longrightarrow CH_4 + CH_2COCH_3 \qquad (2)$$

$$CH_3 + CH_2COCH_3 \longrightarrow C_2H_5COCH_3 \qquad (3)$$
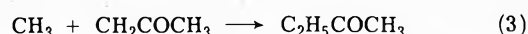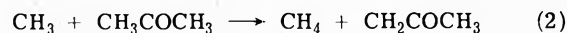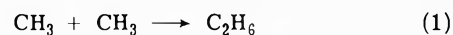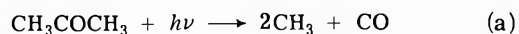
The addition of methyl radical to acetylene at 180° produces a propenyl radical with an average energy of 41.41 kcal/mol (see Discussion section) and when formed at 129°, 40.96 kcal/mol. These radicals can either react or be stabilized by collisional energy transfer.

In the photolyses of acetone and acetylene mixtures products were methane, ethane, carbon monoxide, propylene, 1-butene, *cis*- and *trans*-2-butene, *cis*- and *trans*-1,3-pentadiene, benzene, and toluene. The reaction conditions and rates of formation of products are given in Table II and III for the 180 and 129° runs, respectively. The presence of a large amount of propylene is evidence for the existence of propenyl radicals formed by addition of methyl radicals to acetylene

$$CH_3 + C_2H_2 \longrightarrow CH_3CH = CH^* \qquad (4)$$

$$CH_3CH = CH^* \xrightarrow{\omega} CH_3CH = CH \qquad (5)$$

$$CH_3CH = CH + CH_3COCH_3 \longrightarrow C_3H_6 + CH_2COCH_3 \qquad (6)$$
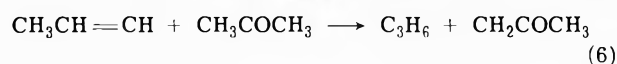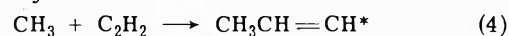
where ω is the specific deactivation rate constant.

B. Influence of Intensity of Incident Light. Carbon monoxide formed under the present conditions is produced primarily by the photodecomposition of acetone and it undergoes no reaction afterward. Therefore the rate of formation of CO is considered to be a measure indicating the intensity of the incident light.

Table IV shows the variation of the formation of products when the rates of CO formation were reduced to about 10% by interposition of a wire net coated by soot to reduce light intensity, while total pressure and the ratio of acetylene to acetone were kept constant. It is clear from the table that although the relative rates of formation of methane and 1-butene were constant independently of reaction conditions the formation of 2-butene could not be observed

TABLE I: Some Literature Values of the Arrhenius Parameters for Unimolecular Radical Isomerization

Reaction	log A, sec^{-1}	E_0, kcal/mol	Method used to obtain the parameters	Ref
n-Hexyl → s-hexyl	7.30 ± 1.0	8.3	Thermal	3
	9.41	11.2	Thermal	4
n-Pentyl → s-pentyl	7.15	10.8	Thermal	1
	8.52	15.1	Thermal	2
		$\sim$15		5
		18	RRKM	6
	11.7	21 ⎱	Recalculation	7
	10.6	18 ⎰		
	11.0	20		
4-Penten-1-yl → cyclopentyl		18	RRKM	9
3-Methyl-1-buten-1-yl → 2-methyl-3-buten-1-yl		17.1	RRKM	8

TABLE II: Experimental Results at 180°

No.	Acetone pressure[a]	C_2H_2 pressure	Total pressure	Temp, °C	t,[b] sec	CH_4[c]	C_2H_6	C_3H_6	$1\text{-}C_4H_8$	$t\text{-}2\text{-}C_4H_8$	$c\text{-}2\text{-}C_4H_8$	$t\text{-}1,3\text{-}C_5H_8$	$c\text{-}1,3\text{-}C_5H_8$	C_6H_6	$C_6H_5CH_3$
26	16.5	15.3	31.8	181.0	60	4.339	24.93	7.088	1.936	0.1751	0.2182	0.7921	3.066	3.117	nd[d]
31	15.2	19.8	35.0	180.0	60	2.814	13.93	5.299	1.812	0.1132	0.1419	1.160	3.025	4.352	0.3928
20	11.2	32.9	44.1	180.5	60	2.471	13.04	4.753	1.983	0.1035	0.1242	0.9431	2.763	5.883	nd
30	32.4	16.8	49.2	180.0	60	11.03	42.99	15.04	1.976	0.2388	0.3453	2.111	2.353	2.650	0.3757
23	37.0	12.8	49.8	180.0	60	14.48	50.29	16.12	1.777	0.2428	0.3228	1.955	1.890	1.129	nd
21	20.3	37.2	57.5	180.5	60	4.930	15.24	9.312	2.645	0.1432	0.2018	2.209	4.733	10.24	nd
29	32.0	34.9	66.9	179.5	60	9.610	28.84	16.23	2.866	0.2247	0.3265	3.508	4.497	8.361	0.6978
27	20.0	64.1	84.1	180.0	60	3.788	nd	7.892	2.037	0.1053	0.1410	2.389	4.931	11.96	0.7874
28	64.7	43.9	108.6	180.0	60	24.29	45.82	36.34	3.014	0.3046	0.4331	6.656	3.949	7.814	0.8408
32	61.5	91.8	153.3	180.3	60	15.16	17.47	29.37	2.973	0.1854	0.2692	6.629	4.474	10.92	1.948

[a] Pressures are expressed in Torr. [b] Photolysis time. [c] Products are expressed in terms of their rates of formation in mol ml^{-1} sec^{-1} $\times$ 10^{12}. [d] Not determined.

TABLE III: Experimental Results at 129°[a]

No.	Acetone pressure	C_2H_2 pressure	Total pressure	Temp, °C	t, sec	CH_3	C_2H_6	C_3H_6	$1\text{-}C_4H_8$	$t\text{-}2\text{-}C_4H_8$	$c\text{-}2\text{-}C_4H_8$	$t\text{-}1,3\text{-}C_5H_8$	$c\text{-}1,3\text{-}C_5H_8$	C_6H_6	$C_6H_5CH_3$
13	20.1	14.1	34.2	129.0	120	1.942	51.19	3.923	0.4465	0.1991	0.2750	0.6329	0.8386	1.221	0.1472
18	18.1	20.4	38.5	129.0	120	1.818	36.80	3.776	0.5802	0.1757	0.2366	0.7693	1.126	2.053	0.2131
11	16.1	31.0	47.1	128.6	60	1.521	29.08	3.459	0.7416	0.1792	0.2323	0.9516	1.585	3.758	0.5919
12	16.2	42.9	59.1	129.0	60	1.544	24.69	3.560	0.7708	0.1582	0.2169	1.114	1.775	5.091	0.5397
14	32.3	30.5	62.8	129.0	90	3.888	64.88	8.019	0.7342	0.3152	0.4552	1.675	1.437	3.045	0.6524
15	33.7	45.6	79.3	129.0	90	4.122	57.34	9.542	0.9379	0.3093	0.4581	2.246	1.921	5.518	0.5203
17	54.3	37.7	92.0	129.0	75	8.243	98.80	15.34	0.7692	0.3745	0.5657	2.860	1.605	3.991	0.6742
16	19.7	81.5	101.2	129.0	120	1.816	20.25	4.511	0.7072	0.1455	0.2168	1.513	2.049	9.688	0.6824

[a] See Table II for units.

TABLE IV: Influences of Incident Light on Products Formation[a]

Acetone[b]	Photolysis time[c]	Products (propylene = 1.00)				
		CH_4	C_2H_6	$1\text{-}C_4H_8$	$2\text{-}C_4H_8$	CO[d]
7.53	90	0.602	2.52	0.078	0.042	87.9
7.61	180	0.633	2.82	0.075	0.044	96.0
7.62	300	0.635	2.70	0.064	nd[e]	89.3
7.63	600	0.800	3.27	0.065	0.045	87.6
7.65	600	0.640	0.482	0.081	$\sim$0	8.96
7.42	600	0.658	0.528	0.077	$\sim$0	9.38
7.46	1200	0.703	0.579	0.057	$\sim$0	9.30
7.37	2400	0.684	0.444	0.065	$\sim$0	8.60

[a] The ratio of acetylene to acetone was kept at 0.954, and reaction temperature was 180°. [b] Concentrations are expressed in mol ml^{-1} × 10^7. [c] Photolysis time is expressed in seconds. [d] Rates of formation of CO are expressed in terms of mol ml^{-1} sec^{-1} × 10^{12}. [e] Not determined.

at the reduced incident light. It may be natural that 2-butene was formed by the reaction of stabilized propenyl radicals with methyl radicals

$$CH_3CH = CH + CH_3 \longrightarrow 2\text{-}C_4H_8 \qquad (7)$$

Since Reactions 6, 7, and 11 (to be proposed later) are competitive reactions, it is inferable that the ratio of 2-butene to propylene decreases at the reduced incident light which yields low steady-state concentrations of methyl radicals.

For 1-butene formation the relative rate of the production was not influenced by incident light, but was affected by variations of total pressures (see next section), suggesting that the mechanism for 1-butene formation differs from that for 2-butene.

C. Pressure Effect on the Formation of 1-Butene. The presence of 1-butene in the products would indicate the existence of species formed by chemically activated propenyl radicals. If so, it is expected that the rate of formation of 1-butene will be affected by the total pressure of the reaction system.

Table II and III show the pressure effects on the rate of formation of 1-butene. It can be seen that the relative rate of 1-butene formation to propylene is suppressed by increasing total pressure. This means that the precursor of 1-butene is chemically activated radicals formed by unimolecular isomerization. Allyl radical is the most probable species which is formed *via* H atom migration in the excited propenyl radicals

$$CH_3CH = CH^* \xrightarrow{k_a} CH_2CH = CH_2^* \qquad (8)$$

$$CH_2CH = CH_2^* \xrightarrow{\omega} CH_2CH = CH_2 \qquad (9)$$

$$CH_3 + CH_2CH = CH_2 \longrightarrow 1\text{-}C_4H_8 \qquad (10)$$
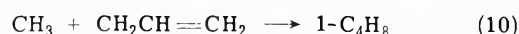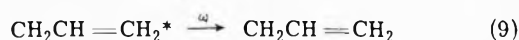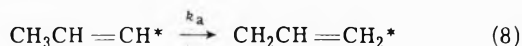
where k_a is the average rate constant for the isomerization.

The cross-disproportionation reaction of allyl with methyl radicals has been considered to be difficult because of high activation energies[14,15]

$$CH_3 + CH_2CH = CH_2 \longrightarrow CH_2 = C = CH_2 + CH_4 \qquad (10')$$
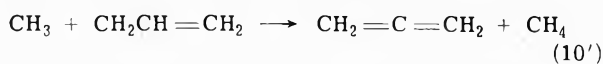
Holroyed and Klein[16] have predicted the value of $k_{10'}/k_{10}$ to be 0.023, which has been supported by James and Troughton.[14] In the present work allene was not identified. Therefore reaction 10' can be neglected in the present conditions. On the other hand, if the reaction of allyl radicals with molecules can occur, this reaction will compete with reaction 10. Then, the ratio of 1-butene to propylene should be decreased at reduced incident light, whereas Table IV shows the value to be independent of the intensity of light as mentioned in the previous section. Conse-

quently every allyl radical formed seems to be consumed to form 1-butene by reaction 10.

D. 1,3-Pentadiene, Benzene, and Toluene Formation. The product benzene makes up 5–40% of the yield of addition products at 180°, and 20–50% at 129°. Moreover the larger is the ratio of acetylene to acetone, the more is the formation of benzene. Drew and Gordon[17] have studied the formation of benzene in mixtures of acetone and acetylene which were irradiated at temperatures between 200 and 500°. Benzene was the major product and toluene was the minor. They noted that a methyl radical adds to acetylene, and this radical then adds to another acetylene in a typical free-radical-initiated polymerization. When three acetylene molecules were added the produced radical would be large enough to undergo intramolecular reaction to yield benzene and methyl radical. They have not observed 1,3-pentadiene, but suggested its existence.

Then, the reactions which can explain the products distributions are proposed as

$$CH_3CH = CH + C_2H_2 \longrightarrow C_5H_7^*(1,3\text{-pentadien-1-yl}) \qquad (11)$$

$$C_5H_7^* \xrightarrow{\omega} C_5H_7 \qquad (12)$$

$$C_5H_7 + CH_3COCH_3 \longrightarrow 1,3\text{-}C_5H_8 + CH_2COCH_3 \qquad (13)$$

$$C_5H_7 + C_2H_2 \longrightarrow C_7H_9^*(1,3,5\text{-heptatrien-1-yl}) \qquad (14)$$

$$C_7H_9^* \longrightarrow C_6H_6 + CH_3 \qquad (15)$$

$$C_7H_9^* \longrightarrow C_6H_5CH_3 + H \qquad (16)$$

$$C_7H_9^* \xrightarrow{\omega} C_7H_9 \qquad (17)$$

$$C_7H_9 + n\text{-}C_2H_2 \longrightarrow polymer \qquad (18)$$
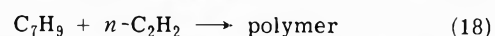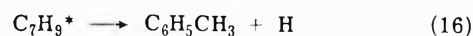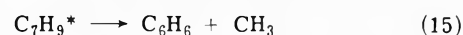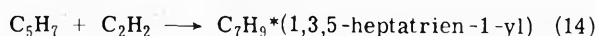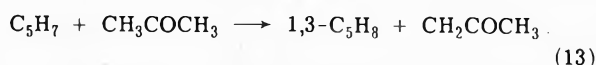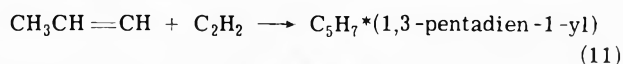
E. Kinetic Treatments. For reactions a–18, the steady-state treatments are applied, which lead to the following equation

$$\frac{R(CH_4)}{R(C_3H_6)} =$$

$$\frac{\omega + k_a}{\omega} \frac{k_2}{k_6} \frac{k_6[\text{acetone}] + k_{11}[\text{acetylene}] + k_7[CH_3]}{k_4[\text{acetylene}]}$$

Since $R(2\text{-}C_4H_8) \ll R(C_3H_6)$ in every run and $k_a/\omega \leq 0.01$ (see Discussion section), the above equation is rewritten as

$$\frac{R(CH_4)}{R(C_3H_6)} = \frac{k_2}{k_4}\left(\frac{[\text{acetone}]}{[\text{acetylene}]} + \frac{k_{11}}{k_6}\right)$$

Plots of $R(CH_4)/R(C_3H_6)$ *vs.* [acetone]/[acetylene] from the data in Table II and III give the value of k_{11}/k_6 as 2.88 and 3.84 at 180 and 129°, respectively.

In a chemical activation system the average rate constant k_a for a unimolecular reaction is given by $k_a = \omega(I/S)$,[18] where S is the total rate of formation of stabilized products and I is the total rate of formation of the isomerization products. In the present work I and S are given by

$$I = R(1\text{-}C_4H_8)$$

$$S = R(C_3H_6) + R(2\text{-}C_4H_8) + R(1,3\text{-}C_5H_8) +$$
$$R(C_6H_6) + R(C_6H_5CH_3) + R(18)$$
$$= R(C_3H_6) + R(2\text{-}C_4H_8) + R(11)$$

In order to estimate $R(11)$, the value of $R(11)/R(C_3H_6)$ was calculated at each run by

$$\frac{R(11)}{R(C_3H_6)} = \frac{k_{11}}{k_6}\frac{[\text{acetylene}]}{[\text{acetone}]}$$

The following expression was found to have the value 0.4–0.7 and 0.4–0.5 at 180 and 129°, respectively.

$$S_{obsd}/S_{calcd} = [R(C_3H_6) + R(2\text{-}C_4H_8) +$$
$$R(1,3\text{-}C_5H_8) + R(C_6H_6) + R(C_6H_5CH_3)]/[R(C_3H_6) +$$
$$R(2\text{-}C_4H_8) + R(11)]$$

The value has a tendency to increase with increasing ratio of acetylene to acetone, which was also observed in benzene formation as mentioned above. This suggests that the polymerization reaction of acetylene catalyzed by radicals occurs easily. Benson[11] has noted that acetylenes and conjugated dienes are much more susceptible to polymerization because the activation energy for radical addition to these species is about 4 kcal/mol, rather than 8 kcal/mol for addition to monoolefins. Fessenden and Shuler[19] observed that vinyl radicals add much more readily to ethylene than alkyl radicals.

Despite efforts to uncover further products of propenyl radical reactions, none could be detected (i.e., no substantial chromatographic peaks eluted after toluene) and therefore to proceed further we have to make the assumption that $S = S_{calcd}$.

A plot of I/S vs. $1/\omega$ from the data in Table II and III is shown in Figure 1. The collision diameters used to calculate the collision frequency of $CH_3CH=CH^*$ were $\sigma(C_2H_2) = 4.11$ Å, $\sigma(\text{acetone}) = 4.67$ Å, and $\sigma(CH_3CH=CH) = 4.67$ Å.[20]

A least-squares treatment of the data gave an intercept 0.0024 and $k_a = 4.04 \times 10^7$ sec^{-1} at 129°; and an intercept 0.0055 and $k_a = 8.38 \times 10^7$ sec^{-1} at 180°.

Discussion

Equations for the calculation of the average rate constant for the reaction of vibrationally excited molecules produced by chemical activation have been proposed by Rabinovitch and coworkers[18]

$$k_a = \omega(I/S) =$$
$$\omega\left\{\int_{E_{min}}^{\infty}\frac{k_E}{k_E + \omega}f(E)\,dE\middle/\int_{E_{min}}^{\infty}\frac{\omega}{k_E + \omega}f(E)\,dE\right\} \quad (I)$$

where k_E is the rate constant for isomerization at a specified energy E and $f(E)$ is the energy distribution above E_{min} of the chemically activated propenyl radical. k_E is given by[18]

$$k_E = \frac{\sigma Z^\dagger}{h Z^*}\frac{\Sigma P(E^\dagger)}{N^*(E)} \quad (II)$$

where $\Sigma P(E^\dagger)$ is the sum of energy eigenstates of the active degrees of freedom for the complex at energy $E^\dagger$,
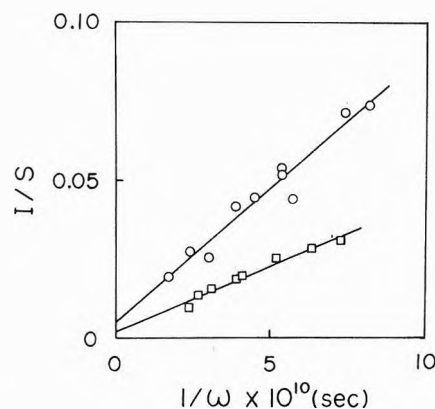
Figure 1. Plots of I/S vs. $1/\omega$: ○, 180°; □, 129°.

TABLE V: Frequency Assignments for Dissociation Complex and Isomerization Complex[a]

Motion	Dissociation complex	Motion	Isomerization complex
C–H str	3013	C–H str	3013
	2954 (2)		2954
	2992		3097
	2933		2940
C=C str	1800	C=C str	1800
HCH bend	1443	Ring expansion	1270
	1419		1300
HC=C bend	1298	Ring puckering	325
	1172	Ring deform	875
C–C=C bend	214	CH$_2$ deform	1435
CH$_3$ wag	456	CH$_2$ wag	918
HCC bend	600	CH$_2$ rock	638
	489 (2)	CH$_2$ twist	1087
	523	CH in plane bend	1276
CH$_3$ rot	113	CH in plane bend	1288
		CH out of plane bend	800
			846

[a] Frequencies are in units of cm^{-1}.

$N^*(E)$ is the density of energy eigenstates of the active degrees of freedom for molecule at energy E, $Z^\dagger$ and Z^* and the partition functions for adiabatic degrees of freedom of the complex and molecule, respectively, h is Plank's constant, and σ is the reaction path degeneracy.

$\Sigma P(E^\dagger)$ and $N^*(E)$ were calculated from the Haarhoff approximation.[21] Rabinovitch and Diessen[22] have described the distribution function, $f(E)\,dE$, for simple bimolecular combination reactions

$$f(E) = k'_E K(E)\,dE\middle/\int_{E_{min}}^{\infty} k'_E K(E)\,dE \quad (III)$$

where $K(E)$ is the Maxwell–Boltzmann distribution function and $k_{E'}$ is the specific rate of back reaction, i.e., the microscopic reverse of reaction 4.

For the calculation of k_a, the dissociation complex was specified as

$$CH_3\text{--}CH\!=\!\!=\!CH$$
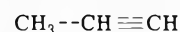
and the isomerization complex as

$$CH\text{---}H$$
$$\|\quad\vdots$$
$$CH\text{---}CH_2$$
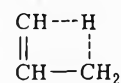
The frequency assignment for propenyl radical was taken from propylene,[23] and the following three frequencies were removed: CH stretch (3090 cm^{-1}), two HCH

T. Ibuki, T. Murata, and Y. Takezaki
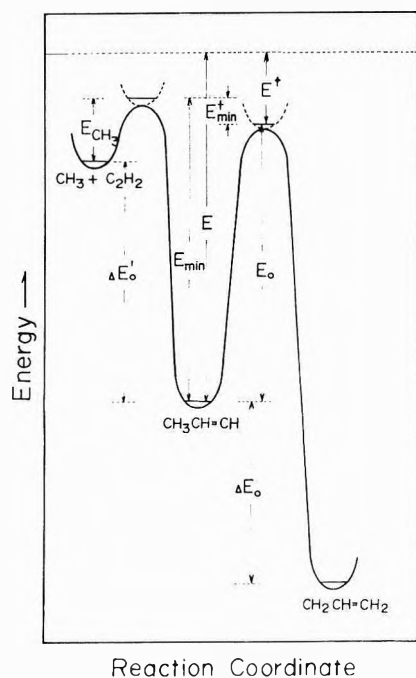
Figure 2. Schematic potential energy diagram.
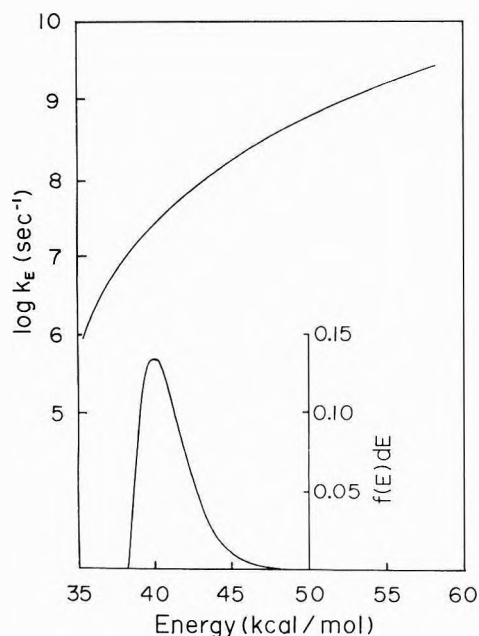
Figure 3. Calculated RRKM rate constants and the distribution function at 129°.

bends (1474, 1378 cm^{-1}). For the dissociation complex modifications were made according to those by Rabinovitch.[24] The vibration frequencies for the isomerization complex were taken from cyclobutene,[25] and are given in Table V together with those for decomposition complex model.

Figure 2 is a schematic energy diagram starting with CH_3 + C_2H_2 and leading to the observed products. This figure also serves to define the quantities, E_{min}, $E_{min}^\dagger$, and E_0 (for energy parameters see Appendix).

The best agreement between the theoretical and experimental rate constant k_a was obtained when $E_0 = 34.5$ kcal/mol. The calculated specific rate constants k_E are shown in Figure 3, and the theoretical average rate constants are

TABLE VI: Comparison of Calculated and Experimental Results

Temp, °C	$\bar{E}$, kcal/mol	k_a, sec^{-1} (obsd)	k_a(calcd), $E_0 = 34.5$ kcal/mol
129	40.96	4.04×10^7	4.80×10^7
180	41.41	8.38×10^7	6.04×10^7

TABLE VII: Enthalpies of Formation and Bond Energy at 0°K (kcal/mol)

$\Delta H_f^\circ(CH_3)$	34.4[a]	ΔH_f°(propylene)	8.47[a]
$\Delta H_f^\circ(H)$	51.62[a]	ΔH_f°(allyl)	37.8[c]
$\Delta H_f^\circ(C_2H_2)$	56.96[b]	$D(CH_3CH=CH-H)$	104[d]

[a] Reference 18. [b] J. G. Calvert and J. N. Pitts, Jr., "Photochemistry," Wiley, New York, N.Y., 1967; value corrected to 0°K. [c] Reference 9. [d] Reference 23.
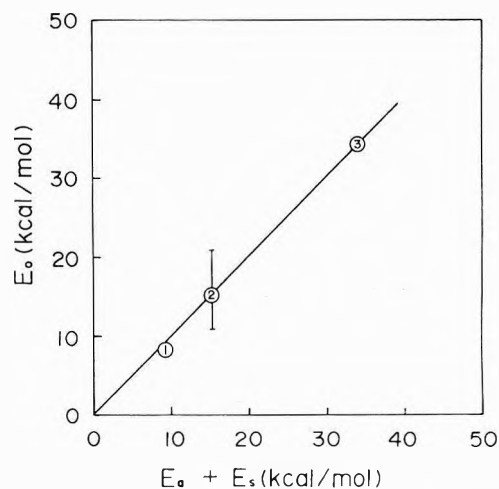
Figure 4. Plots of E_0 vs. $(E_a + E_s)$: ①, ref 3 and 4, isomerization through a six membered, cyclic activated complex; ②, ref 1, 2, and 5-9, five-membered; ③, present work, four-membered.

given in Table VI. The activation energy, $E_0 = 34.5$ kcal/mol, for the isomerization of propenyl radicals has not been measured hitherto. Walsh[10] has calculated the activation energy for the isomerization of the 1-buten-4-yl radical to the cyclobutyl radical as 38 ± 6 kcal/mol.

In the reactions of intramolecular hydrogen atom migration via a cyclic activation complex, the expression by Walsh[10] is considered to be $E_0 = E_a + E_s$, where E_a is the activation energy for a bimolecular H atom abstraction the values of which are in the range 7–11 kcal/mol for simple alkanes and alkenes,[26] generally ~8 kcal/mol, and E_s is the strain energy of a four-, five-, or six-membered ring, which is tabulated by Schleyer, et al.[27] In the present work we can adopt the $E_a = 7.2$ kcal/mol[28] and $E_s = 30.6$ kcal/mol, the strain energy for cyclobutene.[27]

The observed values of E_0 in Table I vs. calculated $E_a + E_s$ are plotted in Figure 4. From this figure it is concluded that the average rate constant k_a for a unimolecular reaction via H atom migration in a cyclic complex can be calculated by using the expression $E_0 = E_a + E_s$.

Appendix

The quantity of E_{min} is given by $E_{min} = \Delta E_0 + E_{CH_3}$, where E_{CH_3} is the activation energy for addition of methyl radicals to acetylene. The value of E_{CH_3} has been found to be 7.7 kcal/mol.[29] The heats of formation of all the free radicals observed in this work are given in Table VII.

References and Notes

(1) L. Endrenyi and D. J. LeRoy, *J. Phys. Chem.*, **70**, 4081 (1966).
(2) K. W. Watkins, *J. Amer. Chem. Soc.*, **93**, 6355 (1971).
(3) K. W. Watkins and L. A. Ostereko, *J. Phys. Chem.*, **73**, 2080 (1969).
(4) K. W. Watkins, *J. Phys. Chem.*, **77**, 2938 (1973).
(5) E. A. Hardwidge, C. W. Larson, and B. S. Rabinovitch, *J. Amer. Chem. Soc.*, **92**, 3278 (1970).
(6) K. W. Watkins and D. R. Lawson, *J. Phys. Chem.*, **75**, 1632 (1971).
(7) K. W. Watkins, *Can. J. Chem.*, **50**, 3738 (1972).
(8) K. W. Watkins and L. A. O'Deen, *J. Phys. Chem.*, **75**, 2665 (1971).
(9) K. W. Watkins and D. K. Olsen, *J. Phys. Chem.*, **76**, 1089 (1972).
(10) R. Walsh, *Int. J. Chem. Kinet.*, **2**, 71 (1970).
(11) S. W. Benson, "Thermochemical Kinetics," Wiley, New York, N.Y., 1968.
(12) D. D. Zakaib, *Anal. Chem.*, **32**, 1107 (1960).
(13) S. W. Benson, "The Foundation of Chemical Kinetics," Wiley, New York, N.Y., 1960.
(14) D. G. L. James and G. E. Throughton, *Trans. Faraday Soc.*, **62**, 145 (1966).
(15) (a) D. A. Dominey and C. J. Danby, *J. Chem. Soc.*, 4656 (1962); (b) J.

R. McNesby and A. S. Gordon, *J. Amer. Chem. Soc.*, **79**, 825 (1957).
(16) R. A. Holroyed and G. W. Klein, *J. Phys. Chem.*, **67**, 2273 (1963).
(17) C. M. Drew and A. S. Gordon, *J. Chem. Phys.*, **31**, 1417 (1959).
(18) (a) B. S. Rabinovitch and D. W. Setser, *Advan. Photochem.*, **3**, 1 (1964); (b) B. S. Rabinovitch and M. C. Flowers, *Quart. Rev., Chem. Soc.*, **18**, 122 (1964).
(19) R. W. Fessenden and R. H. Schuler, *J. Chem. Phys.*, **39**, 2147 (1963).
(20) J. O. Hirschfelder, C. F. Curtiss, and R. B. Bird, "Molecular Theory of Gases and Liquids," Wiley, New York, N.Y., 1964.
(21) P. C. Haarhoff, *Mol. Phys.*, **7**, 101 (1963).
(22) B. S. Rabinovitch and R. Diessen, *J. Chem. Phys.*, **30**, 735 (1959).
(23) J. W. Shimons, *J. Phys. Chem.*, **70**, 1076 (1966).
(24) M. J. Pearson and B. S. Rabinovitch, *J. Chem. Phys.*, **42**, 1624 (1965).
(25) R. C. Lord and D. G. Rea, *J. Amer. Chem. Soc.*, **79**, 2401 (1957).
(26) A. F. Trotman-Dickenson and G. S. Milne, *Nat. Stand. Ref. Data Ser., Nat. Bur. Stand.*, **No. 9** (1967).
(27) P. v. R. Schleyer, J. E. Williams, and K. R. Blanchard, *J. Amer. Chem. Soc.*, **92**, 2377 (1970).
(28) J. C. Cvetanovic and R. S. Irwin, *J. Chem. Phys.*, **46**, 1694 (1967).
(29) J. A. G. Dominguez and A. F. Trotman-Dickenson, *J. Chem. Soc.*, 940 (1962).

The Exchange of Hydrogen Bromide and Deuterium behind Reflected Shock Waves[1a]

R. D. Kern* and G. G. Nika

Department of Chemistry, University of New Orleans,[1b] New Orleans, Louisiana 70122 (Received May 28, 1974)

A complementary shock tube facility was used to study the reaction of equimolar mixtures of HBr and D_2 diluted by inert gases over the temperature range 2030–2515 K. The total gas density in the reflected shock zone was varied, 1.68–1.92×10^{-6} mol/cm^3. One set of experiments involved the analysis of infrared emission from HBr and DBr. The second set of data was collected using a time-of-flight mass spectrometer to sample the reacting gas mixture at 20-μsec intervals. Both sets exhibited a quadratic time dependence with respect to product formation. The combined order with respect to the reactants was found to be second order. Due to experimental difficulties, attempts to determine the order with respect to inert gas dependence were not successful. The kinetic profiles were fit to the equation $[1 - \tfrac{3}{2}f_{DBr}] = \exp(-k\,[HBr]_0, t^2)$, $k = 10^{22.31 \pm 0.48} \exp(-83,020 \pm 4970/RT)$ cm^3 mol^{-1} sec^{-2}. Assuming an order of one for the inert gas dependence, reaction profiles for an atomic mechanism were calculated using the experimental data presented herein and a collection of literature rate constants for the dissociation and three-center steps. Good agreement was obtained. This is the first report of a shock tube study involving the exchange of a diatomic molecule with deuterium that may be explained in terms of an atomic mechanism.

Introduction

Using quartz vessels and thermal conductivity measurements, Gross and Steiner[2] were the first investigators to report on the thermal exchange involving D_2 and a heteronuclear molecule. Data collected from the reaction of HCl with D_2 (765–843 K) were interpreted in terms of a homogeneous and essentially bimolecular mechanism. These workers used a packed vessel to assess wall effects. Heterogeneous atomic reactions resulting from collisions with the flask were determined to contribute about 15% to the overall reaction at the higher temperatures. The homogeneous portion proceeded with an activation energy of 54 kcal/mol. This study was extended by Steiner and Rideal[3] to 900 K. Exchange was reported to occur *via* superposition of the bimolecular reaction HCl + D_2 → DCl + HD and a wall-induced chain reaction: D + HCl → HD + Cl and Cl + D_2 → DCl + D. The activation energy increased to 57 kcal/

mol. The increase of 3 kcal/mol was attributed to the three-center reactions neglected in the earlier work.

Continuing the studies of exchange reactions of D_2 with hydrogen halides, Steiner[4] investigated the HBr + D_2 system. The apparatus used was similar to the previous HCl + D_2 studies. A packed vessel was used to evaluate wall effects. The reaction was found to proceed in a homogeneous straight chain fashion. In the range 821–984 K the activation energy for production of DBr was found to be 54 kcal/mol and was explained using the values for the dissociation energies of D_2 and HBr, their respective equilibrium constants, and several three-center exchange steps. Thus, it was concluded that the mechanism for exchange of D_2 with HBr was altogether different from D_2 + HCl.

Recently the shock tube has been used to study the HCl + D_2 exchange reaction under strictly homogeneous conditions.[5] Dynamic sampling of the reacting gases *via* infrared emission (IRE) and time-of-flight (TOF) mass spectrome-

try yielded data which are at variance with the previous studies. The activation energy is 34 kcal/mol and the products are formed as a nonlinear function of time. The reaction order is two (first order with respect to inert gas diluent and combined first order in reactants).

Several mechanisms which were tested failed to predict all of the experimental findings. The homogeneous bimolecular mechanism leads to a linear growth rate for DCl and zero order with respect to inert gas dependence. When the symmetry rules proposed by Pearson[6] are applied to the four-center mechanism, the exchange is deemed to be symmetry forbidden. Within the framework of these symmetry rules, a forbidden pathway could be traversed but only with a high energy barrier. Calculations of the magnitude of this barrier for the $H_2 + D_2$ exchange[7] have consistently revealed values in excess of 110 kcal/mol, which is the expected value for an atomic mechanism proceeding with atom concentrations far less than equilibrium amounts.[8]

An atomic mechanism was tried which is in partial agreement with the $HCl-D_2$ experiments; namely, a quadratic time dependence and an inert gas dependence. This reaction scheme requires a rate law which is first order in each reactant rather than the observed combined first-order dependence with respect to HCl and D_2. The activation energy which emerges from this process is dependent on which steps are taken from the straight chain sequence. Values range from 77 to 112 kcal/mol.[5] Finally, a vibrational energy chain mechanism can be written but when evaluated under the experimental conditions leads to a linear time dependence for product formation.

Study of the $HBr-D_2$ exchange reaction under high-temperature homogeneous shock tube conditions was undertaken to determine if the reaction proceeded in a homogeneous straight chain fashion as previously reported.[4] Of equal importance and interest are the time dependence and Arrhenius parameters for product formation.

Experimental Section

Dilute gas mixtures were prepared in neon–1% argon (Matheson research grade, 99.999%) and argon (Linde, 99.998%). The latter diluent was used for infrared emission experiments, while the blended diluent was used for the TOF test mixtures. Deuterium (Matheson CP, 99.5%) and hydrogen (Linde, 99.998%) along with the inert gas diluents were used as supplied. Hydrogen bromide (Matheson, 99.8%) was further purified as discussed below.

Analysis of several sources of HBr revealed the repeated presence of about 0.2% HCl. Certain purification procedures were tried; namely, sparging condensed HBr with a stream of helium, liquid N_2 bulb-to-bulb distillation, liquid N_2–ethanol slush, and liquid N_2–(CCl$_4$ + CHCl$_3$) slush. Of these procedures for reducing the HCl content below 500 ppm, the method of choice appears to be liquid N_2 bulb-to-bulb distillation.

During the course of these purification attempts, it was noted that extracted samples of HBr from lecture bottles contain differing amounts of HCl. The first few withdrawals from any cylinder contain the lowest concentration of the contaminant. Another factor is the cylinder itself. Several bottles were thought to have previously contained HCl. This was surmised by scraping the color code paint from the outer surface of the cylinder exposing the color code representing an HCl storage bottle. Hence, the best samples of HBr were obtained from the top third of a lecture bottle which were subsequently distilled and the last third

portion only from the distillation was accepted for gas mixtures. The final level of HCl in HBr was calculated to be about 450 ppm using static TOF measurements and infrared absorption techniques.

A dwell time of no longer than 30 sec existed from time of introduction of a dilute gas sample into the TOF shock tube until rupture of the aluminum diaphragm. During this residence time, the O_2 content of the mixture was recorded as an analog signal and compared to a background O_2 signal obtained prior to sample introduction. Previously prepared O_2 calibration mixtures permitted establishing a 20-ppm O_2 background level and all shock experiments were carried out with O_2 contents less than 17–20 ppm. Ultimate vacuums were 2×10^{-7} Torr in the shock tube, and 5×10^{-7} Torr in the TOF main chamber. Outgassing rates were less than 0.01 μ min^{-1} l.$^{-1}$ in the TOF shock tube.

Mass spectrometric analysis of mixtures used for infrared emission shock experiments indicated O_2 levels of 20 ppm. Residence times for gas mixtures were no longer than 45 sec in the IRE shock tube whose outgassing rate was 0.015 μ min^{-1} l.$^{-1}$.

Execution of a computer program which calculates vibrational–rotational energy levels as a function of temperature[5] aided selection of interference filters to observe HBr and DBr. An Infrared Industries 3.60-μ (0.22-μ half-band width) filter and an Optical Coating Laboratory 5.37-μ (0.2-μ half-band width) filter were used to follow emissions from HBr and DBr, respectively. Both shock tubes and detection equipment have been previously reported.[9]

Results

In the temperature range of this study, the exchange reaction equilibrium constant is at its predicted statistical thermodynamic limit of $K_1 = 2$.

$$HBr + D_2 \xrightleftharpoons{K_1} DBr + HD$$
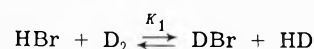
The low mass product self-exchanges through the reaction

$$\tfrac{1}{2}H_2 + \tfrac{1}{2}D_2 \xrightleftharpoons{K_2} HD$$
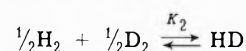
The value of K_2 is equal to 4 under the experimental conditions reported herein. It is convenient to use a mole fraction basis of $f_{HBr} + f_{DBr} = 1$ since virtually all of the bromine atoms are found in either HBr or DBr. All experiments performed contained equimolar amounts of the reactants. Utilizing the two equilibrium constants and solving the three material balance equations yields the values for HBr and DBr at equilibrium, 0.34 and 0.66, respectively. Plots of experimental mole fraction profiles (f_{DBr} vs. t) were observed to equilibrate at a value of 0.66. Neglect of the HD self-exchange results in a predicted equilibrium value of 0.58 for f_{DBr}.

Reaction profiles can be represented by the empirical equation

$$1 - f_{DBr}[1 + (f_{HBr}/f_{DBr})_{eq}] =$$
$$\exp[-k_1[HBr]_0^x[M]^y(t - t_{ind})^z] \quad (1)$$

Mole fraction f_{DBr} is obtained by $[DBr]/[HBr]_0$, where $[HBr]_0$ is the initial concentration of HBr. Experimental records indicate the absence of an induction period (t_{ind}). Growth profiles for f_{DBr} are best fit with a value of 2 for z (the time dependence). All data were tested via the expression

$$1 - \tfrac{3}{2}f_{DBr} = \exp(-k't^2) \quad (2)$$

TABLE I: Rate Constants for Exchange of HBr with D_2 via a Generalized Atomic Mechanism[a]

Reaction		Ref
5	$k_{d_1} = 10^{19.08} T^{-2} \exp(-88,000/RT)$	10a
	$k_{d_2} = 10^{21.78} T^{-2} \exp(-88,000/RT)$	10b
	$k_{d_3} = 10^{12.19} \exp(-50,000/RT)$	10c
6	$k_{ex_1} = 10^{14.43} \exp(-19,700/RT)$	10b
7	$k_{ex_2} = 10^{13.69} \exp(-9390/RT)$	12a
8, 9	$H + DBr \xrightarrow{k_a} HD + Br$	12b
	$H + DBr \xrightarrow{k_{ex}} HBr + D$	
	$k_{ex}/k_a = 0.09$	
	$H + HBr \xrightarrow{k_a} H_2 + Br$	
	$k_a = 10^{13.1} \exp(-900/RT)$	
	and	13
	$D + HBr \xrightarrow{k_a} HD + Br$	
	$D + HBr \xrightarrow{k_{ex}} DBr + H$	
	$k_a/(k_a + k_{ex}) = 0.88$	

[a] Values in $cm^3 \, mol^{-1} \, sec^{-1}$.
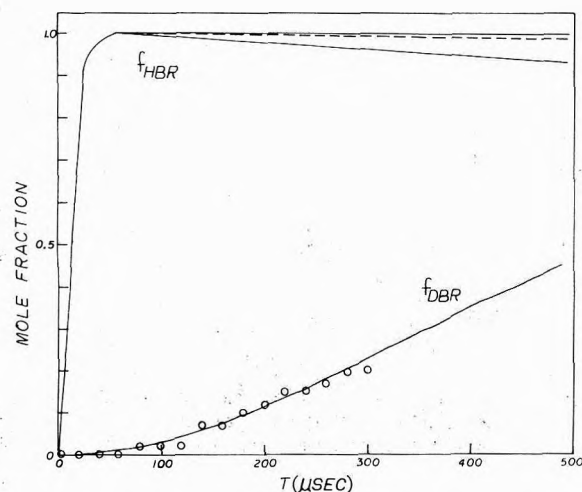
Figure 1. Upper curves (f_{HBr}) represent calculated and observed dissociation of HBr at 2200 K. Lower solid curve is fit to the experimental mole fraction (f_{DBr}) data, O, for an exchange reaction at 2200 K. See text for complete description.

Initially a series of IRE experiments was conducted with 3% HBr and 3% equimolar HBr + H_2 mixtures. Both sets were shocked in the range 1800–2500 K. Digitized emission signals at 3.60 μ were used to test the HBr decomposition profiles against the kinetic parameters reported in recent shock tube studies.[10] A listing of the various decomposition rate constants, k_d, is given in Table I. Curve f_{HBr} in Figure 1 consists of three parts. The uppermost solid line and the dashed line are generated by using k_{d_2} and k_{d_3}, respectively. The lowest solid line of curve f_{HBr} is the experimental profile for HBr thermal dissociation at 2200 K, in the presence of H_2. The data deviate from the reported values by about 7% excess decomposition at the conclusion of the 500-μsec observation period. By limiting subsequent analyses of DBr exchange reaction profiles to the first 350-μsec portion of experimental time, the observed HBr dissociation is held to a 5% level. This amount of decomposition for 3% HBr dilute in inert gas results in a temperature decrease of about 25 K, within the uncertainty limits associated with incident shock wave velocity measurements used to calculate reflected shock zone temperatures. It should be

noted that IRE is not suitable for obtaining kinetic data for HBr decomposition at the temperatures and densities spanned for these exchange rate studies. The purpose of limiting the exchange reaction profile to the aforementioned 5% decomposition is to minimize the effect of secondary reactions with regard to decomposition and to approach more closely the condition of a thermoneutral reaction environment.

These 3% equimolar HBr–H_2 runs exhibited IRE in the 5.37-μ region. Corrections to the DBr signals at 5.37 μ during exchange experiments were made in the same fashion as reported for the HCl–D_2 study.[5] However, the magnitudes of these corrections were significantly greater (70% of the DBr equilibrium signal at 5.37 μ is attributable to HBr emitting at this wavelength) than those necessary for HCl–D_2. For this reason, efforts to test for the inert gas dependence y in eq 1 were not successful and only the value of x was determined. Therefore, in eq 2, $k' = k \, [HBr]_0^x$.

One set of 3% equimolar HBr + D_2 experiments was analyzed by using signals obtained from both regions of the IRE spectrum. For a single experiment, the corrected 5.37-μ signal leads to a set of time-dependent f_{DBr} values. Simultaneous recording of the HBr decay at 3.60 μ leads to a constructed set of f_{DBr} values coincident in time with those obtained at 5.37 μ. An arithmetic average mole fraction basis was used to test Arrhenius parameters. All other IRE experiments, including another equimolar 3% series, used only HBr signals for construction of f_{DBr} profiles. Both sets of 3% data agree within one standard derivation. A plot of eq 2 and the experimental points for an exchange experiment at 2200 K is displayed in the lower portion of Figure 1.

An attempt was made to determine the order with respect to the reactants by changing their initial equimolar concentrations by a factor of 2 while holding the initial total pressure constant at 5 Torr. Within the errors associated with the experiments, the growth of [DBr] is second order with respect to the reactants HBr and D_2. As in previous work, the individual orders were not determined, but were assumed to be each first order.[9] Equation 2 takes the form
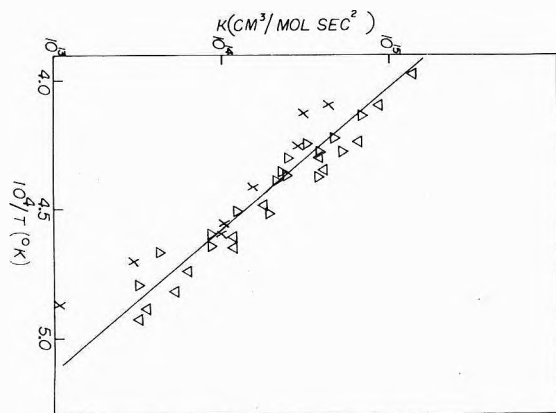
Figure 2. Arrhenius plot of data in Table II: mixture A △; B, ▽; C, ✕.

$$1 - \tfrac{3}{2}f_{\mathrm{DBr}} = \exp(-k[\mathrm{HBr}]_0 t^2) \qquad (3)$$

IRE results fit to eq 3 are listed in Table II.[11] The temperature range is 2029–2514 K.

Several experiments were carried out using the TOF shock tube. A 2% HBr–2% D_2 mixture in Ne–1% Ar was shocked in the range 2053–2438 K at an initial pressure of 5 Torr. The mass spectral peaks P_i observed were m/e 79, 80, 81, 82, and 83. The resolution of these mass peaks was limited by the thermal kinetic energy possessed by the respective ions. The peak height at m/e 83 separates from that of m/e 82 when the former is about 25% of the height of the latter, which in turn corresponds to a mole fraction for HBr of 0.1. The argon signal at m/e 40 was used in normalizing the reaction signals to account for pressure fluctuations in the TOF ion source chamber; thus, $R_i = P_i/P_{40}$. Of the two equally occurring isotopes, ^{79}Br and ^{81}Br, only the former is free of interference from HBr or DBr. Appearance of D^{79}Br was observed by subtracting from R_{81} the value of R_{79}. This corrected product signal was then added to R_{83} (D^{81}Br). The total HBr signal was obtained by direct sum ($R_{80} + R_{82}$). Mole fraction DBr was then calculated from the expression

$$f_{\mathrm{DBr}} = R_{\mathrm{DBr}}/(R_{\mathrm{HBr}} + R_{\mathrm{DBr}})$$

The TOF data yielded support for a quadratic time dependence for f_{DBr} growth and the Arrhenius parameters are within one standard derivation of IRE results. Individual values for this series of experiments are recorded in Table II.[11]

When all data in this table are expressed by eq 3, the exchange reaction is described by the Arrhenius equation

$$k = 10^{22.31 \pm 0.48} \exp(-83,020 \pm$$

$$4970/RT) \text{ cm}^3 \text{ mol}^{-1} \text{ sec}^{-2} \qquad (4)$$

Figure 2 is the Arrhenius plot of the combined IRE and TOF data.

Discussion

Notwithstanding the uncertainties associated with the determination of x and the failure to determine y in eq 1, there does exist throughout the data reported herein the important finding of an activation energy and a quadratic time dependence that is consistent with the proposal of an atomic mechanism for the exchange. This is the first time that such a result has been found for a shock tube investigation involving a diatomic molecule composed of an ele-
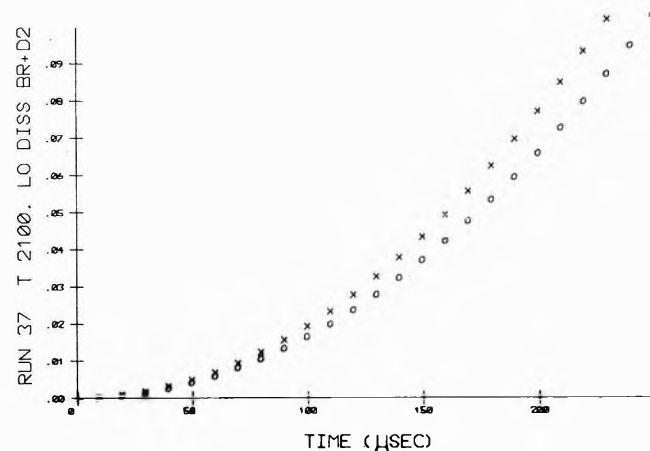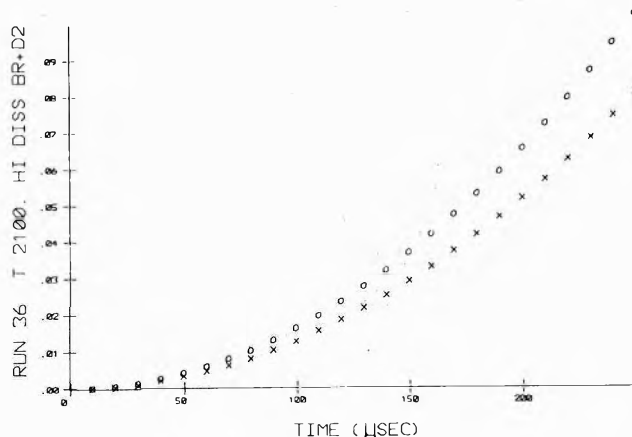
Figure 3. Comparison of experimental values of f_{DBr}, O, with calculated values, ✕, at 2100 K. The upper portion is calculated using a value for k_{d_2}, while the lower portion uses a value for k_{d_3}.

ment higher than the third row exchanging with deuterium. All other studies (see ref 5 and 8, and the citations therein) have dealt with diatomics in the first three rows and the mechanism for exchange with deuterium was not explainable in terms of an atomic mechanism. The possibilities of a direct molecular mechanism or a vibrational energy chain mechanism for the HBr + D_2 system are ruled out for the same reasons outlined in previous work.[8]

An atomic mechanism is represented by the following sequence. The back reactions are neglected.

$$\mathrm{HBr} + \mathrm{M} \xrightarrow{k_d} \mathrm{H} + \mathrm{Br} + \mathrm{M} \qquad (5)$$

$$\mathrm{Br} + \mathrm{D}_2 \xrightarrow{k_{\mathrm{ex}_1}} \mathrm{DBr} + \mathrm{D} \qquad (6)$$

$$\mathrm{H} + \mathrm{D}_2 \xrightarrow{k_{\mathrm{ex}_2}} \mathrm{HD} + \mathrm{D} \qquad (7)$$

$$\mathrm{D} + \mathrm{HBr} \xrightarrow{k_{\mathrm{ex}_3}} \mathrm{DBr} + \mathrm{H} \qquad (8)$$

$$\mathrm{D} + \mathrm{HBr} \xrightarrow{k_a} \mathrm{HD} + \mathrm{Br} \qquad (9)$$
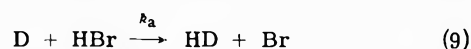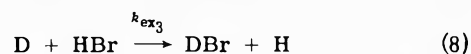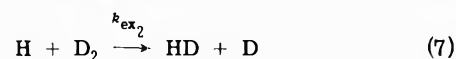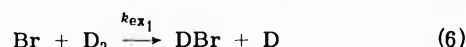
The pertinent rate constants are listed in Table I. Upon examination of the table, step 6 appears to be rate determining. A rate expression which neglects reverse reactions and contains only steps 5 and 6 may be derived.

$$\mathrm{d}[\mathrm{DBr}]/\mathrm{d}t = k_{\mathrm{ex}_1}[\mathrm{Br}][\mathrm{D}_2] \qquad (a)$$
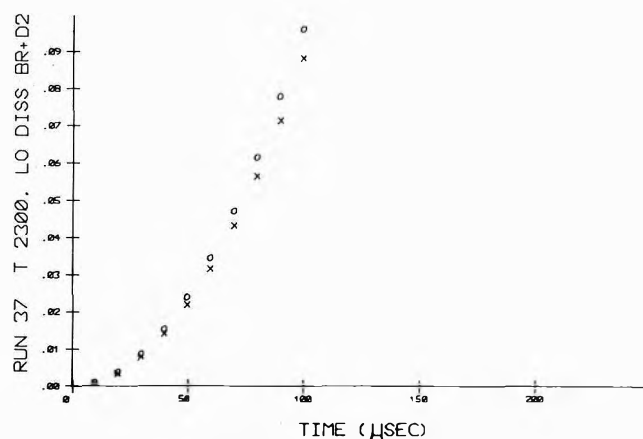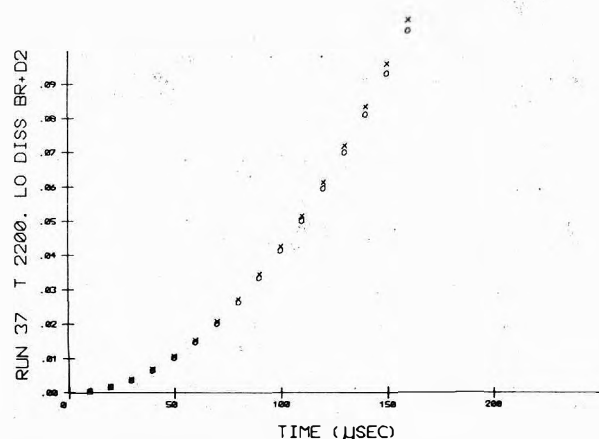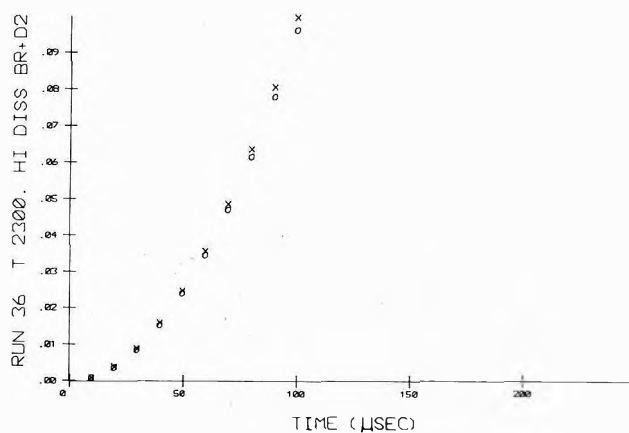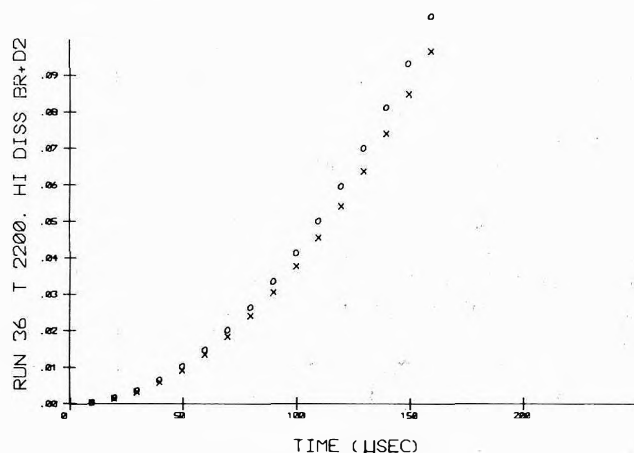
Figure 4. Same as Figure 3 except at 2200 K.

Figure 5. Same as Figure 3 except at 2300 K.

During the initial period of HBr decomposition, the back reaction of step 5 can be ignored, leading to

$$[Br] = k_d[HBr]_0[M]t \qquad (b)$$

When eq b is inserted in eq a and integrated, the growth of DBr is given by

$$[DBr] = \frac{1}{2}k_d k_{ex_1}[HBr]_0[D_2]_0[M]t^2 \qquad (c)$$

Equation c may be expressed as follows on a mole fraction basis when equimolar amounts of reactants are employed

$$f_{DBr} = \frac{1}{2}k_d k_{ex_1}[HBr]_0[M]t^2 \qquad (d)$$

Definition of "early times," or that portion of a reaction profile where back reaction(s) are neglected, can be expressed in the following way as it pertains to this study. Expansion of eq 3 and neglect of higher order terms leads to an expression which is valid up to a mole fraction value of 0.10.

$$f_{DBr} = \frac{2}{3}k[HBr]_0 t^2 \qquad (10)$$

The rate constant k from eq 10 can now be compared to the collection of constants derived from the proposed atomic mechanism, eq d.

$$k = \frac{3}{4}k_d k_{ex_1}[M] \qquad (11)$$

Profiles generated by using eq 10 were compared to plots obtained from eq d. By varying preexponential and activa-

tion energy values for k_{d_2} and k_{ex_1} and for k_{d_3} in combination with k_{ex_1}, close fits were obtained when compared to experimental results over the temperature range 2100–2400 K. In the uppermost plots for Figures 3–6, the trial values of k_{d_2} and k_{ex_1} are

$$k_{d_2} = 10^{22.08} T^{-2} \exp(-85,000/RT)$$

and

$$k_{ex_1} = 10^{14.73} \exp(-18,000/RT)$$

The agreement is better when k_{d_3} is used. The adjustments to the Arrhenius parameters are less severe; namely

$$k_{d_3} = 10^{12.19} \exp(-50,000/RT)$$

and

$$k_{ex_1} = 10^{14.68} \exp(-19,700/RT)$$

These results are dipicted in the lower plots for Figures 3–6. Further adjustments and/or the inclusion of other elementary steps are of course possible. However, recent work on atom–molecule[14a] and radical–molecule[14b,15] reactions has shown that extrapolation of rate constants determined at lower temperatures may be nonlinear when extended to higher temperatures. The magnitude of the curvature depends on several educated estimates. We feel that the number of parameters is too many to warrant additional calculations of profiles at this time.

It is pleasing to note that the atomic mechanism pro-
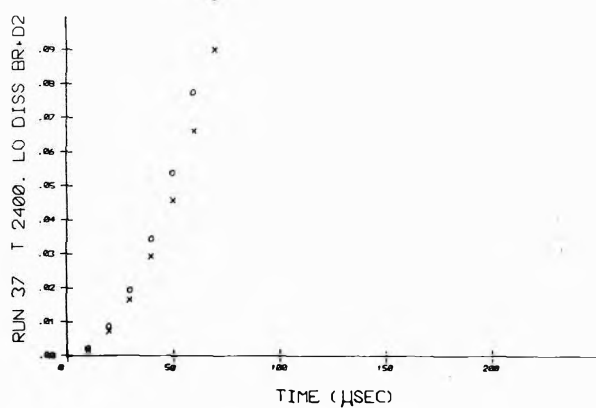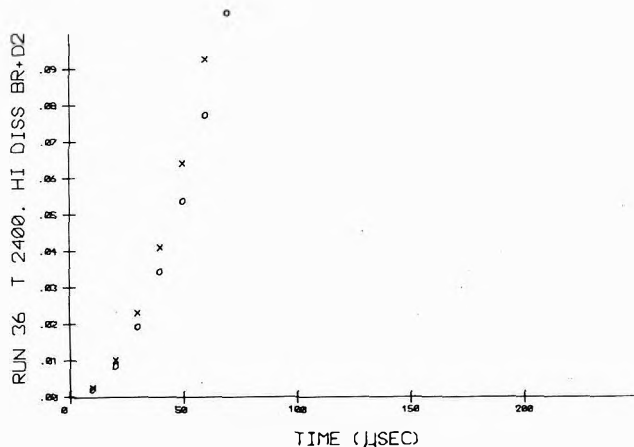
Figure 6. Same as Figure 3 except at 2400 K.

posed by Steiner[4] at the lower temperatures 821–984 K appears to be operative in the temperature range 2050–2500 K covered by this study.

Miniprint Material Available. Full-sized photocopies of the miniprinted material from this paper only (Table II) or microfiche (105 × 148 mm, 24× reduction, negatives) containing all of the miniprinted and supplementary material for the papers in this issue may be obtained from the Journals Department, American Chemical Society, 1155 16th St., N.W., Washington, D. C. 20036. Remit check or money order for $3.00 for photocopy or $2.00 for microfiche, referring to code number JPC-74-2549.

References and Notes

(1) (a) Support of this work by the National Science Foundation under Grant No. GP-33949 X is gratefully acknowledged. Paper presented in part at 168th National Meeting of the American Chemical Society, Atlantic City, N.J., Sept 1974; (b) Formerly Louisiana State University in New Orleans.
(2) Ph. Gross and H. Steiner, *J. Chem. Phys.*, **4**, 165 (1936).
(3) H. Steiner and S. K. Rideal, *Proc. Roy. Soc., Ser. A*, **173**, 503 (1939).
(4) H. Steiner, *Proc. Roy. Soc., Ser. A*, **173**, 531 (1939).
(5) R. D. Kern, Jr., and G. G. Nika, *J. Phys. Chem.*, **75**, 171 (1971).
(6) R. G. Pearson, *Accounts Chem. Res.*, **4**, 152 (1971).
(7) (a) H. Conroy and G. Malli, *J. Chem. Phys.*, **50**, 2014 (1969); (b) C. W. Wilson, Jr., and W. A. Goddard, *ibid.*, **51**, 716 (1969); (c) M. Rubenstein and I. Shavitt, *ibid.*, **51**, 2014 (1969); (d) C. W. Wilson, Jr., and W. A. Goddard, *ibid.*, **56**, 5913 (1972); (e) D. M. Silver and R. M. Stevens, *ibid.*, **59**, 3378 (1973).
(8) R. D. Kern and G. G. Nika, *J. Phys. Chem.*, **75**, 1615, 2541 (1971).
(9) J. M. Brupbacher and R. D. Kern, *J. Phys. Chem.*, **76**, 285 (1972); **77**, 1329 (1973).
(10) (a) K. Westberg and E. F. Greene, *J. Chem. Phys.*, **56**, 2713 (1972); b) N. Cohen, R. R. Giedt, and T. A. Jacobs, *Int. J. Chem. Kinet.*, **5**, 425 (1973); (c) R. R. Giedt, N. Cohen, and T. A. Jacobs, *J. Chem. Phys.*, **50**, 5374 (1969).
(11) See paragraph at end of text regarding miniprinted material.
(12) (a) A. A. Westenberg and N. deHaas, *J. Chem. Phys.*, **47**, 1393 (1967); (b) G. O. Wood, *ibid.*, **56**, 1723 (1972).
(13) J. M. White, *ibid.*, **58**, 4482 (1973).
(14) (a) T. C. Clark and J. E. Dove, *Can. J. Chem.*, **51**, 2147 (1973); (b) *ibid.*, **51**, 2155 (1973).
(15) A. A. Westenberg and N. deHaas, *J. Chem. Phys.*, **58**, 4061 (1973).

Kinetics of Fluorescence Quenching by Inorganic Anions

A. R. Watkins

Max-Planck-Institut für Biophysikalische Chemie, D 3400 Göttingen-Nikolausberg, West Germany (Received March 11, 1974; Revised Manuscript Received July 2, 1974)

The rate constants for the fluorescence quenching of a series of aromatic hydrocarbons by inorganic anions in acetonitrile are reported. For those systems where efficient quenching occurs, a correlation can be observed for any one anion between the measured rate constants k and $\Delta G'$, the excited state reduction potential of the aromatic. A similar correlation is also found between k and the calculated redox potentials of the anion quenchers for any one aromatic. In the region where $\Delta G'$ becomes large and the electron-donating ability of the anion is small, k becomes small and these correlations disappear. The free-energy change accompanying a possible electron transfer process in the excited state can also be calculated; this is, with three exceptions, positive, showing that in the majority of cases an electron transfer mechanism is energetically not favored. The other commonly accepted mechanism, a heavy-atom perturbation of the spin–orbit coupling of the excited aromatic, appears to be relatively unimportant for quenching by these anions, and probably has a slight influence only in the region of weak quenching and for systems quenched by iodides.

There has been much speculation about the mechanism by which fluorescent molecules are quenched by inorganic ions, in particular by inorganic anions. In reviewing the work which had been carried out on such systems up to 1950, Förster[1] came to the conclusion that the quenching process consisted essentially of electron transfer from the anion to the excited molecule with the formation of the corresponding radical anion. This has received support from more recent work[2,3] which has confirmed the earlier observations that the quenching efficiency of inorganic anions bears a direct relation to their oxidation potentials. There have, however, been other proposals to explain quenching by inorganic anions. Chief among these is the suggestion that the so-called "external heavy-atom" effect[4] is responsible for the observed quenching properties of anions containing heavy nuclei;[5–8] the proximity of the anion brings about a perturbation of the spin–orbit coupling in the excited molecule which facilitates a radiationless singlet–triplet transition.

There are, however, some indications that neither the electron transfer mechanism nor the heavy-atom effect are sufficient to explain the fluorescence quenching properties of inorganic anions.[9] It seemed to be of some importance to obtain more information about this type of quenching under conditions where some attempt can be made to calculate the thermodynamics of the electron-transfer process. For this purpose aromatic hydrocarbons were chosen, with acetonitrile as solvent. The electrochemical properties of many of these hydrocarbons in this solvent are well known, as are the singlet and triplet energies. The investigation to be reported here deals with the fluorescence quenching of aromatic hydrocarbons by inorganic anions in acetonitrile; particular attention has been paid to correlating the observed kinetics with the results to be expected from an electron transfer mechanism or a "heavy-atom" mechanism.

Experimental Section

p-Terphenyl, biphenyl, naphthalene, fluoranthene, anthracene, pyrene, perylene, and phenanthrene were all zone-refined samples; the other aromatic hydrocarbons were purified by recrystallization and sublimation. Sodium iodide, potassium iodide, and ammonium iodide were Suprapur quality from Merck; the other salts used in this work were purified as described previously.[9] Measurements of fluorescence quenching were carried out in the conventional way using a Hitachi-Perkin-Elmer MPF2A fluorescence spectrophotometer with digital read out; drifts in excitation light intensity and instrument response were corrected for by using a fluorescence standard. Excitation of the sample occurred at wavelengths as long as possible in order to avoid absorption of light by the added quencher; the only exceptions were the systems *p*-terphenyl–$N(C_4H_9)_4NO_3$ and naphthalene–$N(C_4H_9)_4NO_3$ which were excited at 270 nm under conditions where the nitrate concentration did not exceed 0.02 *M*. The Stern–Volmer plots were in all cases linear; there was no indication that irreversible chemical changes or complex formation in the ground state took place.

It was necessary, in view of the ability of iodide to undergo a light-induced oxidation in the presence of air, to degas all systems in which iodide was used as the quenching species. This had to be done in an apparatus lacking the usual greased stopcocks and joints, since these would be attacked by the solvent used in this work (acetonitrile). The apparatus which was finally used is shown in Figure 1. Solutions of the aromatic hydrocarbon and of hydrocarbon plus quencher are introduced into the reservoirs F and B, respectively, and the apparatus is degassed in the vertical position shown in Figure 1 and sealed off at the constricted openings A and E. The solution in F is transferred to the cell H by rotating in an anticlockwise direction, after which quencher from B can be added by rotating in a clockwise direction, reading off the volume of the solution to be added in D, and then bringing the aliquot so measured into the cell H by anticlockwise rotation. The results from this apparatus are as accurate as those from more conventional systems, as can be seen from Figure 2, which shows a Stern–Volmer plot for the system pyrene–KI obtained with this apparatus.
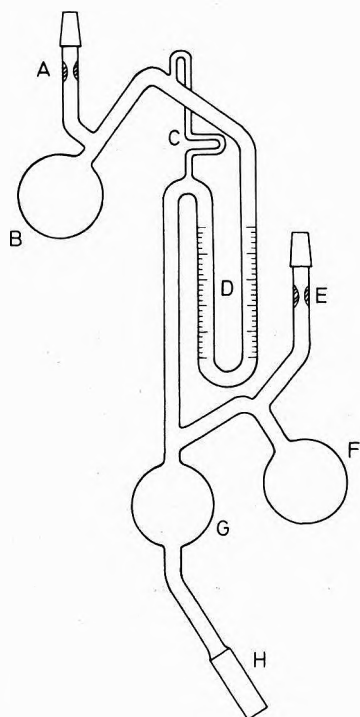
Figure 1. The all-glass apparatus used for quenching measurements with iodides. The letters refer to the description given in the text.
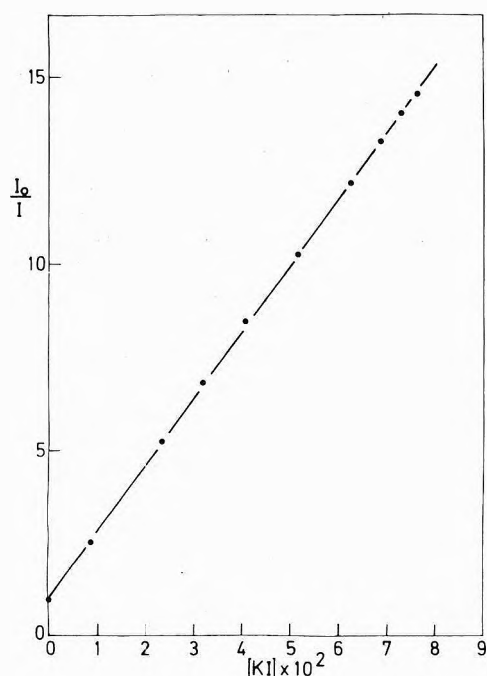
Figure 2. Stern–Volmer plot for the quenching of pyrene fluorescence by KI in acetonitrile.

Results

Rate constants for fluorescence quenching of a range of aromatic hydrocarbons by various inorganic salts are collected in Tables I (quenching by perchlorate, chloride, nitrate, bromide, and thiocyanate) and II (quenching by iodides). The Stern–Volmer quenching constants were measured in air-saturated solution (except for the iodide systems), were corrected to the corresponding air-free value,

and were then converted to quenching rate constants by dividing by the fluorescence lifetime. Fluorescence lifetimes were taken from the literature; although values determined in acetonitrile were lacking in some cases, the error in using a value determined in another solvent is probably not very great.[10,11] Quenching data for anthracene[2] and biphenyl[9] have also been included in these tables. It is well known that the anion plays the dominant role in determining the quenching properties of these salts;[12] the choice of the cation was therefore made mainly on the grounds of solubility. Tetraalkylammonium salts proved to be much more soluble in acetonitrile than the corresponding alkali metal salts; nevertheless, the maximum solubility of the chloride and perchlorate salts proved to be low, and the corresponding rate constants will therefore be less precise.

A possible contribution to quenching by NO_3^- could come from a dipole–dipole energy transfer,[13] since the nitrate ion has an absorption spectrum extending to about 320 nm, partially overlapping the fluorescence spectra of the hydrocarbons p-terphenyl, biphenyl, and naphthalene. Although no way could be found of checking this experimentally, the very small value[14] of the nitrate anion extinction coefficient at 300 nm makes it improbable that this plays any very important part in the quenching effects observed here. It is also to be expected that some of the salts used here exist at least partially as ion pairs in acetonitrile solution;[15] the fact that the Stern–Volmer plots are always linear suggests that the reactivity of the anion toward the quenching process is not affected by the proximity of the cation. Similar conclusions have been reached in other investigations in nonaqueous solvents.[16]

Discussion

Fluorescence quenching by an electron transfer mechanism can be depicted as a diffusing together of the reactants, followed by a subsequent electron transfer and diffusing apart of the radicals so formed

$$^1M^* + A^- \longrightarrow {}^1M^* \ldots A^- \qquad \qquad$$
$$M^- + A\cdot \longleftarrow M^- \ldots A\cdot \quad \Delta G \qquad (1)$$
$$M \ldots A^-$$
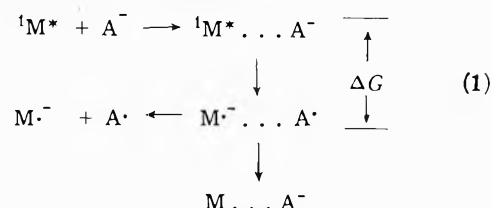
ΔG, the free energy change accompanying the electron transfer step, will be given by

$$\Delta G = E(A^-/A\cdot) - E(M^-/M) - \Delta E \qquad (2)$$

where ΔE is the zero-point energy of hydrocarbon M in its first excited singlet state, and $E(A^-/A\cdot)$ and $E(M^-/M)$ are the standard reduction potentials (vs. SCE) for the radical A· and the hydrocarbon M in acetonitrile. Although experimental values of $E(A^-/A\cdot)$ are not available, the other quantities have been measured for the hydrocarbons used here. If the quantity $\Delta G'$ is defined, where

$$\Delta G' = -E(M^-/M) - \Delta E \qquad (3)$$

it will be expected that the thermodynamic barrier to electron transfer will become larger, and the rate constant smaller, with $\Delta G'$ becoming more positive for any one anion.

The behavior reflected in Tables I and II is more complex than would be expected from this simple picture. Values of $\Delta G'$ have been included in these tables and the aromatic hydrocarbons studied here have been arranged so

TABLE I: Rate Constants k (in units of 10^9 M^{-1} sec^{-1}) for Fluorescence Quenching in Acetonitrile

	N(Bu)$_4$ClO$_4$	N(Hex)$_4$Cl	N(Bu)$_4$NO$_3$	N(Et)$_4$Br	NH$_4$CNS	$\Delta G'$, eV
p-Terphenyl	1.1	1.5	12.5	18.5	11.0	−1.66
Biphenyl[a]	0.16	0.71	7.3	5.0	8.6	−1.50
Fluorene			7.0	1.10	2.2	−1.50
Naphthalene	0.005	0.18	3.5	1.02	2.6	−1.41
Fluoranthene	0.004	0.03	0.004	1.05	2.3	−1.39
Anthracene[b]		0.095		1.9	3.5	−1.32
Pyrene	0.01	0.07	0.032	<0.005	0.044	−1.23
Phenanthrene	<0.02	0.16	0.16	0.035	<0.003	−1.12

[a] From ref 9. [b] From ref 2.

TABLE II: Rate Constants k (in units of 10^9 M^{-1} sec^{-1}) for Fluorescence Quenching by Iodides in Acetonitrile

	KI	NaI	N(Hex)$_4$I	NH$_4$I	$\Delta G'$, eV
p-Terphenyl	24.6				−1.66
Biphenyl	18.2[a]				−1.50
Fluorene	11.3				−1.50
Naphthalene	11.9				−1.41
Fluoranthene	11.9[b]				−1.39
Anthracene	11.0[b]				−1.32
Pyrene	4.46	4.36	4.18	3.58	−1.23
Perylene	10.6	11.6[c]			−1.20
Phenanthrene	4.68	4.00			−1.12
1,2;3,4-Dibenzo-pyrene	6.9				−1.11
Coronene	0.14				−0.91

[a] The value for k given in ref 9 is incorrect, and should be replaced by the value given here. [b] From ref 2. [c] From ref 6.

TABLE III: Calculation of One-Electron Reduction Potentials in Acetonitrile (See Text)

Radical	$E(A^-/A\cdot)$[a] in H$_2$O, V	$E(A^-/A\cdot)$[b] in H$_2$O, V	ΔG_{tr},[c] eV	$E(A^-/A\cdot)$[b] in CH$_3$CN, V
Cl·	2.55	2.79	0.44	2.35
NO$_3$·	2.3	2.5	0.22	2.3
Br·	2.0	2.2	0.33	1.9
I·	1.4	1.6	0.20	1.4

[a] Vs. standard hydrogen electrode, taken from ref 29. [b] Vs. sce. [c] Free energies of transfer from water to acetonitrile from ref 30.

that $\Delta G'$ increases on going from top to bottom. To facilitate further discussion Table I has been arbitrarily divided into two sections by a dashed line. The results in the upper right-hand section of Table I show a tendency, for any one anion, to decrease with increasing $\Delta G'$. On going from left to right in this section (in the direction of increasing electron-donating ability of the anions[17]) a similar tendency, although not quite so marked, can be detected: the quenching rate constants tend to increase. In the lower left-hand section, where the magnitude of the quenching effect is smaller, the vertical trend seems to reverse, so that k now increases with increasing $\Delta G'$. The rate constants in Table II conform, in magnitude and trend, to those in the upper right-hand section of Table I.

The tendency for the quenching efficiency to increase with increasing electron-donating ability of the anion has frequently been used as an argument in favor of an electron transfer quenching process.[1,12] This trend has been observed not only for aromatic hydrocarbons,[2,18] but also for the anion quenching of fluorescein,[3,19-22] Rhodamine B, Rhodamine 6G, acriflavin,[3,21] quinine bisulfate,[23] sodium salicylate,[24] and phenosafranine, eosin, and Rhodamine C[19] in aqueous solution, and it has been generally assumed that electron transfer quenching leads to the observed effects.[2,3,19-21,23-25] This is further supported by the effect of electron-withdrawing substituents on the quenching rate,[26] and by the observation of intermediates corresponding to an electron transfer step in the fluorescence quenching of hydroquinone by cobalticyanide ions.[27]

The same arguments could be applied to the results in the upper right-hand section of Table I and in Table II; a similar trend of quenching efficiency with anion can be observed, and the trends with $\Delta G'$ would also appear to support an electron transfer mechanism. However, the change

in k with changing $\Delta G'$ is unexpectedly slow. Systems in which electron transfer is known to occur show a change in k of a factor of 10^3 for a change of 0.3 eV in ΔG (or, correspondingly, in $\Delta G'$) for the non-diffusion-controlled region.[28] The systems studied here, which have k values which are generally not diffusion controlled, show a much smaller change for the same change in $\Delta G'$. For example, k changes by a factor of only ~5 on going from p-terphenyl–NH$_4$CNS to fluoranthene–NH$_4$CNS. A further argument against electron transfer fluorescence quenching in these systems is that the intermediates expected from an electron transfer process cannot (with one exception) be detected in the corresponding flash experiments.[5-9]

Recently, calculated values of $E(A^-/A\cdot)$ for a number of radicals in aqueous solution have been published.[29] By using the free energy of transfer from water to acetonitrile of the ions involved,[30] it is possible to calculate $E(A^-/A\cdot)$ in acetonitrile for a number of the ions used here. These are shown in Table III; the free energies of transfer for the corresponding radicals have been assumed to be negligibly small. If the data of Table III are used to calculate ΔG (eq 2) for the aromatic hydrocarbon–anion pairs investigated here, it turns out that ΔG is positive in all cases except for biphenyl–iodide, fluorene–iodide, and p-terphenyl–iodide; naphthalene–iodide and fluoranthene–iodide, where ΔG is about zero, appear to be borderline cases. Rehm and Weller[28] have shown that a value of $\Delta G = +0.2$ eV will lead to $k \simeq 10^6$ M^{-1} sec^{-1} for electron transfer quenching by organic electron donors in acetonitrile, whereas the k values observed here for fluorescence quenching by inorganic anions are much larger for positive ΔG values. For example, p-terphenyl–NO$_3^-$, which has $\Delta G = +0.6$ eV, has a value of $k = 1.25 \times 10^{10}$. Thus, if the results of Rehm and Weller are taken as a guide it appears that the rate constants observed here are orders of magnitude larger than would be expected from an electron transfer mechanism. $\Delta G'$ values can also be calculated[31] for the anion quenching of fluorescein, Rhodamine B, and Rhodamine 6G[3,19-22] in aqueous solution; values of −1.56, −1.49, and −1.45 eV, respective-

ly, are obtained. The values of ΔG calculated from the $\Delta G'$ values and the $E(A^-/A\cdot)$ values in the second column of Table III are all positive, showing that electron transfer is also energetically unfavorable for these systems. It is of interest that the flash spectrum of one of the three systems in Table II having negative ΔG (biphenyl–iodide) shows an absorption around 25 kK which persists regardless of the biphenyl concentration or cut-off filter used;[9] this is in all probability due to the biphenyl radical anion and the I_2^- ion produced by electron transfer in the excited state.

If an electron transfer mechanism is unable to explain the quenching kinetics observed here, it is possible that an alternative mechanism, the heavy-atom effect, is operative.[5–8] In this mechanism the spin–orbit coupling of the excited aromatic is perturbed by the presence of the inorganic anion. Since the intersystem crossing rate is determined primarily by spin–orbit coupling effects, an increase in spin–orbit coupling will lead to increased triplet production and to the disappearance of the excited singlet aromatic. The heavy-atom effect generally depends on some power of the nuclear charge of the perturbing atom.[32] However, the rate constants in Tables I and II show no discernable dependence on the atomic number of the heaviest atom in the anion, biphenyl and naphthalene, for example, being quenched more efficiently by NO_3^- and CNS^- than by Cl^- and Br^-. There is also nothing in the heavy-atom effect that could lead to the observed order of salts and aromatics in Tables I and II. A number of other authors have pointed out that the trend of quenching efficiency with anion is inconsistent with a heavy-atom effect;[1–3,9,19,21,24,25] for example, fluorescein in alkaline solution is quenched by the anions chloride, bromide, thiocyanate, and iodide with Stern–Volmer constants 0.6, 1.1, 47, and 68, respectively;[20] thiocyanate occupies a position which, from the point of view of the heavy-atom mechanism, is anomalous.

A possible explanation for the ineffectiveness of inorganic anions (in particular halide ions) as heavy atom quenchers may be found in the observations of Giachino and Kearns[33] on the polarization of naphthalene phosphorescence in various heavy atom glasses. They were able to show that charge transfer complex formation is relatively unimportant for the perturbation of phosphorescence transitions, and they concluded that a direct coupling mechanism (mixing of singlet and triplet states of the perturbed molecule in the field of an adjacent perturber molecule) would be too weak to account for the observed effects, a conclusion which was subsequently confirmed by the calculations of Lin and Lin.[34] The perturbation brought about by a direct mechanism involving a negatively charged ion would be expected to be even smaller. Coupling *via* the triplet states of the perturber and perturbed molecule appears to be more important,[33] and if this type of mixing (or the analogous case of coupling between singlet states) is also the dominant process in heavy-atom-induced intersystem crossing processes, it might be expected to be very much weaker for the high-lying states of inorganic ions than for, *e.g.*, organic halides.

The results for iodide quenching of pyrene and phenanthrene in Table II show that the cation also possesses quenching properties which are, however, weak in comparison with those of the anions. Cation quenching increases in the order $NH_4^+ < N(Hex)_4^+ < Na^+ < K^+$ (perylene appears to form an exception); a similar effect is observed for 9-phenylanthracene in ethylene glycol.[7] This is the order in

which the nuclear charge of the cation increases; it is thus possible that cation quenching is due to a heavy-atom effect.

If the underlying mechanism for anion quenching is one which entails a dependence of k on $\Delta G'$ (or on the electron-donating properties of the anion) then quenching by NO_3^-, Br^- and CNS^- in the upper right-hand section of Table I shows the expected behavior, anthracene being the only exception, while quenching by iodides (Table II) follows the expected trend with some deviations (*e.g.*, pyrene–I^- and perylene–I^-). These deviations may be due to a weak additional quenching component resulting from the heavy-atom effects induced by the relatively high nuclear charge of the iodide anion. The rate constants to the lower left of the dashed line in Table I are in an area where a quenching mechanism depending on $\Delta G'$ and the electron-donating properties of the anion would be expected to have little effect, and the quenching observed here may be due to other processes, such as the influence of the cation or a heavy-atom effect of the anion.

References and Notes

(1) Th. Förster, "Fluoreszenz Organischer Verbindungen," Vandenhoeck and Ruprecht, 1951, Chapter 10.
(2) R. Beer, K. M. C. Davis, and R. Hodgson, *Chem. Commun.*, 840 (1970).
(3) D. K. Majumdar, *Z. Phys. Chem.*, **217**, 200 (1961).
(4) M. Kasha, *J. Chem. Phys.*, **20**, 71 (1952).
(5) H. Leonhardt and A. Weller, *Z. Phys. Chem. (Frankfurt am Main)*, **29**, 277 (1961).
(6) A. Weller, *Chem. Weekbl.*, **60**, 53 (1964).
(7) A. R. Horrocks, T. Medinger, and F. Wilkinson, *Photochem. Photobiol.*, **6**, 21 (1967).
(8) A. Kearvell and F. Wilkinson, *Mol. Cryst.*, **4**, 69 (1968).
(9) A. R. Watkins, *J. Phys. Chem.*, **77**, 1207 (1973).
(10) J. B. Birks "Photophysics of Aromatic Molecules," Wiley-Interscience, London, 1970; G. Porter and M. R. Topp, *Proc. Roy. Soc., Ser. A*, **315**, 163 (1970); H. Schomburg, private communication.
(11) R. P. van Duyne, *J. Amer. Chem. Soc.*, **95**, 7164 (1973).
(12) P. Pringsheim, "Fluorescence and Phosphorescence," Interscience, New York, N.Y., 1949.
(13) N. Mataga and T. Kubota, "Molecular Interactions and Electronic Spectra," Marcel Dekker, New York, N.Y., 1970.
(14) Landolt-Börnstein, "Physikalisch-Chemische Tabellen," Julius Springer, Berlin, 1923.
(15) C. W. Davies, "Ion Association," Butterworths, London, 1962.
(16) J. R. Jones, "The Ionisation of Carbon Acids," Academic Press, London, 1973, Chapter 7.
(17) W. M. Latimer, "The Oxidation States of the Elements and their Potentials in Aqueous Solution," Prentice-Hall, New York, N.Y., 1952.
(18) K. Kasper, *Z. Phys. Chem. (Frankfurt am Main)*, **12**, 52 (1957).
(19) A. V. Karyakin and G. G. Babicheva, *Opt. Spectrosc.*, **24**, 541 (1968).
(20) J. Glowacki and V. Kaminska, *Acta Phys. Polon.*, **23**, 43 (1963).
(21) J. Glowacki, *Acta Phys. Polon.*, **24**, 555 (1963).
(22) J. Hevesi in "Molecular Luminescence," E. C. Lim, editor, 1969, p 167.
(23) J. Eisenbrand and M. Raisch, *Z. Anal. Chem.*, **179**, 406 (1961).
(24) G. Stein and M. Tomkiewicz, *Trans. Faraday Soc.*, **67**, 1009 (1971).
(25) T. G. Beaumont and K. M. C. Davis, *J. Chem. Soc. B*, 456 (1970).
(26) J. Eisenbrand and M. Raisch *Nahrung*, **6**, 157 (1962).
(27) J. Feitelson and N. Shaklay, *J. Phys. Chem.*, **71**, 2582 (1967).
(28) D. Rehm and A. Weller, *Isr. J. Chem.*, **8**, 259 (1970).
(29) V. M. Berdnikov and N. M. Bazhin, *Russ. J. Phys. Chem.*, **44**, 395 (1970).
(30) B. G. Cox, G. R. Hedwig, A. J. Parker, and D. W. Watts, *Aust. J. Chem.*, **27**, 477 (1974).
(31) K. Schwabe, "Polarographie und Chemische Konstitution Organischer Verbindungen," Akademie Verlag, Berlin, 1957.
(32) S. P. McGlynn, T. Azumi, and M. Kinoshita, "Molecular Spectroscopy of the Triplet State," Prentice Hall, Englewood Cliffs, N.J. 1969, Chapter 5.
(33) G. G. Giachino and D. R. Kearns, *J. Chem. Phys.*, **52**, 2964 (1970).
(34) K. C. Lin and S. H. Lin, *Mol. Phys.*, **21**, 1105 (1971).

Mechanism of Direct and Rubrene Enhanced Chemiluminescence during α-Peroxylactone Decarboxylation

Waldemar Adam,[1] George A. Simpson,* and Faris Yany

Department of Chemistry and Puerto Rico Nuclear Center,[2] University of Puerto Rico, Rio Piedras, Puerto Rico 00931
(Received February 14, 1974; Revised Manuscript Received August 16, 1974)

Direct chemiluminescence measurements during the decarboxylation of the *tert*-butyl and dimethyl α-peroxylactones (**2a** and **2b**) in benzene and carbon tetrachloride afforded singlet yields (α) of 4.7×10^{-4} for both excited *tert*-butylcarboxaldehyde and acetone, respectively. The required fluorescence quantum yields (φ_F) were determined to be 0.91×10^{-3} for *tert*-butylcarboxaldehyde and 1.2×10^{-3} for acetone. The triplet yields (β) were estimated to be 1.5×10^{-1} for *tert*-butylcarboxaldehyde and 5.3×10^{-2} for acetone by means of rubrene-enhanced chemiluminescence measurements. From this data the ratio in efficiencies of triplet and singlet excited state production (β/α) was calculated as 320 ± 55 for the *tert*-butyl and 115 ± 25 for the dimethyl systems, indicating a great preference for the formation of triplet excited carbonyl products in the α-peroxylactone decarboxylation. On the basis of a kinetic analysis of the chemiluminescence intensities (I) and decay times (τ) as a function of α-peroxylactone and rubrene concentration, quenching experiments, and the oxygen effect, a mechanism is proposed in which rubrene functions as an enhancer by way of triplet–triplet annihilation.

A recent conference on chemi- and bioluminescence[3] stresses the tremendous surge of activity in this exciting field. Of particular interest has been the discovery that four-membered ring cyclic peroxides, namely, the 1,2-dioxetanes **1**,[4a] 1,2-dioxetanones or α-peroxylactones **2**,[4b] and the carbon dioxide dimer 1,2-dioxetane-3,4-dione **3**,[4c] thermally decay with tremendously increased light emission in the presence of efficient fluorescers such as polyaromatics.
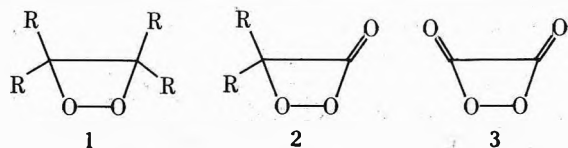
Our understanding of the chemelectronic processes associated with these compounds has been greatly influenced by the pioneering study of Wilson and Schaap.[5] Their chemiluminescence studies of 3,4-diethoxy-1,2-dioxetane (**1a**), utilizing the triplet counting techniques of Vassil'ev,[6] demonstrated efficient excited state production. This understanding has been furthered by the work of Turro's group[7] on tetramethyl-1,2-dioxetane (**1b**), which on thermolysis yields preferentially and efficiently triplet acetone. We anticipate, however, that preferential triplet production may not always be the consequence of thermolysis of these compounds. The work of Darling and Foote,[8] on 3,4-dimethyl-3,4-di-*n*-butyl-1,2-dioxetane (**1c**) showed similar singlet and triplet state production efficiencies. Thus, concern for distinguishing the effects of singlet and triplet states must be maintained.

Our interest in the chemiluminescence of α-peroxylactones (**2**) results from their successful isolation[4b] and the observation of their role as excited state precursors in Luciferin bioluminescence.[9] As a result of this interest, this report is presented to describe the chemiluminescence of two compounds of this class, the *tert*-butyl (**2a**) and dimethyl α-peroxylactones (**2b**). Previous qualitative observations[10] of large enhancement of chemiluminescence from α-peroxylactone in the presence of rubrene have prompted the investigation of the rubrene-enhanced chemiluminescence[11] associated with α-peroxylactone decomposition in order to determine the enhancement mechanism. In addition to possible enhancement *via* singlet energy transfer to rubrene followed by its efficient fluorescence, rubrene may emit *via* triplet–triplet annihilation[12] or triplet–triplet fluorescence,[13] rather than spin–orbit coupling,[6] if triplet energy transfer to rubrene occurs.

Experimental Section

Materials. The *tert*-butyl and dimethyl α-peroxylactones, respectively prepared by Drs. J.-C. Liu and H.-C. Steinmetzer of this laboratory according to reported procedures,[4b] were used as carbon tetrachloride stock solutions. The concentrations of these stock solutions, usually $0.01 \, M$ in α-peroxylactone, were determined by iodometric titration within an error of *ca.* 5%. For the measurements of the chemiluminescence emissions the stock solutions, stored on Dry Ice to minimize decomposition, were diluted to the desired concentration in the appropriate solvent, adjusting the final volume to 3 ml.

The solvents acetone and isomeric hexanes (Eastman spectrograde), dichloromethane, *tert*-butyl alcohol, ethylene glycol (EG) (all Eastman reagent grade), carbon tetrachloride (Baker spectroquality), acetonitrile (Matheson Coleman and Bell reagent grade), and toluene (Packard scintillation grade) were used without further purification. Benzene (gift sample from the Commonwealth Oil Refining Co.) and tetrahydrofuran (THF, Baker reagent grade) were freshly distilled from the benzophenone ketyl radical prior to use, while dimethyl sulfoxide (DMSO) from Fisher Scientific was distilled at reduced pressure from calcium hydride.

The fluorescers 9,10-diphenylanthracene and quinine sulfate dihydrate (Aldrich Chemicals), rubrene (Eastman Organic), 2,5-diphenyloxazole or PPO, and 1,4-bis[2-(5-

TABLE I: Comparative Light Intensities and Decay Times (τ) of the Direct and Enhanced Chemiluminescence of α-Peroxylactones[a]

Peroxide	Solvent	Enhancer	Rel int[b]	τ, min
1. *t*-Bu	CCl₄	None	1.0	15 ± 2
2. Me₂	CCl₄	None	1.2	24 ± 3
3. Me₂	C₆H₆	None	3.4	14 ± 2
4. *t*-Bu	C₆H₆	None	3.4	11 ± 1
5. *t*-Bu	C₆H₆	DPA[c]	560	13 ± 1
6. Me₂	C₆H₆	Rubrene	25000	10
7. *t*-Bu	C₆H₆	Rubrene	18000	13

[a] In the presence of air. [b] Based on $I_0/[P_0]$ values for peroxylactone concentration of the order 10^{-4} M and with enhancer concentration = $1.3 \pm 0.4 \times 10^{-3}$ M. [c] 9,10-Diphenylanthracene.

Figure 2. Dependence of direct initial chemiluminescence intensities (I_0) on initial α-peroxylactone concentration [P_0] of the *tert*-butyl (O) and dimethyl α-peroxylactones (□) in benzene. The center scale (in minutes) shows constant decay times of the intensity for *tert*-butyl α-peroxylactones (●) in benzene and for dimethyl α-peroxylactones in benzene (■) and in carbon tetrachloride (▲). The solid diagonal indicates unit slope.

Figure 1. Time dependence of intensity ($I/[P_0]$) decay of the rubrene-enhanced chemiluminescence of the *tert*-butyl α-peroxylactone in benzene (●) at [P_0] = 7.3 × 10⁻⁵ M, [R] = 5.0 × 10⁻⁴ M, and τ = 9.1 min; of dimethyl α-peroxylactone in benzene (■) at [P_0] = 1.2 × 10⁻³ M, [R] = 1.3 × 10⁻⁴ M, and τ = 20 min; of the direct chemiluminescence of *tert*-butyl α-peroxylactone in benzene (O) at [P_0] = 1.5 × 10⁻³ M and τ = 10.1 min; and of dimethyl α-peroxylactone in benzene (□) at [P_0] = 1.3 × 10⁻³ M and τ = 15 min and in carbon tetrachloride (▲) at [P_0] = 1.3 × 10⁻³ M and τ = 24 min, all in the presence of air.

Figure 3. Dependence of rubrene-enhanced initial chemiluminescence intensities (O) and decay times (center scale, in minutes) of the intensity (●) on the *tert*-butyl α-peroxylactone, [P_0], at [R] = 5.1 × 10⁻² M. The solid diagonal indicates unit slope.

phenyloxazolyl)]benzene or POPOP (both Packard scintillation grade) were used without further purification. The triplet quencher[14] tetramethyl-1,2-diazetidine 1,2-dioxide was kindly supplied by Dr. E. F. Ullman (Syva Research). *n*-Hexadecane-*1-C-14* was obtained from the Radiochemical Center (Amersham) and *tert*-butylcarboxaldehyde (Columbia Organic) was purified by preparative gas chromatography, followed by bulb-to-bulb distillation at reduced pressure. Luminol (Eastman Organic) was recrystallized prior to use from dilute hydrochloric acid.

Apparatus. Total chemiluminescence intensities were measured with a Mitchell–Hastings photometer,[15] using a Perkin-Elmer Model 165 recorder to register the output signal. The photometer consists of a sample and photomultiplier housing, previously described by Hastings and Weber,[16] which accommodates Packard scintillation vials containing 3-ml solutions of the reaction mixture, held in close proximity to a RCA-931A photomultiplier. Power to the photomultiplier dynode chain and amplification of the photomultiplier signal are achieved by the circuit described by Mitchell and Hastings.[15]

Emission spectra and fluorescence quantum yields were

TABLE II: Initial Light Intensities (I_0) and Decay Times (τ) of Direct Chemiluminescence of α-Peroxylactones

Peroxide	$10^4[P_0]$, M	Solvent	Atmosphere	$10^{12}I_0$, einstein/ l. min	$10^8(I_0/[P_0])$, einstein/ mol min	τ, min
1. t-Bu	0.2–100	C_6H_6	Air	0.7–560	4.0 ± 0.7	11 ± 1
2. t-Bu	0.73	C_6H_6	Oxygen	2.48	3.48	11
3. t-Bu	0.73	C_6H_6	Argon	2.48	3.48	12
4. t-Bu	0.73	CCl_4	Air	0.86	1.2	15 ± 2
5. t-Bu	0.73	CH_2Cl_2	Air	0.89	1.2	15
6. t-Bu	0.73	EG^a	Air	1.58	2.1	5 ± 0.4
7. t-Bu	0.73	THF^b	Air	0.92	1.3	5
8. Me_2	13	C_6H_6	Air	49	4.0	15
9. Me_2	13	C_6H_6	Argon	46	3.6	13
10. Me_2	2–33	CCl_4	Air	3.3–46	1.5 ± 0.2	24 ± 2
11. Me_2	15	CCl_4	Oxygen	11	0.73	27
12. Me_2	15	CCl_4	Argon	12	0.82	28

^{a} Ethylene glycol. ^{b} Tetrahydrofuran.

TABLE III: Initial Light Intensities (I_0) and Decay Times (τ) of Rubrene-Enhanced Chemiluminescence of $tert$-Butyl α-Peroxylactone in Benzene and an Air Atmosphere

	$10^4[P_0]$, M	$10^4[R]$, M	$10^3[Q]$, M	$10^{10}I_0$, einstein/ l. min	$10^6(I_0/[P_0])$, einstein/ mol min	τ, min
1.	0.73	0.0042		0.082	0.11	12.3
2.	0.73	0.025		0.82	1.1	9.6
3.	0.73	0.60		9.9	14	9.7
4.	0.73	1.0		14 (12)^c	19 (17)^c	10.0 (10.5)
5.	0.73	3.0		34.3	47	9.8
6.	0.73	5.0		55.0	76	10.1
7.	0.73	7.0		60.6	83	12.5
8.	0.73	10		77.0	110	8.8
9.	0.73	15		143	200	4.8
10.	0.73	46		210	290	3.8
11.	0.73	83		264	360	1.7
12.	0.73	510		660	900	0.4
13.	4.5	3.8		242	51	12
14.	4.3	9.0		511	120	13
15.	4.3	17		937	220	13
16.	4.7	39		1,930	410	11
17.	0.53	510		393	740	0.40
18.	1.0	510		1,150	1200	0.55
19.	2.0	510		2,100	1000	0.60
20.	4.3	510		2,760	640	0.70
21.	10	510		14,400	1400	1.4
22.	4.4	3.7	0.0^a	2,310	52	11
23.	4.4	3.7	0.9^a	135	30	14
24.	4.4	3.7	1.8^a	105	24	13
25.	4.4	3.7	5.4^a	103	23	11
26.	0.73	1.0	100^b	14	19	11
27.	0.73	3.0	100^b	37.0	46	9.8
28.	0.73	7.0	100^b	60.6	83	12.5

^{a} Tetramethyl-1,2-diazetidine 1,2-dioxide. ^{b} Piperylene. ^{c} Values in parentheses are in an argon atmosphere.

determined on a Perkin-Elmer Model MPF-3 spectrofluorimeter.

Measurements. 1. Chemiluminescence Intensities. The direct and enhanced chemiluminescence emission signals of the α-peroxylactone solutions were measured directly after injection into the sample compartment of the Mitchell–Hastings photometer kept at 23 ± 2°, monitoring the emission decays on the recorder continuously. The observed signals were converted into intensity units on multiplication by a calibration factor (C_F) and plotted semilogarithmically against time. From these first-order intensity *vs.* time plots the initial intensities (I_0) and decay lifetimes (τ) were determined. The data are summarized in Tables I–IV and plotted in Figures 1–4. The reproducibility of these results

were within ±15% for the I_0 values and within ±10% for the τ values.

The calibration factor C_F was determined from the ratio of calculated intensity per unit volume from standard emitting solutions to the measured signal of those solutions within the apparatus. The primary standard was a scintillation "cocktail" consisting of PPO, POPOP, and radioactive n-hexadecane in toluene solutions in concentrations suggested by Hastings and Weber.[15] A secondary standard utilized the chemiluminescence exhibited by luminol in potassium $tert$-butoxide-catalyzed, air-saturated DMSO solutions, as described by Lee and Seliger.[17] The POPOP standards gave a calibration factor $C_F = 5.1 \pm 0.2 \times 10^9$ $h\nu$/V ml sec,[18] while the luminol standards gave $C_F = 2.4 \pm$

TABLE IV: Initial Light Intensities (I_0) and Decay Times (τ) of Rubrene-Enhanced Chemiluminescence of Dimethyl α-Peroxylactone in Benzene

10^4[P$_0$], M	10^4[R], M	Atmosphere[a]	$10^{10}I_0$, einstein/ l. min	$10^6(I_0/$ [P$_0$]), einstein/ mol min	τ, min
1. 12	1.3	Air	35.6	3.0	18
2. 24	1.3	Air	76	3.2	20
3. 6	2.6	Air	376	63	11
4. 6	10	Air	1780	300	10
5. 6	29	Air	2380	400	8.3
6. 4	1.3	Helium	5.9	1.5	4.8
7. 12	1.3	Helium	18	1.7	6.7
8. 24	1.3	Helium	53.8	2.2	15
9. 3.6	2.4	Helium	33.4	9.3	9.1
10. 15	85	Helium	1280	86	1.8
11. 15	510	Helium	5940	400	0.2

[a] Flushed vigorously with the appropriate gas.
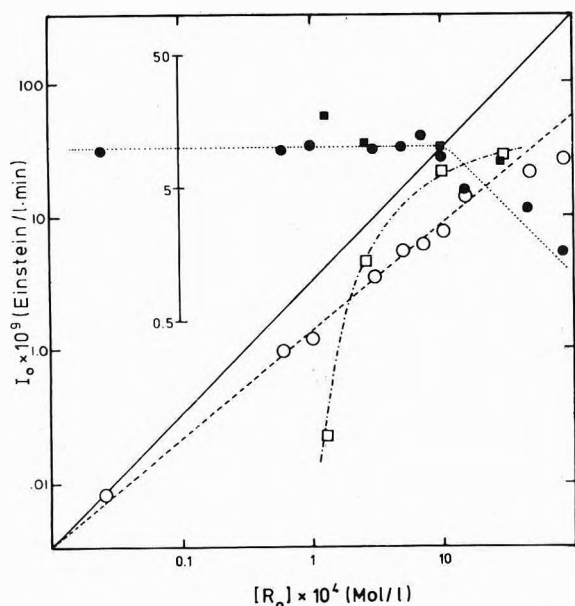
Figure 4. Dependence of rubrene-enhanced initial chemiluminescence intensities (I_0) on initial rubrene concentration [R] of the *tert*-butyl (O) and dimethyl α-peroxylactone (□) in benzene at [P$_0$] = 7.3 × 10^{-5} M. The center scale (in minutes) shows dependence of decay times of the intensity on initial rubrene concentration for the *tert*-butyl (●) and dimethyl α-peroxylactone (■) in benzene. The solid diagonal indicates unit slope.

$0.8 \times 10^9\ h\nu/V$ ml sec. The differences in the two calibration factors lies in part with the relative response of the photomultiplier (to be discussed shortly), and to a larger degree with the difficulty in reproducing the luminol results. In view of these complications we decided to standardize our intensity data in Tables I–IV exclusively against the POPOP calibration factor. However, the luminol calibration factor, corrected for photomultiplier response, is 65% of the POPOP value.

2. Relative Spectral Response. Due to differences in the emission spectra of the fluorescers and the variable wavelength response of the photomultiplier, different signals will result from equal emission intensities of the compounds. To compensate for this relative response factors (RRF) were determined for the emissions according to the method of Hastings and Weber[15] using the formula

$$RRF = \int_{\lambda_i}^{\lambda_f} S_\lambda I_\lambda\ d\lambda \Big/ \int_{\lambda_i}^{\lambda_f} I_\lambda\ d\lambda$$

where λ_i and λ_f are initial and final wavelengths corresponding to onset and fall off of the fluorescence intensity, S_λ is the normalized response of the RCA-931A photomultiplier per unit wavelength interval and per photon, provided by RCA data,[19] and I_λ is the corrected emission intensity per unit wavelength interval, normalized to unity maximum intensity according to literature data.

Thus, for POPOP the corrected spectral data of Berlman[20] was utilized and the RRF was normalized to unity since POPOP was used as standard. For acetone and *tert*-butylcarboxaldehyde, the respective decarboxylation products of dimethyl and the *tert*-butyl α-peroxylactones, measurements reported here indicate that their corrected emission spectra are similar to that of POPOP. The fluorescence maxima are at 413 ± 10, 416, and 420 ± 10 nm respectively for acetone, POPOP,[20] and *tert*-butylcarboxaldehyde. The value of the relative response factor (RRF) measured for *tert*-butylcarboxaldehyde from our data was 0.93 and the value of 1.02 was used for acetone. For luminol, with maximum chemiluminescence at 484 nm in DMSO, RRF = 0.74 relative to POPOP was calculated, using the spectral data of Lee and Seliger.[17] For rubrene the correction was most serious since its fluorescence maximum occurs at 605 nm. Employing the spectral data of Strickler and Berg,[21] a RRF = 0.22 relative to POPOP was determined. Thus, in the calculation of the rubrene-enhanced chemiluminescence quantum yields (Φ_{EC}) a correction factor of C_{RRF} = 4.5 was used to account for the relative response of the photomultiplier to POPOP standard and rubrene emissions.

3. Reabsorption by Rubrene. The spectral data of rubrene[21] show appreciable overlap between the absorption and fluorescence emission bands. Thus, at the high rubrene concentrations, *i.e.*, [R] $\geq 10^{-3}$ M, reabsorption by rubrene was expected to be a problem requiring correction. To test the importance of this effect, we assessed the dependence of the initial intensities I_0 per unit volume against the volume of fixed concentrations of peroxylactone and rubrene solution. The results are summarized in terms of the semilogarithmic expression

$$\log{(I_0/V)} - \log{(1.5 \pm 0.1)} = -0.10 \pm 0.02\ (Mi)^{-1}V$$

for [R] = 5.1 × 10^{-2} M, I_0 in arbitrary units, and where V is the volume of reaction mixture expressed in milliliters. Thus, a 3-ml sample of α-peroxylactone solution containing [R] = 5.1 × 10^{-2} M leads to ca. 50 ± 3% reduction in the emission signal due to rubrene reabsorption. For this reason it was necessary to apply a reabsorption correction factor of C_R = 2.0 at the maximum rubrene concentrations (5.1 × 10^{-2} M), at which the rubrene-enhanced chemiluminescence quantum yields (Φ_{EC}) were determined. Consequently, the corrected rubrene-enhanced emission intensity (I_{corr}^R) is given by the formula

$$I_{corr}^R = I_{max}^R C_{RRF} C_R$$

in which the maximum possible emission intensity (I_{max}^R) is corrected for relative spectral response (C_{RRF}) of the photomultiplier toward rubrene *vs.* POPOP standard fluorescence and for reabsorption (C_R) by rubrene. From these corrected intensity values the enhanced chemiluminescence quantum yields in Table VII were calculated.

4. Fluorescence Quantum Yields. The fluorescence

TABLE V: Fluorescence Spectral Data of Quinine Sulfate, Acetone, and *tert*-Butylcarboxaldehyde

Compd	Excitation wavelength, nm	Excitation slitwidth, nm	Emission slitwidth, nm	Concn, $M \times 10^3$	Solvent	B^a	I^b	N
Quinine	280	4	2	0.054	1.0 N H₂SO₄	0.19	15	1.333
sulfate	280	4	2	0.109	1.0 N H₂SO₄	0.31	28	1.333
	280	4	2	0.272	1.0 N H₂SO₄	0.63	53	1.333
	290	5	20	0.000996	1.0 N H₂SO₄	0.008	9.8	1.333
	290	5	20	0.00398	1.0 N H₂SO₄	0.028	10.7	1.333
	290	5	20	0.00797	1.0 N H₂SO₄	0.057	19.7	1.333
	290	5	20	0.00996	1.0 N H₂SO₄	0.071	26.7	1.333
	335	4	2	0.054	1.0 N H₂SO₄	0.62	120	1.333
Acetone	280	4	2	17	Hexanes^c	0.34	0.074	1.375
	280	4	2	34	Hexanes^c	0.54	0.12	1.375
	280	4	2	64	Hexanes^c	0.78	0.14	1.375
	280	4	2	34	CCl₄	0.64	0.081	1.460
	335	4	2	13,600	Acetone	0.35	0.17	1.359
tert-Butyl-	290	5	20	7.21	Hexanes^c	0.323	0.189	1.375
carbox-	290	5	20	8.24	Hexanes^c	0.390	0.171	1.375
aldehyde	290	5	20	9.27	Hexanes^c	0.451	0.261	1.375
	290	5	20	10.3	Hexanes^c	0.386	0.193	1.375
	290	5	20	20.6	Hexanes^c	0.550	0.280	1.375
	290	5	20	30.9	Hexanes^c	0.750	0.377	1.375

^{a} Average absorptions over excitation band. ^{b} Integrated corrected fluorescence intensities in arbitrary units. ^{c} Isomeric mixture.

TABLE VI: Fluorescence Quantum Yields of Acetone

Substance	Excitation wavelength, nm	Solvent	$10^3 \phi_F$	Ref
Acetone	280	Hexanes^a	1.2 ± 0.2	This work
Acetone	280	Cyclohexane	0.93	b
Acetone	313	n-Hexane	10	c
Acetone	280	CCl₄	0.66	This work
Acetone	335	Acetone	1.3	This work
Acetone	313	Vapor	0.61, 1.2	d, b
tert-Butyl-carbox-aldehyde	290	Hexanes^a	0.91 ± 0.06	This work

^{a} Mixture of isomers. ^{b} Reference 27. ^{c} R. F. Borkman and D. R. Kearns, *J. Chem. Phys.*, **44**, 945 (1966). ^{d} S. J. Collier, D. H. Slater, and J. G. Calvert, *Photochem. Photobiol.*, **7**, 735 (1968).

yields (φ_F) required to calculate the efficiency of excited state production were determined according to procedures discussed by Demas and Crosby.[22] In this treatment the fluorescence efficiency of the unknown ($\varphi_F{}^X$) is given in terms of the fluorescence efficiency ($\varphi_F{}^S$) of the standard by the formula

$$\varphi_F{}^X = \varphi_F{}^S \frac{B_X I_X N_S{}^2}{B_S I_S N_X{}^2}$$

where B_X and B_S are the respective average fractions of light absorbed over the excitation band, I_X and I_S are the respective integrated fluorescence intensities, and N_X and N_S are the respective refractive indices at the excitation wavelength. The $\varphi_F{}^S = 0.55$ value was taken for the quinine sulfate standard in 1 N aqueous sulfuric acid.[23]

The quantities B_X and B_S were determined from the measured absorbances $A_\lambda{}^X$ and $A_\lambda{}^S$ and the relative intensity of the excitation band E_λ, using the relationship

$$B_S = \int_{\lambda_i}^{\lambda_f} E_\lambda(1 - 10^{-A_\lambda{}^X}) \, d\lambda \Big/ \int_{\lambda_i}^{\lambda_f} E_i \, d\lambda$$

where the integration extends over the excitation bandwidth (width at half-height was ca. 4 nm in these experiments) and was performed graphically. The results are summarized in Table V. The spectral data of the excitation band were measured by placing a reflector into the sample compartment of MPF-3A instrument and determining the apparent emission spectra at a narrow band pass.

The quantities I_X and I_S were obtained from the equation

$$I_S = \int_{\lambda_i}^{\lambda_f} k_\lambda I_{\lambda S} \, d\lambda$$

where k_λ is an instrumental correction factor, determined by comparison of the corrected spectrum (for quinine sulfate in 1 N H₂SO₄ the data of Berlman[20] were used) with the observed one. The same correction factors as for the quinine sulfate standard were also used for the unknown. In the case of acetone and *tert*-butylcarboxaldehyde corrected emission spectra that were obtained were broad and structureless with maximum emission at 413 ± 10 and 420 ± 10 nm, respectively. The graphically integrated I_X and I_S values are reported in Table V, employing several concentrations, excitation wavelengths, and solvents. Plots of the I vs. B values at the 280-nm excitation of the standard and acetone and at the 290-nm excitation for *tert*-butylcarboxaldehyde gave straight lines with ca. 10% scatter in the data points. These slopes were used in the calculation of the fluorescence efficiencies. The refractive indices listed in Table V are at the sodium doublet line and were taken from the literature.[24] On the basis of the experimental data in Table V, the fluorescence quantum yields in Table VI were computed, which in turn were employed to determine the efficiency of excited state production in Table VII.

Discussion of the Results

From the experimental information, which is summarized in Tables I–VII and illustrated in Figures 1–4, on the kinetics of chemiluminescence accompanying the decarboxylation of α-peroxylactones, we wish now to project their most salient features and attempt to amalgamate

TABLE VII: Direct and Rubrene-Enhanced Chemiluminescence Quantum Yields (Φ), Singlet (α) and Triplet (β) Yields, and Triplet–Singlet Ratio (β/α) in the Decarboxylation of α-Peroxylactones

Peroxide	Solvent	$\phi,$[a,b] einstein/mol	α	β[c]	β/α
1. t-Bu	C_6H_6	4.6×10^{-7}	4.7×10^{-4}		
2. t-Bu	CCl_4	2.3×10^{-7}			
3. t-Bu	C_6H_6	7.2×10^{-2}		1.5×10^{-1}	320 ± 55
4. Me_2	C_6H_6	5.5×10^{-7}	4.6×10^{-4}		
5. Me_2	CCl_4	3.2×10^{-7}	4.8×10^{-4}		
6. Me_2	C_6H_6	2.7×10^{-2}		5.3×10^{-2}	115 ± 25

[a] Values are within 30%. [b] Entries 3 and 6 are rubrene enhanced, otherwise direct chemiluminescence. [c] The fluorescence yield of rubrene was taken as $\Phi_F{}^R = 1.0$.

them into a mechanism consistent with these data. Figure 1 exhibits the clean first-order decay of the emission intensities of the direct and rubrene-enhanced chemiluminescence of the *tert*-butyl and dimethyl α-peroxylactones over two orders of magnitude in the intensities I and several half-lives. Since these measurements were made at different initial α-peroxylactone concentrations $[P_0]$, it was necessary to plot $I/[P_0]$, in order to correct for the dependence of the initial intensity I_0 on $[P_0]$, enabling better comparison of the results.

Several important features become immediately apparent in Figure 1. The intercepts of the emission decay lines with the ordinate at t_0, which represent the I_0 values, reflect the efficiencies of light production, while the slopes exhibit the time dependence of the intensities or decay times of each system. The comparative results are collected in Table I. The most dramatic fact is that the chemiluminescence is significantly enhanced in the presence of efficient fluorescers such as rubrene and 9,10-diphenylanthracene. For example, in the case of the *tert*-butyl system in benzene with air the emissions are intensified about two order of magnitude (entry 5, Table I) by 9,10-diphenylanthracene and about four orders of magnitude (entry 7, Table I) by rubrene (R), compared to its direct chemiluminescence (entry 4, Table I). Similar enhancements of the direct chemiluminescence by rubrene are observed for the dimethyl system (entries 3 and 6, Table I).

In this connection it is important to point out that in the enhanced chemiluminescence the weak emissions at 400–430 nm of the excited product molecules are completely replaced by the fluorescence emissions of the enhancer, as evidenced by the recorded spectra.[25] Yet, the decay times of the emissions are not changed by the enhancer (entries 4, 5, and 7, Table I), indicating that the enhanced light intensities are not a result of an alteration in the rate of α-peroxylactone decomposition caused by the enhancer. This was independently checked by following the consumption of α-peroxylactone in the infrared, giving the same decay times within experimental error for the α-peroxylactones and the emission decay times.[25]

In Table II are collected the quantitative data of the direct chemiluminescence of both α-peroxylactones. Neither the initial intensities I_0 nor the decay times of the emissions are consistantly affected by the presence or absence of oxygen for the *tert*-butyl (entries 1–3, Table II) and for the dimethyl (entries 8 and 9, Table II) system both in benzene. Thus, the lack of intervention by oxygen indicates it to be an inefficient quencher in the direct chemiluminescence of α-peroxylactones.

A solvent effect, both on the initial intensities and decay times, is clearly discernible for the α-peroxylactones, except that the data are more abundant for the *tert*-butyl

case. Thus, as already evidenced in Figure 1 and Table I, compared to benzene carbon tetrachloride reduces the initial intensities of the *tert*-butyl (entries 1 and 4, Table II) and dimethyl (entries 8 and 12, Table II) systems, but the decay times are increased. The same behavior is portrayed by the *tert*-butyl α-peroxylactone in methylene chloride (entries 1 and 5, Table II); however, in ethylene glycol and tetrahydrofuran (entries 1, 6, and 7, Table II) the τ as well as the values of the emissions are both significantly reduced. In other words, the lower initial intensities in these solvents confirm a much faster α-peroxylactone consumption. This observation is supported for tetrahydrofuran in the infrared.[25] This solvent effect is most dramatically exhibited by acetonitrile, in which the α-peroxylactones are too short-lived to even obtain an infrared or luminescence measurement. Yet the reduction of the initial intensities of the α-peroxylactones in the halogenated solvents must have clearly a different origin since the decay times of the emissions are increased appreciably, indicating slower α-peroxylactone disappearance.

A significant kinetic result exhibited by the direct chemiluminescence data in Table II is the first-order dependence of the I_0 values over almost four orders of magnitude in $[P_0]$. As demonstrated in Figure 2, the slope $d \ln I_0/d \ln [P_0]$ is unity for the *tert*-butyl system (entry 1, Table II). Also the few data points for the dimethyl system (entry 8, Table II) fit in well. In Figure 2 we also illustrate the constancy of the decay times with respect to $[P_0]$, showing that within experimental error the slope $d \ln \tau/d \ln [P_0]$ is zero in the direct chemiluminescence.

The quantitative kinetic data for the rubrene-enhanced chemiluminescence of the *tert*-butyl system in benzene are given in Table III. As shown in Figure 3 (entries 17–21, Table III), at constant rubrene concentration the initial intensities of the enhanced chemiluminescence show first-order dependence on initial α-peroxylactone concentration. Although the error in the data points is appreciable, they scatter about the unit slope line, i.e., $(\partial \ln I_0/\partial \ln [P_0])_{R_0} = 1$. The respective decay times also increase with increasing $[P_0]$ since the slope $(\partial \ln \tau/\partial \ln [P_0])_{R_0}$ is positive and linear, but not first order.

The bulk of the data of Table III (entries 1–12) is plotted in Figure 4, which reveals that the logarithmic dependence of I_0 of the enhanced chemiluminescence of the *tert*-butyl system in benzene with air on the initial rubrene concentration $[R_0]$ at constant initial α-peroxylactone concentration $[P_0]$ is linear (dashed line), i.e., the slope $(\partial \ln I_0/\partial \ln [R_0])_{P_0} = 0.83$, but not first order (solid line) over four orders of magnitude in $[R_0]$. At high rubrene concentration, e.g., $[R_0] \geq 10^{-3}\ M$, the initial intensities begin to drop off from the 0.83 line due to reabsorption by rubrene (cf. Experimental Section). Unfortunately, we could not operate

at $[R_0]$ values above $5 \times 10^{-2} \, M$ because this concentration represents the maximum solubility of rubrene in benzene. Thus, saturation of energy transfer to rubrene could not be achieved for the *tert*-butyl system.

The dependence of the decay times of the enhanced emissions for the *tert*-butyl system is shown by the dotted line in Figure 4. Over three orders of magnitude in $[R_0]$ up to $10^{-3} \, M$ the values are independent of $[R_0]$, *i.e.*, the slope $(\partial \ln \tau / \partial \ln [R_0])_{P_0}$ is zero; but at $[R_0] \geq 10^{-3} \, M$ the decay times fall off inversely, *i.e.*, the slope is -1.0, with increasing $[R_0]$ at constant $[P_0]$ (entries 6–12, Table III). However, when the initial α-peroxylactone concentration is increased at these high rubrene concentrations, then the τ values (entries 13–16, Table III) recover the initially constant values at low $[R_0]$.

Furthermore, it is important to stress that molecular oxygen does not quench the enhanced chemiluminescence of the *tert*-butyl system (entry 4, Table III). Even $0.1 \, M$ piperylene, a popular triplet quencher,[26] was entirely ineffective in quenching the rubrene-enhanced chemiluminescence of the *tert*-butyl α-peroxylactone (entries 26–28, Table III). However, the very efficient triplet quencher tetramethyl-1,2-diazetidine 1,2-dioxide[14] was effectively quenching the enhanced emissions of the *tert*-butyl system without, however, altering the decay times (entries 22–24, Table III). As these data show, the triplet energy transfer to $3.7 \times 10^{-4} \, M$ rubrene is essentially completely intercepted by $5.4 \times 10^{-3} \, M$ tetramethyl-1,2-diazetidine 1,2-dioxide since the I_0 values were observed to be reduced to a constant, limiting value which was 60% of that found in the absence of the quencher. The residual emission intensity must be due to singlet energy transfer to rubrene. It is, therefore, not surprising that the quenching by tetramethyl-1,2-diazetidine 1,2-dioxide does not follow Stern–Volmer kinetics.

Data on the rubrene-enhanced chemiluminescence of the dimethyl system in benzene are collected in Table IV, and part of it (entries 1–15, Table IV) are also plotted in Figure 4 to illustrate its contrasting behavior to the *tert*-butyl case. First of all, as revealed by the dash–dotted curve, the logarithmic dependence of the initial intensities with initial rubrene concentrations is complex. The slope $(\partial \ln I_0 / \partial \ln [R_0])_{P_0}$ varies continually, starting from a value larger than two at low $[R_0]$ and leveling off to zero at high $[R_0]$ due to saturation of energy transfer. This complex behavior is distinct from the *tert*-butyl system which followed a constant slope of 0.83. Still more astounding is the effect of excluding oxygen (entries 6–11, Table IV). While the *tert*-butyl system showed no oxygen effect in its rubrene-enhanced chemiluminescence (entry 4, Table III), the dimethyl system shows in the absence of oxygen complex kinetics, much smaller decay times, and the initial intensities drop significantly. In fact, the initial rubrene concentration in the absence of oxygen must be increased *ca.* 20-fold over that in the presence of oxygen in order to achieve saturation in energy transfer to rubrene (entries 5 and 11, Table IV).

Other trends revealed by our data for the rubrene-enhanced emissions of the dimethyl system, which are consistant with the *tert*-butyl system, are that the I_0 and τ values increase with increasing $[P_0]$ at constant $[R_0]$ (entries 6–8, Table IV), *i.e.*, the slopes $(\partial \ln I_0 / \partial \ln [P_0])_{R_0}$ and $(\partial \ln \tau / \partial \ln [P_0])_{R_0}$ are positive. However, the decay times decrease with increasing $[R_0]$ at constant $[P_0]$ (entries 9–11, Table IV), *i.e.*, the slope $(\partial \ln \tau / \partial \ln [R_0])_{P_0}$ is negative.

Let us now extract the chemiluminescence quantum yields of the direct and enhanced emissions accompanying the decarboxylation of α-peroxylactones from the above experimental data. We saw that the rate of α-peroxylactone consumption followed the first-order rate law $[P_t] = [P_0] \exp(-t/\tau)$. Since the decay of the emission intensities I_A, defined as the rate of photon production $\mathrm{d}(h\nu)/\mathrm{d}t$, is proportional to the rate of α-peroxylactone consumption $-\mathrm{d}[P]/\mathrm{d}t$, we can express I_A in terms of measurable experimental parameters. The emission intensity is expressed as the product of the fraction of excited singlet molecules generated (α), their fluorescence quantum yield ($\varphi_F{}^A$) and the α-peroxylactone concentration per unit decay time in eq 1.

$$I_A = \mathrm{d}(h\nu)/\mathrm{d}t = \alpha \varphi_F{}^A [P]/\tau_1 \qquad (1)$$

Here we imply that in the direct chemiluminescence the fraction of excited triplet products (β) generated do not contribute to the emission intensity. The direct chemiluminescence quantum yield (Φ_{DC}), given by the product of α and $\varphi_F{}^A$, is then experimentally defined by the total number of photons produced per α-peroxylactone molecule decomposed. Thus, integration of I_A over time per initial α-peroxylactone concentration allows the computation of Φ_{DC} (eq 2) in terms of the experimental parameters I_0, τ,

$$\Phi_{DC} = \alpha \varphi_F{}^A = \int_0^\infty I_A \, \mathrm{d}t / [P_0] = I_0 \tau_1 / [P_0] \qquad (2)$$

and $[P_0]$. Thus, the Φ_{DC} value allows the computation of the α value if the fluorescence efficiency associated with the excited singlet product is known. The above empirical equations can be derived in terms of a proposed kinetic scheme and is presented in an available appendix (see paragraph at end of text regarding supplementary material).

For this purpose we have measured (*cf.* Experimental Section for details) the fluorescence quantum yield of acetone and *tert*-butylcarboxaldehyde, the respective products obtained on decarboxylation. The data are summarized in Tables V and VI. While no fluorescence quantum yields appear to be reported for *tert*-butylcarboxaldehyde, our φ_F value for acetone in hexanes (entry 1, Table V) checks well with the literature value of Halpern and Ware[27] (entry 2, Table V). In pure acetone (entry 5, Table V) our φ_F value is within experimental error of that in hexanes, indicating that there should be a negligible solvent effect on φ_F for acetone in nonhalogenated solvents. In other words, we expect that the fluorescence efficiencies of acetone are the same in hexanes and benzene. (Experimental complications prevented us from determining φ_F for acetone directly in benzene.) However, in carbon tetrachloride (entry 4, Table V) the fluorescence efficiency of acetone is about half of that in hexane, indicating some fluorescence quenching of excited acetone singlets by carbon tetrachloride. Consequently, it is explicable now why the initial intensities of the direct chemiluminescence of the dimethyl and the *tert*-butyl α-peroxylactones in carbon tetrachloride are lower than those in benzene (Table I) as a result of fluorescence quenching.

With eq 2 and the data of Tables II and VI, the direct chemiluminescence efficiencies Φ_{DC} and the fraction of singlet excited product molecules were calculated for the *tert*-butyl (entries 1 and 2, Table VII) and for the dimethyl (entires 4 and 5, Table VII) α-peroxylactones in benzene and carbon tetrachloride. It is apparent that both α-peroxylactones have about the same very low efficiency in generating

singlet excited carbonyl products, *i.e.*, per 10^4 α-peroxylactone molecules that decarboxylate only about five singlet excited product molecules are formed.

Already in Table I and Figure 1 we called attention to the fact that in the presence of efficient fluorescers such as rubrene, the emission intensities are dramatically enhanced. Using the data of Table III (entry 12) and Table IV (entry 5) for the *tert*-butyl and dimethyl α-peroxylactones with a variation of eq 2 we estimate the enhanced chemiluminescence quantum yields (Φ_{EC}) taking φ_F^R as unity.[28] In these estimates the enhanced emission intensities had to be corrected for rubrene reabsorption and photomultiplier response. Furthermore, the maximum possible Φ_{EC} value for the *tert*-butyl system, for which saturation of energy transfer could not be achieved even at the highest possible $[R_0]$ of 5.1×10^{-2} M, was extrapolated by means of a Φ^{-1} vs. $[R_0]^{-1}$ relationship, using the data of Table III (entries 12 and 22–25). As seen in Table VII, the Φ_{EC} values (entries 3 and 6) are *ca.* 10^5-fold larger than the Φ_{DC} values (entries 1, 2, 4, and 5).

Complete singlet energy transfer could only account for a 10^3-fold enhancement factor by rubrene since its fluorescence efficiency is 10^3-fold greater than that of acetone or *tert*-butylcarboxaldehyde. Consequently, the additional 10^2-fold enhancement must arise by triplet energy transfer from triplet excited products to rubrene, which in turn fluoresces. Therefore, the rubrene-enhanced emissions of the α-peroxylactones in benzene derive almost entirely from triplet energy transfer at the maximum rubrene concentrations. Thus, the Φ_{EC} values represent triplet counting.

The fraction of triplet excited product molecules formed in the decarboxylation of α-peroxylactones is calculated by eq 3 (see paragraph at end of text regarding supplementary

$$\Phi_{EC} = \beta\varphi_F^R/2 \qquad (3)$$

material)[29] and are given in Table VII (entries 3 and 6), again taking φ_F^R as unity. Clearly, the efficiency of triplet state production is still low, but outweighs the efficiency of singlet state production by a large factor.

One important internal cross check of our data for the *tert*-butyl α-peroxylactone is provided by comparing the efficiency of singlet state production between the direct (entry 1, Table II) and the rubrene-enhanced (entry 25, Table III) chemiluminescence. In the latter case at 5.4×10^{-3} M tetramethyl-1,2-diazetidine 1,2-dioxide triplet quencher, effectively all triplet product molecules are scavenged, as indicated by the saturation of quenching, so that the residual 40% emission intensity must be attributed to singlet energy transfer to rubrene. From this data we calculate a value of α within the order of magnitude 10^{-4}, as obtained in the direct chemiluminescence. The result of entry 5 in Table I is also in accord with this value if one assumes that diphenylanthracene counts only singlet state species.

The effect of the quenchers used in this study provides an interesting contrast. Piperylene appears to be inefficient with either aldehyde or rubrene triplets. The tetramethyl-1,2-diazetidine 1,2-dioxide may be efficient in quenching both triplets. However, in view of the lack of effect of oxygen on the *tert*-butyl enhanced luminescence and the similiar limiting intensities, in the presence or absence of oxygen for the dimethyl-enhanced luminescence, one may conclude oxygen to be inefficiently quenching rubrene triplets.

One final experimental result worth mentioning concerns the possibility that in the aerated runs triplet ground state oxygen quenches triplet excited products and forms singlet oxygen, which transfers its energy to rubrene thereby enhancing the chemiluminescence efficiency. The importance of such a relay mechanism involving oxygen could be discounted, since we observed that high concentrations of singlet oxygen, produced chemically by the hydrogen peroxide–sodium hypchlorite reaction,[30] in the presence of rubrene gave emissions only a factor of 10^{-3} as intense as observed in the rubrene-enhanced chemiluminescence of α-peroxylactone.[31]

Mechanistic Interpretations

The results shown in Tables I–VII and Figures 1–4 concerning the chemiluminescence of the *tert*-butyl and dimethyl α-peroxylactones show qualitative similarities to the chemiluminescences of dioxetane compounds.[5,7] These similarities will be utilized in our analysis. The predominant kinetic feature of both peroxylactone compounds is the appearance of first-order kinetics in the absence and pseudo-first-order kinetic in the presence of sufficiently high concentration of enhancer. This is presented as evidence for the conclusion that the rate-limiting step is the peroxylactone decomposition. The large enhancement of luminescence accompanying the occurrence of the pseudo-first-order kinetics indicates that processes associated with excited states, *sic*, triplets, compete with the peroxylactone decomposition. The differences between the enhanced chemiluminescence of the *tert*-butyl and dimethyl α-peroxylactone are thus interpreted in terms of quantitative changes in the excited triplet state processes, rather than in terms of mechanistically distinct decarboxylations. It may be anticipated that structural variation such as *tert*-butyl *vs.* dimethyl α substitution, may modify the amounts of triplet or singlet state production, the net lifetimes of these excited states and their rates of triplet energy transfer. Utilizing these general concepts, it is possible to present a unified mechanistic picture which incorporates the experimental observations from the direct and enhanced chemiluminescences of both the *tert*-butyl and dimethyl α-peroxylactones, rather than interpret them individually.

It would be heuristic to reiterate some of the key experimental observations in terms of mechanistic clues. Clearly, the direct and enhanced chemiluminescence efficiencies demand that singlet (A^S) and triplet (A^T) excited state and ground state (A) product molecules are formed in the decarboxylation of α-peroxylactones (P), *i.e.*

$$P \longrightarrow \alpha A^S + \beta A^T + \gamma A + CO_2$$
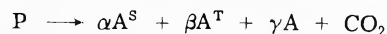
in which γ, similar to α and β, represents the fraction of ground state product molecules. The fact that in the direct chemiluminescence the emissions are due to product fluorescence and in the enhanced chemiluminescence due to rubrene fluorescence, both decaying by first-order kinetics equal to the rate of α-peroxylactone decarboxylation, testifies that the steps

$$A^S \longrightarrow A + h\nu_A$$
$$R^S \longrightarrow R + h\nu_R$$
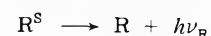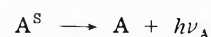
are producing the light emissions. Singlet and triplet energy transfer by excited product molecules to rubrene is most emphatically exhibited by the tetramethyl-1,2-diazetidine 1,2-dioxide quenched, rubrene-enhanced chemiluminescence of *tert*-butyl α-peroxylactone, shown in steps

$$A^S + R \longrightarrow A + R^S$$
$$A^T + R \longrightarrow A + R^T$$
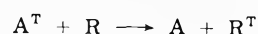
of which the latter dominates in the enhanced chemiluminescence. Furthermore, the enhanced emissions of the dimethyl system, which exhibits the more complex kinetics, are decreased in the absence of molecular oxygen ($O_2{}^T$), the "inverse oxygen effect," first reported by Wilson and Schaap.[5] The occurrence of the "inverse oxygen effect" and the dependence of the decay constants on rubrene concentration suggest the involvement of triplet states in an induced decarboxylation reaction of the α-peroxylactone by either the carbonyl product or fluorescer molecules[5,7] such as

$$A^T + P \longrightarrow \delta A^T + CO_2$$

$$R^T + P \begin{array}{c} \longrightarrow \delta R^T + A + CO_2 \\ \longrightarrow \delta A^T + R + CO_2 \end{array}$$
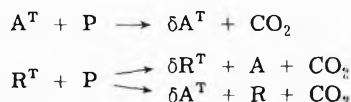
where δ represents the fraction of triplet products generated in the induced decomposition. However, the decay constants, which may reflect the importance of such induced reactions, show near-linear rubrene concentration dependence for both the *tert-* butyl and dimethyl α-peroxylactone results. If the rubrene triplet induced reaction were important, then the decay constants would have displayed a greater variation with increasing rubrene concentration (see also footnote 32). For this reason the induced reaction involving rubrene triplets may be discounted. The occurrence of oxygen quenching reactions, such as

$$A^T + O_2{}^T \longrightarrow A + O_2{}^S$$
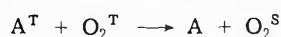
are also supported by the inverse oxygen effect.

Very significant is the complex kinetic dependence of the enhanced emission of the dimethyl α-peroxylactone on rubrene, being essentially quadratic at low [R] and leveling off to a constant value at high [R]. Such behavior is indicative of triplet–triplet annihilation, as given by

$$R^T + R^T \longrightarrow R^S + R$$

and has been apply demonstrated in the electrochemical generation of rubrene triplets.[12,32-34] Besides, merely on energy grounds reverse intersystem crossing, *i.e.*

$$R^T \longrightarrow R^S$$

is inefficient since the triplet energy is about half the singlet energy of rubrene.[12] The unit fluorescence efficiency of rubrene[28] negates the importance of phosphorescence, *i.e.*

$$R^T \longrightarrow R + h\nu_R{}'$$
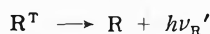
which may have resulted from an intersystem crossing of excited rubrene singlets, in accounting for the 10^5-fold enhancement of the direct chemiluminescence efficiency. Also the direct triplet–singlet energy transfer

$$A^T + R \longrightarrow A + R^S$$

is improbable since spin–orbit coupling for rubrene is of the order of that of 9,10-diphenylanthracene.[6] However, we observed that the latter fluorescer is an inefficient enhancer of the α-peroxylactone chemiluminescence. The possibility of triplet–triplet fluorescence[13] must be discouraged since it will not predict a quadratic dependence of the enhanced emission intensity on the rubrene concentration. Furthermore, singlet oxygen, produced by quenching of product triplets A^T, was shown to be ineffective in accounting for the large enhancement by energy transfer to rubrene, *i.e.*

$$R + O_2{}^S \longrightarrow R^S + O_2{}^T$$

a process which is difficult to accept in view of the fact that singlet oxygen undergoes cycloaddition to rubrene forming an endoperoxide.[35]

Furthermore, the reaction

$$R^T + O_2{}^T \longrightarrow R + O_2{}^S$$
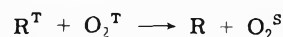
is not considered to be important in view of the lack of an O_2 effect in the *tert-* butyl α-peroxylactone enhanced chemiluminescence as well as the similiar limiting intensities in the presence or absence of air in the enhanced dimethyl α-peroxylactone results.

The minimum number of steps that must be used to cover the above facts in terms of a unified mechanism for both the direct and enhanced chemiluminescence in the decarboxylation of both the *tert-* butyl and dimethyl α-peroxylactones are collected in Scheme I. In addition to the steps

Scheme I

$$P \xrightarrow{k_1} \alpha A^S + \beta A^T + \gamma A + CO_2$$

$$A^S \xrightarrow{k_2} A + h\nu_A$$

$$A^S \xrightarrow{k_3} A$$

$$A^S \xrightarrow{k_4} A^T$$

$$A^S + O_2{}^T \xrightarrow{k_5} A + O_2{}^S$$

$$A^T + P \xrightarrow{k_6} \delta A^T + CO_2$$

$$A^T \xrightarrow{k_7} A$$

$$A^T + O_2{}^T \xrightarrow{k_8} A + O_2{}^S$$

$$A^S + R \xrightarrow{k_9} A + R^S$$

$$A^T + R \xrightarrow{k_{10}} A + R^T$$

$$R^S \xrightarrow{k_{11}} R + h\nu_R$$

$$R^S + O_2{}^T \xrightarrow{k_{12}} R + O_2{}^T$$

$$R^T + R^T \xrightarrow{k_{13}} R^S + R$$

$$R^T \xrightarrow{k_{14}} R$$
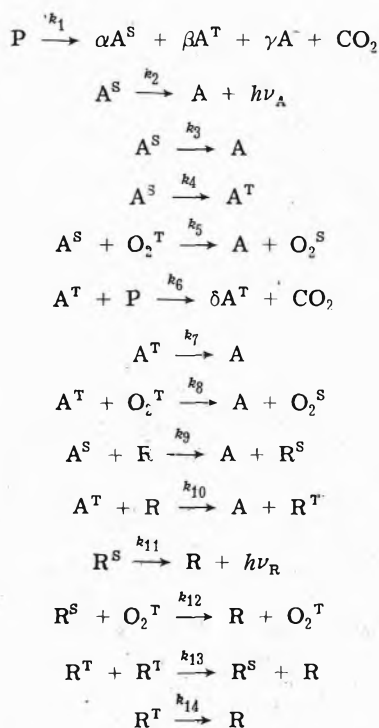
argued previously the usual nonradiative deactivations of excited states were added.

The proposed Scheme I is quite complex. An attempt at a rigorous derivation of kinetic equations describing the experimentally observed intensity and decay dependence on concentrations is possible. However, rather than being useful herein in obtaining additional quantitative information about the processes, which we do not feel is justified, such a treatment would prove distracting. Thus, the remainder of the discussion will concentrate on those qualitative mechanistic conclusions of Scheme I which are justifiable. Since the ultimate justification of those conclusions and, more importantly, the origin of eq 2 and 3, on which the estimation of α and β is made, all derive from the kinetic analysis, the derivations will be relegated to an available Appendix (see paragraph at end of text regarding supplementary material). Also given in the Appendix is a mathematical treatment which may be of general interest for use with other kinetic problems. This concerns use not only of the predicted intensity and decay dependence on concentration, but also that of the partial derivative of the logarithm of the

dependent variables in terms of the logarithm of its independent variables.

The primary conclusion from the direct chemiluminescence data is that only small amounts (ca. 4.7×10^{-4}) of excited singlet carbonyl products are formed in the decomposition of both the dimethyl and *tert*-butyl α-peroxylactones in inert solvents. The lack of phosphorescence emissions and the absence of deviations of the first-order decay constants in the direct chemiluminescence emissions discriminates against the involvement of triplet excited carbonyl products. Yet, the ca. 10^5-fold amplification of the emission intensity by rubrene undeniably demonstrates the production of triplet excited carbonly products. It is difficult to conceive a mechanism involving only singlet excited states to account for these extremely high initial emission intensities and their concentration dependences observed in the rubrene-enhanced chemiluminescence. Our present data tentatively support triplet–triplet annihilation as the principal mechanism for rubrene fluorescence. Thus, we calculate with eq 3 (based on Scheme I) a *tert*-butylcarboxaldehyde triplet yield of ca. 15% and an acetone triplet yield of ca. 5% from the respective *tert*-butyl and dimethyl α-peroxylactones (Table VII).[36] A number of assumptions have entered into these estimates, paramount of these is that the rubrene triplet–triplet annihilation was taken to be maximally efficient, *i.e.*, two rubrene triplets give rise to one rubrene excited singlet. Thus, our triplet yields are at worst a lower limit, especially since Bezman and Faulkner[12] suggest that triplet annihilation observed in electrochemiluminescence can be as low as 1%. Clarification of this uncertainty about the triplet yields must be postponed until absolute triplet annihilation efficiencies become available.

Our observations of triplet annihilation and the effect of oxygen are of considerable photophysical relevance concerning rubrene triplet lifetimes. Since the probability of triplet annihilation requires long triplet lifetimes, we believe that the rubrene triplet lifetime is considerably longer than the 10^{-4} sec, estimated by Yildiz, Kissinger, and Reilly.[13] In this connection the lack of efficient quenching of rubrene triplets by molecular oxygen is surprising. Since it has been shown that the efficiency of molecular oxygen as a triplet quencher depends on the energy level of the triplet excited state,[37] our observations imply that the energy of the rubrene triplet, an excited species that has as yet defied direct detection, is below that of singlet oxygen ($^1\Delta_g$). Thus, endothermicity in the energy transfer would render molecular oxygen quenching of rubrene triplet improbable.

The implications of the induced decomposition reaction (step k_6) incorporated into Scheme I requires discussion. The necessity of this process has been presented by Wilson and Schaap,[5] and Turro and coworkers[38] in the case of decomposition of simple 1,2-dioxetanes. Their interpretations involve quantum chain and solvent cage processes. Thus, the degree of induced decomposition, and thereby the overall kinetic behavior of the system, is dictated by a delicate balance between the rate of triplet state production, the efficiency of triplet transfer to the parent compound, and the probability of escape of triplet product of this reaction from its solvent cage. In terms of the peroxylactone compounds in question here, it is expected on steric grounds that the induced decomposition by *tert*-butylcarboxaldehyde triplets is less effective than that by acetone triplets, accounting for the "inverse oxygen effect," in the dimethyl but not in the *tert*-butyl α-peroxylactone decarboxylation. However, neither the present result on the α-peroxylactones nor the earlier results on the 1,2-dioxetanes[39] can be understood unless production of carbonyl triplets exceeds its consumption in the induced decomposition step k_6. Under these conditions the concept of triplet lifetimes is radically changed since triplet quenching by step k_6 effectively increases triplet lifetime. Furthermore, our kinetic treatment reveals that this reaction is the probable cause of the presence or absence of a quadratic intensity dependence. Associated with a lower rate of induced reaction in the *tert*-butyl system is a longer triplet lifetime than may occur with acetone triplets. This longer lifetime would be associated with more efficient energy transfer, which in turn is associated with linear rather than quadratic dependence of intensity on fluorescer concentration.

Additional kinetic complexity would result, if induced decomposition by fluorescer triplets occurs. Not only could the fluorescer triplet be efficiently replenished, but when energetically feasible, the carbonyl triplet could be produced as well under these circumstances. Also it is anticipated that at very large α-peroxylactone concentrations induced decomposition may manifest itself directly by exhibiting pronounced deviations from first-order kinetics. Preliminary results confirm these predictions and the full details shall be reported.[40]

Supplementary Material Available. The mathematical analysis referred to in the text (Appendix I) will appear following these pages in the microfilm edition of this volume of the journal. Photocopies of the supplementary material from this paper only or microfiche (105 × 148 mm, 24× reduction, negatives) containing all of the supplementary material for the papers in this issue may be obtained from the Journals Department, American Chemical Society, 1155 16th St., N.W., Washington, D. C. 20036. Remit check or money order for $3.00 for photocopy or $2.00 for microfiche, referring to code number JPC-74-2559.

References and Notes

(1) A. P. Sloan Fellow 1968–1972, J. S. Guggenheim Fellow 1972–1973.

(2) "This paper was prepared in connection with work under contract No. AT-(40-1)-1833 with the U.S. Atomic Energy Commission. The Commission retains a non-exclusive, royalty-free license in and to any copyright covering this paper, with the right to authorize others to reproduce all or any part of the copyrighted paper."

(3) "Chemiluminescence and Bioluminescence," N. J. Cormier, D. M. Hercules, and J. Lee, Ed., Plenum Press, New York, N.Y., 1973.

(4) (a) K. R. Kopecky and G. Mumford, *Can. J. Chem.*, **47**, 709 (1969); "Cyclic Peroxide Symposium" of Metrochem 71, Regional Meeting of the North Jersey–New York–Puerto Rico Section of the American Chemical Society, San Juan, Puerto Rico, April 1971; (b) W. Adam and J.-C. Liu, *J. Amer. Chem. Soc.*, **94**, 2894 (1972); (c) M. M. Rauhut, *Accounts Chem. Res.*, **2**, 80 (1969); J. Stauff, W. Yaeschke, and G. Schlögl, *Z. Naturforsch. B*, **27**, 1434 (1972).

(5) T. Wilson and A. P. Schaap, *J. Amer. Chem. Soc.*, **93**, 4126 (1971).

(6) R. F. Vassil'ev, *Progr. React. Kinet.*, **4**, 305 (1967); *Russ. Chem. Rev.*, **39**, 529 (1970); V. A. Belyakov and R. F. Vassil'ev, *Photochem. Photobiol.*, **11**, 179 (1970).

(7) N. J. Turro and P. Lechtken, *J. Amer. Chem. Soc.*, **94**, 2886 (1972); N. J. Turro, H.-C Steinmetzer, and A. Yekta, *ibid.*, **95**, 6468 (1973).

(8) T. R. Darling and C. S. Foote, *J. Amer. Chem. Soc.*, **96**, 1625 (1974).

(9) W. Adam, *Chem. Zeit.*, **7**, 182 (1973).

(10) W. Adam and H.-C. Steinmetzer, *Angew. Chem., Int. Ed. Engl.*, **11**, 540 (1972).

(11) The choice of an adequate term for this effect has been difficult. McElroy and Seliger "Light: Physical and Biological Action," Academic Press, New York, N.Y., 1965, (p. 151) use the term "sensitized chemiluminescence" while Turro (*e.g.*, ref 34, herein) uses the term "indirect chemiluminescence." Of the two choices the former conveys the greater implications. However its use may be misleading, since the fluorescer compound added to these reaction mixtures are not the primary cause of the chemiluminescence (*cf.* "mercury photosensitized decomposition"). We prefer the term "enhanced chemiluminescence" because of prior usage,[10] and because it conveys no more significance than an increase in the emissions accompanying the chemiluminescence reactions. In order to distinguish this term from that of the process "electrogenerated chemiluminescence," abbreviated ecl, we use herein the abbreviation EC.

(12) R. Bezman and L. R. Faulkner, *J. Amer. Chem. Soc.*, **94**, 6324 (1972).

(13) A. Yildiz, P. T. Kissinger, and C. N. Reilley, *J. Chem. Phys.*, **49**, 1403 (1968).

(14) E. F. Ullman and P. Singh, *J. Amer. Chem. Soc.*, **94**, 5077 (1972).

(15) G. W. Mitchell and J. W. Hasting, *Anal. Biochem.*, **39**, 243 (1971).

(16) J. W. Hasting and G. Weber, *J. Opt. Soc. Amer.*, **53**, 1410 (1963).

(17) J. Lee and H. H. Seliger, *Photochem. Photobiol.*, **4**, 1015 (1965).

(18) Intensity of one POPOP standard was measured in Professor's J. W. Hastings Laboratory, Harvard University.

(19) RCA Tube Handbook, RCA Electronic Components, Harrison, N.J.

(20) I. A. Berlman, "Handbook of Fluorescence Spectra of Aromatic Compounds," Academic Press, New York, N.Y., 1965.

(21) S. J. Strickler and R. A. Berg, *J. Chem. Phys.*, **37**, 814 (1962).

(22) J. N. Demas and G. A. Crosby, *J. Phys. Chem.*, **75**, 991 (1971).

(23) M. H. Melhuish, *J. Phys. Chem.*, **65**, 229 (1961).

(24) "Handbook of Chemistry and Physics," 46th ed, R. C. West, S. M. Selby, and C. D. Hodgman, Ed., The Chemical Rubber Co., Cleveland, Ohio, 1966.

(25) J. C. Liu and H.-C. Steinmetzer, unpublished results.

(26) N. J. Turro, J. C. Dalton, K. Dawes, G. Farrington, R. Hautala, D. Morton, M. Niemczyk, and N. Schore, *Accounts Chem. Res.*, **5**, 92 (1972).

(27) A. M. Halpern and W. R. Ware, *J. Chem. Phys.*, **54**, 1271 (1971).

(28) B. Stevens and B. E. Algar, *J. Phys. Chem.*, **72**, 2582 (1968).

(29) The rationale behind eq 3 is that in a triplet–triplet annihilation reaction not more than one excited singlet state is produced per triplet pair disappearance.

(30) C. S. Foote, *Accounts Chem. Res.*, **1**, 104 (1968).

(31) T. Wilson, *J. Amer. Chem. Soc.*, **91**, 2387 (1969), has also shown that singlet molecular oxygen induces rubrene fluorescence.

(32) N. Duran, U.P.R. Visiting Fellow, 1974, has examined the rubrene enhanced chemiluminescences of tetramethyl-1,2-dioxetane at 70°. With rubrene concentrations in excess of 10^{-3} M a maximum chemiluminescence yield of the order 10^{-5} einstein/mol was observed. The intensity varied with rubrene concentration according to the expression, $I = k[R]^{0.4}$. The decay constants at these concentrations varied according to the relation $\tau = k'[R]^{-2}$. A reaction such as $R^T + O \rightarrow R^T + 2A$, where O is the dioxetane, in competition with the triplet–triplet annihilation reaction may account for this effect. The low yield is attributed to reduction in triplet–triplet annihilation efficiency under these conditions.

(33) Although our data for the dimethyl α-peroxylactone are less abundant, it is of the same accuracy as that for the *tert*-butyl system, and it supports our conclusion for rubrene triplet–triplet annihilation in the enhanced chemiluminescence. Even if the data for the dimethyl system were omitted, an enhancement mechanism involving the annihilation reaction would be a reasonable explanation of the high intensities.

(34) It is possible to obtain a quadratic intensity dependence of fluorescer concentration if an excimer was the emitting species. However, high emission intensities could not be achieved from either singlet or triplet excimers, in view of the low α values for the former, and the presumed infrared emissions (to which our detector is insensitive) for the latter.

(35) K. Gollnick and G. O. Schenk, "The Diels-Alder Reaction in Heterocyclic Synthesis," J. Hamer, Ed., Academic Press, New York, N.Y., 1966.

(36) N. J. Turro, P. Lechtken, G. Schuster, J. Orell, H.-C. Steinmetzer, and W. Adam, *J. Amer. Chem. Soc.*, **96**, 1629 (1974), have reported ratios of triplet to singlet excited state products of 9,10-dibromoanthracene activation of dimethyl α-peroxylactone chemiluminescence. We have no rigorous explanation for the difference between the rubrene and dibromoanthracene triplet counting results, except that preliminary work[40] indicates that induced decomposition for the latter is more pronounced.

(37) *E.g.*, R. Benson and W. E. Geacintov, *J. Chem. Phys.*, **59**, 4428 (1973).

(38) N. J. Turro, N. E. Schore, H.-C. Steinmetzer, and A. Yekta, *J. Amer. Chem. Soc.*, **96**, 1936 (1974).

(39) P. Lechtken, A. Yekta, and N. J. Turro, *J. Amer. Chem. Soc.*, **95**, 3027 (1973).

(40) W. Adam, O. Cueto, N. Duran, J. Pulgar, G. A. Simpson, and F. Yany, unpublished results.

Heats of Hydrogenation of Sixteen Terminal Monoolefins. The Alternating Effect

Donald W. Rogers* and Somchitra Skanupong

Chemistry Department, The Brooklyn Center, Long Island University, Brooklyn, New York 11201 (Received June 7, 1974)

We have determined the heats of hydrogenation of all 16 terminal monoolefins from C_5 to C_{20} under identical conditions so as to search for the existence or nonexistence of the alternating effect on the stability of terminal double bonds referred to by Kistiakowsky. Because the alternating effect, if it exists, is small, collection of a sufficient body of information to permit valid statistical treatment was necessary. Accordingly, we present data for 10 determinations each for the 16 monoolefins in question. We present a statistical treatment of the data to support our conclusion that an alternating effect does not exist for the olefins studied.

Some years ago Kistiakowsky[1,2] obtained the values −30.115, −30.341, and −30.137 kcal/mol for the heats of hydrogenation of 1-propene, 1-butene, and 1-heptene, respectively, suggesting that the odd-numbered chain might confer some stability on a terminal double bond as contrasted to the even-numbered chain. If an alternating effect exists, it should be in evidence all along a homologous series of terminal olefins and an alternation of higher and lower stabilities should be observed. Such an effect would be small, however, and with admirable scientific reserve, Kistiakowsky remarked, "Whether the slight difference between propylene and heptene on one side and butene on the other is real and is due to an alternating even–odd effect is very doubtful."

Subsequent studies[3-7] on terminal olefins were carried out in liquid solution and at 25° and are not comparable to Kistiakowsky's gas-phase data measured at 82°. Having been carried out in different laboratories and by different methods, the latter values are probably not even comparable to each other when seeking such small enthalpy differences as the alternating effect would confer on terminal double bonds. We have determined the heats of hydrogenation of all terminal olefins from C_5 through C_{20} under identical conditions so as to shed some light on the existence or nonexistence of the alternating effect.

Experimental Section

Apparatus. The calorimeter and method have evolved beyond the one previously described[7] in several ways. A thicker-walled plastic container with wider threads[8] was substituted for the one in previous use so as to reduce the possibility of cracks and leaks. The cap was drilled with three equidistant 0.25-in. holes which were plugged with three inverted serum bottle stoppers[9] two of which were secured by a pin as shown in Figure 1. The unnecessary part of the serum bottle stoppers was trimmed off as indicated by the dotted line in Figure 1. One of the septa, pierced with a sharp instrument and lubricated with silicone grease, served as a hydrogen tight seal through which a thermistor probe[10] was thrust. The new steel-jacketed thermistor probe is more sensitive and has a faster response than the thermistor–thermistor well arrangement previously used. Shorter extrapolations of the time–temperature curve improved accuracy. The other two serum-bottle stoppers served as septa, one to receive a 19-gauge hydrogen inlet needle and the other to receive injections of the sample.

The calorimeter was insulated from drafts and sudden ambient temperature changes by a cylindrical insulating blanket about 2 cm thick which covered about half its exposed area. The remaining surface of the reaction chamber was left exposed to facilitate cooling after a hydrogenation run as described below. No serious attempt was made to maintain the laboratory at constant temperature (~25°) other than the avoidance of gross temperature changes. Slow temperature drifts in the laboratory sometimes necessitated warming or cooling of the calorimeter so as to keep it slightly above ambient temperature.

The thermistor probe was connected as the unknown arm of a Wheatstone bridge as in our previous paper[7] but a more sensitive potentiometric recorder[11] was used to indicate the degree of imbalance of the bridge. The voltage across the bridge was controlled as previously described.[7] Typical series resistances were 1000 to 5000 ohms, bridge input voltages were between 1 and 2 V, and the thermistor resistance was about 2100 ohms. The potentiometric recorder has a sensitivity control which was set at 0.5 or 1.0 mV full scale deflection (10 in.) in these experiments.

Reagents. All terminal monoolefins reported here were obtained from Chemical Samples Co.[12] The calorimeter fluid was n-hexane from Burdick and Jackson.[13] Although this hexane was inhomogeneous under glc investigation in this laboratory, it did not poison the catalyst and hence was useful as a calorimetric fluid. Most impurities seem to be isomeric hexanes and, in any case, any unsaturated impurities would be hydrogenated during the catalyst activation period. Palladium catalyst (5% on charcoal) was obtained from Mathesen Coleman and Bell.[14]

Procedure. The calorimeter was charged with 0.6 g of

sample hydrogen thermistor   septa   pin   slurry   magnet   magnet
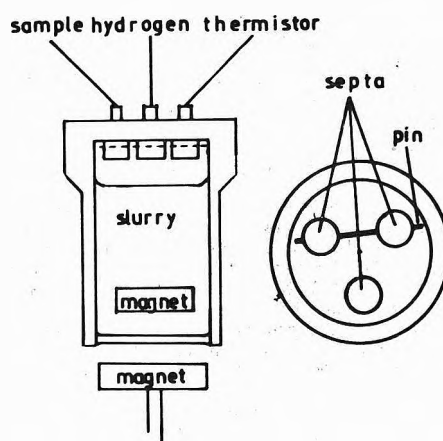
Figure 1.

catalyst and 30 ml of hexane. The threads of the calorimeter vessel were smeared with silicone sealant and the calorimeter cap was screwed down as firmly as could be done by hand. The silicone seal was allowed to set for 1 hr before the calorimeter was ready for hydrogen to be admitted.

The hydrogen inlet tube and needle were swept clear of air by allowing hydrogen to flow for approximately 20 sec. Hydrogen pressure was turned off, the needle, lubricated with silicone grease, was passed through one of the two septa not occupied by the thermistor probe, and the hydrogen valve was reopened to commence activation of the catalyst.

The calorimeter, which had been previously clamped into place in its blanket of insulation and stirred for some time, had almost come to temperature equilibrium as indicated by a steady reading on the potentiometric recorder. Upon admission of hydrogen, the temperature change caused by adsorption of hydrogen on the catalyst surface and reduction of any PdO which might have been formed by air oxidation, caused a sharp deflection of the recorder pen. Catalyst activation is a very exothermic process, releasing eight to ten times as much heat as a typical hydrogenation at these catalyst:olefin ratios.

It is not necessary, in principle, to observe the potentiometer deflection during activation of the catalyst because the heat of catalyst activation is not used in our calculations as it has been in previous studies. In practice, however, we found it useful to observe the potentiometer deflection so as to spot experimental troubles early and, if possible, to remedy some of them. Normal activation was indicated by a slight dip in temperature immediately upon hydrogen injection followed by a sharp rise.

After activation of the catalyst, the calorimeter was above ambient temperature and commenced a slow drift toward thermal equilibrium. Within 15 min, the calorimeter was only slightly above ambient temperature and the recorder base line showed a smooth downward drift. The calorimeter was now ready to receive sample injections. In these experiments, 40 μl of standard or unknown solution in hexane was injected through the remaining of the three septa by means of a 50-μl syringe. The syringe was fitted with a Reprojector[15] to ensure maximum reproducibility of sample volume. According to the manufacturer's statement, injections made with a good syringe and a Reprojector are reproducible to within 0.6%.

Hydrogenation of all alkenes was very rapid and caused a deflection in the potentiometric recorder reading which

was proportional to the amount of heat given off during reaction. Within 9–12 sec, the reaction and instrumental response time were complete and the recorder pen had started a slow drift back toward thermal equilibrium resulting in a temperature vs. time curve which was treated by the graphical method previously discussed.[7] The sensitivity of recorder response was adjusted so that the recorder deflection was 90% of full scale. Alternate 40-μl samples of ~20% (by weight) unknown and a thermochemically equivalent concentration of standard were injected under identical conditions. These sample sizes are of the order of 20–100 μmol. Temperature rise was of the order of 0.1–0.3°.

In the case of the terminal olefins described here, we assumed that they all had ΔH_h very nearly that of 1-hexene and made up the 1-hexene standard at a concentration by weight such that the two peak heights were very nearly the same. This was necessary because recorder deflections differing by 10% or more gave erroneous results, probably due to different heat-leak characteristics of the calorimeter for reactions which differ significantly in their total heat output. Accurately weighed 1-ml samples of the pure terminal monoolefin to be studied were diluted to 5 ml with n-hexane, eliminating the necessity of knowing accurate densities. Standards were made up by diluting an appropriate volume of 1-hexene, with accurate weighing, to 25 ml. Standards were made up in such large amounts to minimize weighing and dilution errors. Standard solutions were made up fresh each day to avoid concentration changes due to evaporation of liquids of different volatility.

A series of 20 or more hydrogenations was carried out, alternating aliquot portions of standard and unknown.

If the recorder trace height per millimole for the standard is R_s and that for the unknown is R_u then the corresponding unknown heat of hydrogenation follows from the ratio

$$\Delta H_u / \Delta H_s = R_u / R_s \qquad (1)$$

Results and Discussion

By way of verifying the method, we obtained a series of 12 R values for 40-μl aliquot portions of 1-hexene in n-hexane solution. The standard deviation from their mean was 0.47%. Blanks of pure n-hexane gave null results.

We then determined the ΔH_h of seven aliquot portions of six different synthetic unknowns of 1-hexene in n-hexane using 1-hexene solutions of (slightly) different concentrations as standards. Taking as the accepted[16] value −29.56, we obtained a mean of the means of −29.64 and a standard deviation of the means of 0.11 kcal/mol. These tests for accuracy and precision along with others are discussed in more detail elsewhere.[17]

The actual hydrogenation reaction is

C_nH_{2n} (hexane soln, C_i) + H_2 (g, 2 atm) =
$\qquad\qquad$ C_2H_{2n+2} (hexane soln, C_f)
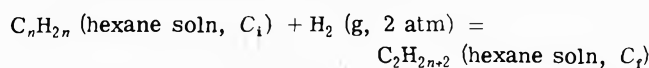
where C_i is the initial olefin concentration and C_f is the final concentration of reaction product in hexane, essentially infinitely dilute. This is not the same as previous work in which pure sample is introduced into the calorimeter. We felt that using hexane as the calorimeter fluid and introducing the sample in the form of a ~20% solution in hexane would reduce interference from heats of solution, the ΔH of mixing of hexane in itself being, of course, zero. Although the results are not strictly comparable with other studies, they should be comparable to each other.

TABLE I: Enthalpies of Hydrogenation of Terminal Olefins, C_nH_{2n}

n	% purity[a]	$-\Delta H_h$[b]	σ, kcal/mol[c,d]
5	99.9	29.30	0.57
6	99.9	29.64	0.25
7	99.5	29.71	0.36
8	99.9	29.40	0.34
9	99.9	29.71	0.24
10	99.6	29.69	0.29
11	99.7	29.58	0.42
12	99.9	29.98	0.35
13	99	30.07	0.46
14	99	29.85	0.38
15	99	29.72	0.23
16	99.8	29.60	0.44
17	99	29.66	0.43
18	99	30.08	0.41
19	99	29.96	0.43
20	99	30.34	0.31

[a] By manufacturers statement, Chemical Samples Co. [b] Each entry is the mean of 10 experimental runs. [c] Mean standard deviation $\bar{\sigma} = 0.37$. [d] Mean standard error $\bar{\sigma}/N^{1/2} = 0.12$.

Results for the heats of hydrogenation of 10 replicate samples of each of 16 homologous terminal olefins are shown in Table I.

From the beginning, we anticipated that we would not be able to present a simple "yes" or "no" answer to the question of the existence of the alternating effect because the standard error[18] of a typical set of 10 runs on any one terminal monoolefin is 0.12 kcal/mol, about half the magnitude of the alternating effect we seek. We felt, however, that this handicap would be partially overcome by the principal advantages of our apparatus, speed of operation and repetitive injection of small, highly purified samples. Our method permits one to obtain, at a reasonable time expenditure, a sufficient body of data for valid statistical treatment.

Standard least-squares treatment of the data shows that the entire set of 160 runs conforms to the linear eq 2 while the results for olefins with an odd number of carbon atoms conform to (3) and those with an even number conform to (4).

$$-\Delta H = 0.03896n + 29.28 \qquad \hat{\sigma} = 0.407 \qquad (2)$$

$$-\Delta H = 0.02928n + 29.36 \qquad \hat{\sigma} = 0.425 \qquad (3)$$

$$-\Delta H = 0.04692n + 29.21 \qquad \hat{\sigma} = 0.383 \qquad (4)$$

Both odd and even series show a small trend in ΔH toward more negative values with the number of carbon atoms in the olefin. We attribute this to solvent effects which increase in magnitude with increasing chain length. A much larger solvent effect has been observed for similar studies in glacial acetic acid.[6] To compare the odd and even series, we calculated the heat of hydrogenation from (3) and (4) for the hypothetical olefin with 12.5 carbon atoms which represents the midpoint of the range C_5 to C_{20}. We shall call these means μ_1 and μ_2.

The value from the odd series, μ_1, is −29.72$_6$ and that for the even series, μ_2, is −29.79$_9$ kcal/mol and the difference between the means is 0.07$_3$ kcal/mol. To evaluate this difference, we calculated the standard error, $\hat{\sigma}_\mu = \hat{\sigma}/N^{1/2}$, of each series from its least-squares straight line to be $\hat{\sigma}_{\mu_1} = 0.048$ for the odd series and $\hat{\sigma}_{\mu_2} = 0.043$ for the even series.

The standard error for the difference between the means, $\hat{\sigma}_{\mu_1-\mu_2}$, is[19]

$$\hat{\sigma}_{\mu_1-\mu_2} = (\hat{\sigma}_{\mu_1}^2 + \hat{\sigma}_{\mu_2}^2)^{1/2}$$

Computing the standard score, $\bar{z} = \mu_1 - \mu_2/\hat{\sigma}_{\mu_1-\mu_2} = 1.14$, leads us to conclude that the difference is significant only at the 0.25 level using a two-tailed test. If an alternating effect of about 0.23 kcal/mol had existed, as inferred from Kistiakowsky's data, we compute $\bar{z} = 3.59$ which leads us to a significance level of about 0.0004 using the same test. We take the large difference between these significance levels to indicate the absence of a measurable alternating effect among linear terminal monoolefins from C_5 to C_{20}.

The least reliable values of ΔH are those of C_5, because of its volatility and consequent handling difficulties and C_{20}, because it has the least unsaturation per double bond, placing the maximum demand on the sensitivity of the method. When these two are deleted, the mean of the remaining seven odd olefins is -29.76_4 while that of the remaining even olefins is -29.76_6. These results lead, *a fortiori*, to the rejection of an alternating effect.

References and Notes

(1) G. B. Kistiakowsky, J. R. Ruhoff, H. A. Smith, and W. E. Vaughan, *J. Amer. Chem. Soc.,* **57**, 876 (1935).
(2) G. B. Kistiakowsky, J. R. Ruhoff, H. A. Smith, and W. E. Vaughan, *J. Amer. Chem. Soc.,* **58**, 137 (1936).
(3) R. B. Williams, *J. Amer. Chem. Soc.,* **64**, 1395 (1942).
(4) T. Flirtcroft, H. A. Skinner, and M. C. Whiting, *Trans. Faraday Soc.,* **53**, 784 (1957).
(5) H. A. Skinner and A. Snelson, *Trans. Faraday Soc.,* **55**, 404 (1959).
(6) D. W. Rogers and E. Bretschneider, *Mikrochim. Acta,* 482 (1970).
(7) D. W. Rogers and F. J. McLafferty, *Tetrahedron,* **27**, 3765 (1971).
(8) Bolab Inc., Derry, N.H. 03038.
(9) E. H. Sargent, Springfield, N.J. 07081. No. S-9055.
(10) Time constant 2.5 sec., Cole-Parmer Inst. Co., Chicago, Ill., 60684. Model 8436.
(11) Microcord 44, Photovolt Corp., New York, N.Y. 10010.
(12) Chemical Samples Co., Columbus, Ohio 43220.
(13) Burdick and Jackson Labs., Muskegon, Mich. 49442.
(14) Matheson Coleman and Bell, The Matheson Co., East Rutherford, N.J.
(15) Shandon Scientific Co., Siwickley, Pa. 15143.
(16) H. F. Bartolo and F. D. Rossini, *J. Phys. Chem.,* **64**, 1685 (1960).
(17) D. W. Rogers, P. M. Papadimetriou, and N. A. Siddiqui, *Mikrochim. Acta,* in press.
(18) N. M. Downie and R. W. Heath, "Basic Statistical Methods," Harper and Brothers, New York, N.Y., 1959, p 117.
(19) Reference 18, pp 123–127.

Solvation of Extracted Complex Metal Acids. VII. An Improved Model[1a]

D. K. K. Liu,[1b] D. T. Shioshita, and R. L. McDonald*

Department of Chemistry, University of Hawaii, Honolulu, Hawaii 96822 (*Received September 20, 1973; Revised Manuscript Received August 2, 1974*)

New data are presented for the distribution of HFeCl₄ between 8 M HCl and bis(2-chloroethyl) ether ($\beta\beta$) in 1,2-dichloroethane or hexane or neat. A simple model based on only two organic phase species will explain these data and those for $\beta\beta$–benzene mixtures reported earlier. The hydrated proton is solvated with three molecules of $\beta\beta$; one $\beta\beta$ molecule is lost when the hydrated proton combines with FeCl₄⁻ to form an ion pair. These species show surprising stability; they are unaffected by gross changes in the composition of the organic phase.

Several papers from this laboratory[2–5] have dealt with the extraction of HMX₄ (M = Fe, In, or Au; X = Cl or Br) from fairly concentrated aqueous HX solutions into mixed organic phases of varying composition. We have used the law of mass action to interpret these data. This yields solvation numbers larger than can be accounted for by any reasonable model. Nonetheless, we continued these studies in the belief that as sufficient data became available, a better model of ion extraction would evolve.

In this paper, we describe the distribution of HFeCl₄ between *ca.* 8 M HCl and solutions of bis(2-chloroethyl) ether ($\beta\beta$) in 1,2-dichloroethane (DCE) or hexane. The former solution essentially obeys Raoult's law while the latter shows a large positive deviation. A simple model, based on only two organic phase metal species, hydrated [H⁺($\beta\beta$)₂FeCl₄⁻] ion pairs and hydrated H⁺($\beta\beta$)₃ + FeCl₄⁻ (free ions), will explain all of these extraction data and those for neat $\beta\beta$ and $\beta\beta$–benzene mixtures[5] as well. The

free energies of the solvated ions vary linearly with the inverse of the organic phase bulk dielectric constant as predicted.[6,7] This fact was omitted from our earlier interpretations.[2–5]

Experimental Section

Distribution Measurements. Eastman White Label bis(2-chloroethyl) ether was purified by distillation under a reduced pressure of N₂. The middle fraction was collected and diluted with spectroquality DCE or reagent grade hexane to the desired concentrations. These solutions were stored in the dark and used within 6 weeks of preparation. Reagent grade HCl was diluted with deionized water to 8.15 M as determined by titration. Approximately 0.1 M FeCl₃ (in 8.15 M HCl) stock solutions were prepared from reagent grade FeCl₃·6H₂O; the Fe(III) concentration was determined spectrophotometrically.[8] Other solutions of lesser Fe(III) concentrations were made by successive
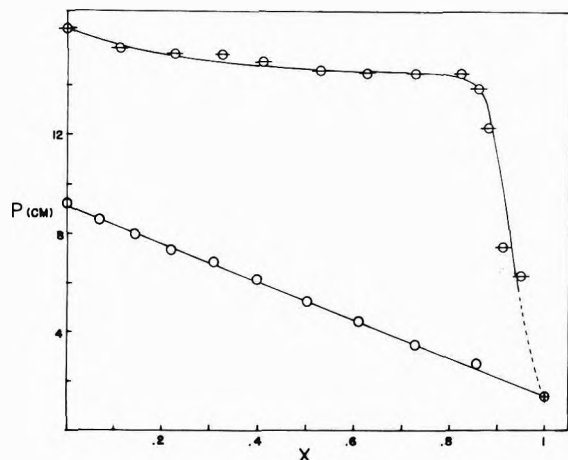
Figure 1. Plots of the vapor pressure over the solutions at 25° vs. mole fractions of bis(2-chloroethyl) ether in 1,2-dichloroethane (O) or hexane (⊖).

TABLE I: Dielectric Constants of Bis(2-chloroethyl) Ether—1,2-Dichloroethane Mixtures at 25°

Mole fraction of ether	$\bar{D}$	Mole fraction of ether	$\bar{D}$
0.00[a]	10.3	0.40	15.0
0.07	11.4	0.50	16.2
0.14	12.2	0.61	17.2
0.22	13.3	0.73	18.4
0.31	14.3		

[a] Literature value: 10.36. A. A. Maryott and E. R. Smith, *Nat. Bur. Stand.* (U.S.), *Circ.*, **No. 514** (1951).

quantitative dilutions of the stock solutions with 8.15 M HCl. Radioactive iron-59 chloride in aqueous HCl was purchased from International Chemical and Nuclear Corp. and diluted with 8.15 M HCl before use.

The distribution experiments were done in triplicate at 25° as described elsewhere.[4] The reproducibility between triplicates was almost always better than ±10%.

Vapor Pressure Measurements. Each solution was shaken with 8.15 M HCl before its vapor pressure was measured. The isoteniscope consisted of a U tube containing mercury, a flask containing the sample, and a stopcock to isolate the sample side of the U tube from the vacuum pump. Air was removed by the freeze–pump–thaw technique. The entire device was placed in a glass jar containing water at 25 ± 0.1° and the difference in mercury levels was measured with a cathetometer. The apparatus was left in the water bath for at least 30 min before any measurements were made. After this, readings were taken at 5-min intervals for 30 min and averaged.

Dielectric Constant Measurements. Each $\beta\beta$–DCE mixture was shaken with 8.15 M HCl before its dielectric constant was measured. The heterodyne beat method[9] was used to measure the change in capacitance of a parallel plate capacitor in air and in the liquid mixture at 25 ± 0.1°. Carefully dried Mallinckrodt Nanograde benzene was used to calibrate the apparatus.

Results

The vapor pressures of both $\beta\beta$–DCE and $\beta\beta$–hexane solutions at 25° are shown in Figure 1. Since the solutions were equilibrated with 8.15 M HCl, all of the vapor pressures are too large by about 1.4 cm, the vapor pressure of 8 M HCl.[10a] However, we are more interested in the shapes of the curves. Clearly $\beta\beta$–DCE can be considered ideal for our purposes, but the activity coefficients of the $\beta\beta$–hexane solutions are significantly different from unity. Calculation using our data (after subtracting 1.4 cm from each point; the vapor pressure of $\beta\beta$ over the solution is negligible) produced activity coefficients identical within experimental error to those reported by Neckel and Volk[11] for the dry solutions at 30°. The latter were used calculate $\beta\beta$ activities.

The dielectric constants of the $\beta\beta$–DCE mixtures (equilibrated with 8.15 M HCl) are tabulated in Table I. Log–log plots of the distribution ratio, E (= ratio of organic phase

to aqueous phase total metal concentrations), vs. the equilibrium aqueous phase metal concentration, C_M, have the general shapes predicted for systems in which both $H^+MX_4^-$ ion pairs and dissociated $H^+ + MX_4^-$ are present in the organic phase.[2-5] The E values for solutions containing ≤ 15 mol % $\beta\beta$ in DCE were corrected for DCE extraction by subtracting from the observed E the product of the volume fraction of DCE times E for pure DCE at the same C_M. As before, we write the distribution equilibrium

$$H^+ + FeCl_4^- + n\overline{\beta\beta} \overset{K'}{=} \overline{[H^+ + FeCl_4^-]\cdot n\beta\beta} \quad (1)$$
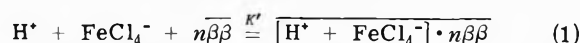
where the bar represents the organic phase, and the ion pair dissociation

$$\overline{H^+FeCl_4^-\cdot(n-p)\beta\beta} + \overline{p\beta\beta} \overset{K_M}{=} \overline{[H^+ + FeCl_4^-]\cdot n\beta\beta} \quad (2)$$
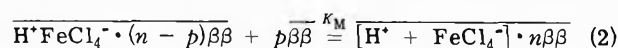
The proton is of course hydrated, probably with four water molecules.[2] For intermediated values of C_M, extracted HCl makes a negligible contribution to the ionic strength of the organic phase,[2-5] thus E can be written[5]

$$E = (K/\bar{K}_M)[\beta\beta]^{(n-p)} + \bar{g}_\pm(K[\beta\beta]^n/C_M)^{1/2} \quad (3)$$

$\bar{g}_\pm$ is mean ionic activity coefficient of $\bar{H}^+$ and $\overline{FeCl_4^-}$ in the organic phase; the Debye–Hückel limiting law predicts it to be near unity at the ionic strengths of interest here. $[\beta\beta]$ represents the activity of $\beta\beta$ and the distribution constant, K, although proportional to K', depends also on the aqueous phase HCl concentration[2] which is constant.

As predicted by eq 3, plots of E vs. $C_M^{-1/2}$ for a fixed organic phase are good straight lines. Values of $K[\beta\beta]^n$ and $\bar{K}_M[\beta\beta]^p$ obtained from such plots are given in Tables II and III.

Discussion

In earlier papers,[2-5] we chose a simple law of mass action approach to explain data similar to those in Tables II and III. This extreme approach assumes that K' (thus K) and $\bar{K}_M$ are truly constant even though the composition of the organic phase changes drastically. The slopes of plots of log $K[S]^n$ or log $\bar{K}_M[S]^p$ vs. log [S] are taken as the solvation numbers n and p. These plots are shown in Figures 2 and 3. Values of n so obtained range from 3 in the dilute $\beta\beta$–DCE mixture to near infinity in the $\beta\beta$–hexane mixtures; p is ca. 1.5 in the former and infinite in the latter.

Another extreme approach that has had some success,[6,12] at least for neat solvents, is to assume that K' and $\bar{K}_M$ are described by expressions based on the assumptions of the Born charging equation;[7] i.e., that $n = p = 0$ and that log K' and log K_M vary linearly with the inverse of the organic phase dielectric constant, $1/\bar{D}$. Figures 4 and 5, where we have included also data for $\beta\beta$–benzene,[5] show plots to test this hypothesis. ($\bar{D}$ values for $\beta\beta$–hexane mixtures were estimated from data for $\beta\beta$–octane.[10b])

TABLE II: Apparent Distribution and Ion Pair Dissociation Constants for $HFeCl_4$ Extracted from 8.15 M HCl by Bis(2-chloroethyl) Ether in 1,2-Dichloroethane

Mole fraction of $\beta\beta$	$K[\beta\beta]^n$	$\bar{K}_M[\beta\beta]^p$
0.03	1.02×10^{-7}	3.03×10^{-5}
0.04	2.23×10^{-7}	5.57×10^{-5}
0.05	5.33×10^{-7}	8.90×10^{-5}
0.07	1.35×10^{-6}	9.97×10^{-5}
0.09	3.46×10^{-6}	1.70×10^{-4}
0.11	6.25×10^{-6}	1.80×10^{-4}
0.15	2.27×10^{-5}	3.41×10^{-4}
0.25	2.46×10^{-4}	8.90×10^{-4}
0.30	5.86×10^{-4}	1.31×10^{-3}
0.35	1.30×10^{-3}	1.66×10^{-3}
0.40	2.35×10^{-3}	1.87×10^{-3}
0.45	4.11×10^{-3}	1.97×10^{-3}
0.50	6.85×10^{-3}	2.14×10^{-3}

TABLE III: Apparent Distribution and Ion Pair Dissociation Constants for $HFeCl_4$ Extracted from 8.15 M HCl by Bis(2-chloroethyl) Ether in Hexane

Mole fraction of $\beta\beta$	$K[\beta\beta]^n$	$\bar{K}_M[\beta\beta]^p$
0.40	1.29×10^{-7}	2.47×10^{-6}
0.53	1.00×10^{-5}	2.59×10^{-5}
0.60	7.69×10^{-5}	9.72×10^{-5}
0.70	8.96×10^{-4}	3.83×10^{-4}
0.80	9.13×10^{-3}	2.20×10^{-3}
1.00	2.5×10^{-1}	8.2×10^{-3}
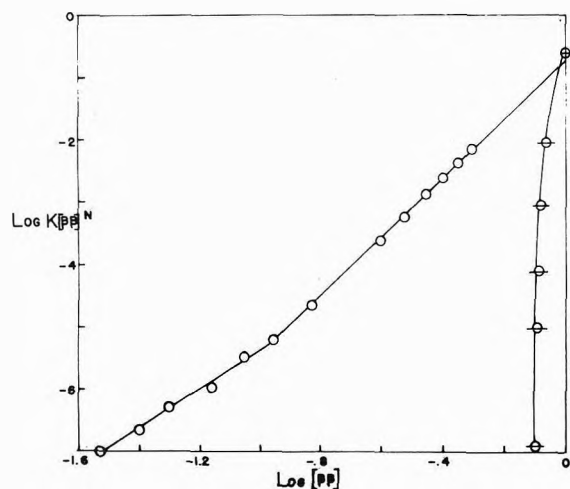
Figure 2. Log–log plots of the apparent distribution constant of $HFeCl_4$ vs. the activity of bis(2-chloroethyl) ether in 1,2-dichloroethane (O), hexane (⊖), or neat (⊕).

Figure 3. Log–log plots of the apparent ion pair dissociation constant of $HFeCl_4$ vs. the activity of bis(2-chloroethyl) ether in 1,2-dichloroethane (O), hexane (⊖), or neat (⊕).
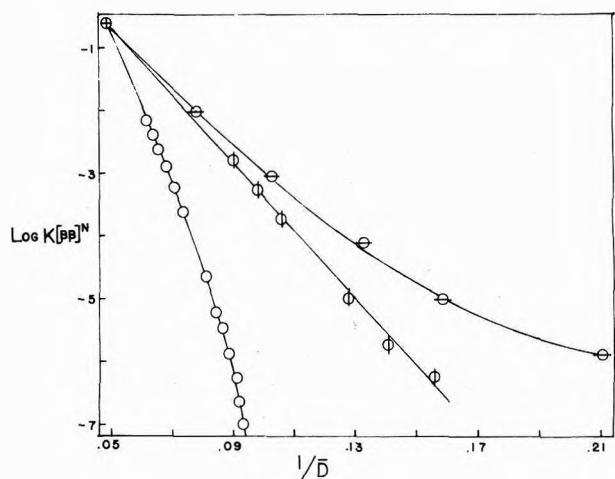
Figure 4. Plots of the apparent distribution constant of $HFeCl_4$ (log scale) vs. the inverse organic phase dielectric constant for bis(2-chloroethyl) ether in 1,2-dichloroethane (O), hexane (⊖), benzene (⊘), or neat (⊕).
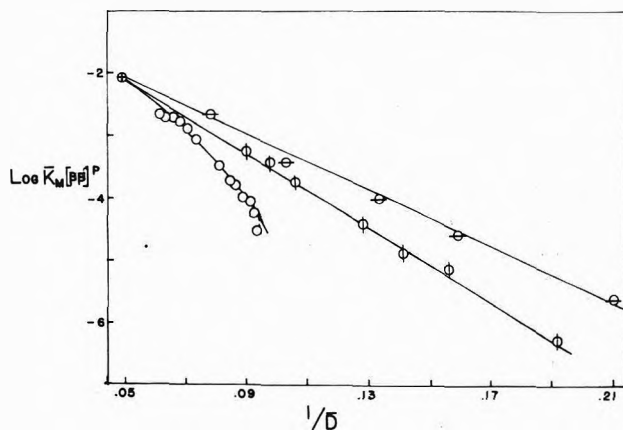
Figure 5. Plots of the apparent ion pair dissociation constant of $HFeCl_4$ (log scale) vs. the inverse organic phase dielectric constant for bis(2-chloroethyl) ether in 1,2-dichloroethane (O), hexane (⊖), benzene (⊘), or neat (⊕).

Both of these extreme approaches are unsatisfying, the first because it often yields solvation numbers too large to fit any reasonable model[2-5] and the second because the K (or $\bar{K}_M$) data do not fall on a single line as predicted by the Born charging equation.[5,13]

Improved models of ion solvation have been suggested which allow for specific interactions between an ion and its nearest neighbor solvent molecules, but treat the solvent as a continuum beyond the first shell.[14] To apply this approach we assume that the apparent value $n = 3$, which obtains at low $\beta\beta$ concentrations in DCE where $\bar{D}$ is nearly constant, is the "true" solvation number of the dissociated $H^+ + FeCl_4^-$, and that this true n is independent of $\beta\beta$

concentration and diluent. That is, we break 1 into two steps: an aqueous equilibrium,
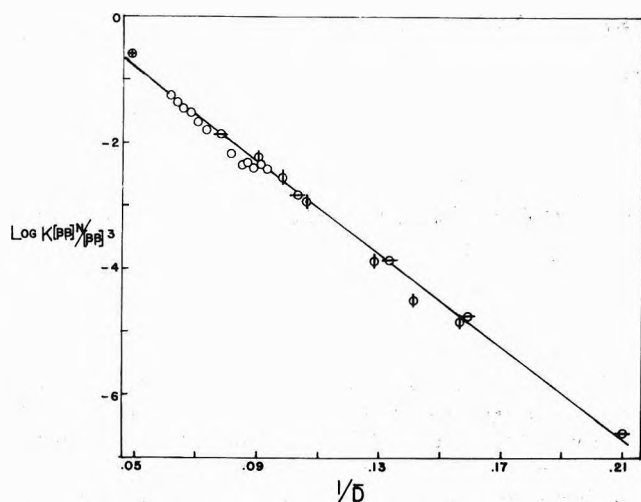
Figure 6. Plot of the distribution constant of $HFeCl_4$ (log scale) vs. the inverse organic phase dielectric constant for bis(2-chloroethyl) ether in 1,2-dichloroethane (O), hexane (⊖), benzene (∅), or neat (⊕).

$$H^+ + FeCl_4^- + 3\beta\beta \overset{K_1'}{=} [H^+ + FeCl_4^-]\cdot 3\beta\beta \qquad (1a)$$
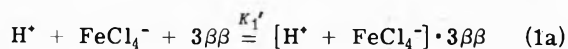
followed by a transfer step

$$[H^+ + FeCl_4^-]\cdot 3\beta\beta \overset{K_2'}{=} \overline{[H^+ + FeCl_4^-]\cdot 3\beta\beta} \qquad (1b)$$
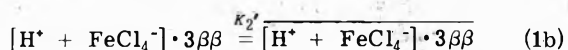
We further assume that K_1' is in fact constant but $\log K_2'$ varies linearly with $1/\bar{D}$; K' is of course $K_1'K_2'$.

If this is valid, plots of $\log \{K[\beta\beta]^n/[\beta\beta]^3\}$ vs. $1/\bar{D}$ should yield a single line for all diluents so long as the aqueous phase is constant. Figure 6 shows vividly that the data conform to our expectations. We use a similar approach on the $\bar{K}_M[\beta\beta]^p$ values. At low $\beta\beta$ concentrations in DCE, the apparent p is near unity (see Figure 6). Figure 7, a plot of $\log \{\bar{K}_M[\beta\beta]^p/[\beta\beta]\}$ vs. $1/\bar{D}$ shows that $p = 1$ will fit all of the solutions.

Note that n and p are insensitive to both ether concentration and diluent. Apparently there is a single value for the number of solvent molecules associated with the ions (or ion pairs) and these solvated species have surprising stability. The solvation number 3 has been reported before for acids in a variety of solvents, most of them stronger bases than $\beta\beta$. The structure of the hydrated proton in these solutions, probably $H_9O_4^{+}$,[2] is not known. Nonetheless, there is much evidence to suggest that it possesses three sites to hydrogen bond to a weakly basic donor solvent.[15] It is reasonable to postulate that the ionic species present in our organic phases are $H_9O_4^{+}(\beta\beta)_3$, $FeCl_4^-$, and $[H_9O_4^{+}(\beta\beta)_2FeCl_4^-]$. $\beta\beta$ is a poor donor; apparently $FeCl_4^-$ can compete successfully for one hydrogen bonding site in
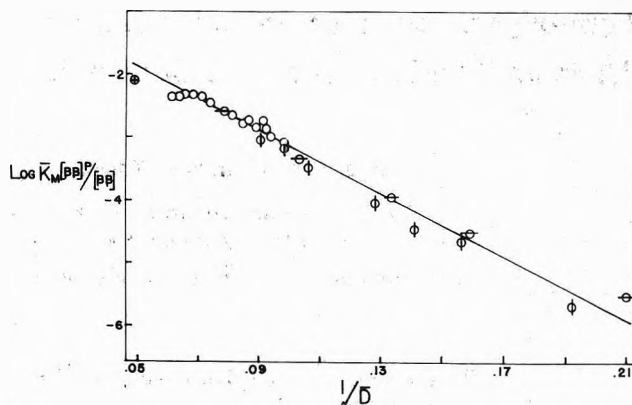
Figure 7. Plot of the ion pair dissociation constant of $HFeCl_4$ (log scale) vs. the inverse organic phase dielectric constant for bis(2-chloroethyl) ether in 1,2-dichloroethane (O), hexane (⊖), benzene (∅), or neat (⊕).

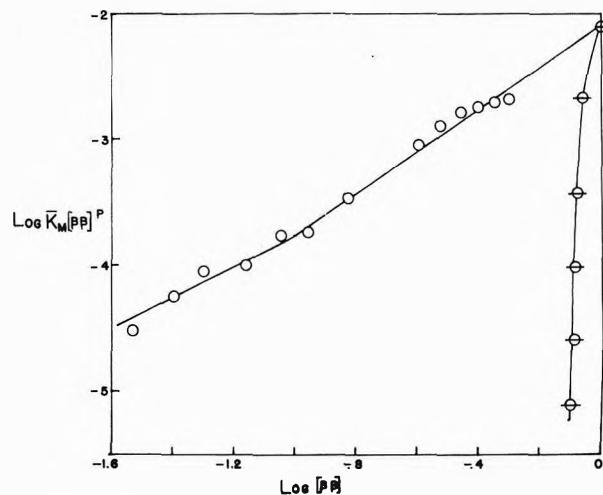the ion pair. Far-infrared spectra have shown that $FeCl_4^-$ hydrogen bonds to R_3NH^+ in benzene.[16] The constancy of the cation solvation number despite significant changes in the composition of the solvent mixtures deserves further discussion. Not only does it emphasize the usefulness of thinking chemically in terms of definite solvated species in solution, it also suggests that information concerning these species obtained from dilute solution studies can be extrapolated even to neat solvents. It is hoped that additional studies of this type in the future will test the generality of this hypothesis.

References and Notes

(1) (a) Work supported in part by the Air Force Office of Scientific Research under Grant No. AFOSR-68-1387. (b) NSF Undergraduate Research Participant.
(2) R. L. Erickson and R. L. McDonald, J. Amer. Chem. Soc., **88**, 2099 (1966).
(3) D. A. Meyers and R. L. McDonald, J. Amer. Chem. Soc., **89**, 486 (1967).
(4) S. L. Law and R. L. McDonald, J. Phys. Chem., **72**, 1617 (1968).
(5) R. L. McDonald and T. H. Hufen, J. Phys. Chem., **74**, 1926 (1970).
(6) J. T. Denison and J. B. Ramsey, J. Amer. Chem. Soc., **77**, 2615 (1955).
(7) M. Born, Z. Phys., **1**, 45 (1920).
(8) D. A. Skoog and D. M. West "Fundamentals of Analytical Chemistry," Holt, Rinehart and Winston, New York, N.Y., 1969, pp 689–90.
(9) D. P. Shoemaker and C. W. Garland, "Experiments in Physical Chemistry," McGraw-Hill, New York, N.Y., 1962, pp 280–283.
(10) (a) J. Timmermans, "The Physico-chemical Constants of Binary Systems in Concentrated Solutions," Vol. 4, Interscience, New York, N.Y., 1959, p 442; (b) ibid., Vol. 1, p 399.
(11) A. Neckel and H. Volk, Monatsh. Chem., **88**, 925 (1957).
(12) G. R. Haugen and H. L. Friedman, J. Phys. Chem., **72**, 4549 (1968).
(13) D. Feakens, "Physico-Chemical Processes in Mixed Aqueous Solvents," F. Franks, Ed., American Elsevier, New York, N.Y., 1967, pp 71–89.
(14) A. D. Buckingham, Discuss. Faraday Soc., **24**, 150 (1957).
(15) D. C. Whitney and R. M. Diamond, J. Phys. Chem., **67**, 209 (1963).
(16) R. A. Work, III, and R. L. McDonald, J. Inorg. Nucl. Chem., **34**, 3123 (1972).

Thermodynamics of Ion Solvation of the Alkali Metal Chlorides in Aluminum Chloride–Propylene Carbonate Solution

Jacob Jorné*[1] and Charles W. Tobias

Inorganic Materials Research Division, Lawrence Berkeley Laboratory and Department of Chemical Engineering, University of California, Berkeley, California 94720 (Received May 30, 1974)

The free energies of solvation of the alkali metal chlorides in unit molality $AlCl_3$–propylene carbonate solution were obtained from emf measurements. The individual free energies of solvation were estimated using the method of Latimer, Pitzer, and Slansky. Free energies of transfer, $\Delta G_t^\circ(M^+)$, estimated by comparing the results to similar data for aqueous solution, are −0.6, −4.2, −4.7, −3.1, and −5.0 kcal/mol for Li^+, Na^+, K^+, Rb^+, and Cs^+, respectively. The negative sign indicates that the cations are on a lower energy level and strongly solvated by the local negative charge of the solvent dipole. The estimated free energy of transfer of Cl^- is +10.3 kcal/mol, and the molal association constant of Cl^- with $Al(PC)_6^{3+}$ in PC is 1.9×10^5. The standard entropies of transfer of the alkali metals are discussed in terms of internal structure and order in the solution.

Introduction

In a previous paper,[2] the standard electrode potentials of the alkali metals in unit molality $AlCl_3$ solution in propylene carbonate (PC) were evaluated using emf measurements at 25 and 35° of the general cell

M(s)|MCl (solution in $AlCl_3$ (1 m) in PC)|.TlCl(s)|Tl(Hg).
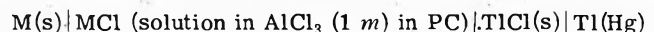
where M represents Li, Na, K, Rb, and Cs. With the exception of LiCl, the alkali metal chlorides are practically insoluble in PC, however, in the presence of $AlCl_3$ a complex is formed between the chloride and $AlCl_3$

$$MCl + AlCl_3 = M^+ + AlCl_4^-$$
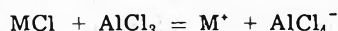
This reaction and the stability of the alkali metals in alkali metal chloride–$AlCl_3$ solutions in PC enables the electrodeposition of the alkali metal at ambient temperature and the evaluation of the standard electrode potentials and activity coefficients.[2]

In the present paper, the standard electrode potentials of the alkali metals and their temperature dependence are used to estimate the free energies and entropies of solvation of individual ions in $AlCl_3$(1 m)–PC solution. The evaluation of single-ion solvation energies and the establishment of a universal scale of standard potentials are fundamental problems in solution chemistry. The solvation free energies, enthalpies, and entropies are of great importance because they reveal the nature of the ion–solvent interactions.

Review of Related Work

The following brief review covers thermodynamic measurements in PC and related aprotic solvents; the direct work in PC is presented at the end of this section in greater detail. Most of the studies were performed in the following common aprotic solvents: acetonitrile (AN), formamide (FA), *N*-methylformamide (NMF), dimethyl sulfoxide (DMSO), dimethylformamide (DMF), and propylene carbonate (PC).

Emf and heat of solution measurements were performed in NMF,[3,4] DMF,[5–8] DMSO,[9–16] FA,[17–20] and AN.[21–23] The measured standard potentials were used to evaluate stan-

dard ionic free energies and entropies of solvation. Enthalpies of solvation were obtained mostly by direct calorimetric measurements in FA,[24,25] NMF,[4,5,24,26,27] DMF,[4,5,28] DMSO,[24,29] and PC.[24,30,31]

In a series of papers, Friedman and coworkers estimated the enthalpies of transfer of ions from water to PC.[30,32] The individual ionic enthalpies of transfer were estimated using the method Latimer, Pitzer, and Slansky.[33] Ion associations in PC were checked by conductance measurements.[30] Regularities and specific effects in enthalpies of transfer of ions from water to PC, DMSO, FA, and NMF were discussed by Friedman.[34] The trend of the halide ions is the same in each case, while a varying trend of the alkali metal ions reflects differences in solvent basicity. The basicity of the solvent is suggested to be in the order PC < FA < DMSO < NMF. The assumption that PC is a nearly ideal solvent for ions is discussed in light of the disagreement with the Born equation, although the agreement is better for PC than for water. A summary of the solvation enthalpies of various ions in water, PC, and DMSO is presented by Krishnan and Friedman.[35] Solvation enthalpies of nonelectrolytes, mostly alcohols and hydrocarbons, were measured in water, PC, and DMSO.[36] Enthalpies of transfer of various 1:1 electrolytes from PC to methanol and DMF are presented elsewhere.[37] Solvation enthalpies of hydrocarbons and normal alcohols in several highly polar solvents, including PC, are reported by Krishnan and Friedman.[38]

The thermodynamics of LiCl and LiBr,[39] NaI,[40] LiI and KI[41] were measured by Salomon using the emf method. The potentials of the cell type M|MX in PC|TlX(s)|Tl(Hg) were measured, where M represents Li, Na, and K, and X represents Cl^-, Br^-, and I^-. In the case of the potassium system, potassium amalgam replaced the metallic potassium. The data were corrected for the free energy of formation of the Tl amalgam,[42] and the standard potentials were obtained by extrapolation to infinite dilution following the Guggenheim equation.[43] The thermodynamic quantities ΔG°, ΔH°, and ΔS° for the cell reactions were calculated from the standard potentials and their temperature dependence.

The thermodynamics of single ion solvation in PC and

water is summarized by Salomon.[44a] The free energies and enthalpies of solvation of individual ions were evaluated from the corresponding values of the salts, and by extrapolation (to infinite ionic radius) of the plot of the differences of cation and anion conventional energies vs. $1/r$. According to Salomon, this method of splitting the solvation energies into individual ionic contributions is preferable to the traditional method of Latimer, Pitzer and Slansky,[33] which introduces a single adjustable parameter in the Born equation.
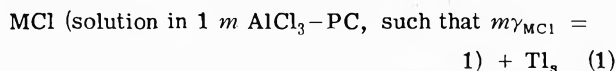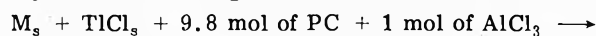
Cogley, Butler, and Grunwald[45] studied the selective solvation of ions by water in PC. The equilibrium constants for the association of water with individual ions were obtained under a relatively mild set of extrathermodynamic assumptions from protic magnetic resonance (chemical shift) measurements. The affinity of water at low concentrations in PC for alkali metal cations correlated well with the free energy of transfer of these ions from PC to bulk water.

A general equation for the estimation of ionic entropies in various solvents, including PC, is presented by Criss.[44b] It is concluded that the solvent structure, rather than basicity, plays the predominant role in determining the value of the ionic entropies.

Parker[46] gives an extensive review on the protic–dipolar aprotic solvent effects on rates of organic bimolecular reactions. The observations that dipolar aprotic solvents are excellent media for many organic reactions are explained by positive free energies of transfer of anions. The review contains extensive and very useful information on the solvation of ions in aprotic solvents and on solvent activity coefficients (medium effects). On the general subject of solvation of individual ions in nonaqueous solvents, the reader is referred to a review of Popovych.[47]

Free Energies of Solvation of Single Ions in AlCl$_3$ (1 m)–PC Solution

Using the standard cell potentials which were obtained for the alkali metals in AlCl$_3$ (1 m)–PC solution,[2] it is now possible to calculate the free energy of solvation for the salt MCl (where M is Li, Na, K, Rb, or Cs) in AlCl$_3$ (1 m)–PC. The free energy of solvation of single alkali metal ions will then be estimated according to Latimer, Pitzer, and Slansky's method.[33] Using $\Delta G°_{emf}$ for the cell reaction

M$_s$ + TlCl$_s$ + 9.8 mol of PC + 1 mol of AlCl$_3$ $\longrightarrow$

MCl (solution in 1 m AlCl$_3$–PC, such that $m\gamma_{MCl}$ =

$$1) + Tl_s \quad (1)$$

plus the formation and lattice energies, it is possible to calculate the free solvation of MCl for all the alkali metals

$$\Delta G°_{solv}(MCl) = \Delta G°_{emf} + \Delta G°_f[TlCl_s] -$$

$$\Delta G°_f[MCl_s] + \Delta G°_{lat}[MCl_s] \quad (2)$$

where

$$\Delta G°_{lat}[MCl_s] = \Delta G°_f(M_g) + \Delta G°_f(Cl_g) -$$

$$\Delta G°_f(MCl_g) + I - A \quad (3)$$

Free energies of formation, $\Delta G°_f$, were taken from Wagman,[48] JANAF,[49] and Latimer.[50] Ionization potentials, I, were obtained from Jesson and Muetterties,[51] and the electron affinity, A, of the chloride ion was obtained from Berry and Reimann.[52] Table I presents the results. The last column gives the crystal ionic radii of the corresponding alkali metal according to Pauling.[53]

Since the chloride ions are being complexed by the Al^{3+} ions to form AlCl$_4^-$ ions, one can assume that the free energy of solvation of chloride ion in AlCl$_3$ (1 m)–PC solution is constant and independent of the nature of the alkali metal cation. Therefore, we assume that the free energy of solvation of the alkali metal chloride in AlCl$_3$ (1 m)–PC solution behaves according to

$$\Delta G°_{solv}(MCl) = \Delta G°_{solv}(Cl^-) + \frac{A}{r_i + \delta_c} \quad (4)$$

where r_i is the Pauling crystal ionic radius of the alkali metal and δ_c is the Latimer, Pitzer, and Slansky's parameter[33] for cations in PC. Figure 1 presents the plot of $\Delta G°_{solv}(MCl)$ vs. $1/(r_i + \delta_c)$. A linear plot was obtained for the alkali metal cations for $\delta_c = 0.50$. The intercept at infinite crystal radii gives the free energy of solvation of Cl$^-$ as $\Delta G°_{solv}(Cl^-) = -90.0$ kcal/mol. Using this result the free energies of solvation of the individual alkali metal cations can be estimated. Table II summarizes the estimated free energies of solvation of single ions at 25° in AlCl$_3$ (1 m)–PC solution. Also included, for comparison, are the free energies of solvation in pure PC and in water estimated by Salomon.[44a]

It can be seen from Table II that the free energies of solvation of the individual cations, obtained in the present work in AlCl$_3$ (1 m) solution in PC, show similar trend to those estimated by Salomon[44a] in pure PC. The presence of AlCl$_3$ in the solvent changes the free energies of solvation by approximately 1–5 kcal/mol. Li$^+$, Na$^+$, and K$^+$ are more strongly solvated in the presence of AlCl$_3$. However, the solvation of Rb$^+$ and Cs$^+$ remain almost the same, probably because of their large size, and in agreement with the popular assumption that the large alkali metal cations have no specific interaction with solvents, and therefore their energies of solvation are independent of the solvent. The free energies of solvation of all the alkali metals are lower in AlCl$_3$ (1 m)–PC than in water, which indicates that the cations are more strongly solvated in AlCl$_3$–PC than in water.

The free energy of solvation of the chloride ion in AlCl$_3$ (1 m)–PC solution is lower than in pure PC. The chloride ions are believed to be complexed by the Al^{3+} ions according to the following exchange reaction[54]

$$4Cl^- + Al(PC)_6^{3+} \overset{K}{\rightleftharpoons} AlCl_4^- + 6PC \quad (5)$$
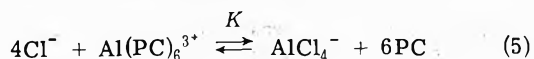
The free energy of transfer of Cl$^-$ from pure PC to AlCl$_3$ (1 m)–PC solution is estimated from the difference between its free energies of solvation in AlCl$_3$ (1 m)–PC and pure PC (see Table II) as -1.8 kcal/mol, hence the equilibrium constant for the exchange reaction can be estimated from

$$4[\Delta G°_{solv}(Cl^-)_{AlCl_3-PC} - \Delta G°_{solv}(Cl^-)_{PC}] = -RT \ln K \quad (6)$$

$K = \exp[(4 \times 1800)/(1.98 \times 298)] = 1.9 \times 10^5$. This is the molal association constant of Cl$^-$ with Al(PC)$_6^{3+}$ in PC solution. It should be mentioned here that a large association constant of Cl$^-$ with Al(PC)$_6^{3+}$ was predicted by nmr studies.[54] Indeed, this should be the reason for the high solubility of the alkali metal chlorides in AlCl$_3$–PC solution, while they are nearly insoluble in pure PC. The association constant can be used to estimate Cl$^-$ concentrations in AlCl$_3$–PC systems. The error in the estimated value of K may be quite large, since it was obtained from the difference between two values which were obtained by extrapolation. K

TABLE I: Free Energies of Solvation of the Alkali Metal Chlorides in AlCl₃ (1 *m*)–PC Solution[a]

Salt	$E°$	$\Delta G°_{emf}$	$\Delta G°_f(TlCl_s)$	$\Delta G°_f(MCl_s)$	$\Delta G°_{lat}(MCl)$	$\Delta G°_{solv}(MCl)$	r_p
LiCl	2.045	−47,170	−44,460	−91,700	−188,500	−188,430	0.607
NaCl	1.885	−43,475	−44,460	−91,890	−170,600	−166,640	0.958
KCl	2.116	−48,800	−44,460	−97,760	−154,100	−149,600	1.331
RbCl	2.116	−48,800	−44,460	−98,480	−149,000	−143,780	1.484
CsCl	2.122	−48,940	−44,460	−96,600	−144,900	−141,700	1.656

[a] Free energies are given in calories per mole, $E°$ in volts, and r_p in ångströms.

TABLE II: Free Energies of Solvation of Individual Ions at 25° in AlCl₃ (1 *m*)–PC in Pure PC and in Water

Ion	$\Delta G°_{solv}(M)_{AlCl_3–PC}$[a]	$\Delta G°_{solv}(M)_{PC}$[b]	$\Delta G°_{solv}(M)_{H_2O}$[b]
Li⁺	−98.4	−95.0	−97.8
Na⁺	−76.6	−71.9	−72.4
K⁺	−59.6	−56.6	−54.9
Rb⁺	−53.8	−54.5	−50.7
Cs⁺	−51.7	−52.7	−46.7
Cl⁻	−90.0	−88.2	−100.3

[a] Present work. Solvent: AlCl₃ (1 *m*)–PC solution. [b] Reference 44a. Free energies of solvation in kilocalories per mole on a molal basis.
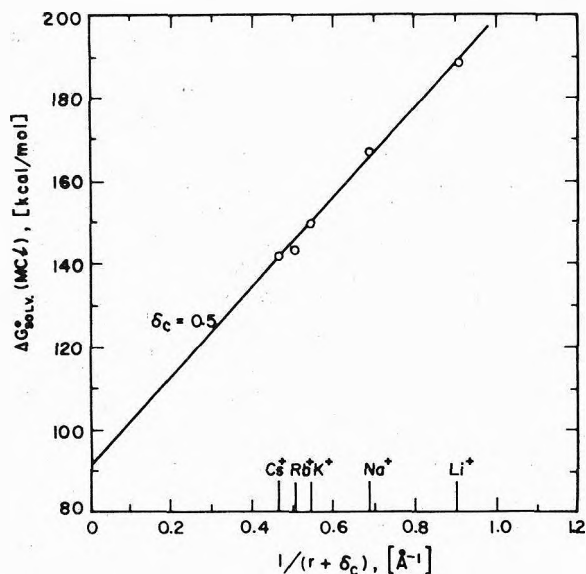
Figure 1. Free energies of solvation of the alkali metal chlorides vs. $1/(r + \delta)$ in AlCl₃ (1 *m*)–PC solution at 25°.

is a measure of the expected strong tendency of the free chloride ions to substitute the PC molecules around the Al³⁺ ions, which is responsible for "forcing" metal cations into the solution.

Free Energy of Transfer

Frequently, the medium effect or the free energy of solvation is expressed in the form of the free energy of transfer of a solute from a reference solvent (usually water) to the particular solvent. This interpretation of the free energy of transfer as the difference between the solvation energies in the two solvents is precise only for neutral molecules. For individual ions, the free energy of transfer includes an additional term $ze\chi$, where χ is the potential difference across the interface between the two phases. A distinction should be made between a "real" and a "chemical" solvation energy of single ions. "Chemical" solvation energies express only the solute-solvent interactions, while "real" solvation energies include the potential step across

the vacuum–solvent interface. Free energies of transfer, in the present work, are referred to as the "chemical" free energy. Table III summarizes the estimated free energies of transfer of individual ions from water to AlCl₃ (1 *m*)–PC solution and to pure PC. The negative values for the alkali metal cations indicate that these ions are more bound in PC than in water. The positive free energy of transfer of chloride ion means that Cl⁻ is loose in PC and poorly solvated, in agreement with the general observation that anions are poorly solvated in aprotic solvents.[46]

Standard Entropies of Transfer of the Alkali Metal Chlorides AlCl₃ (1 *m*)–PC Solution

The standard molal entropies for the general cell reaction

$$M_s + TlCl_s \longrightarrow MCl[AlCl_3(1\ m)-PC] + Tl_s \qquad (7)$$

were calculated from the temperature dependence of the standard cell potentials.[2] These values are tabulated in Table IV, along with the values for the corresponding cell reactions in water. The aqueous standard entropies were calculated from Latimer's tables.[50] The difference between the standard entropies corresponds to the following transfer process: MCl (solution in H₂O such that $m\gamma_{MCl} = 1$) + 9.8 mol of PC + 1 mol of AlCl₃ → MCl [solution in AlCl₃ (1 *m*)–PC such that $m\gamma_{MCl} = 1$] + 55.55 mol of H₂O. The calculated standard molal entropies of transfer are presented in the third column of Table IV. However, if one wants to express the entropy of transfer on a volume basis, a small correction is necessary for the difference in the specific volumes of the two solvents[55]

$$\Delta S_{corr} = R \ln (v_{AlCl_3(1\ m)-PC}) - R \ln (v_{H_2O}) \qquad (8)$$

The specific volume of water at 25° is 1.0019 cm³/g, and the specific volume of AlCl₃ (1 *m*)–PC solution was measured to be 0.7919 cm³/g.[2b] The correction is therefore −0.46 eu for one ion, and −0.92 eu for the transfer of a pair of ions (M⁺, Cl⁻), which was added to the difference between the standard molal entropies. The calculated standard entropies of transfer on a volume basis are presented in the last column of Table IV.

The uncertainty in the calculated entropies is quite high, because these values were calculated from differences between extrapolated values. Therefore, we will refer here only to the sign and the order of magnitudes of the standard entropies of transfer. The standard entropies of transfer are negative for lithium, sodium, and potassium chlorides, while the values for rubidium and cesium chlorides are positive. This can be explained in terms of the internal structures of the solvents. Water exhibits a large amount of hydrogen bonding, which causes a high degree of order in the pure state. Pure PC shows a low degree of order; it is considered to be an ideal orderless solvent. However, we are dealing here with AlCl₃ solution in PC as the solvent, and this reference state exhibits a high degree of order because of the orientation of the PC molecules around the

TABLE III: Free Energies of Transfer of Individual Ions from Water to $AlCl_3$ (1 m)-PC and Pure PC

Ion	$\Delta G^\circ{}_t(M)_{H_2O \rightarrow AlCl_3-PC}{}^a$	$\Delta G^\circ{}_t(M)_{H_2O \rightarrow PC}{}^b$
Li^+	-0.6	$+2.8$
Na^+	-4.2	$+0.5$
K^+	-4.7	-1.7
Rb^+	-3.1	-3.8
Cs^+	-5.0	-6.0
Cl^-	$+10.3$	$+12.1$

[a] Present work. Aqueous values were taken from Salomon.[44a] [b] Reference 44a. Free energies of transfer in kilocalories per mole on a molal basis.

TABLE IV: Standard Entropies of Transfer of the Alkali Metal Chlorides from Water to $AlCl_3$ (1 m)-PC[a]

	$\Delta S^\circ{}_{AlCl_3-PC}$	$\Delta S^\circ{}_{H_2O}$	$\Delta S^\circ{}_t$	$(\Delta S^\circ{}_t)_{vol}$
LiCl	-18.4	-0.6	-17.8	-18.7
NaCl	-16.1	$+4.9$	-21.0	-21.9
KCl	$+9.2$	$+12.0$	-2.8	-3.7
RbCl	$+55.3$	$+15.8$	$+39.5$	$+38.6$
CsCl	$+64.7$	$+14.7$	$+50.0$	$+49.1$

[a] Entropies are given in eu (calories/mole °K) and on a molal basis, except for the last column, which is on a volume basis.

Al^{3+} ions. $AlCl_3$ dissociates in PC solution according to

$$AlCl_3 + \tfrac{3}{2}PC \longrightarrow \tfrac{1}{4}Al(PC)_6{}^{3+} + \tfrac{3}{4}AlCl_4{}^- \qquad (9)$$
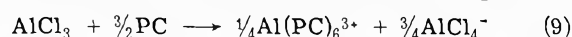
The addition of alkali metal chloride MCl to this solution reduces the amount of solvated $Al(PC)_6{}^{3+}$ species and converts them into $AlCl_4{}^-$ ions, which are poorly solvated. Consequently, the addition of MCl reduces the initial order in $AlCl_3$-PC solution and increases the entropy. On the other hand, the introduction of alkali metal ions causes reorientation of the solvent molecules around the ions, causing an entropy decrease. In the case of lithium, sodium, and potassium, the order gained by the introduction of these ions, due to strong reorientation of the PC molecules around them, is larger than the disorder resulting from the conversion of $Al(PC)_6{}^{3+}$ ions to $AlCl_4{}^-$. In the case of Rb and Cs, these large cations are poorly solvated, and the reorientation due to their presence is smaller than the loss of order due to the disappearance of $Al(PC)_6{}^{3+}$ species.

References and Notes

(1) Address correspondence to this author at the Department of Chemical Engineering and Material Sciences, Wayne State University, Detroit, Mich. 48202.
(2) (a) J. Jorné and C. W. Tobias, *J. Electrochem. Soc.*, submitted for publication; (b) J. Jorné, Ph.D. Thesis, LBL-1111, University of California, Berkeley, 1972.
(3) E. Luksha and C. M. Criss, *J. Phys. Chem.*, **70**, 1496 (1966).
(4) R. P. Held and C. M. Criss, *J. Phys. Chem.*, **69**, 2611 (1965).
(5) R. P. Held and C. M. Criss, *J. Phys. Chem.*, **71**, 2487 (1967).
(6) C. M. Criss and E. Luksha, *J. Phys. Chem.*, **72**, 2966 (1968).
(7) C. M. Criss, R. P. Held, and E. Luksha, *J. Phys. Chem.*, **72**, 2970 (1968).
(8) J. N. Butler and J. C. Synnott, *J. Amer. Chem. Soc.*, **92**, 2602 (1970).
(9) W. H. Smyrl and C. W. Tobias, *J. Electrochem. Soc.*, **115**, 33 (1968).
(10) D. R. Cogley and J. N. Butler, *J. Electrochem. Soc.*, **113**, 1074 (1966).
(11) G. Holleck, D. R. Cogley, and J. N. Butler, *J. Electrochem. Soc.*, **116**, 952 (1969).
(12) J. S. Dunnett and R. P. H. Gasser, *Trans. Faraday Soc.*, **61**, 922 (1965).
(13) T. Slerlak, B. Nikov, and V. Sislov, *Glas. Hem. Tehnol. Bosne Hercegovine*, No. 11, 39 (1962); *Chem. Abstr.*, **61**, 2461c (1962).
(14) J. N. Butler, "Reference Electrodes in Aprotic Organic Solvents," in "Advances in Electrochemistry and Electrochemical Engineering," Vol. 7, P. Delahay and C. W. Tobias, Ed., Interscience, New York, N.Y., 1970.
(15) M. Salomon, *J. Electrochem. Soc.*, **116**, 1392 (1969).
(16) M. Salomon, *J. Electrochem. Soc.*, **117**, 325 (1970).
(17) R. K. Agarwall and B. Nayak, *J. Phys. Chem.*, **70**, 2568 (1966).
(18) R. K. Agarwall and B. Nayak, *J. Phys. Chem.*, **71**, 2062 (1967).
(19) M. Mandel and P. Decroly, *Nature (London)*, **182**, 794 (1958).
(20) R. W. C. Broadband, et al., *Trans. Faraday Soc.*, **64**, 3311 (1968).
(21) G. Spiegel and H. Ulich, *Z. Phys. Chem.*, **A148**, 187 (1937).
(22) J. F. Coetzee and J. J. Campion, *J. Amer. Chem. Soc.*, **89**, 2513 (1967).
(23) J. F. Coetzee and J. J. Campion, *J. Amer. Chem. Soc.*, **89**, 2517 (1967).
(24) H. L. Friedman, *J. Phys. Chem.*, **71**, 1723 (1967).
(25) G. Somsen, *Recl. Trav. Chim. Pays-Bas*, **85**, 517, 526 (1966).
(26) Yu. M. Kessler, *Elektrokhimiya*, **2**, 1467 (1966).
(27) L. Weeda and G. Somsen, *Recl. Trav. Chim. Pays-Bas*, **85**, 159 (1966); **86**, 263 (1967).
(28) R. C. Paul, et al., *Indian J. Chem.*, **3**, 300, 305 (1965).
(29) E. M. Arnett and D. R. McKelvey, *J. Amer. Chem. Soc.* **88**, 2598 (1966).
(30) Y. Wu and H. L. Friedman, *J. Phys. Chem.*, **70**, 501 (1966).
(31) H. Strehlow in "The Chemistry of Non-Aqueous Solvents," Vol. 1, J. J. Lagowski, Ed., Academic Press, New York, N.Y., 1966.
(32) Y. Wu and H. L. Friedman, *J. Phys. Chem.*, **70**, 2020 (1966).
(33) W. M. Latimer, K. S. Pitzer, and C. M. Slansky, *J. Chem. Phys.*, **7**, 108 (1939).
(34) H. L. Friedman, *J. Phys. Chem.*, **71**, 1723 (1967).
(35) C. V. Krishnan and H. L. Friedman, *J. Phys. Chem.*, **73**, 3934 (1969).
(36) C. V. Krishnan and H. L. Friedman, *J. Phys. Chem.*, **73**, 1572 (1969).
(37) C. V. Krishnan and H. L. Friedman, *J. Phys. Chem.*, **75**, 3606 (1971).
(38) C. V. Krishnan and H. L. Friedman, *J. Phys. Chem.*, **75**, 3598 (1971).
(39) M. Salomon, *J. Phys. Chem.*, **73**, 3299 (1969).
(40) M. Salomon, *J. Electroanal. Chem.*, **25**, 1 (1970).
(41) M. Salomon, *J. Electroanal. Chem.*, **26**, 319 (1970).
(42) T. W. Richards and F. Daniels, *J. Amer. Chem. Soc.*, **41**, 1732 (1919).
(43) E. A. Guggenheim, "Thermodynamics," 4th ed, North-Holland Publishing Co., Amsterdam 1959.
(44) (a) M. Salomon, *J. Phys. Chem.*, **74**, 2519 (1970); (b) C. M. Criss, *ibid.*, **78**, 1000 (1974).
(45) D. R. Cogley, J. N. Butler, and E. Grunwald, *J. Phys. Chem.*, **75**, 1477 (1971).
(46) A. J. Parker, *Chem. Rev.*, **69**, 1 (1969).
(47) O. Popovych, *Crit. Rev. Anal. Chem.*, **1**, 73 (1970).
(48) D. D. Wagman, et al., *Nat. Bur. Stand., Tech. Note, No. 270* (1968).
(49) "JANAF Thermochemical Tables," The Dow Chemical Co., Midland, Mich., August 1965 and addenda.
(50) W. M. Latimer, "Oxidation Pctentials," Prentice-Hall, Englewood Cliffs, N.J., 1952.
(51) J. P. Jesson and E. L. Muetteries, "Basic Chemical and Physical Data," Marcel Deker, New York, N.Y., 1969.
(52) R. S. Berry and C. W. Reimann, *J. Chem. Phys.*, **38**, 1540 (1963).
(53) L. Pauling, "The Nature of the Chemical Bond," 3rd ed, Cornell University Press, Ithaca, N.Y., 1960.
(54) R. Keller, et al., Final Report, Contract NAS 3-8521, Dec 1969.
(55) W. M. Latimer and C. M. Slansky, *J. Amer. Chem. Soc.*, **62**, 2019 (1940).

Kinetics of the Reaction between Iron(II) and Silver(I) Catalyzed by Silver Nuclei on Titanium Dioxide Surfaces

Paul D. Fleischauer* and John R. Shepherd

The Aerospace Corporation, El Segundo, California 90245   (Received March 18, 1974; Revised Manuscript Received August 21, 1974)

Publication costs assisted by the U. S. Air Force

The one-electron reduction of Ag(I) by Fe(II) in aqueous solution is catalyzed by nuclei of Ag metal on TiO_2 single-crystal and thin-film surfaces. The reaction results in the selective precipitation of silver on the catalytic nuclei, forming spherically shaped Ag particles. The kinetics of the reaction show that adsorption of Ag(I) on the substrate TiO_2 surface is an important step in the mechanism, the adsorption follows a Langmuir isotherm, and the rate-determining step of the reaction is the electron transfer from Fe(II) to adsorbed Ag(I). The net reaction is an electrochemical process in which the catalytic nucleus serves simultaneously as cathode for Ag(I) reduction and anode for Fe(II) oxidation.

I. Introduction

Electron-transfer reactions on surfaces of titanium dioxide (TiO_2) are important because of their role in practical applications of this material as a catalyst,[1] as a pigment,[2] and as an unconventional photographic material.[3] Investigations of the mechanisms of surface reactions on TiO_2 and on other metal oxides[4] have centered on the transport of charges at interfaces, adsorption on reactive surfaces, and changes in other physical and chemical parameters of such systems that occur during reaction. The objective of this study was to determine the kinetics and mechanism of the electron-transfer reaction between Fe(II) and Ag(I) ions when it is catalyzed by metallic silver nuclei on TiO_2 surfaces.

Titanium dioxide, slightly nonstoichiometric TiO_{2-x}, is a defect semiconductor. It is inert with respect to thermal electron transfer to adsorbed silver ions, but under near-ultraviolet irradiation, surface electrons are generated that can reduce Ag(I) with quantum efficiencies up to 0.1.[5] After such an irradiation, additional Ag(I) can be reduced thermally by treatment with an appropriate reducing agent such as Fe(II). This type of electron-transfer reaction, in which the oxidant can be precipitated at the catalytic sites, forming nuclei that grow into microscopic particles, is the basis of a type of photographic development process called "physical development."[6]

Various studies of the mechanism of physical development, where Ag(I) is reduced by numerous different reducing agents (developers), both organic and inorganic, have demonstrated that the process is most likely an electrochemical one in which a Ag nucleus behaves simultaneously as the cathode and anode.[7-9] Most previous studies have involved Ag particles (nuclei) embedded in a gelatin or in another polymer matrix. In such systems, the importance of adsorption of oxidant or reductant varies with the structure of the reductant.[7,9] In this work, the primary silver particles were formed on smooth surfaces of thin films and single crystals. Because they were in direct contact with reaction solutions, the measured kinetics describe the process at the solid–aqueous solution interface, with no complications due to a surrounding polymer matrix.

II. Experimental Section

A. Materials and Sample Preparation. All chemicals used were of reagent grade and were used as received. $AgNO_3$ and $Fe(NH_4)_2(SO_4)_2 \cdot 6H_2O$ were used to prepare the Ag(I) and Fe(II) solutions, respectively. The Fe(II) salt contained small amounts of Fe(III) impurity, which had an effect on the stability of the reagent solutions, but did not influence the kinetics of the catalyzed reaction.

Two different TiO_2 sample configurations, {001} oriented rutile single crystals and thin polycrystalline films on Pyrex or quartz substrates, were used for silver deposition. The Vernuiel-grown single crystals were prepared by an elaborate polishing procedure.[10] The thin films, which were used in most of the experiments, were prepared by reactive radiofrequency sputtering in a 20% oxygen–80% argon atmosphere at a total pressure of 7.5×10^{-3} Torr with the substrate at ~50°. The TiO_2 films were 0.3 to 0.5 μm thick and consisted of a mixture of rutile and anatase.[11] The films were colorless and had no visible surface features when observed under a microscope at 350× magnification.

A number of extraneous contaminants such as dust particles and minute deposits on glassware were found to catalyze the reaction between Fe(II) and Ag(I). Extreme care was therefore taken in the cleaning of reaction chambers (spectrophotometer cells), in the preparation of substrates, and in the purification of water used to prepare all solutions. Glassware was cleaned carefully with detergent and water and then with hot dichromate sulfuric acid cleaning solution. Samples were prepared for Ag deposition by extensive washing (soaking) with concentrated HNO_3 and, after water rinsing, with hot cleaning solution, again followed by copious water rinsing. The water used in all rinsing, as well as in the preparation of all solutions, was doubly distilled, once from alkaline $KMnO_4$. Commercial bottled water that had not been treated in this fashion gave traces of silver halide precipitate that were not visible to the eye, but that made the reaction solution degrade immediately.

B. Measurement Procedures. The nuclei that were to selectively catalyze the reaction between Fe(II) and Ag(I) were deposited onto TiO_2 sample surfaces by a photochem-

ical process that consisted of irradiation with 366-nm light of a sample in contact with Ag(I) solution.[5] After irradiation, a known volume of Fe(II) solution was injected into the Ag(I) solution with a 1- or 2-ml syringe, and the kinetics of the catalyzed reaction between Fe(II) and Ag(I) were followed by measuring the increase in the optical density of the chemically deposited Ag film. The TiO_2 substrate was mounted in a 1-cm spectrophotometer cell such that the beam of a Beckman Model DU passed through the exposed portion of the sample. The spectrophotometer was monitored continuously at 620 nm by the energy recording attachment (ERA) and a strip chart recorder. The optical density from Ag was obtained by subtracting contributions from the cell, solutions, and unexposed film. Mixing of the two solutions appeared to be complete within 1 to 2 sec because the recorder trace smoothed within that time. All of the Ag deposits, which were clearly visible but not opaque after reaction, were very uniform, indicating that no inhomogeneity existed in the solution during the reaction time. In most cases, only the very early stages of reaction (optical density <0.15) were examined; therefore, the reported results correspond to initial reaction rates.

Experiments were performed in a thermostated cell compartment, at room temperature (22–24°). The pH of the solutions, which was adjusted to the desired value with HNO_3, was measured with a Beckman Research pH meter.

The optical densities of Ag films on TiO_2 surfaces were calibrated in terms of the mass of deposited Ag by atomic absorption spectrophotometric analysis. Immediately after development, a sample of measured optical density was removed from solution, washed well with water, and soaked first in saturated KNO_3 and then in 0.01 M KNO_3 solution for 15 min each. After further water washing, the silver was dissolved off the TiO_2 with 0.05- to 0.1-ml concentrated HNO_3. The TiO_2 was washed with a few drops of water and again soaked in dilute HNO_3 for 5 min.[12,13] The HNO_3 and subsequent washings were collected in a 10- to 25-ml volumetric flask and diluted to the mark with water. A sample of this solution was then injected into the Model HGA 2000 heated graphite atomizer attachment of a Perkin-Elmer Model 303 atomic absorption spectrophotometer. The measured absorption of silver was recorded directly as optical density[14] and compared with a calibration curve that was prepared by an identical procedure with solutions of known amounts of $AgNO_3$.

III. Results and Discussion

Preliminary experiments demonstrated that the one-electron transfer reaction between Fe(II) and Ag(I) ions in aqueous solution is catalyzed by submicroscopic silver nuclei on the surfaces of TiO_{2-x} thin films and single crystals. This type of reaction has been reported previously for TiO_2 powder emulsion systems[7,15,16] and has been studied in some detail.[8,17] The reactivities of solutions of these reagents have been characterized in terms of the effects of their concentrations and of complexing agents on the electrode potentials of the two half-cell reactions. The rate of the silver-catalyzed reaction, although not on TiO_2 substrates, has also been related to the cell potential (ΔE) for the reduction reaction. At relatively high ΔE ($\geq \sim 100$ mV), the rate was comparatively insensitive to changes in this potential.[8] The experiments described here involved solutions with ΔE values in this insensitive, high region. Consequently, the influence of redox potentials on the rate of the

catalyzed reaction has not been considered in the following derivation of a reaction mechanism.

A. Effect of Complexing Fe(II). In contrast to their effects on the catalyzed reaction, cell potentials are important in determining the stabilities of the reagent solutions. One way to alter cell potentials is by the addition of complexing agents that change the effective concentrations and the electron configurations of reagents. In this study, a number of different Fe(II) and Ag(I) complex ions were examined in order to measure variations in solution reactivities and hence to determine the degree of catalytic specificity at the surface sites of the thin-film and crystal substrates. The various reaction pairs investigated and their specificity for the catalyzed reaction are listed in Table I.

Aqueous solutions of Fe(II) and Ag(I) are unstable from the standpoint of spontaneous electron transfer to produce a fine metallic silver precipitate. The rate of this spontaneous reaction is slowed, however, by the presence of complexing agents. The mechanism of oxidation of Fe(II) and the stability of its complexes depend on the ligands that are coordinated to the metal ion and on the identity of the oxidizing agent. Thus, for example, for $Fe(phen)_3{}^{2+}$, where the metal has the low-spin d^6 electronic configuration, oxidation by $S_2O_8{}^{2-}$ obeys second-order kinetics and is relatively fast compared with ligand dissociation, whereas oxidation by $P_2O_8{}^{4-}$ is a first-order reaction whose rate is approximately equal to that of dissociation.[18]

The data of Table I indicate that neither of the two low-spin complexes of Fe(II) studied, *i.e.*, No. 11 through 13, demonstrated any observable reactivity with Ag(I). This was true for both the homogeneous and the catalyzed reaction. In the case of $Fe(phen)_3{}^{2+}$ and presumably $Fe(en)_3{}^{2+}$, the oxidation potentials for the undissociated complexes are unfavorable for reaction with Ag^+ and there was no evidence of dissociation during the time of our experiments.

On the contrary, aqueous Fe(II) ions and their high-spin citric acid (HCit) complexes reduce Ag(I) with reaction rates that can be controlled by adjusting the conditions of the solutions. The difference between the rate of the catalyzed reduction of Ag(I) and that of the homogeneous reaction is small for solutions of $Fe(NH_4)_2(SO_4)_2$ in the absence of HCit. However, the addition of HCit and adjustment of the solution pH to approximately 1 slow the homogeneous reaction such that the kinetics of the surface process are readily discernible. The pH of the reaction solutions cannot be reduced to this value in the absence of HCit because the Fe(II) is rapidly air oxidized, and reaction with Ag(I) is slow, apparently because of the high Fe(III) concentration, which causes a substantial decrease in the cell potential.[8] The presence of HCit does not appear to affect the reactivity of Ag(I), although the low pH drastically alters the adsorption properties of Ag(I) on the TiO_2 surface.[13,19] The formation constants of Ag(I)–citrate complexes are considerably smaller than the constants for Fe(II) complexes.[20]

B. Kinetics and Mechanism. Some typical kinetic plots of the increase in optical density due to the deposition of silver on TiO_{2-x} thin films *vs.* reaction time are shown in Figure 1. The interpretation of these plots and the data of Table II and the postulation of a mechanism for this silver-metal-catalyzed electron-transfer reaction between Fe(II) and Ag(I) on TiO_2 surfaces are based on three important considerations: (1) the order of the reaction with respect to the catalyst, *i.e.*, the mass of silver; (2) the orders with respect to reagents Ag(I) and Fe(II); and (3) comparisons of these results with those from independent adsorption *and*

TABLE I: Fe(II) and Ag(I) Complexes Examined for Catalytic Specificity[a]

Fe(II)	Ag(I)	Homogeneous reaction	Surface reaction
$Fe(NH_4)_2(SO_4)_2$	$AgNO_3$	M	F
$Fe(NH_4)_2(SO_4)_2$ + surfactant	$AgNO_3$	F	F
$Fe(NH_4)_2(SO_4)_2$	$Ag(S_2O_3)_2^{3-}$	ppt(VF?)	
$Fe(NH_4)_2(SO_4)_2$	$Ag(SO_3)_2^{3-}$	ppt(VF?)	
$Fe(NH_4)_2(SO_4)_2$	$Ag(NH_3)_2^+$	VF	
$Fe(NH_4)_2(SO_4)_2$	$Ag(CN)_2^-$	M	M
$Fe(EDTA)^-$	$Ag(CN)_2^-$	M	M
Fe(II)/HCit, 1:3	$Ag(CN)_2^-$	ppt	
Fe(II)/HCit, 1:3[b]	$AgNO_3$	S	F
Fe(II)/HCit, 0.5 M[a]	$AgNO_3$	S	F
$Fe(en)_3^{2+}$	$Ag(CN)_2^-$	VS	VS
$Fe(en)_3^{2+}$	$AgNO_3$	VS	VS
$Fe(phen)_3^{2+}$	$AgNO_3$	VS	VS

[a] EDTA ≡ ethylenediaminetetraacetic acid; en ≡ ethylenediamine; phen ≡ 1,10-phenanthroline; VF, very fast ($t_{1/2} < {\sim}5$ sec); F, fast ($t_{1/2} = 5-30$ sec); M, moderate ($t_{1/2} = 30-90$ sec); S, slow ($t_{1/2} = 1.5-5$ min); VS, very slow ($t_{1/2} > 5$ min). [b] pH of solution after mixing, 1.2; for pH >1.2, homoeneous reaction M to F.

photochemical studies of Ag(I) on the same surfaces. The net reaction

$$Fe(II) + Ag(I) \xrightarrow{Ag} Fe(III) + Ag \qquad (1)$$
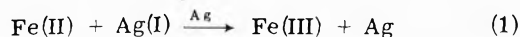
is an autocatalytic process; it is catalyzed by product silver metal. As such, the mechanism and rate law are considerably more complex than the situation that is indicated by this reaction.

1. Influence of Silver Particle Shape. A general form of the rate law for reaction 1 may be written as follows

$$dM(Ag)/dt = k_{app}f(C_{Ag(I)})g(C_{Fe(II)})M(Ag)^j \qquad (2)$$

$M(Ag)$ is the mass of product silver deposited, k_{app} is an apparent rate constant that contains terms such as the specific rate constant and the density of silver in the nuclei, $f(C_x)$ and $g(C_y)$ represent functions of the solution concentration of species x(y), and j is the order of the reaction with respect to the catalyst. Integration of eq 2 yields

$$\frac{1}{1-j}\left[M(Ag)^{1-j} - M_0(Ag)^{1-j}\right] =$$
$$k_{app}f(C_{Ag(I)})g(C_{Fe(II)})t \qquad (3)$$

where $M(Ag)$ is the mass of product silver at time t, and $M_0(Ag)$ is the mass at the onset of the reaction (the amount deposited in the exposure). The quantities of Ag(I) and Fe(II) that are reduced and oxidized, respectively, are extremely small compared with the solution concentrations. Thus, the effective changes in reagent concentrations during reaction are negligible. The optical densities shown in Figure 1 are proportional to the mass of deposited silver; the relationship is 1.5×10^{-4} g(Ag) D^{-1} cm^{-2}, where D ≡ optical density unit.

As shown in Figure 1b and Table II, for sufficiently high reagent concentrations, a very good fit to the data is obtained, for the early stages of the reaction, if $j = 2/3$. However, as the reaction proceeds, the two-thirds dependence does not hold; the rate of increase in silver mass decreases, and the value of j approaches zero.

For an autocatalytic reaction where the catalyst is a solid, it is not unusual to have a reaction order of two-thirds. Such a situation indicates that an important vari-
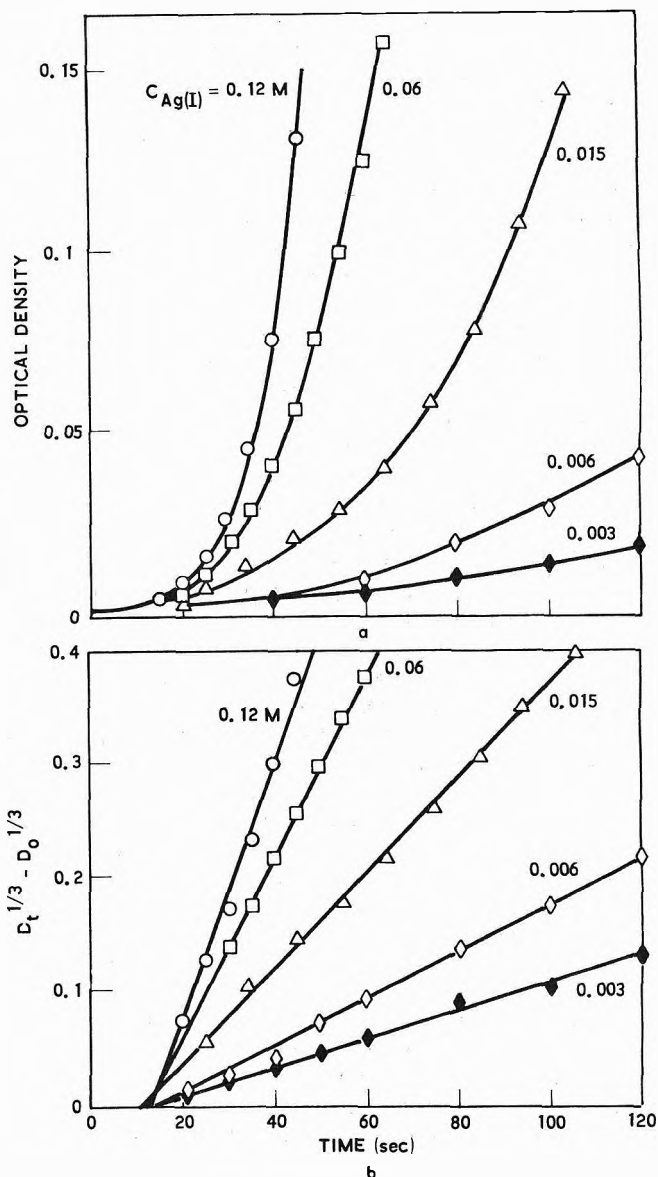
Figure 1. Chemical deposition of silver on photonucleated TiO_{2-x} thin films. (a) Optical density at 620 nm as a function of reaction time. The ordinate intercept is the initial density from nucleation D_0. (b) Rate plots of the cube root of density vs. reaction time: $C_{Fe(II)} = 0.0125$ M, $C_{Ag(I)}$, as indicated, pH = 1.2, $C_{HCit} = 0.5$ M.

able in the catalytic process is the surface area of the catalyst particles, and that the shape of the growing (during reaction) particles is nearly spherical. The normal crystal structure for silver metal is face-centered cubic, but it is considered unlikely that the particles grow as cubes. It is more probable that spherical or hemispherical particles are involved, and this shape is assumed. This assumption has been supported by electron microscopy.[21]

The decrease in the value of j as the reaction proceeds suggests that the particles expand radially until they grow together, forming a continuous silver film. At this stage, apparently, the surface area of the silver changes very little; the film simply increases its thickness as the reaction continues, and the reaction order j becomes zero.

There are other possible geometrical arrangements that could have prevailed during this reaction. Their presence also would have been indicated by the order of the reaction with respect to the mass of silver. For example, there is evi-

TABLE II: Kinetic Data for Fe(II) + Ag(I) Reaction[a]

$C_{Ag(I)}$, M	$C_{Fe(II)}$, M	pH	C_{HCit}, M	$10^2 k_{meas}$, $D^{1/3}$ sec^{-1}
Thin Films				
0.12	0.015	1.2	0.045	0.74
0.06	0.015	1.2	0.045	0.69
0.03	0.015	1.2	0.045	0.68
0.015	0.015	1.2	0.045	0.55
0.015	0.0375	1.2	0.1125	1.58
0.015	0.025	1.2	0.075	0.62
0.015	0.005	1.2	0.015	0.14
0.12	0.0125	1.2	0.50	1.2
0.06	0.0125	1.2	0.50	0.85
0.015	0.0125	1.2	0.50	0.42
0.006	0.0125	1.2	0.50	0.20
0.003	0.0125	1.2	0.50	0.11
0.015	0.05	1.2	0.50	2.5
0.015	0.025	1.2	0.50	1.5
0.015	0.005	1.2	0.50	0.26
Single Crystal				
0.06	0.0125	1.2	0.50	1.6
0.03	0.0125	1.2	0.50	0.18
0.015	0.0125	1.2	0.50	0.78
0.0075	0.0125	1.2	0.50	0.52

[a] Each k value is an average of two or more runs.

Figure 2. Dependence of measured rate constants on solutions Ag(I) ($\triangle$, $\bigcirc$) and Fe(II) ($\square$) concentrations.

dence that, in the photochemical deposition of silver on TiO_2, Ag(I) is reduced on the TiO_2 surface with subsequent agglomeration of metal to form pancake-shaped islands. If Fe(II) reduction of Ag(I) had produced similarly flat-shaped particles, the increase in particle area would have been directly proportional to M(Ag), and j would have equaled unity until the entire TiO_2 surface again became covered with silver. [The postulation of spherical growth of silver particles permits the expression of k_{app} in terms of geometrical parameters, viz., $k_{app} = (1/\rho(2/3\pi)^{1/2})^{2/3}k$, where ρ is the density of the silver particle and k is the specific rate constant in units of A(TiO_2)/A (Ag) M^{-1} sec^{-1}; A (x) is the surface area of x.]

This silver deposition in the early stages of reaction, then, appears to consist of spherically shaped metal particles growing on the oxide surface, with the rate of Ag(I) reduction constant in all directions. Although the reaction rate is proportional to the surface area of the particles, there are additional factors that determine the details of the mechanism. The most significant of these is the dependence of the reaction rate on the concentration of reagent Ag(I).

2. Adsorption of Reagents. The dependence of the measured rate constant for the catalyzed reaction on solution Ag(I) and Fe(II) concentrations is shown in Figure 2. The variation with Ag(I) concentration is nonlinear; it increases rapidly at first then reaches a limiting rate as $C_{Ag(I)}$ increases. The dependence on Fe(II) concentration is first-order (linear) under the conditions of our experiments. The integrated rate expression derived from these data is

$$M(\text{Ag})^{1/3} - M_0(\text{Ag})^{1/3} = \tfrac{1}{3} k_{app}\left[\frac{abC_{Ag(I)}}{1 + bC_{Ag(I)}}\right]C_{Fe(II)}t \quad (4)$$

where a and b are empirical constants.

This expression of the Ag(I) concentration dependence is analogous to that reported for the photolytic deposition process[5] and can be interpreted to indicate that Ag(I) is adsorbed onto the silver–TiO_2 surface prior to (and during) reaction, that the adsorption follows a Langmuir isotherm, and that only adsorbed Ag(I) is reduced by Fe(II). Lang-

muir plots (reciprocal of the observed rate constant vs. reciprocal of the Ag(I) solution concentration) are shown in Figure 3 for the thin-film and single-crystal surfaces. The values of the product $k_{app}a$ and of the constant b may be evaluated from the intercept and the intercept-to-slope ratios, respectively.
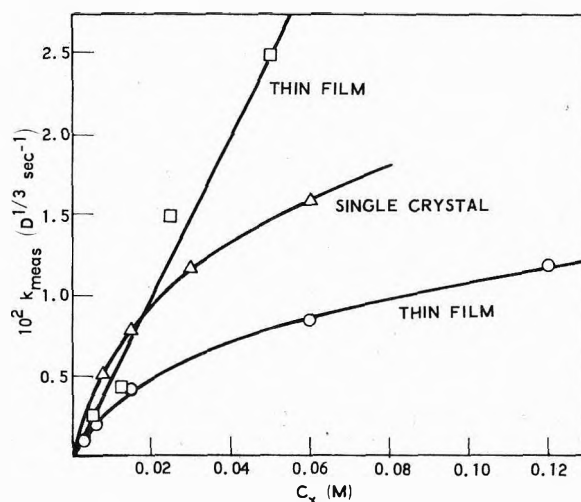
The reaction is first order in reagent Fe(II) in all cases studied, indicating that Fe(II) is either not adsorbed or adsorbed very weakly. Thus, the following mechanism is proposed to explain the rate expression of eq 4

$$\text{Ag(I)} \underset{}{\overset{b}{\rightleftharpoons}} \text{Ag(I)}_{ads} \quad (5)$$

$$\text{Fe(II)} + \text{Ag(I)}_{ads} \xrightarrow{A(Ag)} \text{Fe(III)} + \text{Ag} \quad (6)$$
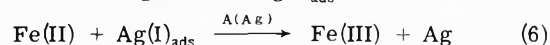
By assuming that reaction 6 is rate determining and substituting the Langmuir dependence for the concentration of adsorbed Ag(I), one obtains eq 4. The constant b becomes the Langmuir adsorption equilibrium constant, and a is the number of adsorption sites per unit area of active surface.

There is at least one other mechanism that could explain the rate law of eq 4. That mechanism would involve, as the rate-limiting step, the dissociation of an Fe(II)–citrate complex with a subsequent fast electron transfer to Ag(I), again on the surface of silver nuclei. (See, for example, the mechanism given in ref 18.) For three reasons, we believe that this dissociation mechanism is not involved in the catalyzed reaction: (1) the values of b calculated from the kinetics results agree quite well with those from independent adsorption studies,[13] (2) the high-spin Fe(II)–citrate complexes are quite labile and should undergo rapid ligand dissociation, and (3) there is no evidence for a retardation in rate in the low Ag(I) concentration region as HCit concentration is increased.

The important features of the proposed mechanism, *i.e.*, the dependence of reaction rate on the Ag surface area and the first-order kinetics in Fe(II), are analogous to the electrochemical description of such a reaction.[22] There is, however, one essential difference between the systems studied here and those reported in the photographic literature: the nature of the Ag(I) adsorption and its influence on the electron-transfer reaction.

There are two surfaces, silver particles and TiO_{2-x} substrate, on which Ag(I) ions can be adsorbed. For each sur-

Paul D. Fleischauer and John R. Shepherd
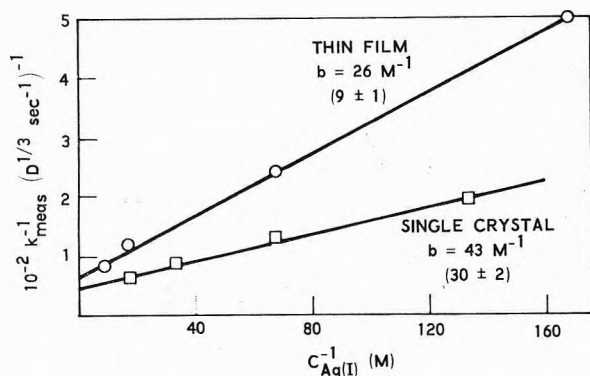
Figure 3. Langmuir plots for reduction of Ag(I) by Fe(II) on thin film and single crystal TiO_2 surfaces. $C_{Fe(II)} = 0.0125$ M, pH = 1.2, and $C_{HCit} = 0.5$ M. Values of b in parentheses are from ref 13.

Figure 4. Surface-catalyzed reduction of Ag(I) by Fe(II).

face, there is an adsorption isotherm that depends on various chemical and physical properties of the material. These properties include the number and type of bonding sites and the surface potential, which depends on the electrical properties of the material, *e.g.*, conductivity, space charge. Within the precision of our kinetic data, a single-step Langmuir isotherm is sufficient to describe all applicable adsorption behavior. This result means that either the isotherms for the two surfaces (Ag and TiO_{2-x}) are the same, or that adsorption on one of the surfaces dominates and controls the concentration of the reagent Ag(I) in the region of the reaction site.

Apparently, the actual reduction of Ag(I) occurs at the silver surface, as evidenced by the aforementioned surface-area dependence. However, the adsorption of reagent Ag(I) is determined by equilibration with Ag(I) solution before commencement of the reduction, *i.e.*, before the addition of Fe(II). For the initial stages of reaction, for which these kinetics are applicable, the surface area of TiO_2 exposed to the solution is approximately 50 to 100 times greater than that of silver. In addition, for a given set of solution conditions, the adsorption behavior, *i.e.*, the value of b, is very similar to that obtained in independent adsorption-desorption measurements on unexposed and exposed or nucleated TiO_2 surfaces; the adsorption constant appears to be unaffected by the small amounts of silver introduced by exposure.[13] All of these observations suggest that the adsorption isotherm that determines the concentration of Ag(I) for reactions with Fe(II), eq 6, is that for the TiO_{2-x} substrate surface.

The adsorption isotherm

$$\frac{N_{Ag(I)}}{N_s} = \frac{bC_{Ag(I)}}{1 + bC_{Ag(I)}} \tag{7}$$

where $N_{Ag(I)}$ and N_s ($\equiv a$) are the number of adsorbed silver ions and the number of adsorption sites, respectively, is determined essentially by the properties of the oxide surface. It is interesting to note the variation in the number of adsorption sites with variations in the substrate TiO_2 surface. The value of a cannot be determined directly from the kinetics, but the product $k_{app}a$ (eq 4) is obtained from the limiting region of the Ag(I) concentration dependencies of k_{meas} at constant $C_{Fe(II)}$. As shown in Figure 2, this product is quite different for the two different TiO_2 samples; the values for the films are consistently lower than for the single crystals. This relative ordering of reactivities is the same as the expected ordering of the surface areas of
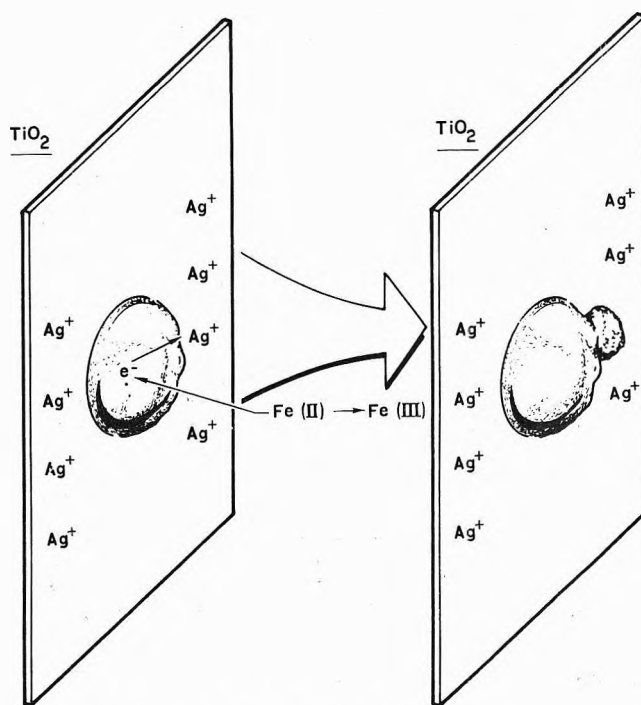
the TiO_2 surfaces, *i.e.*, the faster limiting rates are obtained on samples with larger surface areas.

It is possible that the adsorption sites in the isotherm for this electron-transfer reaction are actually the silver nuclei on the oxide surface. However, the variation in limiting rates with different surfaces and the similarity between the adsorption constants (the b values in eq 4) obtained in these kinetics studies and those from the adsorption-desorption studies[13] support the interpretation that the adsorption sites in the rate expression (4) are those of the bare TiO_2 surface, *i.e.*, the surface with no predeposited silver. The number of these sites ($\sim 2.5 \times 10^{15}$ cm^{-2})[13] is 10^3 to 10^4 cm^{-2} larger than the number of silver nuclei.[21]

IV. Conclusions

Results of these studies of the kinetics and mechanism of the one-electron reduction of Ag(I) by Fe(II), catalyzed by silver nuclei on TiO_2 surfaces, show that the overall reaction consists of the two half-cells as shown in Figure 4. An anodic reaction consists of diffusion of Fe(II) up to a silver particle and injection of an electron. Simultaneously, a Ag(I), adsorbed on the TiO_2 at the edge of the silver particle, captures the injected electron in the cathodic step. After reduction, the silver atom can diffuse on the surface of the particle until it is bound in the silver lattice. The electron conduction is believed to occur through the silver particle because it has a much higher conductivity than does TiO_2, which is an insulator. The alternative possibility, reaction in solution followed by precipitation of silver on the nuclei, is ruled out because of the nature of the Ag(I) concentration dependence and the agreement of the results with adsorption studies.[13]

References and Notes

(1) M. Che, C. Naccache, and B. Imelik, *J. Catal.*, **24**, 328 (1972).

(2) T. Purcell and R. A. Weeks, *J. Chem. Phys.*, **54**, 2800 (1971).

(3) G. L. McLeod, *Photogr. Sci. Eng.*, **13**, 93 (1969).

(4) J. Cunningham, J. J. Kelly, and A. L. Penny, *J. Phys. Chem.*, **75**, 617 (1971); H. J. Price, *Photogr. Sci. Eng.*, **14**, 391 (1970); P. J. Boddy, *J. Electrochem. Soc.*, **115**, 199 (1968); R. A. L. Vanden Berghe, F. Cardon, and W. P. Gomes, *Surface Sci.*, **39**, 368 (1973).

(5) P. D. Fleischauer, H. K. A. Kan, and J. R. Shepherd, *J. Amer. Chem. Soc.*, **94**, 283 (1972).

(6) Physical development, where the source of metal ions for precipitation is the developer solution, is distinguished in photographic literature from the more common "chemical or direct development," where the source of the oxidant is the lattice of the exposed grain in the photographic emulsion.[7]

(7) T. H. James in "The Theory of the Photographic Process," 3rd ed, C. E. K. Mees and T. H. James, Ed., Macmillan, New York, N.Y., 1966, Chapter 15.

(8) H. Jonker, A. Molenaar, and C. J. Dippel, *Photogr. Sci. Eng.*, **13**, 38 (1969).

(9) D. C. Shuman and T. H. James, *Photogr. Sci. Eng.*, **15**, 42 (1971).

(10) P. D. Fleischauer and A. B. Chase, *J. Phys. Chem. Solids*, **35**, 1211 (1973).

(11) L. F. Goldstein, unpublished results.

(12) These soaking procedures were necessary in order to remove Ag(I) adsorbed on the surface of TiO_2. The influence of adsorption on reaction rates is discussed later in this paper, and more details will be presented in a subsequent paper.[13]

(13) P. D. Fleischauer and J. R. Shepherd, Presented at the 9th Western Regional Meeting of the American Chemical Society, San Diego, Calif., 1–3 Nov 1973; submitted for publication in *J. Phys. Chem.*

(14) J. R. Shepherd and H. Hedgpeth, *Rev. Sci. Instrum.*, **44**, 338 (1973).

(15) H. Jonker, C. J. G. F. Janssen, C. J. Dippel, Th. P. G. W. Thijssens, and L. Postma, *Photogr. Sci. Eng.*, **13**, 45 (1969).

(16) E. J. DeLorenzo, L. K. Case, E. M. Stickles, and W. A. Stamoulis, *Photogr. Sci. Eng.*, **13**, 95 (1969).

(17) R. Matejec and E. Moisar, *Photogr. Korresp.*, **100**, 39 (1964).

(18) E. Chaffee, Ph.D. Dissertation, Brown University, 1971; A. A. Green, J. O. Edwards, and P. Jones, *Inorg. Chem.*, **5**, 1858 (1966).

(19) A novel method involving the use of surfactants for stabilizing the type of solutions studied here has been reported.[8] However, this method is unsatisfactory for use with TiO_2 thin-film substrates because the same mechanism that stabilizes the solution, *i.e.*, interaction of the surfactant with nuclei that tend to form spontaneously in solution, would prevent reaction at the surface catalytic nuclei since these nuclei are not masked from the surfactant by a gelatin binder.

(20) L. G. Sillan and A. E. Martell, "Stability Constants of Metal-Ion Complexes," The Chemical Society, London, 1964.

(21) P. D. Fleischauer, unpublished results.

(22) R. B. Pontinus, R. G. Willis, and R. J. Newmiller, *Photogr. Sci. Eng.*, **16**, 406 (1972).

Hydrogen Bonding. IV. Correlation of Infrared Spectral Properties with C–H···X Hydrogen Bonding and Crystal Habit in Tetramethylammonium Ion Salts[1]

Kenneth M. Harmon,* **Irene Gennick,**[2a,b] **and Susan L. Madeira**[2a]

Department of Chemistry, Oakland University, Rochester Michigan 48063 *(Received January 21, 1974; Revised Manuscript Received June 14, 1974)*

Examination of the solid state infrared spectrum of the tetramethylammonium cation in twelve salts shows that three areas of the readily accessible sodium chloride region are sensitive to crystal environment, and demonstrates the existence of cation C–H to anion hydrogen bonding in a number of salts such as the fluoride, chloride, bromide, iodide, perchlorate, and borohydride. The C–H stretching region gives characteristic hydrogen bonding shifts in the above salts; this effect is particularly intense in the fluoride. The C–H deformation modes in the 1400–1500-cm^{-1} region and the N–C breathing band near 950 cm^{-1} show perturbations which can be qualitatively used to identify crystal type, and which can be reasonably explained by site symmetry and factor group analysis considerations. Intensity changes in some absorptions can be empirically related to steric size and packing effects. Infrared spectra are correlated with known crystal structures and bond distances for seven of the salts.

Introduction

Although C–H···X hydrogen bonding has been demonstrated in a number of instances[3–6] in which the carbon in question is substituted with electron-withdrawing groups, there have not been reports of such hydrogen bonding involving the α hydrogens of tetraalkylammonium ions except in the case of a number of cholinergic compounds,[7] where an intramolecular C–H···O bond has been suggested.

We were interested in investigating the nature, extent, and spectroscopic detection of possible hydrogen bonding from simple tetraalkylammonium ions to anions for two reasons. In the first place, as part of a continuing research program on novel water–anion moieties containing very strong hydrogen bonds,[8,9] we have been examining hydrates of tetramethylammonium fluoride and hydroxide,[10] and it is essential to the elucidation of the structures of these compounds and the interpretation of their unusual infrared spectra to know the extent to which the cation interacts with the anion–water species present. Secondly, we are initiating an investigation of the specific interactions of biologically important quaternary cholinergic compounds with solvent water and protein substrate, and wish to determine the extent to which hydrogen bonding, rather than the usually proposed electrostatic interactions,[7] may be operative; simple tetramethylammonium ion salts can serve as model systems for such compounds.

TABLE I: Infrared Spectra of Tetramethylammonium Ion Salts[a]

Anion	ν_sC–H, cm^{-1} [b]		δ_{as}C–H, cm^{-1} [b]	δ_{sym}C–H, cm^{-1} [b]		ν_{rock}CH$_3$, cm^{-1} [c]		ν_BC–N, cm^{-1} [c]	
F$^-$	3200–2500(bs)		1508(vs)	1418(m)		1263(w)		965(vs)	950(w)
Cl$^-$	3050(s)	2920(bm)	1495(vs)	1410(m)	1402(m)	1306(w)	962(m)	952(vs)	922(sh)
Br$^-$	3020(s)	2940(bm)	1488(vs)	1404(m)	1398(m)	1305(w)	958(m)	949(vs)	922(sh)
I$^-$	3010(s)	2930(bm)	1484(vs)	1405(m)	1399(m)	1298(w)	952(m)	946(vs)	919(m)
ClO$_4^-$	3048(s)	2975(bm)	1492(vs)	1416(sh)	1411(m)			951(vs)	922(w)
BH$_4^-$	3030(s)	2960(bm)	1489(vs)	1409(m)	1401(m)	1300(w)	952(sh)	948(vs)	920(sh)
CdCl$_3^-$	3035(s)	2970(m)	1484(vs)	1420(m)		1290(m)	970(sh)	950(vs)	920(sh)
SiF$_6^{2-}$	3045(s)	d	1507(vs)	1437(m)^e				968(vs)	
SnCl$_6^{2-}$	3038(s)	2970(vw)	1490(vs)	1420(m)^f		1296(m)		952(vs)	
SnBr$_6^{2-}$	3038(s)	2965(vw)	1483(vs)	1419(s)^g		1294(s)		952(vs)	
Ph$_4$B$^-$	3060(s)		h	h		h		950(vs)	
SbF$_6^-$	3060(s)	i	1490(vs)	1420(m)				949(vs)	

[a] Symbols used: (vw) very weak, (w) weak, (m) medium, (s) strong, (vs) very strong, (bw) broad weak, (bm) broad medium, (sh) shoulder. [b] Fluorolube mulls. [c] Nujol mulls. [d] Complex set of six weak bands also present. [e] Peak at 1477(m) also present. [f] Peak at 1452(m) also present. [g] Peak at 1448(s) also present. [h] Region obscured by phenyl bands. [i] Region not well defined; salt appears to react with Fluorolube.

We also wished to see if it would be possible to use infrared spectra of solid salts to derive structural information about the hydrate salts mentioned above. It is extremely difficult, if not impossible, to prepare single crystals of these species suitable for diffraction studies; the available methods of preparation give microcrystalline powders. If the infrared spectrum of the tetramethylammonium ion in crystalline salts could be correlated with known crystal structures, it might then be possible to predict the crystal habit of salts where diffraction data are not available, and most particularly to determine if the tetramethylammonium fluoride and hydroxide monohydrates contain discrete anions in an identifiable crystal environment.

Experimental Section

A. *Materials*. Tetramethylammonium fluoride,[11,12] hexachlorostannate(IV),[13] hexabromostannate(IV),[13] and trichlorocadmate(II)[14] were prepared by previously reported routes. Eastman Kodak White Label tetramethylammonium chloride, bromide, iodide, and borohydride were used as supplied. Tetramethylammonium hexafluorosilicate(IV) was prepared by addition of the chloride to a solution of pure silica in 48% hydrofluoric acid, followed by precipitation with ethanol; the presence of the hexafluorosilicate(IV) anion was confirmed by its infrared spectrum[8,9] and the absence of chloride by a negative test with silver nitrate. Tetramethylammonium perchlorate, tetraphenylborate, and hexafluoroantimonate(V) were made by adding the calculated amount of perchloric acid, sodium tetraphenylborate, and 65% hexafluoroantimonic acid, respectively, to Eastman Kodak White Label tetramethylammonium hydroxide, 10% in water; these salts precipitate from aqueous solution. Characteristic anion bands were present in each salt.

All of the above salts were dried at 56° and 0.1 Torr over phosphorus pentoxide for several days before use, and subsequently only handled in a glove box under dry nitrogen; the absence of water or other solvent was confirmed in each case by infrared spectra. The anhydrous fluoride removes water from even slightly filmed phosphorus pentoxide; mulls free of water can be prepared only in a glove box undergoing dynamic scrubbing with freshly activated molecular sieve columns.

B. *Measurements*. Infrared spectra were recorded on a Beckman IR-12 spectrophotometer using NaCl plates;
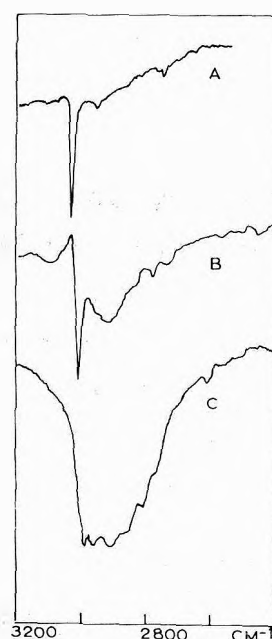
Figure 1. C–H stretching region (Fluorolube mulls) of tetramethylammonium ion salts: (A) hexabromostannate, (B) chloride, (C) fluoride; approximate relative concentrations of A = C = ½B.

mulls were prepared in the glove box using predried[15] Nujol or Fluorolube.

Results and Discussion

Table I lists the principal infrared absorptions of the tetramethylammonium ion in the spectra of 12 solid salts; the assignment of bands is discussed below.

In Table II seven salts of known crystal structure are classified as to the appearance of the infrared spectrum, and this classification is correlated with crystal structure information either reported directly in the literature or derived geometrically by us from available data. The correlation discussions which follow are primarily based on the information and references to crystal structures contained in Table II. In Table III infrared spectral data for five salts are used to predict information about the nature of the solid state of the salts.

Assignment of Fundamental Infrared Frequencies of the Tetramethylammonium Cation. Infrared and Raman

TABLE II: Correlation of Infrared Spectral Properties with Crystal Structure Data for Tetramethylammonium Ion Salts

Anion	Classification of ir bands					Crystal structure parameters[d]			Symmetry parameters[d]			
	ν_sC–H[a]	δ_{sym}C–H[b]	ν_{rot}[c]	ν_{rock}CH$_3$[c]	ν_BC–N[b]	r_{obsd}C–X[e]	r_{calcd}C–X[g]	$0.5r_{min}$N–N[h]	Crystal[j]	Cation[k]	Site[l]	Unit cell[m]
Cl$^-$	B	D	–	–	T	3.78	3.61	2.75	Tet	Dis	D_{2d}	D_{4h}^7
Br$^-$	B	D	–	–	T	3.70	3.75	2.74	Tet	Dis	D_{2d}	D_{4h}^7
I$^-$	B	D	–	–	T	3.79	3.96	2.81	Tet	Dis	D_{2d}	D_{4h}^7
ClO$_4^-$	B	S	–	–	D	3.04	3.20	2.93	Tet	Undis	D_{2d}	D_{4h}^7
SiF$_6^{2-}$	N	S	+	+	S	3.39	3.16	3.94	Tet	Undis	S_4	C_{4h}^5
SnCl$_6^{2-}$	N	S	+	+	S	3.79	3.61	4.55	Cub	Undis	T_d	O_h^5
CdCl$_3^-$	B	S	–	+	S	3.54	3.61	3.30	Hex	Dis	n	C_{6h}^2

[a] Hydrogen bonded (B) or nonhydrogen bonded (N). [b] Sharp singlet (S), doublet or incipient doublet (D), or triplet or incipient triplet (T). [c] Absent or barely detectable (−) or present and very strong (+). [d] Based on data taken from R. W. G. Wyckoff, "Crystal Structures," 2nd ed, Interscience, New York, N.Y., 1963: Vol. 1, pp 107–109 (Cl$^-$, Br$^-$, I$^-$, ClO$_4^-$); Vol. 5, pp 149–150 (SiF$_6^{2-}$, SnCl$_6^{2-}$), 158–160 (SiF$_6^{2-}$, SnCl$_6^{2-}$), and B. Morosin, *Acta Crystallogr., Sect. B*, **28**, 2303 (1972), (CdCl$_3^-$). [e] Closest approach of methyl carbon to an electronegative anion atom; in halide salts r_{obsd} derived geometrically using C–N bond length of 1.55 Å (values in Å). [f] B. Morosin and E. C. Lingafelter, *Acta Crystallogr.*, **12**, 611 (1959). [g] Calculated with ionic radii from I. Pauling, "The Nature of the Chemical Bond," 3rd ed, Cornell University Press, Ithaca, N.Y., 1960, p 514, and the value of 1.8 Å as r_{vdw} of carbon (see Discussion) (values in Å). [h] One-half of the closest N–N distance between adjacent cations; to be compared with the 3.37-Å spherical radius of the tetramethylammonium ion[i] (values in Å). [i] K. M. Harmon, S. D. Alderman, K. E. Benker, D. J. Diestler, and P. A. Gebauer, *J. Amer. Chem. Soc.*, **87**, 1700 (1965). [j] General classification of crystal lattice: tetragonal (Tet); cubic (Cub); or hexagonal (Hex). [k] Nature of bond angles in cation tetrahedral (Undis) or distorted from tetrahedral (Dis). [l] Site symmetry of cation location. [m] Symmetry space group of unit cell. [n] Cations disordered.
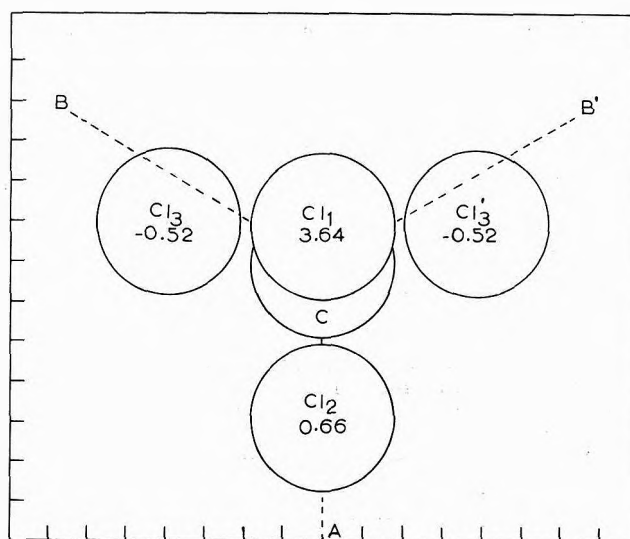

Figure 2. Arrangement of chlorine neighbors about a methyl carbon in tetramethylammonium chloride. The plane of the paper passes through the center of the carbon atom, and is orthogonal to the axis of the C–N bond; the nitrogen lies below the carbon. The numbers on the chlorines indicate the distance above or below this plane in ångströms. We assume one hydrogen lies on axis A and is hydrogen bonding to Cl$_2$; the other two lie on B and B' and are not directed toward chlorines. The C–H bonds make an angle of about 20° above the paper. The grid is in ångströms.

spectra of tetrahedral M(CH$_3$)$_4$ molecules have been discussed in considerable detail.[16–21] Species of this type have seven infrared active T$_2$ bands under T_d symmetry. Two of these bands are classified as C–H stretching modes, two as methyl group deformations, one as a methyl group rock, and two as vibrations of the MC$_4$ skeleton. Assignment of fundamentals to specific bands in the infrared spectrum of the tetramethylammonium ion has been sometimes tentative since data were taken either from solution Raman spectra[16,17] or solid state infrared spectra[22–24] where the spectra can be more complex. We find that the tetramethylammonium ion in aqueous solution, where it should show undisturbed T_d symmetry, shows six sharp singlet infrared bands in the sodium chloride region of the spectrum; this, coupled with the positive identification of the NC$_4$ modes by isotopic substitution of ^{15}N in the cation,[25] allows a clear correlation of the solid state spectral bands with the T_d fundamentals, and essentially supports the assignments of Bottger and Geddes[26] based on the solid state infrared spectrum of the chloride. Table IV lists the fundamental bands in the infrared spectrum of the cation, the designations used in this discussion, and the frequency values observed in our solution spectrum.

Cation C–H to Anion Hydrogen Bonding. In tetramethylammonium ion salts of anucleophilic anions such as hexafluorosilicate, hexachloro- and hexabromostannate(IV), and tetraphenylborate the principal band in the ν_s region appears as a sharp singlet; however, in the spectra of salts with anions which can act as proton acceptors in hydrogen bonding, such as the halides and the perchlorate[15] ion, a new broad band appears at higher wavelength (Figure 1). In the extreme case of the fluoride this band is an intense, structured absorption over 700 cm^{-1} in width (Figure 1). The observed increases in intensity[5] and changes in spectral shape and appearance[4] are essentially identical with those previously observed for C–H hydrogen bonding.

Examination of Table II shows that four salts with hy-

TABLE III: Predicted Crystal Habit for Tetramethylammonium Ion Salts Based on Infrared Spectral Data[a]

Anion	Classification of ir bands					Symmetry parameters	
	ν_aC–H	δ_{sym}C–H	ν_{rot}	ν_{rock}CH$_3$	ν_BC–N	Crystal	Cation
F$^-$	B	S	–	–	D	Tet	Undis
BH$_4{}^-$	B	D	–	–	T	Tet	Dis
SnBr$_6{}^{2-}$	N	S	+	+	S	Cub	Undis
Ph$_4$B$^-$	N	b	b	b	S	Cub	Undis
SbF$_6{}^-$	N	S	–	–	S	Cub	Undis

[a] For abbreviations and symbols used in this table, see footnotes to Table II. [b] Region obscured by phenyl bands.

TABLE IV: Assignment of Infrared Bands of the Tetramethylammonium Cation

Assign-ment[a]	Mode	Symbol[b]	Value in solution[d]
ν_{13}	asym C–H stretch ⎱	ν_s	3030(s) in D$_2$O
ν_{14}	sym C–H stretch ⎰		2985(m) in D$_2$O
ν_{15}	asym CH$_3$ deform	δ_{ns}	1500(vs) in H$_2$O
ν_{16}	sym CH$_3$ deform	δ_{sym}	1418(s) in H$_2$O
ν_{17}	CH$_3$ rock	ν_{rock}	1292(m) in H$_2$O
ν_{18}	skeletal	ν_B	950(vs) in H$_2$O
ν_{19}	skeletal	d	d

[a] According to ref 19. [b] Symbols used for convenience in this work. [c] Recorded on Beckman IR-33 spectrophotometer using silver chloride cavity cell. [d] Not observed in this work.

TABLE V: Relationship of Carbon at (a, b, c) = $(0.17a_0, 0, 0.15c_0)$[a] to Its Four Neighboring Chlorines in Crystalline Tetramethylammonium Chloride

Chlorine (a, b, c)	N–C–Cl angle, deg	Deviation of N–C–Cl angle from 109.5°, deg	r(C–Cl), Å
$(0.50a_0, 0, 0.65c_0)$	164.6	55.1	3.78
$(0.50a_0, 0, -0.35c_0)$	100.2	−9.3	3.78
$(0, 0.50a_0, 0.35c_0)$	83.0	−26.5	4.25
$(0, -0.50a_0, 0.35c_0)$	83.0	−26.5	4.25

[a] See footnote d, Table II.

Figure 3. Methyl group deformation region for tetramethylammonium ion salts: (A) bromide, (B) hexabromostannate(IV). (Composite spectra from Nujol and Fluorolube mulls.)
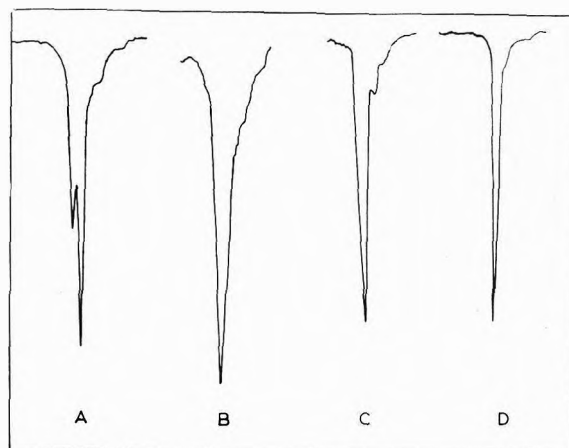
Figure 4. N–C breathing mode region for tetramethylammonium ion salts: (A) chloride, (B) trichlorocadmate(II), (C) perchlorate, (D) hexafluorosilicate. See Table I for wavelength values (Nujol mulls.)

drogen bonding type spectra have known crystal structures; these are the chloride, bromide, iodide, and perchlorate. In the perchlorate salt the observed carbon–oxygen distance of 3.04 Å is significantly less that the sum of the van der Waal's radii[27] of the two atoms, 3.20 Å. At first consideration the chloride and bromide salts appear to have the same carbon–anion distance, which is above the sum of r_{vdw} for carbon and chlorine; however, examination of the nitrogen–nitrogen distance (Table II) in adjacent cations shows that the cation centers are actually closer together than the sum of the two spherical radii of the cations as a result of dovetailing of methyl groups. The cations are packed together as tightly as possible in the bromide and chloride, and thus the available hole in the lattice for the anion is the same size in each; it is the distance from carbon center to hole center that is represented by the 3.78 r_{obsd} in the chloride. Structural confirmation of hydrogen bonding in this salt will have to await an accurate determination of the hydrogen–chlorine distance.[6] In the case of the bromide the anion almost exactly fills the hole. The cations in the iodide are somewhat further apart than in the chloride and bromide, and in the iodide, like the perchlorate, the observed C·····X distance of 3.79 Å is less

than the sum of r_{vdw} for carbon[19] and iodine, 3.96 Å, which indicates hydrogen bonding.

The ν_s region of the four salts discussed above continues to show a sharp peak for free C–H in addition to the hydrogen bonded band (Figure 1). This is in accord with the observation of Sutor[3] that usually only one hydrogen of a given methyl group is involved in hydrogen bonding, and with a consideration of the geometry of the anion environment about an individual methyl group in these salts, all of which have the same tetragonal crystal lattice. In the chloride salt, for example, each individual methyl group has four anion neighbors (Table V); two of these are at the
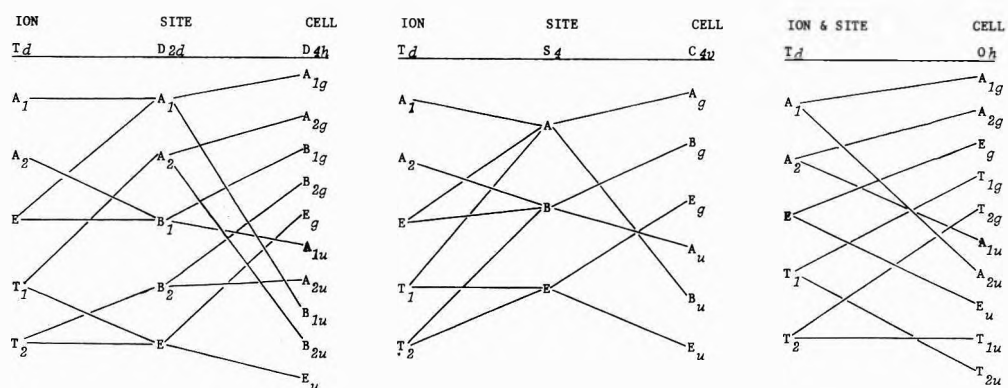
Figure 5. Correlation of spectral bands of the T_d tetramethylammonium ion with site and unit cell symmetry for the three salt types discussed in this work.

same 3.78-Å distance, assuming the chloride to be in the middle of the hole, but only one is at an angle which is likely to provide good interaction for hydrogen bonding; since the methyl group is not rotating[17,30] only one favorable C–H · · · Cl interaction is possible for each methyl group (Figure 2).

In both the hexafluorosilicate and hexachlorostannate(IV) salts the distance between methyl carbon and the nearest anion neighbor is significantly larger than the sum of r_{vdw} for carbon and fluorine or chlorine, respectively; this is in accord with the complete absence of hydrogen bonding effects in the ν_s region of the infrared spectra of these salts.

There is one cation carbon to anion chain chlorine distance in the trichlorocadmate(II) crystal structure that is shorter than the sum of r_{vdw} for carbon and chlorine, and the infrared spectrum shows a very weak broad band at longer wavelength than the principal ν_s band; we have tentatively given this salt a hydrogen bonded designation in Table II, but the effect is not large.

Correlation of Cation Infrared Spectra with Crystal Habit. A. General Observations. Examination of the infrared spectra of the seven salts for which crystal structure data are available (Tables I and II) shows that there are clear correlations between the qualitative appearance of the cation spectrum and the structure of the solid salt. Thus in the ν_s C–H stretching region a sharp singlet band appears as the primary absorption in salts that lack hydrogen bonding to anion, and a second broad, strong band appears at lower wavelength in the spectra of salts in which such C–H to anion hydrogen bonding is present (Figure 1). In the methyl deformation and rocking region the tetragonal and cubic salts show a strikingly different appearance (Figure 3); in particular ν_{rock} is much stronger in the latter salts. In salts where the cations are far apart a new band, which we have designated ν_{rot}, appears in this region. The skeletal breathing mode ν_B is a singlet in cubic salts, a doublet in tetragonal salts, and this doublet is further split in salts where the cation is distorted from the tetrahedral (Figure 4). By examination of the solid state infrared spectrum of a tetramethylammonium ion salt it is possible to predict the lattice type, the approximate size of the anion, the closeness of approach of the cations to each other, the presence or absence of cation to anion hydrogen bonding, and whether or not the cation is distorted from tetrahedral bonding. The correlation of structure with spectral appearance is discussed below for each region of the spectrum.

B. Site Symmetry Effects and Factor Group Analysis.

When a tetramethylammonium ion of T_d symmetry is placed in a lattice site of lower symmetry, the infrared spectrum may be modified through the appearance of previously forbidden bands or the splitting of previously degenerate bands.[31] In addition, further splitting of bands can arise from the coupling of the vibrations of molecules in the same unit cell.[31,32] The correlations of T_d with site and unit cell symmetries[34] for the three types of salts represented by the known crystal structures (Table II) are shown in Figure 5.

In the tetragonal D_{4h} salts such as the halides and the perchlorate, each T_2 infrared active fundamental of the cation is split by the D_{2d} site symmetry into a B_2 and an E mode, both of which are infrared active. No further splitting would be anticipated in the infrared from coupling in the D_{4h} unit cell; however the band designations change to A_{2u} and E_u. In these salts the previously infrared inactive T_1 vibrations are allowed as doubly degenerate transitions under either site or cell symmetry.

In the tetragonal C_{4h} hexafluorosilicate the T_2 fundamentals are again split into B and E bands by the S_4 site symmetry, and again only two infrared active bands, A_u and E_u, would be observed under the influence of the C_{4h} unit cell. However, in this salt A_2, E, and T_1 vibrations of the T_d cation could become infrared active.

In the cubic salt tetramethylammonium hexachlorostannate(IV) (and by structural analogy and spectral identity, the hexabromostannate(IV)) the cation T_2 bands are unchanged by the T_d site, and would transform in the O_h unit cell into an active T_{1u} and an inactive T_{2g} mode; thus the number of bands would remain unchanged. No other vibrations of the cation become active under pure O_h symmetry.

C. The ν_B Region. In the cubic tetramethylammonium hexahalostannates the NC_4 breathing mode ν_B appears as a sharp and symmetrical singlet, in accord with theory. In the tetragonal hexafluorosilicate a shoulder develops on the low wavelength side of this absorption (Figure 4), and in the tetragonal perchlorate salt the band is resolved into two peaks, a strong, sharp band at 951 cm^{-1} and a weak band at 922 cm^{-1} (Figure 4); these presumably represent the E_u and A_{2u} bands expected under the site and cell symmetry of the D_{4h} tetragonal salt. We assign the more intense absorption to the E_u mode, since in salts such as the chloride (where the cation is distorted from the tetrahedral) this band splits into two sharp peaks (Figure 4). Such splitting would result from lifting the degeneracy of the doubly degenerate E_u by distortion from T_d to, say, C_{2v} symmetry.
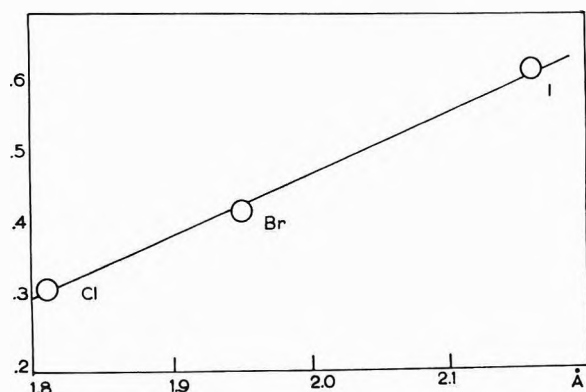
Figure 6. Ratio of δ_{sym}/δ_{as} methyl deformation modes vs. anion radius for tetramethylammonium ion halide salts.

Figure 7. Expanded spectra of the C–H stretching region for tetramethylammonium ion salts: (A) hexafluorosilicate, (B) bromide.

In both the tetragonal salts the bands should be anisotropic; the E_u modes transform as x and y, and the A_u or A_{2u} modes transform as z. Thus single crystal spectra should assist in the definitive assignment of the bands.

D. The Methyl Deformation Region, δ_{as}, δ_{sym}, *and* ν_{rock}. The region between 1200 and 1550 cm^{-1} sharply distinguishes between the cubic and the tetragonal salts. All of these salts show a strong absorption for the asymmetric methyl deformation mode, δ_{as}, near 1500 cm^{-1}; however, the remainder of the spectrum differs sharply. In the tetragonal salts the symmetrical methyl deformation mode, δ_{sym}, near 1400 cm^{-1} is a moderately strong band, and the methyl rocking mode, ν_{rock}, near 1300 cm^{-1} is difficult to detect (Figure 3), while in the cubic salts δ_{sym} is relatively weak compared to the intense ν_{rock} (Figure 3). An anomolous peak in the 1450–1480-cm^{-1} region in the hexafluorosilicate and the hexahalostannates, which we have designated ν_{rot}, is discussed below.

In the cubic salts both the δ_{as} and δ_{sym} modes appear as sharp singlets; however, in the tetragonal salts these bands develop incipient structure on the low wavelength side, presumably due to splitting of the A type bands from the E bands. In the salts with symmetrical cations such as the perchlorate or hexafluorosilicate the δ_{sym} E band is a singlet, while in salts with distorted cations such as the chloride, bromide, or iodide this band splits into a doublet paralleling the appearance of ν_B.

In both the O_h and D_{4h} salts the intensity of δ_{sym} increases with an increase in the size of the anion; this effect is particularly marked in the latter salts. To compare the intensity of these peaks we first assume that the δ_{as} band at about 1500 cm^{-1} would have a similar intensity in the chloride, bromide, and iodide, and then take the ratio of the intensity of δ_{sym} to that of δ_{as}. When this ratio is plotted against anion radius (Figure 6) a fair straight line relationship is obtained.

E. The Carbon–Hydrogen Stretching Region, ν_s. In all of the salts (with the exception of the fluoride where it is masked by hydrogen bonding) the assymetric C–H stretching mode appears as a sharp, reasonably intense singlet in the region of 3010 to 3060 cm^{-1}. The symmetric stretching band, which appears as a much weaker singlet at 2985 cm^{-1} in the solution spectrum (Table IV), can be seen as a very weak peak at 2980 cm^{-1} in a cubic salt of an anucleophilic anion such as the hexabromostannate(IV) (Figure 1). In the tetragonal salts it is more difficult to assign the symmetric C–H stretching band; in the C_{4h} hexafluorosilicate, for example, there are at least seven small bands in the C–
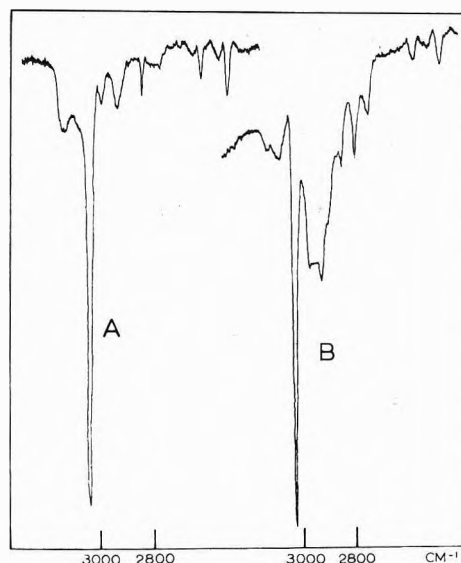
H stretching region (Figure 7). By anology with the cubic salt the slightly larger band at 2940 cm^{-1} might be assigned to this absorption, but this would be extremely tentative, and we cannot say which of these is a fundamental and which are combination or overtone bands. The D_{4h} tetragonal salts such as the halides show a very similar band pattern in this region (Figure 7) with the additional broad hydrogen bonding absorption superimposed on it, in the examples we have studied.

A Possible Methyl Rotation Band, ν_{rot}. In the hexafluorosilicate, hexachlorostannate, and hexabromostannate salts there is an absorption in the 1440–1480-cm^{-1} region (Figure 3 and Table I) which is not associated with a T_2 fundamental (Table IV). This band is clearly marked in all three salts, and in the hexabromostannate is stronger than δ_{sym} or ν_{rock}. Weak bands in this region have been ascribed to previously inactive T_1 or E methyl deformation modes;[23,26] however, the observation that the energy of this band (4.12–4.22 kcal/mol) is the same as that calculated for the barrier to internal methyl group rotation in compounds of this type (4.2 kcal/mol)[30] coupled with the fact that this band is observed only in salts in which the N–N distance between the centers of adjacent cations is greater than the sum of the spherical radii of the two cations suggests that it might be a methyl rotation mode inactive under T_d symmetry. This is in accord with the fact that the band is not observed in solution, where the ion has T_d symmetry, or in salts such as the halides where the cations are tightly interlocked, but is observed under the lower symmetry and looser packing of the hexafluorosilicate. We have no immediate explanation for the appearance on this band in the cubic hexahalostannate(IV) salts; under true O_h symmetry no bands other than the T_{1u} bands, which bear a one to one relationship (Figure 5) with the T_2 fundamentals of the free ion, should be allowed in the infrared.

Structural Predictions for Salts of Unknown Crystal Type. A. Hexabromostannate. The infrared spectrum of the cation in this salt is identical in type (Table III) with that of the hexachlorostannate(IV) salt (Table II). We expect this salt to have an undistorted CaF_2-type lattice with cubic symmetry, to have undistorted bond angles in the cation, to have the cations further apart than the sum of

their spherical radii, and to have no hydrogen bonding between cation C–H and anion.

B. Borohydride. The borohydride has a spectrum (Table III) very similar to the chloride and related salts (Table II). We expect that the borohydride has a tetragonal D_{4h} type lattice with tightly packed cations, has slightly distorted C–N–C angles in the cations, and has cation to anion C–H hydrogen bonding. The observation of a broad new band in the C–H stretching region of this salt suggests a novel C–H $\cdots$ H–B hydrogen bond, and indicates that diffraction structural studies of this salt would be of theoretical interest.

C. Tetraphenylborate. This salt is clearly not hydrogen bonded from the sharp singlet character of ν_8, and appears to have undistorted cations in a symmetrical crystal lattice, as the degeneracy of ν_B is not lifted at all.

D. Fluoride. The fluoride is in some ways the most interesting of the salts. It is extremely strongly hydrogen bonded; the C–H stretching region is much more like an O–H or N–H hydrogen bonded absorption than a C–H absorption in appearance. The radius ratio for this salt, 0.404, suggests that it might crystallize in an anti sodium chloride lattice; this would allow all the hydrogens on the methyl groups to interact equally with fluoride ions, which could account for the extensive hydrogen bonding shown in the infrared spectrum. On the other hand, such an arrangement in the crystal would place the cations in a symmetrical environment, and would not account for the doublet appearance of ν_B, which is similar to that of the perchlorate. We expect that the fluoride is also tetragonal, that the cations, as in the perchlorate, have undistorted tetrahedral bond angles, and that the C $\cdots$ F distance will be significantly shortened between carbon and its most favorably situated fluoride neighbor.[35]

E. Hexafluoroantimonate (V). The cation in this salt is not hydrogen bonded to anion, and is in a highly symmetrical environment. The cations are apparantly tightly packed. We suggest a cesium chloride structure, similar to the CaF_2 type of the halostannate(IV) salts with the vacancies filled by anions.

Conclusions

The tetramethylammonium ion is capable of hydrogen bonding to species as weakly nucleophilic as the iodide or perchloriate ion, and this property can be detected spectroscopically. In addition, the fine structure of the cation solid state infrared spectrum can give information about the crystal lattice symmetry, the packing of cations, and the distortion of the cation from the tetrahedral. The structural parameters of some salts for which crystallographic information is not available have been predicted. X-Ray studies on these salts are in progress.

Acknowledgment. We wish to thank Catherine L. Spix and Dorothy L. Duffy for technical assistance.

References and Notes

(1) Acknowledgment is made to the Donors of the Petroleum Research Fund, administrated by the American Chemical Society, to the National Science Foundation, and to the Biomedical Sciences Support Committee of Oakland University for support of this work.
(2) (a) National Science Foundation Undergraduate Research Participation Fellow. (b) Petroleum Research Fund Scholar.
(3) D. J. Sutor, *Nature (London)*, **195**, 68 (1962).
(4) A. Allerhand and P. v. R. Schleyer, *J. Amer. Chem. Soc.*, **85**, 1715 (1963).
(5) G. C. Pimentel and A. L. McClellan, "The Hydrogen Bond," W. H. Freeman, San Francisco, Calif., 1960, p 197 ff.
(6) W. C. Hamilton and J. A. Ibers, "Hydrogen Bonding in Solids," W. A. Benjamin, New York, N.Y., 1968, pp 16, 182 ff.
(7) P. Pauling in "Structural Chemistry and Molecular Biology," A. Rich and N. Davidson, Ed., W. H. Freeman, San Francisco, Calif., 1968, p 555 ff and references therein.
(8) K. M. Harmon, S. L. Madeira, and R. W. Carling, *Inorg. Chem.*, **13**, 1260 (1974).
(9) K. M. Harmon, I. Gennick, S. L. Madeira, and D. L. Duffy, *J. Org. Chem.*, **39**, 2809 (1974).
(10) K. M. Harmon, I. Gennick, and S. L. Madeira, Abstracts, presented at the 167th National Meeting of the American Chemical Society, Los Angeles, Calif., April 5, 1974, INORG-228.
(11) R. Tunder and B. Siegel, *J. Inorg. Nucl. Chem.*, **25**, 1097 (1963).
(12) The "bifluoroide impurity" reported by Tunder and Siegel[11] to be present in fluoride prepared by neutralization of tetramethylammonium hydroxide with hydrofluoric acid is almost certainly hydrate water.[10]
(13) K. M. Harmon, L. Hesse, L. P. Klemann, C. W. Kocher, S. V. McKinley, and A. E. Young, *Inorg. Chem.*, **8**, 1054 (1969).
(14) B. Morosin, *Acta Crystallogr., Sect. B*, **28**, 2303 (1972).
(15) K. M. Harmon and T. T. Coburn, *J. Phys. Chem.*, **72**, 2950 (1968).
(16) J. T. Edsall, *J. Chem. Phys.*, **5**, 225 (1937).
(17) S. Silver, *J. Chem. Phys.*, **8**, 919 (1940).
(18) C. W. Young, J. S. Koehler, and D. S. McKinney, *J. Amer. Chem. Soc.*, **69**, 1410 (1947).
(19) H. Siebert, *Z. Anorg. Chem.*, **263**, 82 (1950).
(20) H. Siebert, *Z. Anorg. Chem.*, **268**, 177 (1952).
(21) E. R. Shull, T. S. Oakwood, and D. H. Rank, *J. Chem. Phys.*, **21**, 2024 (1953).
(22) V. Lorenzelli and K. D. Moller, *C. R. Acad. Sci.*, **251**, 1483 (1960).
(23) M. A. Hooper and D. W. James, *Aust. J. Chem.*, **24**, 1331 (1971).
(24) E. A. B. Ebsworth and N. Sheppard, *Spectrochim. Acta*, **13**, 261 (1959).
(25) K. G. van Senden, *Recl. Trav. Chim. Pays-Bas*, **84**, 1459 (1963).
(26) G. L. Bottger and A. L. Geddes, *Spectrochim. Acta*, **21**, 1701 (1965).
(27) There is some question of a proper choice of r_{vdw} for carbon.[28] We have chosen to use 1.80 Å, since, when combined with the accepted value of 1.40 Å for oxygen, this gives 3.20 Å which is near the upper limit of the range of bond lengths associated with "short" carbon–oxygen distances[3] indicative of hydrogen bonding. The numerical values in Table II will change slightly if the value of 1.7 Å given by Bondi[29] is used, but the arguments based on them are unaffected.
(28) N. L. Allinger, J. A. Hirsch, M. A. Miller, I. J. Tyminski, and F. A. Van-Catledge, *J. Amer. Chem. Soc.*, **90**, 1199 (1968).
(29) A. Bondi, *J. Phys. Chem.*, **68**, 441 (1964).
(30) K. Pitzer, *J. Chem. Phys.*, **5**, 473 (1938).
(31) For example, see G. Turrell, "Infrared and Raman Spectra of Crystals," Academic Press, New York, N.Y., 1972, p 107 ff.
(32) This effect, which is most active when neutral molecules with highly dipole-active oscillators lie close to each other, would not be expected to operate strongly in these salts.[33]
(33) For example, see F. A. Cotton, "Chemical Applications of Group Theory," New York, N.Y., 1971, p 336 ff.
(34) E. B. Wilson, Jr., J. C. Decius, and P. C. Cross, "Molecular Vibrations," McGraw-Hill, New York, N.Y., 1955, p 333 ff.
(35) The fluoride has been reported to decompose on heating to trimethylamine and methyl fluoride,[36] presumably by an S_N2 displacement. The extreme degree of C–H $\cdots$ F hydrogen bonding observed in this salt suggests that decomposition via ylid formation involving proton abstraction by fluoride ion may be a competing route for decomposition; such ylid formation is observed in the thermal decomposition of tetramethylammonium hydroxide.[37] We are investigating this possibility.
(36) A. T. Lawson and N. Collie, *J. Chem. Soc.*, **53**, 624 (1888).
(37) W. K. Musker, *J. Amer. Chem. Soc.*, **86**, 960 (1964).

Chlorine Kβ X-Ray Emission Spectra of Several Solid Organic Chlorine Compounds[1,2]

H. C. Whitehead and G. Andermann*

Department of Chemistry and Hawaii Institute of Geophysics, University of Hawaii, Honolulu, Hawaii 96822
(Received November 15, 1973; Revised Manuscript Received July 29, 1974)

High-resolution Cl Kβ X-ray emission spectra of several solid organic chlorine compounds were measured to illustrate that molecular orbital theory can also be used for the interpretation of the X-ray emission spectra of certain solids. CNDO/2 calculations and published valence photoelectron spectra were used to identify the X-ray emission peaks and to provide a correlation between the electron emission and X-ray photon emission spectra. Differences in the chemical bonding of chlorine in saturated and unsaturated compounds were clearly evident in the spectra, as well as the effects of π electron conjugation. Varying the substituent and its position on the benzene ring also had some effects on the spectra which could be related to varying degrees of π electron conjugation in a series of substituted chlorobenzenes. A limited amount of conjugation was predicted for several acyl compounds.

Introduction

Chlorine Kβ X-ray emission spectra have been measured by several others[3-7] from simple gaseous molecules. Very few studies of the Cl Kβ spectra of complex solids are known.[8,9] Interpretations of the results of these measurements on gaseous molecules by simple molecular orbital theory and comparisons with valence photoelectron spectra have proved to be reasonably successful in correlating the results of both of the experimental techniques and the theoretical calculations to yield information on the chemical bonding of chlorine and the valence electronic structure of simple gaseous molecules.

The Cl Kβ spectra of the chloromethanes,[3-7] when combined with the results of uv-photoelectron studies[10-12] and molecular orbital theory, have shown that, in saturated organic compounds, $2n$ chlorine 3p lone pair molecular orbitals may be observed, where n is the number of chlorine atoms in the molecule. In addition, carbon 2p–chlorine 3p σ molecular orbitals may also be identified which are subject to the progressively increasing inductive effects of substituting additional chlorines on the methyl carbon.

Klasson and coworkers[13,14] have combined the results of uv-[10,15-17] and X-ray-induced[14] photoelectron spectra with Gilberg's[6] Cl Kβ emission spectra and their own extended Hückel calculations for an interpretation of the valence electronic structure of the chloroethylenes. In keeping with Lake and Thompson's[15] and Turner, et al.'s,[10] conclusions, Klasson and coworkers[13,14] were able to illustrate the effects of the conjugation of the out-of-plane chlorine 3p lone pair electrons with the single carbon–carbon 2p π bond. These latter workers were also able to assign symmetries to most of the molecular orbitals contributing to their ESCA spectra observed for the chloroethylenes.

Uv-photoelectron spectra[10,18,19] of a number of gaseous aromatic chlorine compounds have also indicated that the chlorine 3p π electrons, perpendicular to the benzene ring, participate in conjugation with the benzene ring π electron system leading to significant changes in the electronic energies of the π molecular orbitals. In addition, Baker, et al.,[18] have reported that both inductive effects and isomerism result in changes in the electronic energies of both the σ and π molecular orbitals.

In this paper we propose to illustrate that X-ray emission spectra obtained from several solid organic chlorine compounds can be interpreted in an analogous manner to the spectra obtained from gaseous chlorine compounds. The Cl Kβ emission spectra were all obtained from molecular crystals in which intermolecular perturbations were assumed negligible so that simple molecular orbital theory could be readily applied to the interpretation of their spectra. Most of the compounds studied were also considerably more complex than those whose Cl Kβ spectra have been studied previously in order to illustrate the usefulness of X-ray photon emission spectroscopy in studying complex molecules.

Previous reports[20,21] have illustrated the capability of X-ray photon emission spectroscopy as a central atom probe for studying the valence electronic structure of central atoms bonded to a variety of ligands. This study represents the first systematic investigation of the ability of X-ray photon emission spectroscopy to serve as a ligand atom probe. In this instance, the valence electron X-ray emission spectra of chlorine ligands in saturated and unsaturated organic molecules were measured to assess the effects on the spectra brought about by inductive effects, conjugation, and isomerism.

Theory

In applying molecular orbital theory to the interpretation of the Cl Kβ emission spectra reported here, we have assumed that the main features in each spectrum arise from electronic transitions from specific valence molecular orbitals to a single vacancy in a chlorine 1s molecular orbital. Although LaVilla and Deslattes,[22] for example, have shown that multiple vacancy transitions (Wentzel–Dryvesteyn satellites) do occur in the Cl Kβ X-ray emission spectra of gaseous chlorine compounds, these transitions appear on the high-energy side of the single-vacancy transitions and may be readily identified. However, as we shall show later, some high-energy structure on the high-energy side of the principle peak in the Cl Kβ spectra reported here, especially in the unsaturated compounds, can be assigned to single-vacancy processes.

A further prerequisite, as mentioned above, lies in the se-

lection of the compounds which were studied. All of the organic solids chosen were essentially molecular crystals in which intermolecular perturbations or solid state effects were considered negligible. This assumption has proved to be quite valid in the investigation of other molecular crystals and polyatomic ionic salts.[23,24] In making such an assumption, X-ray emission spectra of solids may then be interpreted in terms of a single molecule or molecular ion, i.e., by molecular orbital theory.

Rigorous ground-state molecular orbital calculations are not available for any of the complex molecules considered here, so, in a few cases, the semiempirical CNDO/2 method of Pople and Beveridge[25] was used as a guide to the valence electronic structure of these compounds. However, the Fortran program available to us at this time was limited to molecules with less than 80 basis functions, so that, in some instances, it was necessary to choose a "model" compound which exhibited the essential features of the chlorine bonding of a particular compound to use for our interpretation.

A distinct advantage of the X-ray emission technique is the operation of specific electric dipole selection rules which can be deduced in the same manner as for uv-visible or ir absorption spectra. These selection rules allow one to select a specific spectral series for a specific element in order to extract information regarding that element's participation in the valence molecular orbitals of the molecule being studied. Manne[26] has shown that, in terms of an LCAO MO approach, the intensity of each Cl $K\beta$ emission line can be related to the chlorine 3p LCAO coefficients

$$I_i \propto \sum_{\mu \in 3p} C_{\mu i}{}^2 \tag{1}$$

Equation 1 is directly applicable to molecules containing a single chlorine atom, but where there is more than one chlorine atom per molecule, transitions may occur from a valence molecular orbital to a vacancy in any one of a number of core-level molecular orbitals of variable symmetry. In using the one-center integral intensity approximation[26] here, an additional factor was considered in predicting the relative intensities contributed by each molecular orbital to a Cl $K\beta$ spectrum, namely, the number of core-level molecular orbitals predicted by molecular selection rules as being able to participate in a Cl $K\beta$ transition. Thus, eq 1 was modified to

$$I_i \propto G_i G_f \sum_{\mu \in 3p} C_{\mu i}{}^2 \tag{2}$$

where G_i is the number of core-level molecular orbitals active in a Cl $K\beta$ transition, G_f is the degeneracy of the valence molecular orbital, and owing to the fact that, in the CNDO/2 calculation, the chlorine 3p LCAO coefficients are not rotationally invariant, an average sum of the squares of the 3p LCAO coefficients was calculated for molecules with more than one chlorine atom. In the figures to follow where the Cl $K\beta$ peaks are assigned to particular molecular orbitals, the height of the vertical lines represent the results of eq 2.

The interpretations of the Cl $K\beta$ emission spectra presented in this paper, then, are based either on the application of very simple concepts from molecular orbital theory or comparisons with valence photoelectron spectra.

Experimental Section

The Cl $K\beta$ spectra were obtained with a double-crystal X-ray spectrometer[27] using calcite crystals. The chlorine

TABLE I: Chlorine Compounds Studied

| Compound (molecular symmetry)	Main peak, eV
Hexachloroethane, C_2Cl_6 (D_{3d})	2816.9
Hexachlorocyclohexane, $C_6H_6Cl_6$	2817.1
Hexachlorobenzene, C_6Cl_6 (D_{6h})	2817.1
p-Dichlorobenzene, p-ClC_6H_4Cl (D_{2h})	2817.3
p-Chloroaniline, p-$ClC_6H_4NH_2$ (C_{2v})	2817.1
p-Nitrochlorobenzene, p-$ClC_6H_4NO_2$ (C_{2v})	2817.2
o-, m-, p-Chlorobenzoic acid, o-, m-, p-ClC_6H_4COOH (C_s)	2817.0
3,5-Dinitrobenzoyl chloride, 3,5-$(NO_2)_2C_6H_3COCl$ (C_s)	2816.8
Diphenylcarbamyl chloride, $(C_6H_5)_2NCOCl$ (C_s)	2816.8
p-Phenylphenacyl chloride, p-$C_6H_5C_6H_4COCH_2Cl$ (C_s)	2817.3
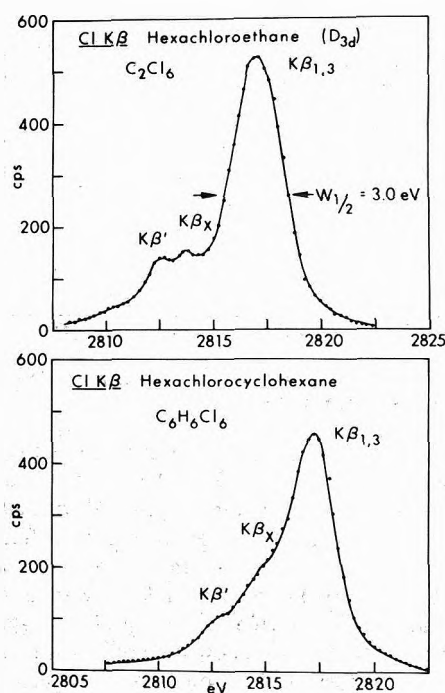
Figure 1. The Cl $K\beta$ emission spectra of hexachloroethane and hexachlorocyclohexane.
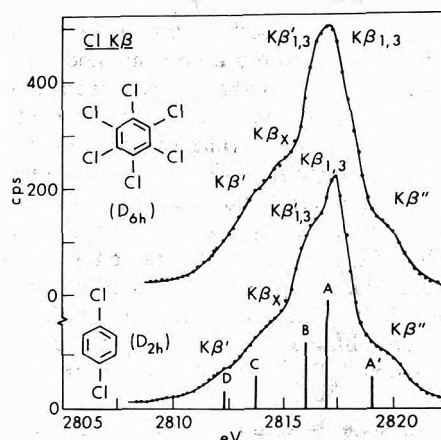

Figure 2. The Cl $K\beta$ emission spectra of hexachlorobenzene, p-dichlorobenzene, and energies and relative intensities from Gilberg's[6] spectrum of gaseous chlorobenzene.
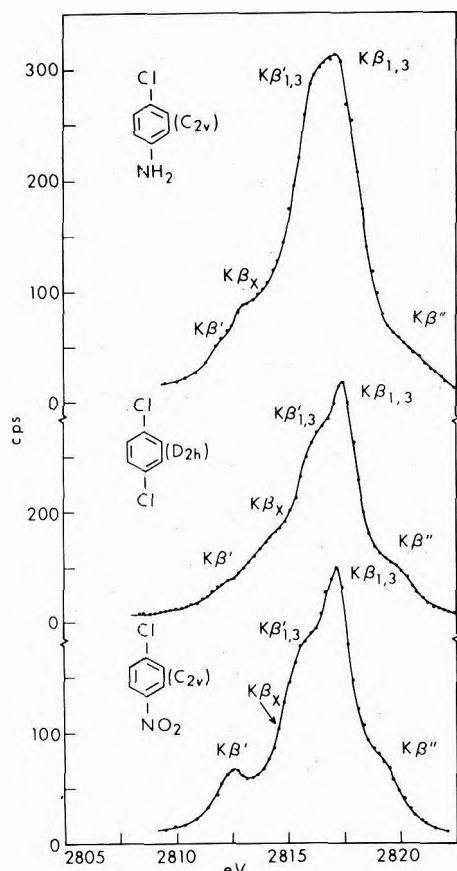
Figure 3. The Cl Kβ emission spectra of p-chloroaniline, p-dichloro-benzene, and p-nitrochlorobenzene.

radiation was excited by a sealed chromium target X-ray tube operating at 60 kV and 25 MA (1.5 kW) and detected with a flow proportional counter equipped with a 6-μ mylar window and using 0.1 ft^3/hr of P-10 gas. Pulse height selection was employed and a helium atmosphere was used. Counting rates in the range of 50–400 cps were obtained.

All of the samples were analytical grade reagents dried, and ground lightly to a fine powder, and pressed onto a Bakelite backing to form 1.25-in. diameter briquettes.

The spectra were measured in a variety of ways to assure that any effects due to the decomposition of the samples were kept at a minimum. Some of the spectra were obtained by point-by-point intensity measurements of sections of a particular spectrum from fresh samples in periods of only 10 or 15 min, normalizing the intensities to that of the main peak, measured each time, and then plotting the complete spectrum. Other spectra were obtained by making point-by-point intensity measurements rapidly over the entire spectrum so that less than 20 min were required for the complete scan. Several spectra were recorded in this manner, the results normalized, averaged, and then plotted to obtain the complete spectrum. For other compounds, reliable spectra could be obtained in a single point-by-point scan taking up to 3 hr. Counting precisions of about 5% in the low-intensity regions to less than 1% over the peaks were obtained. An approximate 30-eV region of the spectra from 2800 to 2830 eV was measured for all samples.

The Cl Kβ spectra were calibrated using the energy of the main Cl K$\beta_{1,3}$ line of solid KCl (λ = 4.043516 Å; 2815.50 eV) as measured against the Pd Lα_1 line (λ = 4.367 Å; 2838.61 eV) reported by Bearden.[28] Peak reproducibility
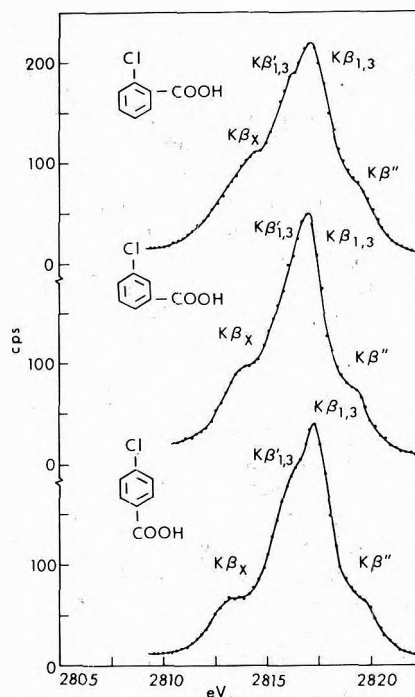
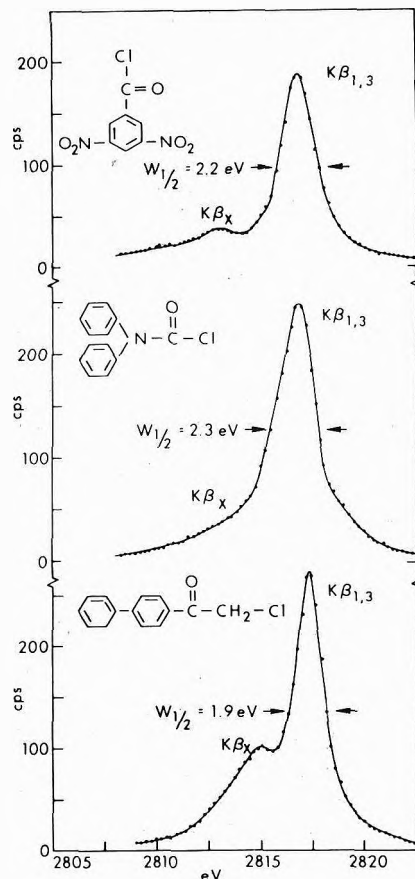**Figure 4.** The Cl Kβ emission spectra of o-, m-, and p-chloroben-zoic acid.

Figure 5. The Cl Kβ emission spectra of 3,5-dinitrobenzoyl chloride, diphenylcarbamyl chloride, and p-phenylphenacyl chloride.

was about ±0.1 eV, whereas the accuracy of the measured values were around ±0.3 to 0.4 eV.

The spectra, as measured, are presented in Figures 1–5. No corrections have been applied to any of the results. The

vertical lines at the bottom of Figure 2 represent the best estimates of the energies and relative intensities obtained from Gilberg's[6] reported spectrum of gaseous chlorobenzene. The resolution obtained here was comparable to that achieved by Gilberg using long focal-length curved-crystal optics, but it was not entirely sufficient to resolve many of the spectral features as shown in Figures 1–5. It was necessary, then, to make some qualitative assumptions of the energies and relative intensities for the main features observed in each spectrum.

Table I lists the compounds studied along with the energy measured for the highest intensity peak in each spectrum. The energy values measured for this peak range over some 0.5 eV, but, in general, the main peak for each compound can be assigned an energy of 2817.0 ± 0.2 eV.

Results and Discussion

Saturated Compounds. The Cl $K\beta$ spectrum of hexachloroethane is shown in Figure 1. This spectrum exhibits a broad (FWHM = 3.0 eV) high-energy, high-intensity peak ($K\beta_{1,3}$) centered at about 2817 eV, and two lower-energy, lower-intensity peaks ($K\beta_x$ and $K\beta'$) separated from the main peak by 3.2 and 4.4 eV, respectively.

Gilberg's[6] Cl $K\beta$ spectra for the chloromethanes also exhibited a high-intensity peak at 2817 eV, which broadened as the number of chlorine atoms increased, but which maintained a relatively constant energy. This peak was identified by Gilberg with the chlorine 3p lone pair electrons. However, only a single low-energy, low-intensity peak appeared in the chloromethane spectra and this peak was attributed to carbon–chlorine σ bonding orbitals. This lower energy peak shifted by about 0.5 eV per additional chlorine atom away from the lone pair peak, so that for three chlorine atoms bonded to a single carbon, its energy was 4.0 eV below that of the lone pair peak. The shifting of this low-energy peak is consistent with the inductive effects of the additional chlorine atoms leading to an increasing stability of the carbon–chlorine σ bonding orbitals.[3,12]

A significant observation which we made from Gilberg's results on the chloromethanes is the fact that while the single low-energy peak did shift to lower energies, this peak did not exhibit any additional broadening as was observed for the lone pair peak; moreover there was no evidence of additional peaks in the low-energy region as the number of chlorine atoms attached to the single carbon atom was increased. On the other hand, lengthening the carbon chain did lead to additional peaks as seen in Gilberg's spectra for ethyl, n-propyl, and n-butyl chloride. For ethyl chloride, two low-energy peaks were observed at 1.8 and 4.2 eV below the lone pair peak. These two peaks may be identified with vertical ionization potentials, I_2 and I_5, as measured by Kimura, et al.,[29] some 2.1 and 4.6 eV higher than the chlorine 3p lone pair ionization potentials. The electrons exhibiting these ionization potentials were assigned by Kimura, et al., as originating from carbon–chlorine σ orbitals (I_2) and pseudo π orbitals (I_5) encompassing the chlorine atom, the α carbon, and the methyl group in ethyl chloride. Similar π molecular orbitals were also presumed by Nefedov[7] in his interpretation of the Cl $K\beta$ spectra of a series of fluorochloromethanes.

Qualitatively, then, the bonding of a chlorine atom to a saturated carbon atom can be described in terms of a single carbon–chlorine σ bond involving one of the 3p orbitals of chlorine, with the other two 3p orbitals representing two chlorine lone pairs. It appears, however, that one, or both,
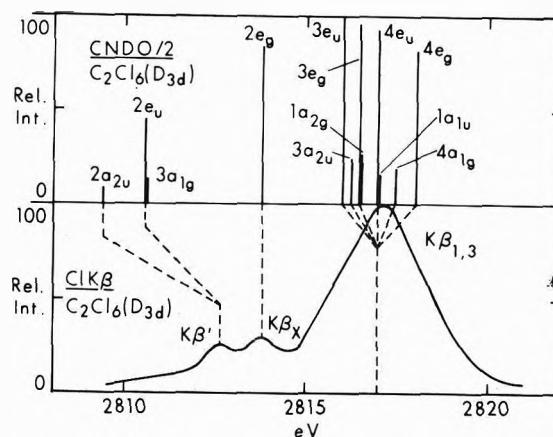

Figure 6. Molecular orbital assignments for the Cl $K\beta$ emission spectrum of hexachloroethane (D_{3d}).

of these two chlorine lone pair orbitals can participate in π orbital formation leading to additional low-energy peaks in the spectra of saturated chlorine compounds.

A CNDO/2 calculation was carried out for hexachloroethane assuming a staggered (D_{3d}) configuration.[30] The LCAO coefficients indicate that the 12 highest energy molecular orbitals ($4e_g$ through $3e_u$) can be assigned as essentially chlorine 3p lone pair orbitals. The next six molecular orbitals ($2e_g$ through $2a_{2u}$) are the only other orbitals predicted by the intensity approximation (eq 2) as contributing any appreciable intensities to the Cl $K\beta$ spectrum of hexachloroethane. The remaining orbitals were composed mainly of either carbon 2s, 2p, or chlorine 3s.

The relative Cl $K\beta$ intensities predicted for the upper 18 molecular orbitals of hexachloroethane are shown in the top half of Figure 6. The eigenvalues from the CNDO/2 calculation have been scaled to the experimental spectrum, which has been replotted in the bottom half of Figure 6, by placing the highest energy nonbonding chlorine 3p molecular orbitals, $4e_u$ and $1a_{1u}$, at the same energy as the $K\beta_{1,3}$ peak. As expected, the uppermost 12 lone pair molecular orbitals can be assigned to the $K\beta_{1,3}$ peak. The CNDO/2 calculation has these molecular orbitals spread over a range of about 2.0 eV which, considering a reasonable amount of instrumental and solid state broadening, agrees extremely well with the experimentally determined breadth of 3.0 eV.

The CNDO/2 calculation for hexachloroethane places the $2e_g$ orbital at the same energy as the $K\beta_x$ peak, but the other four molecular orbitals assumed to be contributing to the Cl $K\beta$ spectra, $3a_{1g}$, $2e_u$, and $2a_{2u}$, are displaced to energies lower than the $K\beta'$ peak. An examination of the LCAO coefficients for this last group of six molecular orbitals revealed that the $2e_g$ orbital was composed entirely of carbon 2p and chlorine 3p orbitals, whereas the other orbitals had contributions from carbon 2s and 2p and chlorine 3s and 3p. The $K\beta_x$ peak, then, was assigned as originating from pure carbon 2p–chlorine 3p σ bonding orbitals, and the $K\beta'$ peak as originating from molecular orbitals of more mixed character; possibly of the pseudo π type mentioned above.

Some additional insight was acquired regarding the molecular orbitals of saturated organic chlorine compounds by considering the Cl $K\beta$ spectrum of hexachlorocyclohexane also shown in Figure 1. The spectrum of hexachlorocyclohexane is similar to that of hexachloroethane, except that
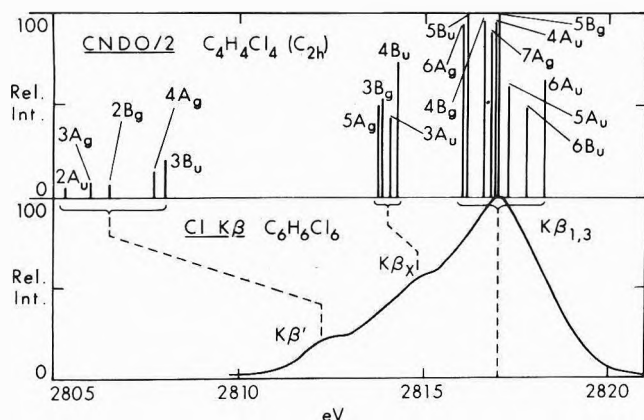
Figure 7. Molecular orbital assignments for the Cl $K\beta$ emission spectrum of hexachlorocyclohexane, using tetrachlorocyclobutane (C_{2h}) as a model.

the $K\beta_x$ peak appears to lie closer to the lone pair peak ($K\beta_{1,3}$). This fact is consistent with the smaller inductive effects predicted for only a single chlorine atom bonded to a saturated carbon atom.

Unfortunately, the CNDO/2 program available to us at this time could not accommodate the $C_6H_6Cl_6$ molecule, so the next smallest even-membered ring compound, i.e., tetrachlorocyclobutane, was selected as a "model" compound upon which to base an interpretation of the hexachlorocyclohexane Cl $K\beta$ spectrum. A planar (C_{2h}) configuration was assumed.

The results of the CNDO/2 calculation[30] for $C_4H_4Cl_4$ indicated four general groups of molecular orbitals for an even-membered cyclic chloro compound: (1) a manifold of upper levels of bonding and antibonding molecular orbitals which contained sizable contributions from the chlorine 3p orbitals, and which were identified as chlorine 3p lone pair orbitals; (2) pure carbon 2p–chlorine 3p σ bonding orbitals some 2 eV lower in energy than the lone pair orbitals; (3) a group of molecular orbitals, spanning a region of about 15 eV below the second group, which were mixtures of carbon 2s, 2p, hydrogen 1s, and chlorine 3s, and 3p; and (4) the lowest energy molecular orbitals representing essentially carbon 2s and chlorine 3s orbitals. Only the first three groups would be likely to contribute to a Cl $K\beta$ spectrum and this is so indicated in Figure 7. Here, each Cl $K\beta$ peak for hexachlorocyclohexane has been assigned to groups of molecular orbitals representing a particular type of molecular orbital which might be expected to occur in such a molecule. Again, the CNDO/2 calculation places those orbitals assigned to the $K\beta'$ peak at a lower energy than that experimentally observed. However, the intensity pattern predicted by the CNDO/2 calculation seems to be borne out by the experimental results.

Unsaturated Compounds. In Figure 2, the Cl $K\beta$ spectra of hexachlorobenzene and p- dichlorobenzene are presented along with an estimate of the energies and relative intensities obtained from Gilberg's[6] spectrum of gaseous chlorobenzene. There are at least five major features which can be discerned in the Cl $K\beta$ spectra of the chlorobenzenes, the most significant of which is the presence of the $K\beta''$ peak which is not seen in the spectra of the saturated chlorine compounds. The absence of any high-energy structure in the Cl $K\beta$ spectra for the saturated compounds implies that the $K\beta''$ peak for the unsaturated compounds may indeed be due to a true single-vacancy transition rather than

a double-vacancy transition (WD) which would also occur in the region of the $K\beta''$ peak. The interpretations to follow also support this contention.

One other noticeable feature in the Cl $K\beta$ spectra of the chlorobenzenes is the variation in the relative intensity of the low-energy side of the $K\beta_{1,3}$ peak ($K\beta_{1,3}'$) which Gilberg[6] has labeled as his peak B. The other peaks in the spectra of the chlorobenzenes do not appear to vary, especially in intensity, as much as the $K\beta_{1,3}'$ peak.

In an attempt to interpret the Cl $K\beta$ spectra of the chlorobenzenes, a CNDO/2 calculation[30] was performed for hexachlorobenzene (D_{6h}). All of the chlorobenzenes were assumed to be planar so that each chlorine atom has, in addition to its 3s and 3p σ orbitals, two 3p lone pair orbitals perpendicular to the carbon–chlorine σ bond.[10,18] One orbital is in the plane of the molecule, while the other 3p orbital is perpendicular to the molecular plane. The out-of-plane chlorine 3p orbitals are capable of interacting with the benzene ring π orbitals leading to conjugation of the chlorine 3p lone pair electrons with the benzene ring π electron system. A key to the conjugation mechanism and its effect on Cl $K\beta$ spectra was found in the works of Klasson and Manne,[13] Lake and Thompson,[15] and Gilberg.[6] Klasson and Manne, along with Lake and Thompson, observed that the out-of-plane chlorine lone pair orbitals mixed significantly with the bonding combination (C_a $2p_z$ + C_b $2p_z$) of the carbon–carbon π bond of ethylene leading to the formation of a carbon–carbon–chlorine π bonding orbital whose energy was lowered by as much as 2 eV relative to the chlorine 3p lone pairs. These two groups of investigators also found evidence for the formation of an antibonding combination of the chlorine 3p lone pair orbitals with the bonding combination of the ethylene π orbital which resulted in a carbon–chlorine antibonding orbital of higher energy (1–2 eV) than the chlorine 3p lone pairs. The in-plane chlorine lone pair orbitals remained essentially localized on the chlorine atoms and did not appreciably change in energy.

The CNDO/2 calculation[30] for hexachlorobenzene indicated the presence of antibonding carbon–chlorine π molecular orbitals ($2e_{1g}$) about 2 eV higher than the chlorine 3p lone pair orbitals, with weakly antibonding ($2a_{2u}$) and bonding ($1b_{2g}$ and $1e_{2u}$) π orbitals in the same energy region (−14 to −16 eV) as the in-plane chlorine 3p lone pair orbitals. Other π bonding orbitals were predicted at about 3 eV ($1e_{1g}$) below the lone pair, which seemed reasonable, but, the presence of the $1a_{2u}$-orbital at about 11 eV below the lone pairs indicated that the CNDO/2 calculation had grossly overestimated the amount of π orbital interaction.

If the assignments of the CNDO/2 calculation are accepted (see Figure 8), then the $K\beta''$ peak would originate from the $2e_{1g}$ orbital; the $K\beta_{1,3}$ peak would originate from the π and chlorine 3p lone pair orbitals; $4e_{2g}$ down through $3e_{2g}$; the $K\beta_x$ peak would be attributed entirely to the carbon–chlorine σ bonding orbitals ($2b_{1u}$ and $3e_{1u}$); and the $K\beta'$ peak would be due mainly to the $1e_{1g}$ π bonding orbital. The energy of the $1a_{2u}$ π orbital and its relative intensity would both be too low to contribute to the Cl $K\beta$ spectrum measured for hexachlorobenzene. Examination of the valence photoelectron spectra of a number of chlorobenzenes[10,18,19] indicated that the assignments made from the CNDO/2 calculation appeared reasonable for the $K\beta''$ and $K\beta_{1,3}$ peaks, but that there was some uncertainty as to which orbitals were contributing to the $K\beta_{1,3}'$ peak and to the $K\beta_x$ and $K\beta'$ peaks. An alternate interpretation based
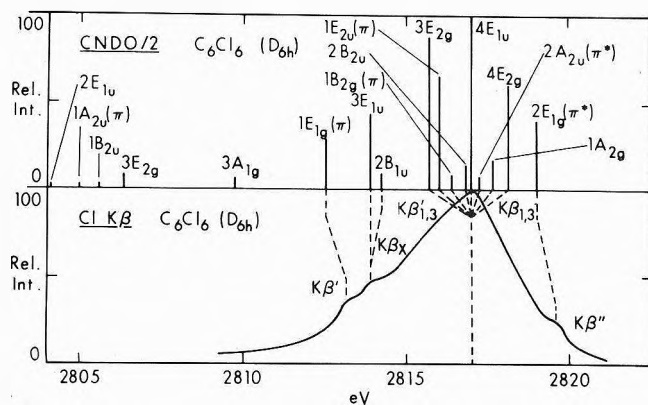
Figure 8. Molecular orbital assignments for the Cl $K\beta$ emission spectrum of hexachlorobenzene (D_{6h}).

Figure 9. Correlation of the ionization potentials of benzene, chlorobenzene, and p-dichlorobenzene and the assignment of the Cl $K\beta$ emission spectra of chlorobenzene and p-dichlorobenzene (see text for references).

on the conjugative interactions of the chlorine 3p lone pair orbitals with the benzene ring π orbitals as observed in the valence photoelectron spectra of some chlorobenzenes seems more appropriate.

A number of *ab initio* SCF–MO calculations[31-37] have indicated that the valence electronic structure of benzene is $(2a_{1g})^2(2e_{1u})^4(2e_{2g})^4(3a_{1g})^2(2b_{1u})^2(1b_{2u})^2(3e_{1u})^4(1a_{2u})^2-(3e_{2g})^4(1e_{1g})^4$. Photoelectron evidence has been offered[38-44] which seems to support this ordering, especially with regard to placing at least one σ orbital between the two π molecular orbitals ($1a_{2u}$ and $1e_{1g}$) and placing the $1a_{2u}$ orbital about 3 eV below the $1e_{1g}$ orbital.

Ionization potentials for benzene which have values below 17 eV are plotted in Figure 9 along with ionization potentials for chlorobenzene and p-dichlorobenzene obtained from several studies.[10,18,19] Since only the $1e_{1g}$ (π) ionization potential (9.20 eV) has been reported for hexachlorobenzene,[45] data for this compound were not included in Figure 9. A correlation has been made between the ionization potentials of the two chlorobenzenes and those of benzene showing the assumed parentage of the chlorobenzene bands. It can be seen that all of the photoelectron bands for both chlorobenzenes can be related to molecular orbitals originating with the benzene molecule except those labeled as chlorine 3p lone pairs. However, except for the chlorine 3p lone pair bands, there is no indication in the photoelectron spectra for the chlorobenzenes of just how much chlorine 3p character is mixed into the original benzene molecular orbitals. The splitting of the $1e_{1g}$ π orbital, for example, has been attributed to conjugation of the chlorine 3p lone pairs with the benzene ring π orbitals, mixing chlorine 3p character into one, or both, of the $1e_{1g}$ orbitals, while mixing carbon 2p character into the chlorine 3p lone pair orbitals.[10,18,19] The Cl $K\beta$ spectra of the chlorobenzenes should indicate which molecular orbitals contain chlorine 3p contributions as well as provide a relative indication of how much chlorine 3p character is given each molecular orbital.

In Figure 9, the best estimates of the energies of the five major peaks in the Cl $K\beta$ spectra of chlorobenzene[6] and p-dichlorobenzene are also plotted. The main $K\beta_{1,3}$ peak has been positioned in the center of the chlorine 3p lone pair photoelectron peaks for each molecule, with the energies of the other X-ray peaks being taken relative to that particular energy. It can be seen that the $K\beta''$ peaks lie in the region of the $1e_{1g}$ orbitals, although it is impossible to make a definite assignment of this peak to the upper or lower component of these orbitals owing to the uncertainties in the
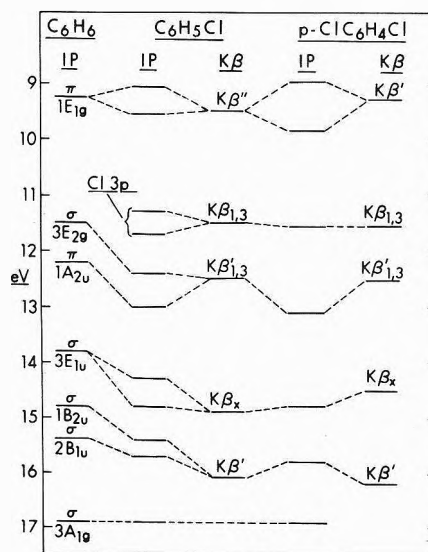
$K\beta''$ peak position. The presence of this peak, however, does confirm that some chlorine 3p character has been mixed into the original $1e_{1g}$ benzene π orbitals. The $K\beta_{1,3}'$ peak is seen to occur in the region of the $3e_{2g}$ (σ) and $1a_{2u}$ (π) ionization peaks for the chlorobenzenes, but, again, a definite assignment is impossible. The $K\beta_{1,3}'$ peak appears to increase in relative intensity as the number of chlorine atoms per molecule increases implying that its main contribution may come from the $3e_{2g}$ σ type orbital. However, these orbitals have been characterized as weakly carbon–hydrogen bonding in benzene,[38] and may also be weakly bonding in the chlorobenzenes so that they may contain very little chlorine 3p character. Thus, the main contribution to the $K\beta_{1,3}'$ peak could arise from conjugative interactions with the $1a_{2u}$ (π) orbitals of benzene. There appears, however, to be no really decisive evidence in any of the chlorobenzene spectra to indicate such an interaction.

The $K\beta_x$ and $K\beta'$ peaks for chlorobenzene and p-dichlorobenzene are about 3.2 and 4.6 eV, respectively, below the energy of the chlorine 3p lone pair peaks ($K\beta_{1,3}$) and lie in the region of σ orbital photoelectron bands. Judging by the separations of the $K\beta''$ peak and the $K\beta_{1,3}'$ peak from the $K\beta_{1,3}$ peak brought about by conjugative effects, there seems to be no reason to suppose that the $K\beta_x$ and $K\beta'$ peaks for these compounds are the result of chlorine 3p lone pair conjugation. Rather, these peaks most likely arise from chlorine 3p σ bonding orbitals. Interaction of the chlorine 3p σ orbitals is allowed by symmetry with the $3e_{1u}$ and $2b_{1u}$ orbitals of benzene, both characterized as originally strongly carbon–hydrogen bonding.[38] The $3a_{1g}$ and $1b_{2u}$ benzene orbitals which are strongly carbon–carbon bonding and nonbonding carbon–hydrogen, respectively, would most likely not acquire any significant degree of chlorine 3p character upon substitution. Thus, we may assign the $K\beta_x$ peak in chlorobenzene and p-dichlorobenzene as originating from molecular orbitals formed from the interaction of the chlorine 3p σ orbitals with the benzene $3e_{1u}$ orbital. Similarly, the $K\beta'$ peak may be assigned to molecular orbitals having their origin primarily in the benzene $2b_{1u}$ orbital.
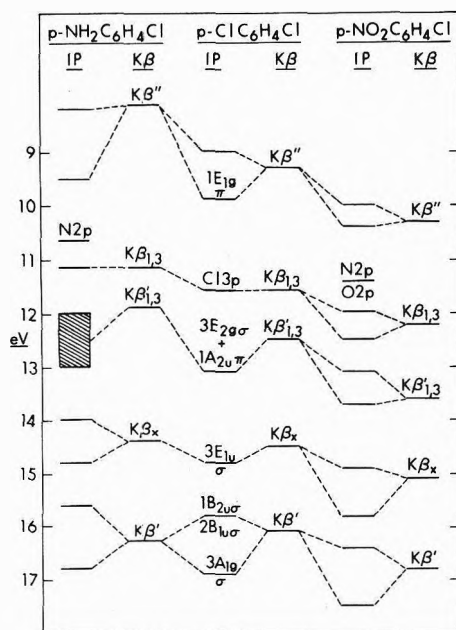
Figure 10. Correlation of the ionization potentials and the assignment of the Cl Kβ emission spectra of p-chloroaniline, p-dichlorobenzene, and p-nitrochlorobenzene (see text for references).

The Cl Kβ spectrum of hexachlorobenzene can be interpreted in a manner analogous to the other chlorobenzenes. The shifting of the $K\beta_x$ and $K\beta'$ peaks for hexachlorobenzene closer to the $K\beta_{1,3}$ peak and their apparently higher relative intensities may represent a saturation of the ring π electron system with conjugated chlorine 3p lone pair electrons. The increased electron density on the ring lowers the binding energies for these predominantly carbon 2p orbitals.[10] An inductive effect acting through the carbon–chlorine σ orbitals would act in the opposite direction.[44]

Substitution and Isomerism Effects. In order to illustrate the effects of various electron-donating and -withdrawing substituents on the Cl Kβ spectra of some para-disubstituted chlorobenzenes, the spectra of p-chloroaniline, p-dichlorobenzene, and p-nitrochlorobenzene were measured and the results shown in Figure 3.

Again, the main peak ($K\beta_{1,3}$) occurs at 2817 eV and may be attributed to the chlorine 3p lone pair orbitals. Differences in the spectral positions and relative intensities of the other peaks for the p-nitro and p-amino compounds can be understood in relation to the Cl Kβ spectrum of p-dichlorobenzene and its previous interpretation.

Upon replacing one of the chlorine atoms of p-dichlorobenzene with a nitro group, the $K\beta''$ peak shifts slightly to lower energy. The appearance of this peak indicates that chlorine 3p π conjugation is still in effect, but that the splitting of the $1e_{1g}$ π orbital of benzene is less than in the p-dichloro compound. The lower intensity of the $K\beta_{1,3}'$ peak, relative to p-dichlorobenzene, indicates a greater delocalization of the carbon–chlorine π electrons away from the chlorine atom. This would be consistent with a greater localization of the carbon–chlorine π antibonding electrons on the chlorine atom as implied by the slightly higher $K\beta''$ intensity. Thus, the highly electronegative nitro group seems to be withdrawing electron density away from chlorine rather than contributing to a conjugative effect of its own with the benzene π electron system.

Just the opposite effects are seen for the $K\beta''$ peak and the $K\beta_{1,3}'$ peak of p-chloroaniline. The nitrogen 2p π lone

pair of the amino group can participate in conjugation with the benzene π electron system leading to an increased splitting of the benzene $1e_{1g}$ orbital. Thus, the $K\beta''$ peak is at a higher energy than for p-dichlorobenzene. More chlorine 3p π bonding electron density is apparently localized in the carbon–chlorine π bonding orbitals for p-chloroaniline than for either p-nitrochlorobenzene or p-dichlorobenzene, as indicated by the greater relative intensity of the $K\beta_{1,3}'$ peak. The lower relative intensity of the $K\beta''$ peak indicates a lower chlorine 3p participation in the upper π antibonding orbitals than in p-dichlorobenzene.

Variations in the region of the low-energy peaks ($K\beta_x$ and $K\beta'$) indicate that the nitro and amino groups also have some effect on the carbon–chlorine σ bonding orbitals, relative to those in p-dichlorobenzene, but these effects can not be determined as readily as for the π orbitals.

The ionization potentials[10,18,45] measured for p-chloroaniline, p-dichlorobenzene, and p-nitrochlorobenzene are plotted in Figure 10 along with the best estimates of the energies of the Cl Kβ peaks for these compounds. Again, the $K\beta_{1,3}$ peak has been centered in the chlorine 3p lone pair photoelectron bands for each compound and the molecular orbital designations are those for the parent benzene molecule. The photoelectron results quite clearly confirm the effects of the p-nitro and p-amino substitution observed in the Cl Kβ spectra presented in Figure 3. The $1e_{1g}$ π orbital splitting is much more pronounced for p-chloroaniline, but much less so for p-nitrochlorobenzene, than that observed for p-dichlorobenzene. In addition, the inductive effects on the p-nitrochlorobenzene orbitals are quite evident, whereas for p-chloroaniline these effects are less evident. The Cl Kβ peaks for all three compounds, again, lie in the appropriate energy regions for assignment to the same type of molecular orbitals as was made previously for the mono-, di-, and hexachlorobenzenes.

In Figure 4, the variations among the Cl Kβ spectra for the three chlorobenzoic acids indicate that the location of the substituent relative to the chlorine atom on an aromatic ring also has an effect on the valence electronic structure of these substances. While the acid group has about the same inductive power as chlorine,[46] it apparently does little to enhance the conjugative effect of chlorine as evidenced from the $K\beta''$ peak being at a slightly lower energy in all of the chlorobenzoic acids than in p-dichlorobenzene. In addition, the lower intensity of the $K\beta_{1,3}'$ peak for the meta isomer may reflect the ability of the acid group to increase the electron density at positions ortho and para to itself.[47] Changes in the $K\beta_x$ peak indicate that the position of the acid group also affects the carbon–chlorine σ bonding orbitals. The apparent absence of the lowest energy peak ($K\beta'$) shows that the acid group also has a different effect on these σ bonding orbitals not observed for the other substituents considered above.

Acyl Compounds. We have seen that chlorine atoms bonded to a benzene ring participate in π electron conjugation with the benzene ring π electron system to yield loosely bound molecular orbitals with sufficient chlorine 3p character to lead to the appearance of the $K\beta''$ peak in the Cl Kβ spectra of all the chlorobenzenes. To see if this conjugation could be extended to chlorine atoms separated from the benzene ring by an atom, or group, with potential conjugation ability, the Cl Kβ spectra for several acyl compounds were measured. The results are shown in Figure 5.

Inspection of the Cl Kβ spectra of 3,5-dinitrobenzoyl chloride immediately reveals two facts: (1) the high-energy

$K\beta''$ peak, observed for the chlorobenzenes, is absent; and (2) there is a relatively narrow (FWHM = 2.2 eV) $K\beta_{1,3}$ peak and a single low-energy, low-intensity peak ($K\beta_x$) about 3.8 eV below the $K\beta_{1,3}$ peak. This spectrum is quite similar to those observed by Gilberg[6] for the chloromethanes. It appears that there is evidence in Figure 5 for only chlorine 3p lone pairs and a carbon–chlorine σ bond. The fact that there is no $K\beta''$ peak indicates that there is negligible interaction of the chlorine 3p π orbitals with the benzene ring. The spectrum of diphenylcarbamyl chloride, where the acyl chloride group is separated from the benzene rings by nitrogen, also supports this contention. It appears, too, that the chlorine σ bonding in this latter molecule is quite different. The spectrum for p-phenylphenacyl chloride is practically identical with Gilberg's spectrum for methyl chloride. In p-phenylphenacyl chloride the chlorine atom is separated from both the benzene ring and the carbonyl (CO) group by a methylene group, a condition which apparently reduces the bonding of chlorine to carbon–chlorine σ bonding and chlorine 3p lone pairs.

In order to assess the type of chlorine bonding which might occur in an acyl chloride, a CNDO/2 calculation[30] was performed for the "model" compound, benzoyl chloride, C_6H_5COCl. The CNDO/2 calculation was carried out on the benzoyl chloride molecule with the acyl chloride group in the plane of the benzene ring. This enabled a separation of the σ (a') and π (a'') orbitals for easy identification.

Of the 23 occupied molecular orbitals of benzoyl chloride, the intensity approximation used here indicated that only 11 of the uppermost 13 orbitals would make any significant contributions to the Cl $K\beta$ spectrum of an acyl chloride. The σ bonding orbitals (10a' through 18a') fell into two categories: (1) those with large chlorine 3p lone pair character, which could be assigned to the $K\beta_{1,3}$ peak; and (2) those with acyl carbon–chlorine σ bonding character, which could be assigned to the $K\beta_x$ peak. There was very little indication of phenyl carbon–acyl carbon σ bonding in any of these upper a' type molecular orbitals.

In regard to the upper four π orbitals, the 5a'' orbital contained acyl carbon 2p–chlorine 3p π antibonding, as well as phenyl carbon–carbon π antibonding, character. The 4a'' and 3a'' orbitals consisted mostly of chlorine 3p π antibonding character, but phenyl carbon–carbon π bonding character. For all three of these upper π orbitals, the CNDO/2 calculation showed that the chlorine 3p π electrons were relatively isolated on the chlorine atom. Thus, these orbitals were also assigned to the $K\beta_{1,3}$ peak. The 2a'' orbital, however, was strongly chlorine 3p–acyl carbon 2p–oxygen 2p π bonding, and, hence, would be lowered in energy relative to the chlorine 3p lone pairs. The 2a'' orbital was, then, assigned to the $K\beta_x$ peak. An interesting feature about this orbital was the presence of a nodal plane between the phenyl carbon bonded to the acyl carbon and the remainder of the benzene ring.

Both the CNDO/2 calculation and the appearance of the Cl $K\beta$ spectra of the acyl chlorides indicated that there was a negligible interaction between the chlorine 3p π orbitals and the benzene ring even though, for the CNDO/2 calculation, the configuration of the "model" benzoyl chloride was such as to provide the maximum opportunity for such an interaction. As the acyl group is turned out of the plane of the benzene ring, the opportunity for π orbital interaction is lessened. As the spectra show (Figure 5), the chlorine atom was relatively isolated from the influence of the ben-

zene ring, but not from the effects of oxygen–acyl carbon–chlorine π conjugation.

Conclusions

X-Ray photon emission spectroscopy has been shown to be quite useful in the study of the valence electronic structure of several different types of chlorine compounds. With the appropriate selection of the X-ray spectral series to be measured and the elements on which to make these measurements, a great deal of information can be acquired on the chemical bonding of individual chlorine ligand atoms in complex molecules. X-Ray photon emission spectroscopy can be used independently, or in conjunction with photoelectron spectroscopy, to provide such information.

Spectra measured on certain types of solids may be interpreted by molecular orbital theory just as successfully as spectra obtained on gaseous molecules. The CNDO/2 calculation used here seems to be useful as a guide for interpreting the Cl $K\beta$ spectra presented in this study, although the lower level molecular orbitals are displaced to lower energies than those observed experimentally. The relative intensities calculated from the results of the CNDO/2 calculation are, however, in reasonable agreement with experiment. Other semiempirical methods, such as extended Hückel theory, or more rigorous *ab initio* calculations may prove more suitable.

The results presented here show conclusive evidence of chlorine 3p π electron conjugation leading to the mixing of chlorine 3p character into the benzene ring π molecular orbitals. The $K\beta''$ peak resulting from this conjugative mixing serves as a means for differentiating between chlorine bonded to saturated or unsaturated molecules. Specific effects due to substitution and isomerism were also seen in the Cl $K\beta$ spectra of the chlorobenzenes. With further study under higher resolution the nature of these effects may be determined with more assurance.

While many of the conclusions drawn here and in the previous discussion may be somewhat speculative, it is clear that molecular X-ray spectroscopy can provide a valuable tool for studying complex molecules in the solid state.

Supplementary Material Available. Listings of the results of CNDO/2 calculations showing eigenvalues, eigenvectors, and calculated relative intensities will appear as Tables II–V following these pages in the microfilm edition of this volume of the journal. Photocopies of the supplementary material from this paper only or microfiche (105 × 148 mm, 24× reduction, negatives) containing all of the supplementary material for the papers in this issue may be obtained from the Journals Deparment, American Chemical Society, 1155 16th St., N.W., Washington, D. C. 20036. Remit check or money order for $3.00 for photocopy or $2.00 for microfiche, referring to code number JPC-74-2592.

References and Notes

(1) This work was supported by a National Science Foundation Grant (GP 9596) and represents part of a dissertation submitted by H.C.W. in partial fulfillment of the Ph.D. Degree, University of Hawaii, Honolulu, Hawaii, 1973.
(2) Hawaii Institute of Geophysics Contribution No. 558.
(3) R. E. LaVilla and R. D. Deslattes, *J. Chem. Phys.*, **45**, 3446 (1966).

(4) R. D. Deslattes and R. E. LaVilla, *Appl. Opt.*, **6**, 39 (1967).
(5) S. M. Blokhin, A. P. Sadovskii, G. N. Dolenko, and V. M. Bertenev, *J. Struct. Chem.*, **10**, 722 (1969).
(6) E. Gilberg, *Z. Phys.*, **236**, 21 (1970).
(7) V. I. Nefedov, *J. Struct. Chem.*, **12**, 276, 476 (1971).
(8) V. I. Nefedov, A. P. Sadovskii, L. N. Mazlov, A. P. Belyaev, and E. S. Gluskin, *J. Struct. Chem.*, **12**, 617 (1971).
(9) V. I. Nefedov and K. N. Narbutt, *J. Struct. Chem.*, **12**, 937 (1971).
(10) D. W. Turner, C. Baker, A. D. Baker, and C. R. Brundle, "Molecular Photoelectron Spectroscopy," Wiley-Interscience, New York, N.Y., 1970.
(11) D. G. Streets, H. J. Lempka, A. W. Potts, and W. C. Price, *Phil. Trans.*, **268A**, 59 (1970).
(12) R. N. Dixon, J. N. Murrell, and B. Narayan, *Mol. Phys.*, **20**, 611 (1971).
(13) M. Klasson and R. Manne in "Electron Spectroscopy," D. A. Shirley, Ed., North-Holland Publishing Co., Amsterdam, 1972, p 471.
(14) M. Klasson, *et al.*, Uppsala University Institute of Physics Preliminary Report No. UUIP-831, Aug 1973 (see also references contained herein).
(15) R. F. Lake and H. Thompson, *Proc. Roy. Soc., Ser. A*, **315**, 323 (1970).
(16) N. Jonathan, K. Ross, and V. Tomlinson, *Int. J. Mass Spectrom. Ion Phys.*, **4**, 51 (1970).
(17) M. B. Robin, N. A. Kuebler, and C. R. Brundle in ref 13, p 351.
(18) A. D. Baker, D. P. May, and D. W. Turner, *J. Chem. Soc. B*, 22 (1968).
(19) J. N. Murrell and R. J. Suffolk, *J. Electron Spectrosc. Rel. Phenom.*, **1**, 471 (1973).
(20) K. Myers and G. Andermann, *J. Phys. Chem.*, **76**, 3975 (1972).
(21) G. Andermann, R. A. Lynch, H. C. Whitehead, and K. Myers, *Proc. Int. Symp. X-ray Spectra Electron. Struct. Matter, 1972*, 283 (1973).
(22) R. E. LaVilla and R. D. Deslattes, *J. Phys. Colloq. C-4*, **32**, (Suppl. 10), C4-100 (1971).
(23) G. Andermann and H. C. Whitehead, *Advan. X-ray Anal.*, **14**, 453 (1971).
(24) V. I. Nefedov, *J. Struct. Chem.*, **13**, 334 (1972).
(25) J. A. Pople and D. L. Beveridge, "Approximate Molecular Orbital Theory," McGraw-Hill, New York, N.Y., 1970, Appendix A.
(26) R. Manne, *J. Chem. Phys.*, **52**, 5733 (1970).
(27) H. C. Whitehead, J. D. Layfield, and G. Andermann, *Rev. Sci. Instrum.*, **43**, 50 (1972).
(28) J. A. Bearden, *Rev. Mod. Phys.*, **31**, 78 (1967).
(29) K. Kimura, S. Katsumata, Y. Achiba, H. Matsumoto, and S. Nagakura, *Bull. Chem. Soc. Jap.*, **46**, 373 (1973).
(30) See paragraph at end of text regarding supplementary material.
(31) J. M. Shulman and J. W. Moskowitz, *J. Chem. Phys.*, **47**, 3491 (1967).
(32) G. Diercksen and H. Preuss, *Int. J. Quantum Chem.*, **1**, 357 (1967).
(33) R. J. Buenker, J. L. Whitten, and J. D. Petke, *J. Chem. Phys.*, **49**, 2261 (1968).
(34) S. D. Peyerimhoff and R. J. Buenker, *Theor. Chim. Acta*, **19**, 1 (1970).
(35) P. M. Stevens, E. Switkes, E. A. Laws, and W. N. Lipscomb, *J. Amer. Chem. Soc.*, **93**, 2603 (1971).
(36) W. C. Ermler and C. W. Kern, *J. Chem. Phys.*, **58**, 3458 (1973).
(37) I. Fischer-Hjalmars and P. Siegbahn, *Theor. Chim. Acta*, **31**, 1 (1973).
(38) B. O. Jonsson and E. Lindholm, *Ark. Fys.*, **39**, 65 (1969).
(39) J. A. R. Samson, *Chem. Phys. Lett.*, **4**, 257 (1969).
(40) L. Asbrink, O. Edqvist, E. Lindholm, and L. E. Selin, *Chem. Phys. Lett.*, **5**, 192 (1970).
(41) L. Asbrink, E. Lindholm, and O. Edqvist, *Chem. Phys. Lett.*, **5**, 609 (1970).
(42) B. Narayan and J. N. Murrell, *Mol. Phys.*, **19**, 169 (1970).
(43) T. A. Carlson and C. P. Anderson, *Chem. Phys. Lett.*, **10**, 561 (1971).
(44) C. R. Brundle, M. B. Robin, and N. A. Kuebler, *J. Amer. Chem. Soc.*, **94**, 1466 (1972).
(45) D. G. Streets and G. P. Caesar, *Mol. Phys.*, **26**, 1037 (1973).
(46) C. R. Noller, "Chemistry of Organic Compounds," 1st ed, W. B. Saunders, Philadelphia, Pa., 1951, p 439.
(47) Reference 46, p 430.

Significant Structure Theory of Multilayer Physical Adsorption

David S. Newsome[1]

Department of Chemical Engineering, Virginia Polytechnic Institute and State University, Blacksburg, Virginia 24061
(Received June 17, 1974)

A new theory of multilayer physical adsorption is developed using a modified form of the significant structure theory of liquids. With adsorption limited to three layers, isotherm equations are developed in which the adsorption process is described from zero surface coverage up to three adsorbed layers. These isotherm equations are used to fit the multilayer adsorption data for the system Ar–hexagonal boron nitride at three different temperatures. The predicted temperature dependence of the theoretical isotherms agrees quite well with the experimental data. The theory not only correctly predicts condensation of Ar in the first adsorbed layer, but in the second layer as well, with the critical temperature in each layer dependent on the degree of lateral interaction of Ar in that layer. All molecular parameters except the gas–solid interaction parameters are taken from outside sources. The gas–solid interaction parameter used in the first layer agrees well with previously used values. There are no independent sources of the gas–solid interaction parameters in the second and third layers.

Introduction

Of particular theoretical interest in physical adsorption are those model systems of rare gases adsorbed on nearly homogeneous surfaces, such as graphitized carbon black and hexagonal boron nitride. Experimental studies of these systems have shown what appear to be phase transitions in the first adsorbed layer.[2] Some measurements have also been taken which show what appears to be phase transitions in the higher adsorbed layers as well.[3-5] A successful theory of multilayer adsorption should somehow be able to

account for the appearance and disappearance of these adsorption steps in a reasonable and consistent fashion.

Most of the recent theoretical work in physical adsorption has been in the area of submonolayer adsorption at intermediate values of surface coverage[6-8] and in the low surface coverage area known as the Henry's law region.[9-11] There has been less work in the multilayer regions, but one theory of multilayer adsorption has been developed by Pace[12] using a statistical mechanical lattice vacancy model. In this model adsorption is allowed to proceed up to three

layers, and the behavior of a molecule in any layer is represented by a two-dimensional lattice liquid model utilizing the Ono approximation to express the variation of the free volume with the fraction of vacant sites in the lattice. In order to test the model, Pace[12] calculated the isosteric heats of adsorption for the system Ar–graphitized carbon black and found good agreement with the experimental data of Beebe and Young[13] for this system up to a coverage of two adsorbed layers. Pace concluded that the adsorbed layers are liquid like in character as a result of this work.

Although Pace did not derive any specific theoretical isotherms, Pierotti and Thomas[14] have shown that the isotherms predicted by Pace's theory are not accurate representations of the actual experimental system, as the data have very pronounced steps, while the theory has only small, undefined steps in the second layer. As pointed out by Bruce and Sheridan,[15] a realistic theory of adsorption must do more than predict thermodynamic quantities, but must in fact be able to fit the primary data, the set of isotherms. This point of view is taken here, since if the isotherms can be correctly fitted, the thermodynamic quantities are correctly predicted, whereas the reverse is not necessarily true.

In this paper a new theory of multilayer adsorption is developed using the general approach of Pace [12] but with a somewhat different model. McAlpin and Pierotti[7,8] have applied the significant structure theory of liquids, originally developed by Eyring, et al.,[16] to submonolayer adsorption with good success for a number of experimental systems. Pierotti[7] points out that two-dimensional adsorbed phases are more amenable to treatment by hole theories than are three-dimensional fluids. A vacancy existing on a surface is not a novel idea, whereas in a three-dimensional fluid, the idea of a hole seems somewhat contrived. Pierotti, et al.,[7,8] are able to predict the two-dimensional critical temperature for the Ar–graphite system closely with this theory as well as fitting the isotherm data for a number of other submonolayer adsorption systems. The significant structure theory is therefore chosen as a basis for a new multilayer adsorption theory. As a test of the new theory, an attempt is made to fit the experimental data of the adsorption system Ar–hexagonal boron nitride. This system consists of multilayer data which show a vertical riser in the second layer indicative of condensation, and the data are taken at three temperatures. These data are an excellent test of a multilayer adsorption theory.

Theory

The Model. The model used here is one where two-dimensional liquid-like layers adsorb on a structureless, energetically uniform surface. The surface therefore imposes no structure on the adsorbed layers, and each layer is assumed to be in a hexagonal close-packed configuration.

The energy of an adsorbed molecule in a layer is made up of two contributions: (1) site energy and (2) lateral interaction energy. The site energy is the energy an isolated molecule derives from the surface and also from its interactions with all the adsorbed molecules in the $(i - 1)$ layers beneath the ith layer. The adsorbate–adsorbate interaction, or lateral interaction, in any layer is assumed to follow a Lennard-Jones potential function as seen in eq 1 and is assumed to be pairwise additive. Here E is the pair interaction energy in calories per mole, R is the gas constant in calories, (ϵ/k) is the potential minimum in degrees, r^* is the internuclear distance at the potential minimum, and r is the internuclear distance. Molecular vibrations of the adsorbed gas normal to the surface are assumed to be the same in every layer and to be given by a harmonic oscillator model. Each adsorbed layer is assumed to have three significant structures, or degrees of freedom, available to it at any given time, and just as in the case of liquids,[16,17] these are a solid-like degree of freedom, a configurational degeneracy of the solid-like degree of freedom due to the presence of holes, or unfilled sites, and a gas-like degree of freedom.

Partition Function. Eyring and Jhon[17] write the partition function for a liquid as

$$Q = \left\{ Q_s \left[1 + n_h \exp\left(-\frac{\epsilon_h}{RT} \right) \right] \right\}^{V_s N / V} [Q_g]^{(V - V_s)N / V}$$

(2)

where Q_s is the solid-like partition function and Q_g is the gas-like partition function. The term multiplying Q_s in eq 2 is the total number of positions available to a molecule in the fluid. Here n_h is proportional to the number of holes available to a solid-like molecule and ϵ_h is the so-called strain energy, or the energy a molecule must possess to enter a hole, thus excluding its competing neighbors. N is Avogadro's number. The fraction V_s/V of the degrees of freedom should be solid-like where V and V_s are the molar volumes of the liquid and solid, respectively. $(V - V_s)/V$ is the fraction of the degrees of freedom of the fluid which are gas like.

Any suitable partition function desired can be used for Q_s and Q_g. Eyring[17] chose to use the ideal gas partition function for Q_g and the Einstein solid partition function for Q_s. Henderson[18] has shown that the Lennard-Jones and Devonshire[19,20] cell model is perhaps a better choice for the solid-like partition function.

For two-dimensional multilayer adsorption, the canonical partition function for the ith adsorbed layer can be written as

$$Q_i = q_{is}{}^{N_i(N_i / N_{i-1})} q_{ig}{}^{N_i[(N_{i-1} - N_i)/N_{i-1}]}$$

(3)

where q_{is} is the partition function for the solid-like structure in the ith layer and q_{ig} is the corresponding partition function for the gas-like structure. N_i is the number of molecules adsorbed in the ith layer, while N_{i-1} is the number of molecules adsorbed in the $(i - 1)$ layer. N_0 would correspond to the number of sites available for adsorption on the surface.

For q_{is} the partition function for the two-dimensional cell model as given by Devonshire[19,20] is used in this model, with a term included for the configurational degeneracy and the strain energy assumed to be zero. Thus

$$q_{is} = (\Lambda^{-2} a_{fi}) \left[\exp\left(\frac{U_i + W_i}{RT} \right) \right] (1 + n_h) q_z$$

(4)

The first term in eq 4 is the partition function for a Lennard-Jones and Devonshire[19,20] two-dimensional fluid, where Λ is $h/(2\pi m k T)^{1/2}$ and a_{fi} is the free area in the ith layer and is given by

$$a_{fi} = \pi a^2 \int_0^{a/2} \exp\left\{ \left(\frac{6\epsilon_i}{kT} \right) [2m_s(y) - l_s(y)] \right\} \, dy$$

(5)

where a is the diameter of the cell containing the molecule and is taken to be equal to the internuclear distance in the bulk adsorbate, ϵ_i is the Lennard-Jones interaction param-

eter in the ith adsorbed layer, $m_s(y)$, $l_s(y)$ are polynomials whose form is given by Lennard-Jones and Devonshire,[19,20] and $y = (r/a)^2$ where r is the distance from the cell center to the molecule. The second term in eq 4 is a correction for the zero point of energy, which is taken as a molecule at rest infinitely removed from the surface. U_i is the molar site energy for an isolated molecule in the ith layer, and W_i is the molar two-dimensional lattice energy of the adsorbate in the ith layer.

The third term in eq 4 is the degeneracy factor for the strained solid state. Eyring[17] expresses n_h for a liquid as

$$n_h = n(V - V_s)/V_s \qquad (6)$$

n is a proportionality constant nearly equal to the coordination number. For this model n_h is expressed as

$$n_h = z(A_i - A_i^0)/A_i^0 \qquad (7)$$

where z is the coordination number, A_i is the area per molecule in the ith layer, and A_i^0 is the area per molecule when the ith layer is filled to capacity.

The last term in eq 4 is the harmonic oscillator partition function for the vibrations normal to the adsorbing surface. This is assumed to be the same for all layers and is given by

$$q_z = \exp\left(\frac{-h\nu}{2kT}\right) / \left[1 - \exp\left(\frac{-h\nu}{kT}\right)\right] \qquad (8)$$

where ν is the vibrational frequency.

The molecular partition function for the gas-like structure in the ith adsorbed layer is assumed to be given by a two-dimensional ideal gas model and is

$$q_{ig} = q_z \left[\exp\left(\frac{U_i}{RT}\right)\right](\Lambda^{-2} A_i e) \qquad (9)$$

The second term in eq 9 is the correction for the zero point of energy of the vibrating molecules in the ith layer while the last term in eq 9 is the partition function for an ideal, two-dimensional gas molecule, where e is the base of the natural logarithm.

Combining eq 3, 4, 7, and 9 the canonical partition function for the ith adsorbed layer is

$$Q_i = \left[\Lambda^{-2} q_z \exp\left(\frac{U_i}{RT}\right)\right]^{N_i} \left[a_{fi}\left\{\exp\left(\frac{W_i}{RT}\right)\right\} \times \right.$$
$$\left.\left(1 + \frac{z(A_i - A_i^0)}{A_i^0}\right)\right]^{N_i(N_i/N_{i-1})} [A_i e]^{N_i[(N_{i-1}-N_i)/N_{i-1}]} \qquad (10)$$

The total partition function Q for all i adsorbed layers is

$$Q = \prod_i Q_i \qquad (11)$$

or

$$\ln Q = \sum_i \ln Q_i \qquad (12)$$

This total partition function Q for the multilayer model is now used to compute theoretical adsorption isotherms.

Theoretical Isotherms. Theoretical isotherms are determined by finding the chemical potential for the adsorbed molecules in each layer and equating these to each other and to the chemical potential of the gas phase. The chemical potential μ_i in the ith layer is given by

$$\frac{\mu_i}{kT} = -\left(\frac{\partial \ln Q}{\partial N_i}\right)_{N_{k\neq i}, T} \qquad (13)$$

If the gas phase is taken to be an ideal monatomic gas, the chemical potential μ_g of the gas phase is given by

$$\frac{\mu_g}{kT} = -\ln\left[\left(\frac{2\pi m kT}{h^2}\right)^{3/2} kT\right] + \ln P \qquad (14)$$

where P is the gas-phase pressure and all other terms have their usual meaning. Equating the chemical potentials yields i equations in i unknowns where i is the number of layers assumed and the i unknowns are the ratios of N_i/N_{i-1}, N_{i-1}/N_{i-2}, ..., N_1/N_0. In the multilayer significant structure theory, the coverage in the ith layer, θ_i, is defined as

$$\theta_i = N_i/N_{i-1} \qquad (15)$$

A set of θ_i's are then the solution of the isotherm equations at a given temperature and set of adsorption parameters. The total statistical coverage, θ, is

$$\theta = \frac{1}{N_0} \sum_{i=1} N_i \qquad (16)$$

which is equal to the total number of molecules adsorbed divided by the total number of sites on the surface, or

$$\theta = \frac{1}{N_0} \sum_{i=1} N_{i-1}\theta_i \qquad (17)$$

The experimental surface coverage θ is usually defined as

$$\theta = V_{ads}/V_m \qquad (18)$$

where V_{ads} is the volume of gas adsorbed and V_m is the volume of gas needed to completely fill the first layer. The experimental and theoretical surface coverages are therefore very comparable as seen from eq 16 and 18. The statistical coverage θ and gas-phase pressure P are the two parameters which are used in comparing the theory to experiment.

In the present treatment the number of layers adsorbed are arbitrarily limited to three, which leads to three simultaneous equations which must be solved for θ_i and P. These equations are found using the method described and are

$$\frac{U_1}{RT} - \frac{U_2}{RT} + 2\theta_1 \ln\left[\frac{a_{f1}}{A_1^0} \exp\left(\frac{W_1}{RT}\right)\right] + $$
$$2\theta_1 \ln (6 - 5\theta_1) - \ln \theta_1 - \left(\frac{6\theta_1}{6 - 5\theta_1}\right) - $$
$$\theta_1 = [2\theta_2 + (\theta_2)^2] \ln\left[\frac{a_{f2}}{A_2^0} \exp\left(\frac{W_2}{RT}\right)\right] + $$
$$[2\theta_2 + (\theta_2)^2] \ln (6 - 5\theta_2) - \left[\frac{6(\theta_2)^2}{6 - 5\theta_2}\right] - $$
$$\left[\frac{6\theta_2}{6 - 5\theta_2}\right] - 2\theta_2 - \ln \theta_2 + \left[\frac{6(\theta_3)^2}{6 - 5\theta_3}\right] - $$
$$(\theta_3)^2 \ln\left[\frac{a_{f3}}{A_3^0} \exp\left(\frac{W_3}{RT}\right)\right] - (\theta_3)^2 \ln (6 - 5\theta_3) + \theta_3 \qquad (19)$$

$$\frac{U_2}{RT} - \frac{U_3}{RT} + 2\theta_2 \ln\left[\frac{a_{f2}}{A_2^0} \exp\left(\frac{W_2}{RT}\right)\right] + $$
$$2\theta_2 \ln (6 - 5\theta_2) - \left(\frac{6\theta_2}{6 - 5\theta_2}\right) - \ln \theta_2 - \theta_2 = $$
$$-\left[\frac{6(\theta_3)^2 + 6\theta_3}{6 - 5\theta_3}\right] + [2\theta_3 + (\theta_3)^2] \times $$
$$\ln\left[\frac{a_{f3}}{A_3^0} \exp\left(\frac{W_3}{RT}\right)\right] + [2\theta_3 + (\theta_3)^2] \ln (6 - 5\theta_3) - $$
$$\ln \theta_3 - 2\theta_3 \qquad (20)$$

and

$$\ln P = -\ln \Lambda + \ln (kT) - \ln q_z - \frac{U_3}{RT} -$$

$$2\theta_3 \ln \left(\frac{c_{f3}}{A_3{}^0}\right) - 2\theta_3 \ln (6 - 5\theta_3) + \ln \theta_3 -$$

$$\ln A_3{}^0 - \left(\frac{2W_3}{RT}\right)\theta_3 + \left(\frac{6\theta_3}{6 - 5\theta_3}\right) + \theta_3 \quad (21)$$

It should be emphasized that no distinction is made between the submonolayer and multilayer regions in the theory. That is, the same model applies to all regions of adsorption from zero surface coverage up to three adsorbed layers.

Comparison with Experiment

Equations 19–21 are now applied to the experimental results of Pierotti[3] for the system Ar–BN. Table I shows the molecular parameters used in the theory and Figure 1 shows the theoretical curves and the experimental multilayer data of the Ar–BN system. Figure 2 shows the fit of the same system in the submonolayer region; these data are taken from Ross and Pultz.[21]

In fitting the data the values of all parameters except U_i, the molar site energy, are taken from outside sources. The lateral interaction parameter W_i is found by summing the Lennard-Jones potential function, eq 1, directly over the nearest 36 neighbors in the hexagonal lattice and integrating over the rest of the lattice. ϵ_1/kT is given the previously used value[8] of 108°K and ϵ_2/kT and ϵ_3/kT are given the gas phase value[22] of 122°K.

A best fit value of U_2 and U_3 is found for the multilayer isotherm at 68.9°K as seen in Figure 1 and the value of U_1 is found by a best fit of the submonolayer data of Ross and Pultz[21] for this system as shown in Figure 2. These values of U_i are then used to derive the other isotherms, changing only the temperature.

The experimental maximum surface coverage V_m is taken to be 6.86 ml(STP)/g. This is somewhat higher than any previously used value of V_m for this system. Pierotti[3] uses 5.3 ml(STP)/g which is the BET value. It should be noted that Steele[6] also had to assume a higher than usual value of surface area in order to maintain agreement between his theory and the experimental data for argon adsorbed on graphitized carbon black.

Discussion

In most equations of state which incorporate an attractive potential, condensation is predicted by the appearance of the so-called van der Waals loop, and the position of the vertical riser in the loop is determined by the equal areas method of Maxwell. In the present theory no such loops appear in the first and second layers when the critical temperature is reached. The vertical risers that do appear are true vertical discontinuities, not loops. The theory does predict loops only in the last layer below its critical temperature. In the present case this is the third layer, which is not shown in Figure 1.

The theory seems to provide an excellent fit of the observed data for the Ar–BN system. At the highest temperature there is no step in the data or in the theory, but as the temperature is lowered, both the theory and data show the development of a well-defined step in the second layer. At the lowest temperature of interest both the theory and data show condensation in the second layer. The isotherm temperature dependence is predicted quite well by the theory.

TABLE I: Molecular Adsorption Parameters for the Ar–BN System

Parameter	Value
$10^{-12}\,\nu$, sec^{-1}	0.95[a]
$A_1{}^0$, $A_2{}^0$, $A_3{}^0$, Å^2	14.8[a]
$(\epsilon/k)_1$, °K	108[a]
$(\epsilon/k)_2$, $(\epsilon/k)_3$, °K	122[b]
W_1, cal/mol	726[c]
W_2, W_3, cal/mol	820[c]
U_1, cal/mol	1900[d]
U_2, cal/mol	1135[e]
U_3, cal/mol	1080[e]
V_m, ml(STP)/g	6.86[f]
a, Å	3.84[a]

[a] Reference 8. [b] Reference 22. [c] Determined as described in text. [d] Best fit of submonolayer data of Ross and Pultz (ref 21). [e] Best fit of isotherm at 68.9°K. [f] Adjusted value for best fit of data.
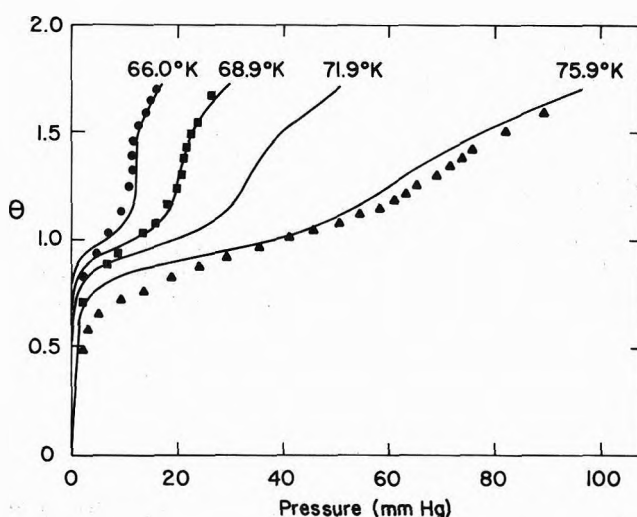

Figure 1. Theoretical isotherms and experimental data for argon on boron nitride.
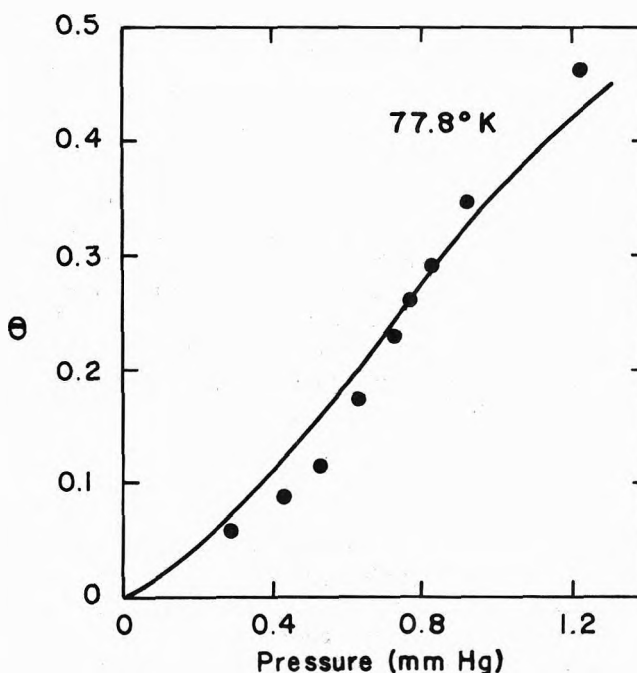

Figure 2. Theoretical isotherm and experimental submonolayer data for argon on boron nitride.

The value of $(\epsilon/k)_i$ determines the critical temperature in each layer, whereas U_i determines the position of the step on the pressure axis. Sinanoglu and Pitzer[23] have determined using third-order perturbation theory that the pairwise interactions of molecules adsorbed on a surface in the submonolayer region are less than in the gas phase. These results are in good agreement with their theory as their theory predicts a 20–40% reduction in the gas-phase Lennard-Jones potential minimum. The critical temperatures predicted by the present treatment are about 65°K for the first layer and 68°K for the second layer. This brings up the very interesting situation where at points intermediate between these two temperatures the first layer is supercritical and the second layer is subcritical. Unfortunately not enough data have been taken with the Ar–BN system to verify whether this is indeed possible. If so, then a smooth transition is seen to take place between the adsorbed state and the liquid state.

The value of U_1 used is very close to that estimated for the Ar–BN system by Pierotti[3] using the Frenkel–Halsey–Hill equation. No independent values are available for U_2 or U_3.

The significant structure theory is often criticized for the intuitive nature of its development and the number of adjustable parameters in the partition functions. Here only U_i is adjusted to fit the data, and, as pointed out by McAlpin and Pierotti,[7] the more or less arbitrary parameter n_h used in the liquid theory is in an adsorption theory related to the experimentally measurable surface coverage. The ex-

traordinarily realistic fit provided in the present case can only lend more credit to this theory.

References and Notes

(1) This work was in part done in partial fulfillment of the requirements for a Ph.D. Degree at the Department of Chemistry, Georgia Institute of Technology, 1972.
(2) (a) A. Thomy and X. Duval, *J. Chim. Phys.*, **67**, 1101 (1970); (b) S. Ross and W. Winkler, *J. Colloid Sci.*, **10**, 330 (1955).
(3) R. A. Pierotti, *J. Phys. Chem.*, **66**, 1810 (1962).
(4) C. F. Prenzlow and G. D. Halsey, Jr., *J. Phys. Chem.*, **61**, 1158 (1957).
(5) J. H. Singleton and G. D. Halsey, Jr., *J. Phys. Chem.*, **58**, 1011 (1954).
(6) W. A. Steele, *J. Phys. Chem.*, **69**, 3446 (1965).
(7) J. J. McAlpin and R. A. Pierotti, *J. Chem. Phys.*, **41**, 68 (1964).
(8) J. J. McAlpin and R. A. Pierotti, *J. Chem. Phys.*, **42**, 1842 (1965).
(9) J. R. Sams, G. Constabaris, and G. D. Halsey, Jr., *J. Chem. Phys.*, **36**, 1334 (1962).
(10) R. N. Ramsey, H. E. Thomas, and R. A. Pierotti, *J. Phys. Chem.*, **76**, 3171 (1972).
(11) W. A. Steele, *Surface Sci.*, **39**, 149 (1973).
(12) E. L. Pace, *J. Chem. Phys.*, **27**, 1341 (1957).
(13) R. A. Beebe and D. M. Young, *J. Phys. Chem.*, **58**, 93 (1954).
(14) R. A. Pierotti and H. E. Thomas, "Surface and Colloid Science," Vol. IV, Wiley-Interscience, New York, N.Y., 1971, pp 93–259.
(15) L. A. Bruce and M. H. Sheridan, *J. Chem. Soc., Faraday Trans. 1*, **69**, 176 (1973).
(16) H. Eyring, T. Ree, and N. Hirai, *Proc. Nat. Acad. Sci. U. S.*, **44**, 683 (1958).
(17) H. Eyring and M. S. Jhon, "Significant Liquid Structures," Wiley, New York, N.Y., 1969, Chapter 3.
(18) D. Henderson, *J. Chem. Phys.*, **39**, 1857 (1963).
(19) J. E. Lennard-Jones and A. F. Devonshire, *Proc. Roy. Soc., Ser. A*, **163**, 53 (1937).
(20) A. F. Devonshire, *Proc. Roy. Soc., Ser. A*, **163**, 132 (1937).
(21) S. Ross and W. W. Pultz, *J. Colloid Sci.*, **13**, 397 (1958).
(22) J. O. Hirschfelder, C. F. Curtiss, and R. B. Bird, "Molecular Theory of Gases and Liquids," Wiley, New York, N.Y., 1954, p 1110.
(23) O. Sinanoglu and K. S. Pitzer, *J. Chem. Phys.*, **32**, 1729 (1960).

Electronic Structures of Cephalosporins and Penicillins. III. EH and CNDO/2D Electron Density Maps of 7-Amino-3-cephem

Donald B. Boyd

Lilly Research Laboratories, Eli Lilly and Company, Indianapolis, Indiana 46206 (*Received July 9, 1974*)

Publication costs assisted by Eli Lilly and Company

Contour maps of electron density computed from EH (extended Hückel) and CNDO/2D (complete-neglect-of-differential-overlap, deorthogonalized) wave functions are reported for the molecular nucleus of cephalosporin antibiotics. Density is computed in planes through the sulfide, ethylenic, and β-lactam functionalities. Comparison of the two MO methods reveals qualitative similarities for most of the charge distributions, but interestingly, CNDO/2D gives greater directionality to the lone pairs on S, N, and O. The charge distributions are discussed in relation to the mechanism of biological activity of β-lactam antibiotics.

Introduction

Recent utilizations of molecular orbital methods in studying structure–activity relationships among β-lactam antibiotics have extended the understanding of the electronic structures of cephalosporins and penicillins. In the first paper of this series, extended Hückel (EH) wave functions were used to assign the uv and circular dichroism bands of cephalosporins, penicillins, and related structures.[1] Despite the simplicity of the theory, reasonable correlations of predicted and experimental absorptions were obtained. In the second paper of the series, the EH charge distributions in the β-lactam ring were correlated with biological activity of antibiotics with different molecular nuclei.[2] A deficiency of electron density on the carbonyl carbon and a lability of the β-lactam C–N bond were found to be among the attributes of good antibiotics. In other words,

the β-lactam ring must have a certain degree of susceptibility to nucleophilic attack for high biological activity. Our findings are consistent with the proposed mode of action of the β-lactam antibiotics; namely, they acylate and thereby inactivate a transpeptidase involved in bacterial cell wall synthesis.[3] The main conclusions regarding the EH derived charge distributions are corroborated in studies using another popular semiempirical MO method, CNDO/2 (complete-neglect-of-differential-overlap).[4-6]

One of the molecular nuclei common to our earlier studies is 7-amino-3-cephem (I). This bicyclic system is the fun-

I
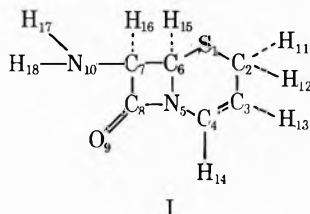
damental moiety of the Δ^3-cephalosporins, compounds of major therapeutic importance.[7] The medicinal cephalosporins have a substituent, such as CH_3, at the 3 position, a carboxyl group at the 4 position, and an acylated 7-amino side chain. The β-lactam ring of the 3-cephem moiety is tipped up (toward the β face of the molecule) with respect to the dihydrothiazine ring.[7] The sulfur atom is also puckered about 0.9 Å above the rest of the atoms in the dihydrothiazine ring. Atomic coordinates for structure I are described elsewhere.[1]

The purpose of this study is twofold. One is to view for the first time the spatial distribution of electrons in 7-amino-3-cephem using electron density maps. These are contour diagrams showing the topography of the electron clouds in selected planes through the molecule. We will examine the interesting regions of the sulfide lone pairs and S-C bonds, the ethylenic C=C bond, the enamine C-N bond, and the β-lactam C-N and C=O bonds. Plots of the total density of the valence electrons give a rather bulbous appearance to the electron clouds (see, e.g., ref 8 and 9) and are not especially revealing about the details of bonding in the molecule. Of more interest than the total density map is the *difference map*, which is obtained by subtracting from the total density the spherically symmetric, ground state, valence electron atomic densities centered at the same positions as the atoms in the molecule.[9-12] The difference maps from valence electron wave functions display vividly and with frequent apparent qualitative validity the effects of bonding: lone-pair formation, σ and π bonding, and other descriptive concepts useful in chemistry.

The second purpose of this paper is to compare *via* electron density maps the EH[13-15] and CNDO/2D[11] methods. The EH wave function of 7-amino-3-cephem is obtained with previously published parameter values.[1] The CNDO/2D wave function is obtained by the standard CNDO/2 procedure[9,16] followed by a Löwdin $S^{-1/2}$ transformation on the LCAO-MO coefficient matrix in order to renormalize the CNDO/2 wave function to the usual basis set of Slater-type orbitals.[9,11,17] We have incorporated the complete CNDO/2D algorithm into a single computer program called BNDO (big NDO) devised from CNINDO.[16] Comparisons of the way in which the EH and CNDO/2D methods distribute electrons in space have been published for adenine[11] and more recently for H_2S_2.[9,12,18] The EH and CNDO/2D shapes of the filled MO's of H_2S_2 were very sim-

TABLE I: Net Atomic Charges in 7-Amino-3-cephem

Atom	EH	CNDO/2D	CNDO/2
S_1	−0.1313	0.0271	−0.1033
C_2	−0.0060	−0.1038	0.0080
C_3	−0.2222	−0.0629	−0.0638
C_4	0.1268	0.1109	0.1049
N_5	−0.1563	−0.2633	−0.1365
C_6	0.2363	0.0012	0.0741
C_7	0.1671	0.0446	0.0594
C_8	0.8214	0.4248	0.3390
O_9	−0.9477	−0.3501	−0.3065
N_{10}	−0.6270	−0.3100	−0.1952
H_{11}	0.0527	0.0423	0.0165
H_{12}	0.0511	0.0463	0.0196
H_{13}	0.0615	0.0352	0.0105
H_{14}	0.0448	0.0262	−0.0005
H_{15}	0.0289	0.0417	0.0108
H_{16}	0.0446	0.0184	−0.0072
H_{17}	0.2273	0.1327	0.0825
H_{18}	0.2281	0.1385	0.0875

[a] The fourth decimal place in these data, as well as those in Table II, is without much significance because of minor round-off errors which can enter from the input atomic coordinates, convergence criterion, conversion factors, etc., even though the calculations are carried out in double precision.

TABLE II: Mulliken Overlap Populations in 7-Amino-3-cephem

Bond	EH	CNDO/2D	Bond	EH	CNDO/2D
S_1-C_2	0.6690	0.5326	C_7-N_{10}	0.7012	0.6866
S_1-C_6	0.7158	0.4750	C_2-H_{11}	0.7966	0.7299
C_2-C_3	0.8104	0.8747	C_2-H_{12}	0.7985	0.7334
C_3=C_4	1.2483	1.2675	C_3-H_{13}	0.8004	0.7605
C_4-N_5	0.8520	0.7502	C_4-H_{14}	0.8072	0.7716
N_5-C_6	0.6939	0.6714	C_6-H_{15}	0.8183	0.7440
C_6-C_7	0.6771	0.7484	C_7-H_{16}	0.7971	0.7146
C_7-C_8	0.8017	0.7926	N_{10}-H_{17}	0.7485	0.6101
C_8=O_9	0.9856	0.7918	N_{10}-H_{18}	0.7480	0.6167
N_5-C_8	0.9151	0.7057			

ilar in appearance, but the difference maps revealed contrasts between the bonding descriptions of these two methods. In addition, we have obtained difference maps from the EH and CNDO/2D methods for adamantane, bicyclo[2.2.2]octane, and *trans*- decalin. The hydrocarbon maps show gains in density along the C-C and C-H bond axes corresponding to σ bonding and losses of density from tetrahedral shaped regions around each carbon and spheroidal shaped regions around each hydrogen. Thus, the semiempirical findings on the large polycyclic alkanes are qualitatively similar to *ab initio* electron density maps of ethane.[19]

Results and Discussion

The gross charge distribution of 7-amino-3-cephem can be seen in the conventional Mulliken[20] population analysis results (Tables I and II). Most of the charges from the three MO methods are reasonable relative to each other, but there are two nonhydrogenic atoms (S_1 and C_2) whose CNDO/2 net atomic charges change sign due to deorthogonalization. Such sign reversals are not too common for nonhydrogenic atoms.[11,21] Previous experience[9,11] indicated that deorthogonalization renders the apparent net atomic charges from a CNDO/2 wave function closer to EH values, but such is not the case for many of the atoms of 7-

amino-3-cephem. The sign reversals in the net charges of S_1 and C_2 are due to the electron density in the S 3p and 3d AO's being partitioned onto the secondary carbon C_2 by the prescription of the deorthogonalization. Differences in directionality of EH and CNDO/2D lone pair regions, which are discussed below, are not apparent from the orbital populations, thus exemplifying the superior acuity of electron density maps compared to a population analysis. The CNDO/2D charges on the hydrogens are expectedly more positive than the CNDO/2 values.[9] The EH and CNDO/2D overlap populations are quite similar for most bonds in the molecule (Table II), but the two wave functions differ in their predictions about the relative strengths of the S_1–C_2 and S_1–C_6 bonds. The lengths of these bonds from X-ray crystallographic data[7] are very close (1.82 and 1.79 Å, respectively), indicating that the EH results better reproduce this subtle difference. The CNDO/2D population analysis is thus yielding misleading results regarding the S–C bonds, perhaps due to the treatment of the S 3d atomic orbitals (*vide infra*).

Electron density maps of 7-amino-3-cephem in Figures 1–7 have contour labels corresponding to the following densities: T or 8 for 0.09, S or 7 for 0.009, and R or 6 for 0.0009 e/bohr^3. The lettered contours correspond to regions where there is greater density in the molecule than in the sum of the constituent atomic densities and may be associated with bonding or lone-pair regions. Numbered contours specify regions where the molecular density is *lower* than in the atoms. The dotted contours (.,) delineate where the molecular and atomic densities are equal. Some contours may appear discontinuous, but this is only an artifact of the limited resolution of the characters of the computer printout. The effects of formation of a molecule from the constituent atoms are most prominent within about 1.8 Å of the nuclei. Consequently, Figures 1–6 cover 3.6 × 4.8 Å, and Figures 7 covers 4.8 × 6.4 Å. Positions or projections of positions of the nuclei on the plane of density calculation are denoted by asterisks. Solid lines connect bonded atoms lying in the plane of calculation of each map; projections of internuclear axes between other bonded atoms within the field of each map are shown by dashed lines. Calculation of Figures 1–7 from the MO's required 44 min on the IBM 370/158 computer.

The buildups seen in Figure 1 on the α (bottom) and β (top) faces of the sulfur mark the regions occupied by the two sulfur lone pairs. A surprising difference between the EH and CNDO/2D maps is to be noted. Whereas CNDO/2D generally produces a smoother charge distribution than EH due to the explicit inclusion of interelectronic repulsions, CNDO/2D gives greater directionality to the lone-pair lobes. CNDO/2D gives a cloven lone-pair region concentrated along the two axes associated with sp^3 hybridization at sulfur. The EH map is suggestive of sp^2,p hybridization like the combined shapes of the individual lone-pair MO's of a simple sulfide. A similar contrast between EH and CNDO/2D was seen in the study of H_2S_2.[9,12,18] Density maps from an *ab initio* wave function of H_2S[22] showed more directionality of the lone-pair lobes than seen in the EH map of Figure 1, but also showed more density buildup in the plane of the R–S–R group than seen in the CNDO/2D map of Figure 1. A final point to notice about Figure 1 is that there is only density loss throughout the middle of
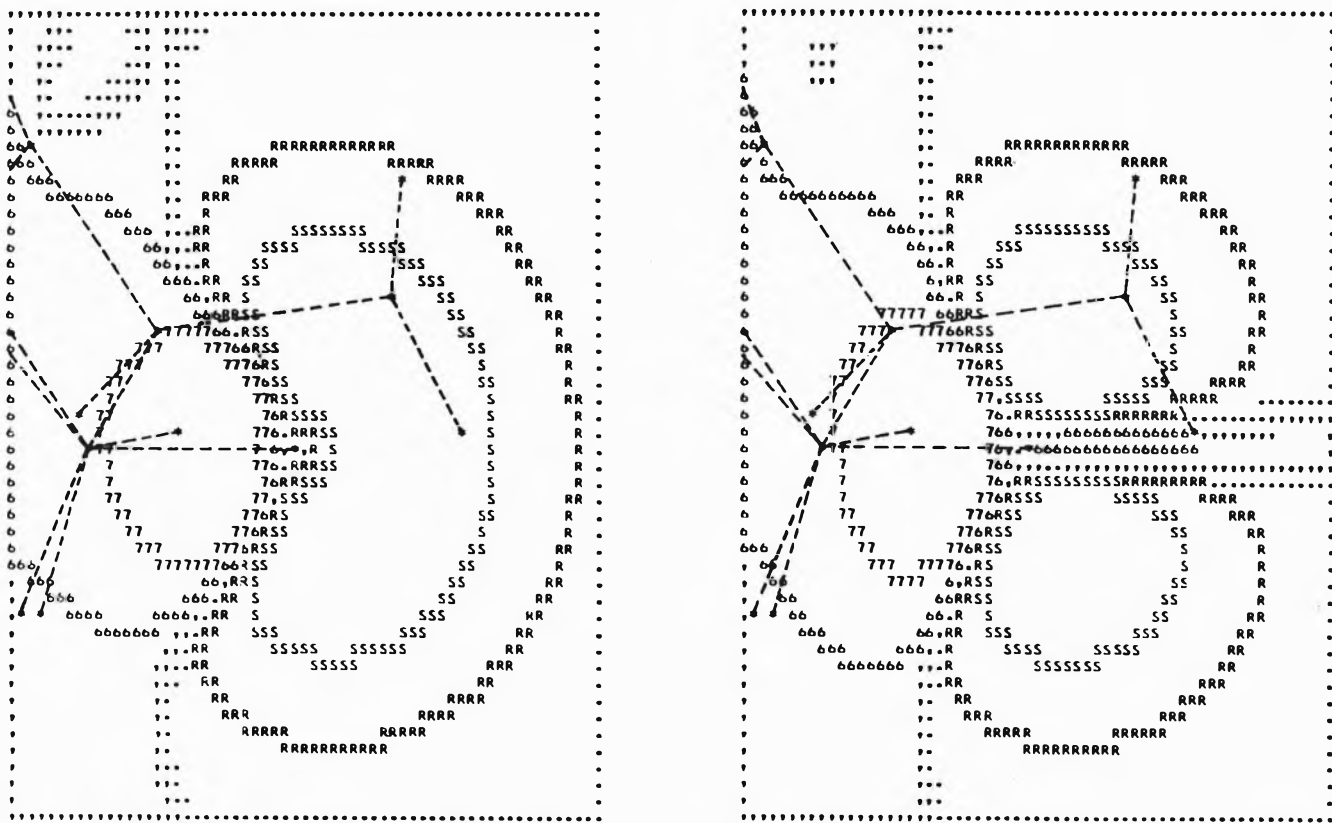

Figure 1. EH (left) and CNDO/2D (right) difference maps of 7-amino-3-cephem computed in the plane through the sulfur and perpendicular to the $C_2 \cdots C_6$ axis. This view looks down the $C_2 \cdots C_6$ axis, so that C_2 and C_6 fall at the same point, and S_1 is to the right of this point near the center of the maps. The β face of the molecule is toward the top of the maps. The peaks in density gain in the lone-pair lobes are 0.0715 and 0.0675 e/bohr^3 in the EH and CNDO/2D maps, respectively.
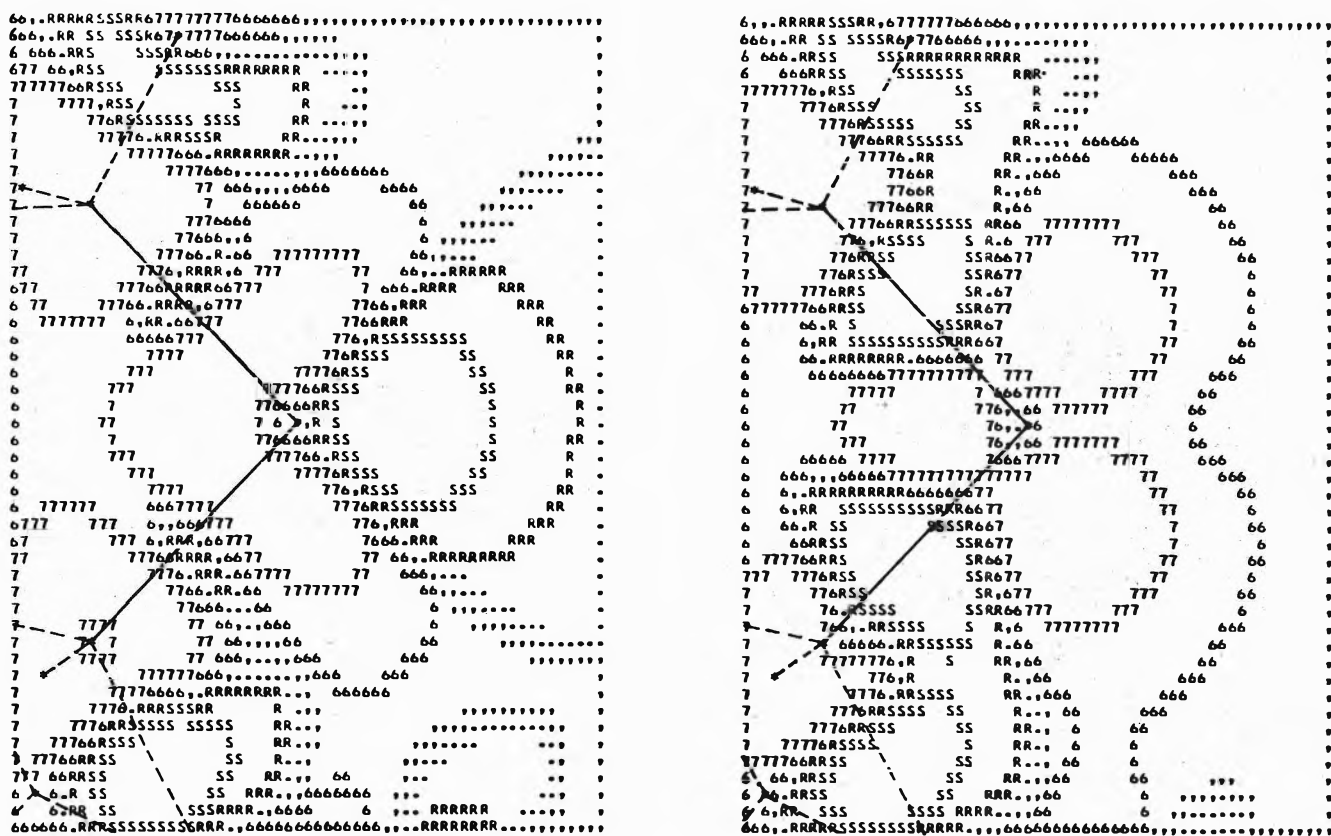
Figure 2. EH (left) and CNDO/2D (right) difference maps of 7-amino-3-cephem computed in the plane of C_6–S_1–C_2. The projection of the β-lactam ring falls in the lower left-hand corner.
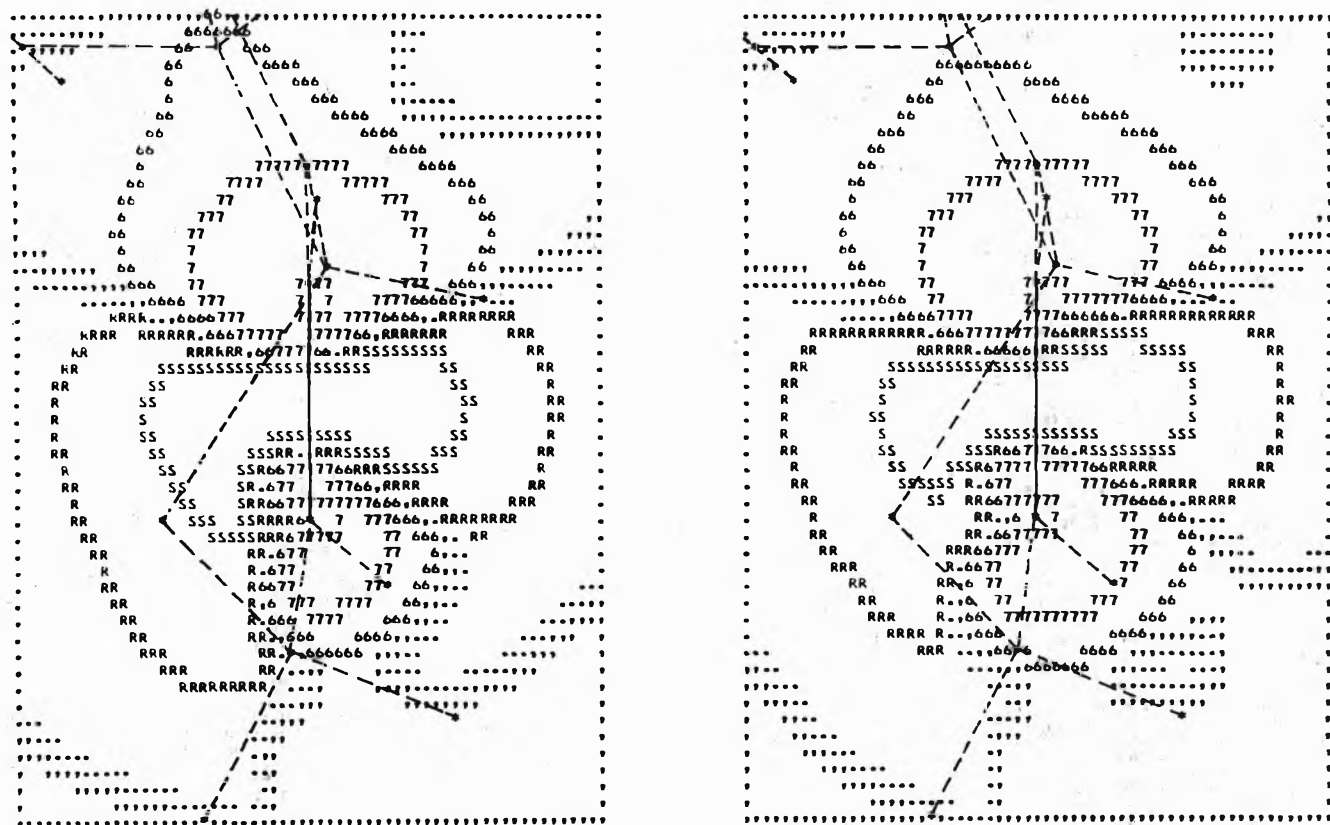

Figure 3. EH (left) and CNDO/2D (right) difference maps of 7-amino-3-cephem computed in the plane which passes through the C_3–C_4 axis and is perpendicular to the C_3–C_4–N_5 plane. The C_3–C_4 axis is the vertical solid line at the center of the maps. The projection of the β-lactam ring extends off the top of the maps. The β face of the molecule is toward the left.

Donald B. Boyd

Figure 4. EH (left) and CNDO/2D (right) difference maps of 7-amino-3-cephem computed in the plane which passes through the C_4–N_5 axis (solid line) and is perpendicular to the C_4–N_5–C_6 plane. The β face of the molecule is toward the left, and the projection of the β-lactam ring extends off the top of the maps.
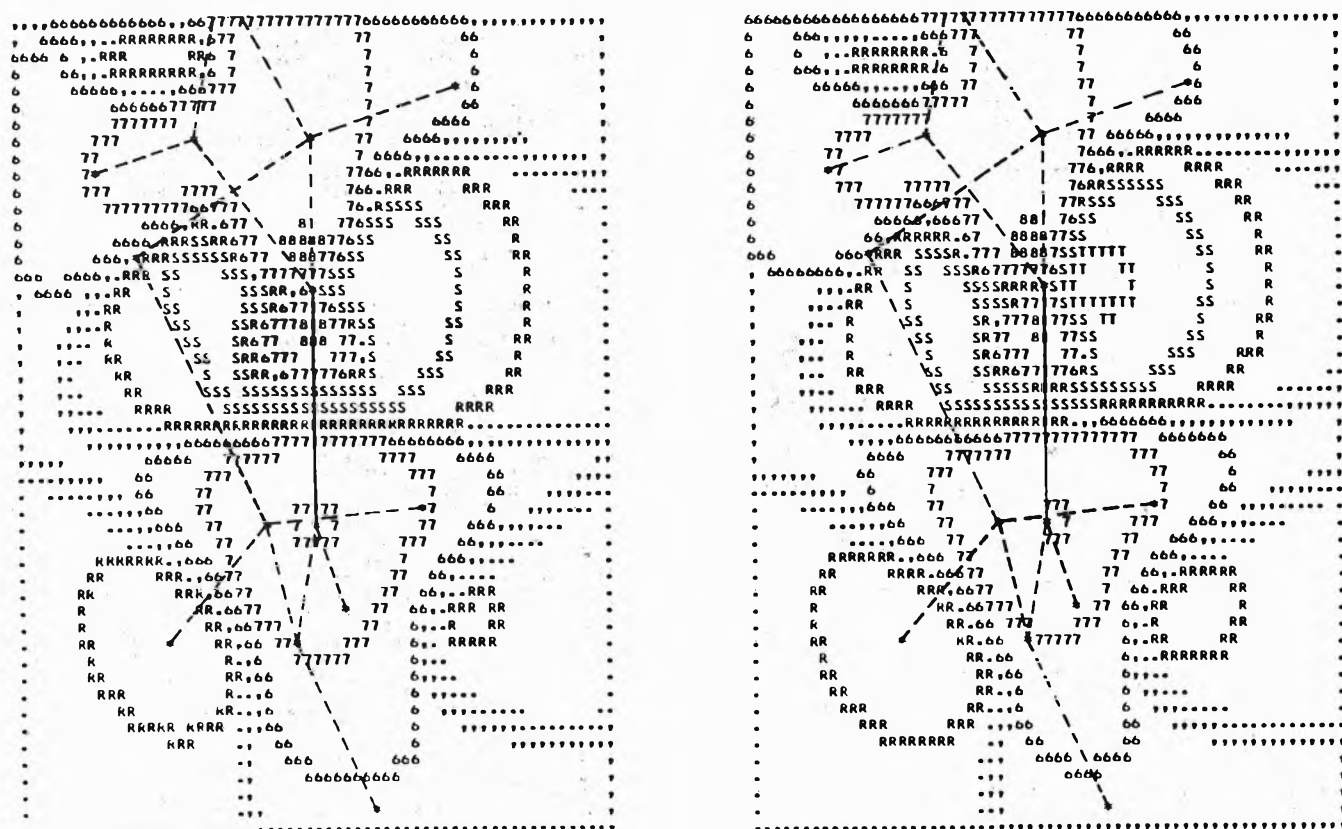

Figure 5. EH (left) and CNDO/2D (right) difference maps of 7-amino-3-cephem computed in the plane which passes through the N_5–C_8 axis (solid line) and is perpendicular to the N_5–C_8–C_7 plane. The projection of the dihydrothiazine ring extends off the lower left-hand corner of the maps. The β face of the molecule is toward the left. In this view C_8 and C_7 fall at the same asterisk. The peaks in density in the N_5 lone-pair lobe are 0.1029 and 0.2022 e/bohr^3 in the EH and CNDO/2D maps, respectively.
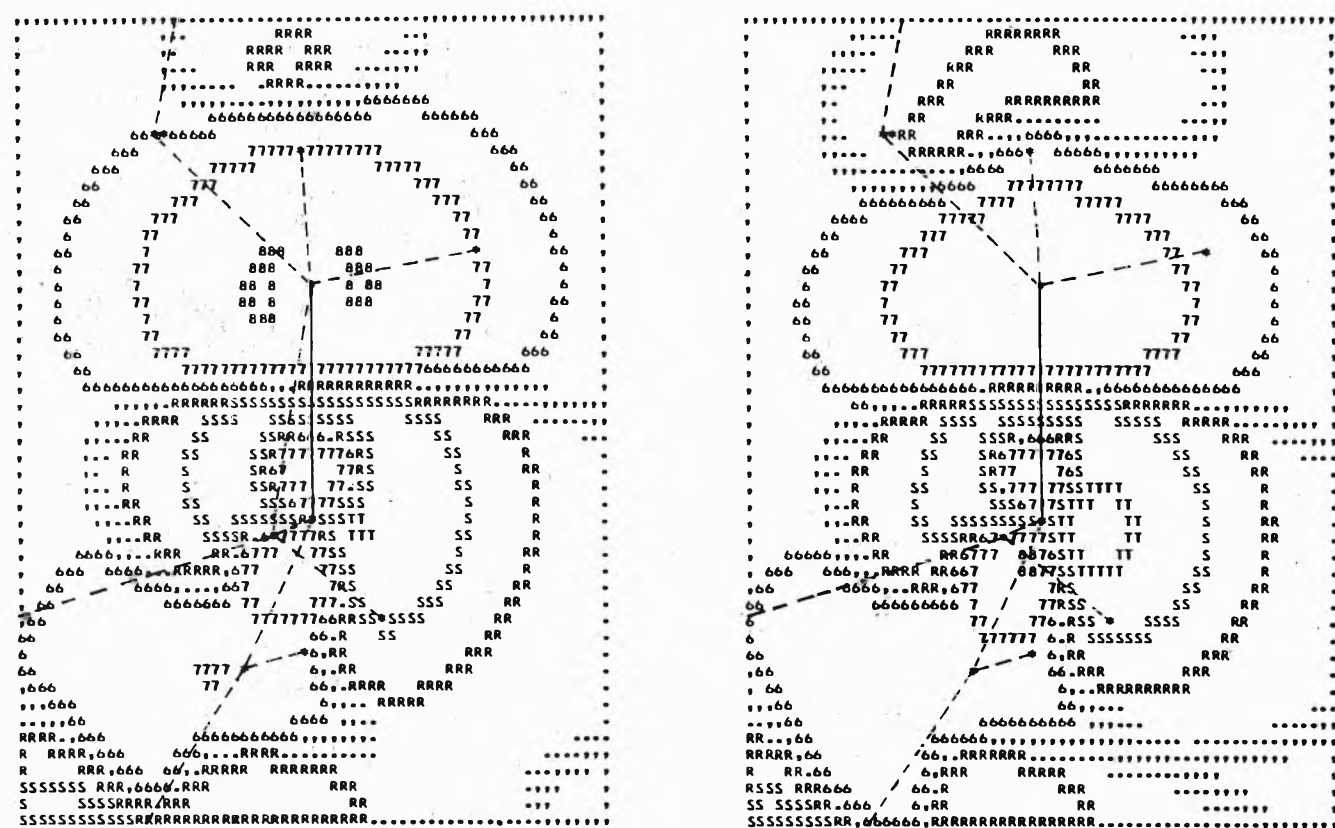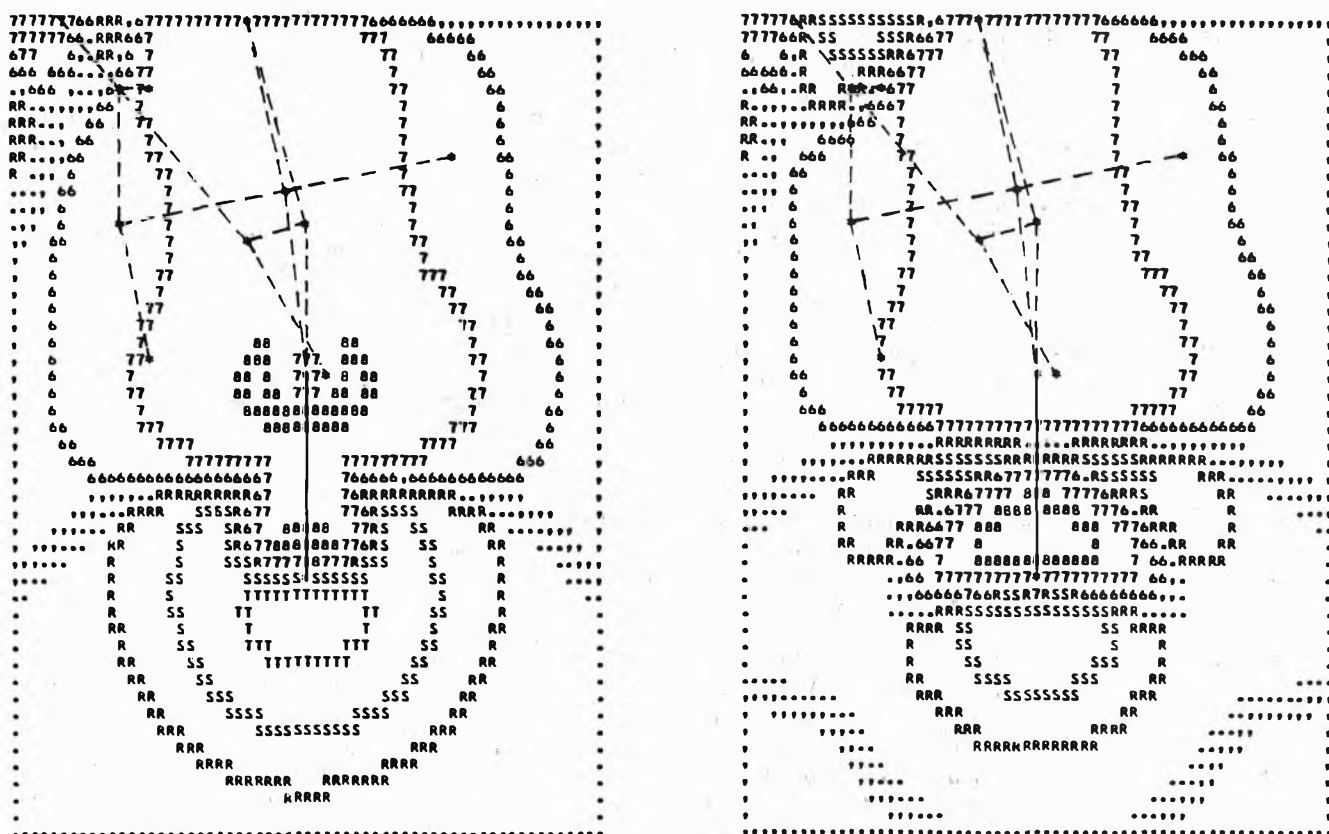
Figure 6. EH (left) and CNDO/2D (right) difference maps of 7-amino-3-cephem computed in the plane which passes through the O_9-C_8 axis (solid line) and is perpendicular to the $O_9-C_8-N_5$ plane. The projection of the dihydrothiazine ring extends off the top of the maps, and the β face of the molecule is toward the left. H_{17} of the amino group and C_3 happen to fall at the same asterisk in the upper left-hand corner of the maps.

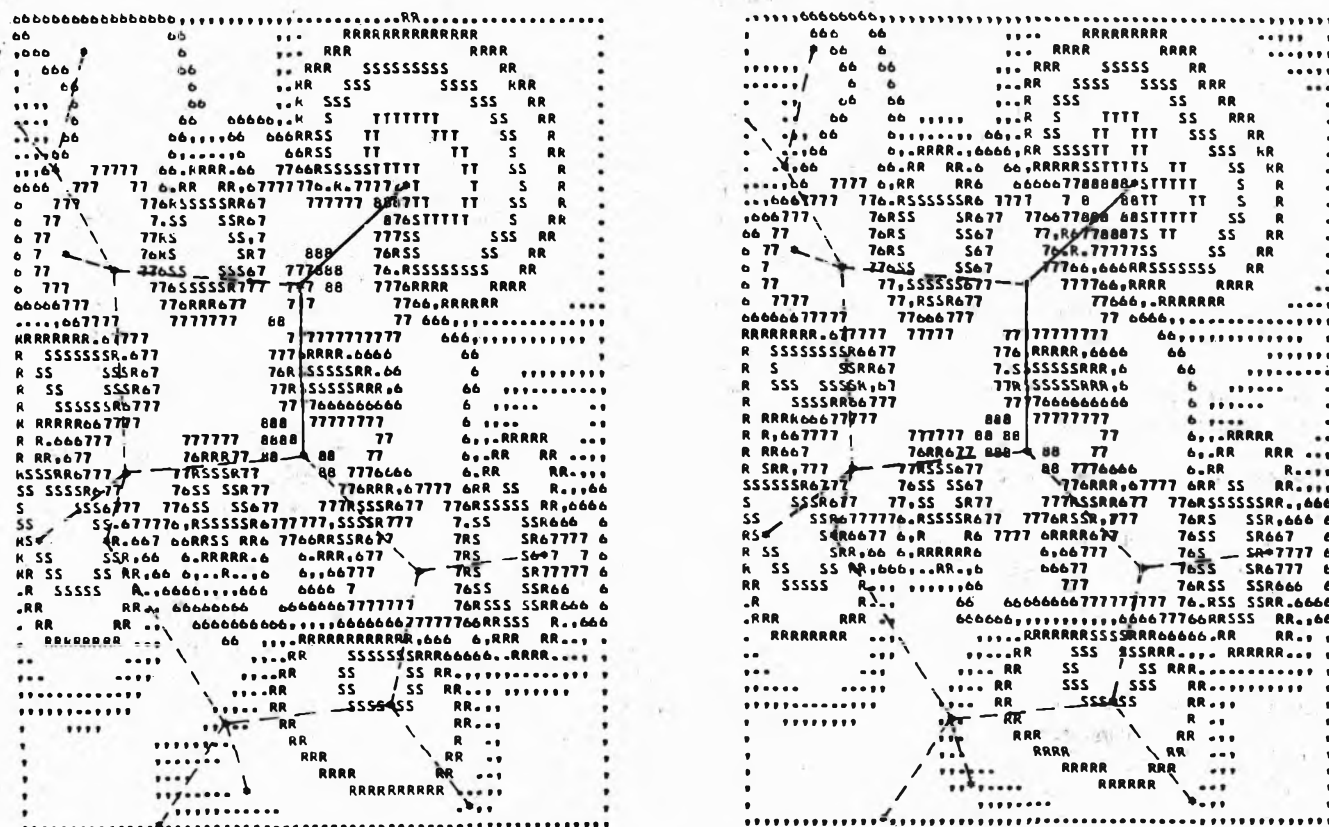**Figure 7.** EH (left) and CNDO/2D (right) difference maps of 7-amino-3-cephem in the plane of $N_5-C_8-O_9$. This plane also slices through the regions near several other nuclei including C_4 (0.34 Å out of the plane), H_{14} (0.13 Å), C_6 (0.36 Å), C_7 (0.12 Å), and H_{15} (0.27 Å). The peaks in density in the O_9 lone-pair lobe are 0.3068 and 0.3026 e/bohr³ in the EH and CNDO/2D maps, respectively.

the dihydrothiazine ring, meaning that transannular bonding is not great in the ground state of the molecule. The excited states also have little transannular character.[1]

The gains along the S–C axes in Figure 2 correspond to σ bonding. The lack of any accumulation of sulfur lone-pair electrons in the plane of C_6–S_1–C_2 is evident in the CNDO/2D map. CNDO/2D puts much more density in the S–C σ bonding regions than does the EH method. Thus, the density maps indicate that CNDO/2D gives stronger S–C bonds compared to EH, which is contrary to the conclusion that would have been surmised from the overlap populations of Table II. The two S–C bonds appear very similar. The volume of density loss around C_2 and C_6 is roughly tetrahedrally shaped.

Figure 3 reveals that electrons have aggregated along the C_3–C_4 axis (σ bonding), as well as on either side of the C_3=C_4–N_5 plane (π bonding). The π cloud is more extensive on the β face of the molecule. The density buildup between the doubly bonded carbons is not unlike that which X-ray crystallographers have tried to see in their electron density maps.[23] The density difference maps do not show a banana-type π bond between C_3 and C_4, but perhaps if the σ density were separable from the π (which it is not due to the slight nonplanarity of the ethylenic moiety) then such bonding would become apparent. Compared to the separated atoms, electrons are lost from the immediate vicinity of each carbon. The loss from around C_4 is seen to be greater than from around C_3, which fits with the positive net atomic charge of the former and negative net atomic charge of the latter (Table I). The EH and CNDO/2D charge distributions in the region of the molecule covered by Figure 3 are remarkably similar.

The C_4–N_5 bond (Figure 4) is the one spanned by an enamine π MO important to the uv absorption of cephalosporins.[1] The EH and CNDO/2D maps yield similar results: there is a small accumulation of electron density on the C–N axis (σ bonding) and considerable gain on either side of this axis (π bonding), which is contiguous with the β-lactam nitrogen lone pair. The N_5 lone pair extends mainly toward the α face of the molecule, but the density buildup on the other face is by no means negligible. No doubt this distribution at N_5 accounts for the partial conjugation of the β-lactam and dihydrothiazine rings and for the effects of substituents at certain positions in the dihydrothiazine ring affecting the chemistry of the β-lactam ring. As in the case of the sulfur lone pairs, the CNDO/2D method concentrates more density along the lone-pair axis on the β face than does the EH method.

Figures 5 and 6 show the density in two planes passing perpendicularly through the N_5–C_8=O_9 plane of the β-lactam ring, and Figure 7 shows the density in the latter plane. The lone-pair density buildup around N_5 is again noted to be hatchet-head shaped with the larger accumulation on the α face of the molecule (Figure 5). CNDO/2D gives a density peak twice as high as the EH method near N_5. The lone-pair region on the carbonyl oxygen O_9 appears as a nub over the end of the C=O bond. The EH and CNDO/2D descriptions of the O_9 lone-pair regions are distinctly different in shape. In the plane perpendicular to the β-lactam amide group (Figure 6) the CNDO/2D wave function puts much less density at the end of the carbonyl group. In the plane of the β-lactam amide group (Figure 7), CNDO/2D has the O_9 lone-pair region somewhat polarized into two fused lobes. This suggests that the two oxygen lone pairs are principally in sp^2-like hybrid orbitals lying in

the O_9=C_8–N_5 plane. EH fails to show more than a kidney-shaped nub of density gain on the carbonyl oxygen, and also fails to show any C–O σ bonding. In fact, the CNDO/2D wave function has much more π, as well as σ, bonding density in the carbonyl bond. In this regard, electron density difference maps of carbon monoxide obtained from *ab initio* wave functions[17,24–26] resemble more closely the CNDO/2D description of the β-lactam carbonyl bond than the EH one. As is evident in Figures 5–7, the charge separation between C_8 and O_9 is much less in the CNDO/2D description, and this fact is apparent in the net atomic charges (Table I). The overlap populations of the C_8=O_9 bond (Table II) do not properly reflect the relative amounts of density in this bond as predicted by the two MO methods.

Electron density plots from both semiempirical methods reveal in Figure 7 various σ bonds of the β-lactam ring, the N_5–C_4 σ bond, and the C_4–H_{14} σ bond, all of which lie in or close to the plane being mapped. Of special interest is that the σ-bonding electron density peaks for the ring bonds lie mostly outside the four-membered ring. In other strained systems a similar phenomenon is observed. For instance, in a cyclopropylidene ring, we have seen the so-called bent C–C bonds.[27] There are many instances where the bent bonds of cyclopropane have been viewed with electron density maps.[28,29] Bent bonds are evident in the four-membered rings of cubane.[30]

In regard to biological activity, the most interesting part of our model compound is the β-lactam ring. This is the portion of cephalosporin molecules which can acylate some bacterial cell wall enzyme and destroy the bacteria, or, conversely, be hydrolyzed by a bacterial β-lactamase and itself be destroyed.[7] Apparent in Figures 5 and 6 is the great loss of electron density around the carbonyl carbon C_8. This loss corresponds to the large positive net atomic charge on this atom (Table I) and relates to the susceptibility of this center to nucleophilic attack. An approaching nucleophile, such as RS$^-$, OH$^-$, or H$_2$O, could easily approach C_8 from either the α or β faces. Electronically, the two modes of attack are not much different, but sterically, other parts of the molecule can partially block one or both paths.[6,31,32] The lone-pair buildups on O_9 and N_5 are seen in Figures 5 and 6 to be spatially disposed such that they would not intercept a nucleophile approaching C_8. Also, there is loss through most of the transannular region of the β-lactam ring (Figures 6 and 7). These factors help explain the reactivity of the β-lactam ring.

Conclusion

From illustrations in the present study, characteristics of the EH and CNDO/2D MO methods and of the Mulliken population analysis on the diverse group of chemical functionalities in 7-amino-3-cephem have been scrutinized. Electron density maps are more useful than the population analysis in assessing details of electron topography, such as lone pair directionality and relative bond populations. Also, we have seen how the electrons distribute themselves about these functionalities, so that the chemical, physical, and biological properties of cephalosporins can be better appreciated. In subsequent papers, the electronic structures of some of the clinically useful cephalosporins and other β-lactam compounds will be explored.

References and Notes

(1) D. B. Boyd, *J. Amer. Chem. Soc.*, **94**, 6513 (1972).
(2) D. B. Boyd, *J. Med. Chem.*, **16**, 1195 (1973).
(3) J. L. Strominger, *Johns Hopkins Med. J.*, **133**, 63 (1973).
(4) R. B. Hermann, *J. Antibiot.*, **26**, 223 (1973).
(5) W. C. Topp and B. G. Christensen, *J. Med. Chem.*, **17**, 342 (1974).
(6) D. B. Boyd, R. B. Hermann, D. E. Presti, and M. M. Marsh, to be submitted for publication; paper IV.
(7) E. H. Flynn, "Cephalosporins and Penicillins: Chemistry and Biology," Academic Press, New York, N.Y., 1972.
(8) O. Martensson, *Acta Chem. Scand.*, **25**, 3763 (1971).
(9) D. B. Boyd, *J. Phys. Chem.*, **78**, 1554 (1974). This paper was part XI of the series "Mapping Electron Density in Molecules," of which the present paper is part XII.
(10) D. B. Boyd, *Theor. Chim. Acta*, **18**, 184 (1970).
(11) D. B. Boyd, *J. Amer. Chem. Soc.*, **94**, 64 (1972), and references therein.
(12) D. B. Boyd, *Theor. Chim. Acta*, **30**, 137 (1973).
(13) R. Hoffmann and W. N. Lipscomb, *J. Chem. Phys.*, **36**, 2179, 3489 (1962); **37**, 2872 (1962).
(14) R. Hoffmann, *J. Chem. Phys.*, **39**, 1397 (1963); **40**, 2480 (1964).
(15) D. B. Boyd and W. N. Lipscomb, *J. Theor. Biol.*, **25**, 403 (1969).
(16) J. A. Pople and D. L. Beveridge, "Approximate Molecular Orbital Theory," McGraw-Hill, New York, N.Y., 1970.
(17) F. A. Van-Catledge, *J. Phys. Chem.*, **78**, 763 (1974).
(18) D. B. Boyd, *Int. J. Quantum Chem., Quantum Biology Symp.*, **No. 1**, 13 (1974); *J. Amer. Chem. Soc*, **94**, 8799 (1972). Regarding the correlation of predicted S–S bond strength and Raman stretching frequency in the first citation, see recent corroborative evidence in paper by H. E. Van Wart, L. L. Shipman, and H. A. Scheraga, *J. Phys. Chem.*, **78**, 1848 (1974).
(19) R. M. Pitzer and W. N. Lipscomb, *J. Chem. Phys.*, **39**, 1995 (1963).
(20) R. S. Mulliken, *J. Chem. Phys.*, **23**, 1833 (1955).
(21) D. D. Shillady, F. P. Billingsley, II, and J. E. Bloor, *Theor. Chim. Acta*, **21**, 1 (1971).
(22) D. B. Boyd, *J. Chem. Phys.*, **52**, 4846 (1970).
(23) R. B. Helmholdt, A. F. J. Ruysink, H. Reynaers, and G. Kemper, *Acta Crystallogr., Sect. B*, **28**, 318 (1972).
(24) R. F. W. Bader and A. D. Bandrauk, *J. Chem. Phys.*, **49**, 1653 (1968).
(25) M. J. Hazelrigg, Jr., and P. Politzer, *J. Phys. Chem.*, **73**, 1008 (1969).
(26) D. A. Kohl and L. S. Bartell, *J. Chem. Phys.*, **51**, 2896 (1969).
(27) D. B. Boyd and R. Hoffmann, *J. Amer. Chem. Soc.*, **93**, 1064 (1971).
(28) O. Martensson and G. Sperber, *Acta Chem. Scand.*, **24**, 1749 (1970).
(29) R. M. Stevens, E. Switkes, E. A. Laws, and W. N. Lipscomb, *J. Amer. Chem. Soc.*, **93**, 2603 (1971).
(30) O. Martensson, *Acta Chem. Scand.*, **24**, 1495 (1970).
(31) P. P. K. Ho, R. D. Towner, J. M. Indelicato, W. A. Spitzer, and G. A. Koppel, *J. Antibiot.*, **25**, 627 (1972).
(32) P. P. K. Ho, R. D. Towner, J. M. Indelicato, W. J. Wilham, W. A. Spitzer, and G. A. Koppel, *J. Antibiot.*, **26**, 313 (1973).

Ultrasound Propagation in Binary Mixtures of Dimethyl Sulfoxide and Water

D. E. Bowen,* M. A. Priesand, and M. P. Eastman

The University of Texas at El Paso, El Paso, Texas 79968 (Received June 24, 1974)

Measurements of the velocity and attenuation of sound have been made for the dimethyl sulfoxide (DMSO)–water binary system as a function of composition and temperature. It has been found that the velocity and attenuation *vs.* composition curves peak in the region $X_{DMSO} \sim 0.3$ for all temperatures studied. No characteristic relaxation frequency was observed for this binary system in the frequency range studied (6–26 MHz). Values for the adiabatic compressibility have been calculated from the velocity measurements and previously published densities. The compressibility decreases rapidly in the region of low DMSO concentration and peaks at $X_{DMSO} \sim 0.3$. The experimental results are discussed in terms of the formation of thermolabile nonstoichiometric 1:2 complexes and recent theories of the structure of water.

I. Introduction

In recent years the dimethyl sulfoxide–water system has been investigated by a wide variety of experimental techniques. These studies have been undertaken because the DMSO–H_2O system is useful as a solvent and as a reaction medium and because DMSO exhibits a number of interesting properties when interacting with biological systems.[1-6] The results of neutron inelastic scattering (nis) experiments have indicated that DMSO is an associated dipolar liquid and that the methyl groups in the DMSO molecule do not take part in hydrogen bonding as had been suggested.[7] In solutions of DMSO–H_2O containing small amounts of DMSO nis and X-ray diffraction data provide evidence for an increased ordering of water molecules. Apparently, however, this increase in molecular order is not accompanied by a change in hydrogen bond energies or by a large change in the distribution of hydrogen bond energies.[7-9] Thus, it seems that there is no clathrate or "iceberg" formation in aqueous solutions containing small amounts of DMSO and that the effect of DMSO on the water structure is not such as to produce a decrease in the so-called "structural temperature" of the water.[8]

In solutions containing larger concentrations of DMSO there is evidence for the breaking down of the water structure and for the formation of hydrogen bonded thermolabile DMSO–H_2O complexes.[7-10] Studies of the DMSO–H_2O system by a variety of experimental techniques indicate that the effect of this complex formation is greatest in the region where the H_2O–DMSO molar ratio is about 2:1.[11-14] However, at present there is no evidence for the formation of a DMSO–H_2O complex having a definite stoichiometry.[10] Nmr measurements show that complex formation leads to reduced translational and rotational mobility for both DMSO and water with the mobility minimum occurring at $X_{DMSO} = 0.35$.[14]

The purpose of this paper is to investigate the DMSO–H_2O system by means of ultrasonic velocity and attenuation measurements.[15] Particular emphasis is placed on

studying the effect of DMSO on the ultrasonic properties of water and on a determination of the ultrasonic properties of DMSO–H$_2$O solutions in the region where complex formation is significant.

II. Experimental Section

Two different sets of experimental apparatus were used in the velocity and the absorption measurements. Both have been described in the literature[16,17] and will not be discussed in detail here. The velocity apparatus operates at 10 MHz and can make measurements to within 0.01% using a pulse superposition technique. The absorption apparatus also uses a pulse technique and can make measurements to within 3% over a 10–100-MHz frequency range. Both sets of apparatus use quartz cells which are placed in cryostats for temperature control.

The DMSO was obtained from Aldrich (99$^+$%) and was used without further purification. The DMSO–water samples were prepared using a weighing technique with deionized water. The concentrations are accurate to within 0.5%. Sound velocity measurements in a dried sample of DMSO did not differ within experimental error from the measurements made in the undried samples; thus no corrections for the effects of H$_2$O in the DMSO were made.

III. Data

A. *Sound Velocity*. The velocity of the 10-MHz compressional waves was determined for 14 different concentrations between 0.5 mol % DMSO and 100% DMSO as a function of temperature. Since water is used to calibrate the system it is not included in this data. We have fitted this data with an equation of the form

$$C_s = C_0 + C_1 T + C_2 T^2 \qquad (1)$$

where C_s is the sound velocity, T is the temperature in Kelvin, and C_0, C_1, and C_2 are constants determined by a least-squares procedure.[18] Table I presents the values for C_0, C_1, and C_2 for the concentrations studied, along with the temperature ranges. For concentrations greater than 24.8 mol % DMSO it was found that the curves of C_s vs. T were linear to within experimental error; consequently no value for C_2 was determined.

Figure 1 depicts sound velocity as a function of the temperature for three concentrations. This clearly shows the transition from the curvature exhibited by water to the linear behavior exhibited by most other liquids. Figure 2 shows the sound velocity as a function of the DMSO concentration at three different temperatures.

B. *Absorption*. The absorption (α) was measured for seven different concentrations between 20 and 100 mol % DMSO as a function of temperature and frequency. These results (presented as α/f^2) are given in Table II. There is clearly little if any frequency dependence over the frequency range studied (6–26 MHz); the apparent frequency dependence which was seen at the low temperatures is probably not real but just indicative of the error which was present.

Figure 3 shows the concentration dependence of the absorption (at 18 MHz) for several temperatures at which data were obtained. Figure 4 shows the temperature dependence of α/f^2 for pure H$_2$O and for 25, 50, and 100 mol % DMSO solutions. The DMSO–water solutions have the same type of temperature dependence for α/f^2 as that exhibited by water up to 50 mol % DMSO. At higher concentrations of DMSO the absorption increased as the tempera-

TABLE I: Sound Velocity Data for DMSO–Water

| Concn, mol % DMSO	C_0, m/sec	C_1, m/sec K	C_2, m/sec K^2	Temp range, K
0.47	−2081.13	21.6312	−0.032162	295–312
3.00	940.586	15.3606	−0.023415	298–320
5.00	−133.797	10.9133	−0.017214	292–327
10.77	1014.87	5.25111	−0.010347	290–327
19.39	1528.75	3.25937	−0.009065	293–322
24.77	2539.70	−2.77987		296–326
27.00	2589.86	−2.94898		304–336
28.00	2579.41	−2.92658		297–327
28.57	2568.18	−2.89358		297–327
33.00	2593.02	−3.02349		297–327
39.13	2589.57	−3.08447		295–327
50.53	2539.38	−3.11068		296–335
70.21	2536.68	−3.29362		293–319
100.00	2495.49	−3.37613		297–330
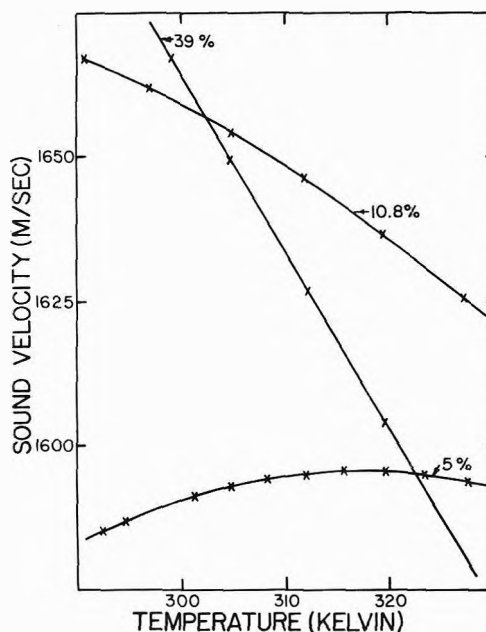
Figure 1. Sound velocity vs. temperature for three DMSO–H$_2$O solutions. The concentrations are in mole per cent DMSO. The circles are the data points and the curves are the fits as given by eq 1.

ture decreased, but the exact functional dependence was not determined.

IV. Discussion

The sound velocity (c) data presented here may be combined with the density (ρ) values from the literature[12] to obtain the adiabatic compressibility (β_s) by use of the equation

$$\beta_s = 1/\rho c^2 \qquad (2)$$

This has been done and the results are shown as a function of concentration (at 18 MHz, 20°) in Figure 5. The compressibility decreases rapidly until a concentration of about 28 mol % DMSO is reached after which there is a rise to the value exhibited by the pure DMSO.

Classically the absorption of ultrasound waves in liquids may be calculated from the well-known equation[15]

$$\alpha_c/f^2 = (8\pi^2/3\rho c^3)[\eta_s + 3(\gamma - 1)K/4C_p] \qquad (3)$$

where α_c is the classical absorption coefficient, ρ the density, c the velocity of sound, η_s the coefficient of shear viscos-

TABLE II: Absorption Data for Water–DMSO Solutions[a]

Concn, mol % DMSO	T = 20°		T = 10°		T = 0°		T = -10°		T = -20°		T = -30°		T = -40°		T = -50°	
	f	α/f^2	f	α/f^2	f	α/f^2	f	α/f^2	f	α/f^2	f	α/f^2	f	α/f^2	f	α/f^2
0	18	25.3	18	36.1	18	56.9										
20	18	34.64	18	49.2	18	66.9	18	104	18	177	18	337				
	10	38.96									14	304				
											10	325				
25	18	39.8	18	54.2	18	73.5	18	112	18	189	18	386				
											10	342	10	738	10	2610
											14	322	14	603		
33	18	43.2	18	55.9	18	78.3	18	114	18	189	18	344				
									10	175	10	287	10	612	10	1281
									14	173	6	379	14	681		
									22	196	14	319	6	740		
									26	179						
40	18	44.0	18	57.6	18	77.3	18	109	18	170	18	303				
50	18	43.3	18	52.9	18	67.5	18	92.2	18	134						
									10	132						
70	18	42.0	18	47.3												
100	14	41.5														
	18	41.7														
	22	41.6														

[a] Frequencies (f) are in MHz; α/f^2 is in 10^{17} nepers sec²/cm.
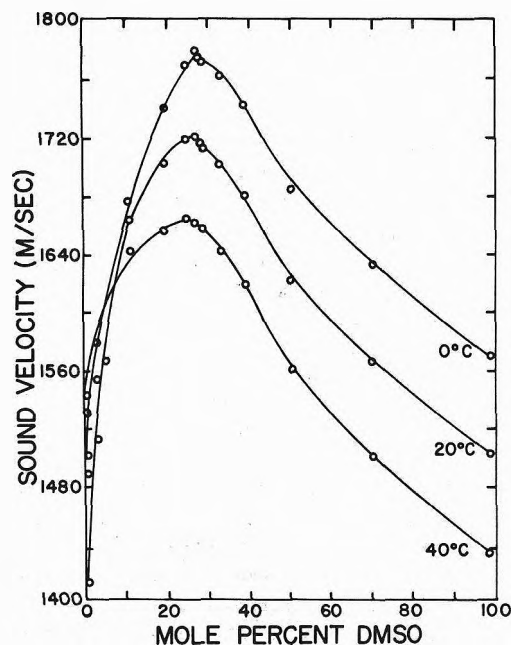
Figure 2. Sound velocity *vs.* concentration for DMSO–H$_2$O solutions at three temperatures.

Figure 3. Absorption (α/f^2) *vs.* concentration for DMSO–H$_2$O solutions at several temperatures (f = 18 MHz).

ity, γ the ratio of specific heats, K the thermal conductivity, C_p the specific heat at constant pressure, and f the frequency of the ultrasonic wave. Values for the density and viscosity for DMSO–water solutions have been reported in the literature;[13] thus, using the sound velocity data reported here it is possible to calculate the contribution to the classical absorption due to the viscosity. It is not possible to calculate the contribution due to the thermal conductivity because of a lack of data on the thermal conductivity. This is not serious, however, as the contribution to the classical absorption due to the thermal conductivity is quite small for most liquids (less than 0.08% for water).[15] Thus, in what follows, we shall assume the classical absorption to be that due only to the viscosity (*i.e.*, the first term in eq 3).

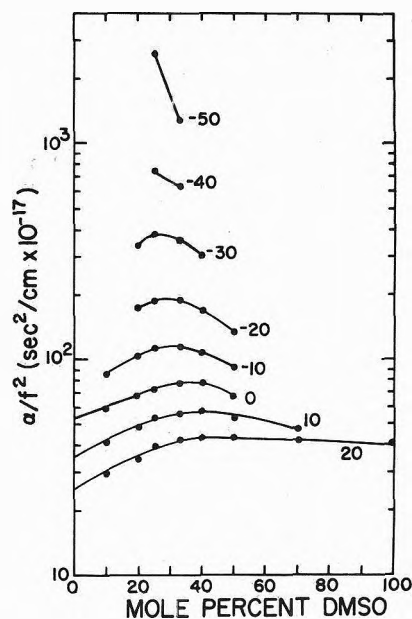Table III presents values for α/f^2 as determined in these

experiments. The temperature dependence of the sound velocity and α/f^2 were fitted with polynomials and these polynomials were used to generate values of c and α/f^2 at the temperatures corresponding to those at which the data for the density and viscosity were reported in the literature. The ratio is equal to about 2 at almost all of the temperatures and concentrations, as expected for associated liquids.

In the absorption experiments no characteristic absorption frequencies were observed in the frequency range investigated. Because of the rapid rise in absorption with frequency it was impossible with equipment used in this study to reliably investigate the frequency range (>30 MHz) in which relaxation effects have been observed in other aqueous binary systems.[18]

Figures 2 and 5 show that the velocity increases and the

D. E. Bowen, M. A. Priesand, and M. P. Eastman

TABLE III: Classical and Measured Absorption for Water–DMSO Solntion[a]

Concn, mol % DMSO	Temp, °C	α_c/f^2	α/f^2	α/α_c
100	20	14.97	41.72	2.79
	30	13.89	41.72	3.00
	40	12.55	41.72	3.15
50	−30	118.4	202.9	1.71
	−15	60.06	110.5	1.84
	−10	49.79	92.20	1.85
	0	30.38	67.49	2.22
	15	23.80	47.70	2.00
	20	21.24	43.34	2.04
33	−55	1066	1269	1.19
	−50	692.9	1018	1.47
	−45	465.2	797.3	1.71
	−30	156.9	343.6	2.19
	−15	71.77	144.2	2.01
	−10	57.77	113.7	1.97
	0	39.31	78.30	1.99
	10	28.09	55.91	1.99
	15	24.30	47.25	1.94
	20	21.18	43.15	2.04
25	−55	1087	3073	2.83
	−50	697.5	2068	2.96
	−45	461.9	1367	2.96
	−30	153.9	385.9	2.51
	−15	66.93	142.4	2.13
	−10	53.12	111.6	2.10
	0	35.81	73.50	2.05
	10	25.56	54.15	2.12
	15	21.68	48.40	2.23
	20	18.89	39.76	2.10
20	−45	434.9	1055	2.43
	−30	141.2	337.4	2.39
	−15	61.82	134.4	2.17
	−10	48.88	104.4	2.14
	0	32.56	66.89	2.05
	10	23.00	49.18	2.14
	15	19.69	43.67	2.22
	20	17.01	34.64	2.04

[a] α_c/f^2 and α/f^2 are measured in 10^{17} sec^2/cm; α/f^2 is given for $f = 18$ MHz.
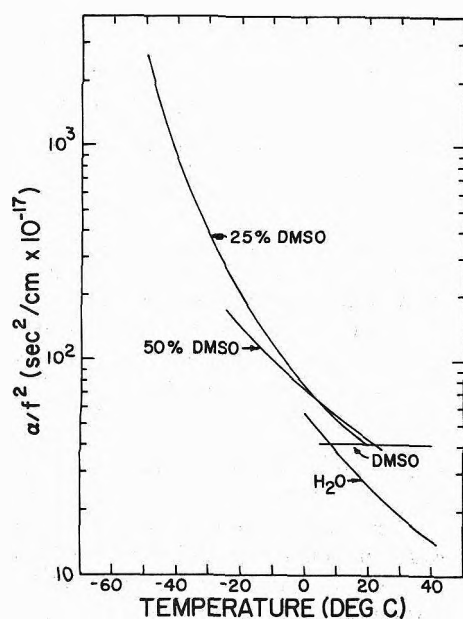

Figure 4. Absorption (α/f^2) vs. temperature for DMSO–H_2O solutions at four different concentrations ($f = 18$ MHz).
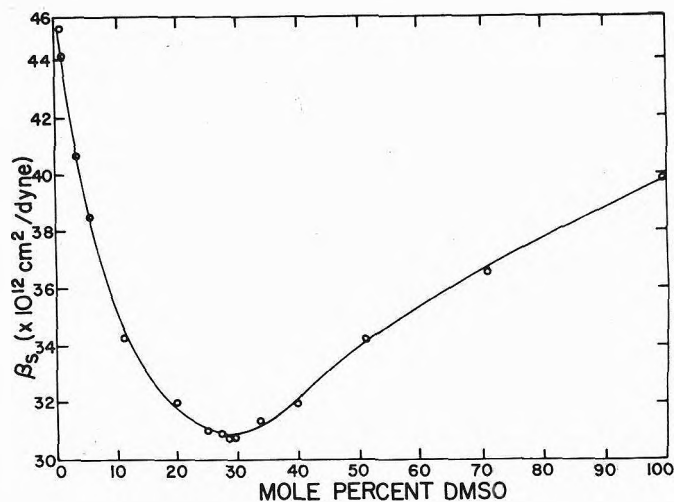

Figure 5. Adiabatic compressibility (β_s) vs. concentration for DMSO–H_2O solutions at 20°.

adiabatic compressibility decreases rapidly in the region of low DMSO concentration. Studies by neutron inelastic scattering[7] have shown this to be the concentration region in which DMSO increases the ordering in the water structure. Since infrared studies have indicated that this ordering is accomplished without an alteration in either the average hydrogen bond energy or the distribution of hydrogen bond energies[8] it seems reasonable to conclude that the rapid decrease in compressibility is due only to increased ordering and not to a "stiffening" of the water structure or to a lowering of the "structural temperature" of the water.

Recent theories of the structure of water suggest that water should not be viewed in terms of a disrupted version of any any known ice or hydrate crystal structure but rather in terms of a distribution of hydrogen bonded polygons.[19] The effect of solutes in this model is to perturb the pattern of hydrogen bonded polygons in water. At present it is unclear whether this pattern reorganization can be accomplished in such a way as to increase the apparent ordering of molecules and to decrease the compressibility while at the same time leaving the hydrogen bond energy distribution unchanged. To the extent that such a conclusion is possible this model would provide an attractive description of the DMSO–water system.

The velocity, compressibility, and attenuation curves peak in the region $X_{DMSO} \sim 0.3$ and show only a slight temperature dependence. A variety of experimental studies have indicated that for $X_{DMSO} = 0.3$ water and DMSO form nonstoichiometric thermolabile complexes with an average water to DMSO ratio of 2.[7-14] Thus, the attenuation, velocity, and compressibility measured at the extremes are taken to be those of a mixture of nonstoichiometric 2:1 complexes.

References and Notes

(1) J. B. Kinsinger, M. M. Tannahill, M. S. Greenberg, and A. I. Popov, *J. Phys. Chem.*, **77**, 2444 (1973); D. Martin, A. Weise, and H.-J. Nidas, *Angew. Chem., Int. Edit. Engl.*, **6**, 318 (1967).
(2) A. J. Parker, *Chem. Rev.*, **69**, 1 (1969).

(3) R. K. Wolford, *J. Phys. Chem.*, **68**, 3392 (1964).
(4) J. R. Jezorek and H. B. Mark, *J. Phys. Chem.*, **74**, 1627 (1970).
(5) S. W. Jacob, D. C. Wood, and J. H. Brown, *Univ. Oreg. Med. Sch. Aerosp. Med.*, **40**, 75 (1969).
(6) G. Rasmussen and R. B. Andersen, *Laeger*, **32**, 830 (1970).
(7) G. J. Safford, P. C. Schaffer, P. S. Leung, G. F. Doebbler, G. W. Brady, and E. F. X. Lyden, *J. Chem. Phys.*, **50**, 2140 (1969).
(8) G. Brink and M. Falk, *J. Mol. Struct.*, **5**, 27 (1970).
(9) J. R. Scherer, M. K. Go, and S. Kint, *J. Phys. Chem.*, **77**, 2108 (1973).
(10) F. Rallo, R. Rodante, and P. Silvestroni, *Thermochim. Acta*, **1**, 311 (1970).

(11) J. J. Lundberg and J. Kenttamaa, *Suom. Kemistilehti B*, **33**, 104 (1960).
(12) J. M. G. Cowie and P. M. Toporowski, *Can. J. Chem.*, **39**, 2240 (1961).
(13) S. A. Schichman and R. L. Amey, *J. Phys. Chem.*, **75**, 98 (1971).
(14) K. J. Picker and D. J. Tomlinson, *Trans. Faraday Soc.*, **67**, 1302 (1971).
(15) R. T. Beyer and S. V. Letcher, "Physical Ultrasonics," Academic Press, New York, N.Y., 1969.
(16) D. E. Bowen, *J. Chem. Phys.*, **51**, 1115 (1969).
(17) D. E. Bowen, *J. Chem. Phys.*, **59**, 4686 (1973).
(18) J. H. Andreae, P. D. Edmonds, and J. F. McKellar, *Acustica*, **15**, 74 (1965).
(19) A. Rahman and F. H. Stillinger, *J. Amer. Chem. Soc.*, **95**, 7943 (1973).

Intermediates Produced from the One-Electron Reduction of Nitrogen Heterocyclic Compounds in Solution

P. N. Moorthy[1] and E. Hayon*

Pioneering Research Laboratory, U. S. Army Natick Laboratories, Natick, Massachusetts 01760 (Received June 24, 1974)

A detailed examination of the one-electron reduction of aromatic nitrogen heterocyclic compounds in water was carried out using the technique of pulse radiolysis and kinetic absorption spectrophotometry. The compounds studied include pyrazine (Pz), pyrimidine (Pm), pyridazine (Pd), quinoxaline (Qx), phthalazine, and acridine. The reducing agents used were e_{aq}^-, $(CH_3)_2\dot{C}OH$ and $(CH_3)_2\dot{C}O^-$ radicals. The efficiency and the rate of electron transfer from the latter two radicals were correlated with the redox potentials of the aza-aromatic compounds. The radical anions of these compounds are very weak acids and undergo fast protonation by water or by other proton donors to form the neutral monohydro radicals and the dihydroradical cations. Based on the determined transient absorption spectra of the intermediates, and their change over the pH range 0–14, it was possible to assign and derive the ionization constants of the radical observed. For $\cdot PzH_2^+$, $\cdot PmH_2^+$, $\cdot PdH_2^+$, and $\cdot QxH_2^+$ dihydroradical cations the pK_a values are 10.5 ± 0.2, 7.6 ± 0.1, 7.6 ± 0.3, and 8.8 ± 0.1, respectively. No ionization of the corresponding neutral radicals $\cdot PzH$, $\cdot PmH$, $\cdot PdH$, and $\cdot QxH$ to the radical anions was observed up to pH 14, and presumably occurs only in very alkaline solution. An interesting feature of the spectral characteristics of these intermediates is the blue shifting of the absorption maxima of the neutral monohydro radicals compared to the dihydro radical cations. Furthermore, the radical cations are relatively inert to oxygen while the neutral radicals react with O_2 with $k > 10^8 M^{-1}$ sec^{-1}.

Introduction

Although considerable amount of work has been done on the electrochemical reduction of aza-aromatic compounds in water and organic solvents[2-7] and on the esr spectra of the radical ions and neutral species produced from N-heterocyclic compounds,[8-13] very little work appears to have been carried out on the electronic absorption spectra and physicochemical properties of these intermediates (except for pyridinyl radicals[14]). The most studied compounds have been the diaza derivatives of benzene, naphthalene, and anthracene. The intrinsic importance of these diaza compounds is their presence in many biologically important molecules, *e.g.*, pyrimidines, purines, pteridines, alloxazines, and imidazoles.

Presented below is an investigation of the intermediates produced from the one-electron reduction of pyrazine, pyrimidine, pyridazine, quinoxaline, phthalazine, and acridine in aqueous solutions. The fast-reaction technique of pulse radiolysis was used to determine the transient optical absorption spectra of these relatively short-lived species, their decay kinetics, and their acid–base properties. The electronic spectra of the radical anions of some of these compounds have been reported at room temperature[15] and at 77°K[16] in organic solvents.

Experimental Section

The pulse radiolytic experimental conditions used have been described previously.[17,18] The radiolysis of water produces e_{aq}^- (2.8), OH(2.8), and H(0.6) radicals, where the numbers in parentheses are the G values of the radicals formed.

The one-electron reduction of the diazines was accomplished in two ways: (1) by direct reaction with e_{aq}^-. The oxidizing OH radical was scavenged by using *tert*-butyl alcohol.[17] The β radical *t*-BuOH produced absorbs very weakly above ~280 nm and does not give rise to the initial intermediates observed.[17] However, this alcohol β radical appears to affect the subsequent decay reactions of the di-

azine radicals (see more below). Typically, the heterocyclic compounds were irradiated in 0.5–2.0 M t-BuOH solutions saturated with argon (1 atm). (2) The one-electron reduction was also accomplished by electron transfer from an α-hydroxyalkyl radical, e.g., $(CH_3)_2\dot{C}OH$ or $(CH_3)_2\dot{C}O^-$. Solutions were irradiated in the presence of N_2O (1 atm) in order to scavenge e_{aq}^-

$$N_2O + e_{aq}^- \longrightarrow N_2 + OH + OH^- \qquad (1)$$
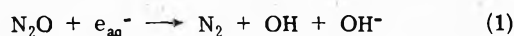
with $k_1 = 8.7 \times 10^9 \ M^{-1} \ sec^{-1}$ (ref 19). The OH radicals produced react with the alcohol, e.g.

$$OH + (CH_3)_2CHOH \longrightarrow (CH_3)_2\dot{C}OH + H_2O \qquad (2)$$
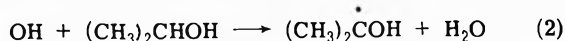
and the $(CH_3)_2\dot{C}OH$ radicals formed subsequently react with the diazines

$$(CH_3)_2\dot{C}OH + D \longrightarrow \cdot DH \ (or \cdot D^-) + CH_3COCH_3(+H^+) \qquad (3)$$
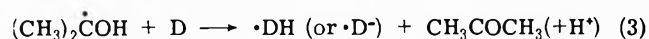
The concentrations of the diazine and alcohol were chosen such that (a) all the e_{aq}^- (>95%) react with N_2O via reaction 1 and none (<5%) with the diazines, (b) all the OH radicals react with the alcohol and none (<2%) react with the diazines; (c) all the α-hydroxyalkyl radicals transfer an electron to the diazines, and none (<5%) disappear by radical–radical reaction. This condition was achieved by working at relatively low concentrations of $\cdot$RHOH radicals (to minimize radical–radical reactions), by determining the rate of reaction 3 in every case, and by making use of the known decay rates of the $\cdot$RHOH radicals.[17] In alkaline solution these radicals can ionize[20]

$$\cdot RHOH \rightleftharpoons \cdot RHO^- + H^+ \qquad (4)$$
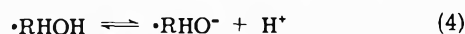
the pK_a of the $(CH_3)_2\dot{C}OH$ radical being 12.2.[21] The $\cdot RHO^-$ can also react with the diazines

$$(CH_3)_2\dot{C}O^- + D \longrightarrow \cdot D^- \ (or \cdot DH) + CH_3COCH_3$$
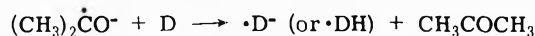
The nitrogen heterocyclic compounds used were the best research grade commercially available and were obtained from Aldrich, Eastman, K & K Laboratories, Mallinckrodt, Calbiochem, and Baker & Adamson. All chemicals were used as received, except quinoxaline which was repurified by vacuum sublimation just prior to use.

All the compounds were dissolved in oxygen-free solutions and were irradiated within a few hours. Solutions were buffered using perchloric acid, potassium hydroxide, and 0.5–1.0 mM borate and phosphates. Photolysis was minimized by using a synchronized shutter between the monitoring light source and the solution.

Dosimetry was carried out using KCNS solutions, as described.[17] The transient spectra were, in all cases, corrected for depletion of the solutes at the wavelengths where they absorb on the basis $G(e_{aq}^-) = G(OH) = 2.8$. The extinction coefficients of the intermediates were subsequently derived from these corrected spectra.

Results and Discussion

The same experimental conditions and technique have been used throughout. The one-electron reduction of the aromatic nitrogen heterocyclic compounds in aqueous solution was brought about primarily by reaction with either e_{aq}^- or $(CH_3)_2\dot{C}OH$ radicals (see Experimental Section above).

Reactivity with One-Electron Reducing Agents. The diaza aromatic compounds are weak bases and protonation of the heteroatom usually occurs at low pH values. For most of the compounds examined here, the pK_a' lies be-

tween 0 and 3 (Table I). For diazines, addition of a second proton occurs only in very strongly acidic solutions. The rate constants for reaction with one-electron reducing agents can be expected to be dependent on the state of protonation of the diazine molecule.[22]

Table I shows these rate constants for various one-electron reducing agents at different pH values. The rates with e_{aq}^- were determined by monitoring the decay kinetics of e_{aq}^- at 700 nm, while all other rates were determined by monitoring the *formation* kinetics of the intermediate produced from this reaction at the appropriate wavelength (see below). In all cases, two–four different concentrations of the compounds were used, and from the pseudo-first-order rates the second-order rate constants were calculated, and are given in the fifth column of Table I.

It can be seen that the reactivity of diazines at pH 7.0 with e_{aq}^- is almost diffusion controlled, with $k = 2$–$3 \times 10^{10} \ M^{-1} \ sec^{-1}$. The rate of electron transfer from organic free radicals is significantly slower. With pyrazine, the reaction with $(CH_3)_2\dot{C}OH$ and $CO_2 \cdot^-$ radicals at pH 5.0–11.0 is very slow,[23] $k \ll 10^7 \ M^{-1} \ sec^{-1}$. On protonation of one of the ring nitrogens of pyrazine ($pK_a = 0.65$), the $(CH_3)_2\dot{C}OH$ radical reacts with $k = 2.8 \times 10^9 \ M^{-1} \ sec^{-1}$ in 1.0 M $HClO_4$ and 100% efficiency is observed for the formation of the pyrazinyl radical cation (see Table I and below). In 70% $HClO_4$, this rate increases to $\sim 5.0 \times 10^9 \ M^{-1} \ sec^{-1}$. Under these conditions, both ring nitrogens in pyrazine are protonated and the donor radical may also be protonated, $(CH_3)_2\dot{C}OH_2^+$. At pH 13.6, electron transfer to neutral pyrazine is observed, with $k = 1.7 \times 10^9 \ M^{-1} \ sec^{-1}$ and 100% efficiency. At this pH the donor radical is present as $(CH_3)_2\dot{C}O^-$.

Some of these observations can be rationalized on the basis of the relative redox potentials of pyrazine and the donor radical. The $(CH_3)_2\dot{C}OH$ radical has a *kinetic* potential[26] of $E_k^{01} = -0.82$ V at pH 7.0. Polarographic results[7] on pyrazine in water gave a $E_{1/2} = -0.87$ V at pH 7.0 vs. sce (i.e., $E^{01} = -0.63$ V). On this basis, electron transfer from $(CH_3)_2\dot{C}OH$ to pyrazine should have occurred. This $E_{1/2}$ value is probably not the potential for one-electron reduction,[12] and indeed that potential[4] is $E_{1/2} = -1.57$ V ($E^{01} = -1.32$ V) in dimethylformamide. Protonation of a ring nitrogen is known[2-6] to increase the reduction potential (i.e., making it more positive) of aza aromatic molecules, though no value is available for pyrazine. This probably explains the observed electron transfer from $(CH_3)_2\dot{C}OH$ to PzH^+ in 1.0 M $HClO_4$. In alkaline solutions, the $(CH_3)_2\dot{C}O^-$ radical present has a kinetic potential $E^{01} < -1.3$ V (ref 26) and hence transfer to pyrazine is feasible.

The results given in Table I for the other nitrogen heterocyclic compounds can be interpreted in the same way. Quinoxaline[6] has a $E_{1/2} = -1.02$ V at pH 4.0 (i.e., $E_m = -0.78$ V). The rate of electron transfer from $(CH_3)_2\dot{C}OH$ radicals ($E_k^{01} = -0.82$ V) is slower, $k = 1.6 \times 10^8 \ M^{-1} \ sec^{-1}$. In 2.0 M $HClO_4$, $k = 3.7 \times 10^9 \ M^{-1} \ sec^{-1}$ (see Table I). Similarly, electron transfer from $CH_3\dot{C}HOH$ radicals (kinetic potential is[26] -0.69 V) occurs with $k = 6.5 \times 10^7 \ M^{-1} \ sec^{-1}$ and only $\sim 70\%$ efficiency.

Absorption Spectra of Intermediates. Pyrazine. The one-electron reduction of pyrazine by e_{aq}^- in neutral solutions produces a transient species with an optical absorption maximum at 315 nm (see Figure 1 and Table II), and an ϵ_{315} of $6.9 \times 10^3 \ M^{-1} \ cm^{-1}$. A second band with λ_{max} 242 nm and ϵ_{242} of $4.5 \times 10^3 \ M^{-1} \ cm^{-1}$ has also been observed[24,25] (under better experimental conditions) in the

TABLE I: Reaction Rate Constants of Some Nitrogen Heterocyclic Compounds with One-Electron Reducing Agents in Water

Compd	pK_a	Reducing agent	pH	k, M^{-1} sec $^{-1}$	Efficiency for formation of reduced radical, %
Pyrazine, Pz	0.65, −6.25	e_{aq}^-	7.0	2.1×10^{10}	100
		$CO_2 \cdot ^-$, $(CH_3)_2\dot{C}OH$	5.0, 11.0	$\ll 10^7$	<10
		$(CH_3)_2\dot{C}OH$	1.0 M HClO₄	2.8×10^9	100
		$(CH_3)_2\dot{C}OH$	70% HClO₄[a]	5.0×10^9	100[b]
		$(CH_3)_2\dot{C}O^-$	13.6	1.7×10^9	100
Pyrimidine, Pm	1.3, −6.92	e_{aq}^-	7.0	2.0×10^{10}	100
		$CO_2 \cdot ^-$, $(CH_3)_2\dot{C}OH$	5.0, 11.0	$\ll 10^7$	<10
		$(CH_3)_2\dot{C}OH$	1.0 M HClO₄	2.2×10^9	100
		$(CH_3)_2\dot{C}O^-$	13.6	$\ll 10^7$	<10
Pyridazine, Pd	2.96	e_{aq}^-	7.0	2.2×10^{10}	100
		$CO_2 \cdot ^-$, $(CH_3)_2\dot{C}OH$	5.0, 11.0	$\ll 10^7$	<10
		$(CH_3)_2\dot{C}OH$	1.0 M HClO₄	2.6×10^9	100
		$(CH_3)_2\dot{C}O^-$	13.6	2.1×10^9	100
Quinoxaline, Qx	0.56, −5.52	e_{aq}^-	7.0	3.1×10^{10}	100
		$(CH_3)_2\dot{C}OH$	6.5	1.6×10^8	100
		$(CH_3)_2\dot{C}OH$	2.0 M HClO₄	3.7×10^9	100
		$(CH_3)_2\dot{C}OH$	70% HClO₄[a]	$\sim 7.0 \times 10^8$	100[b]
		$CH_3\dot{C}HOH$	6.5	6.5×10^7	70
Phthalazine, Pl	3.39	e_{aq}^-	7.0	3.5×10^{10}	100
Acridine, Ad	5.6	e_{aq}^-	9.2	2.2×10^{10}	100
		$(CH_3)_2\dot{C}OH$	7.6	3.0×10^8	~40
		$(CH_3)_2\dot{C}OH$	2.0	3.7×10^9	~90
		$\dot{C}H_2OH$	7.6		0
		$\dot{C}H_2OH$	2.0	5.0×10^8	~30

[a] At this [H⁺], radical may be present as $(CH_3)_2\dot{C}OH_2^+$ and substrate as PzH_2^{2+}. [b] Presumed to be 100%.
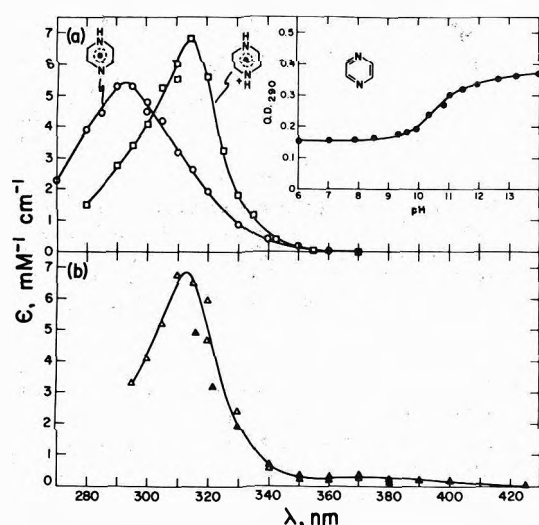

Figure 1. Optical spectra of intermediates produced from the one-electron reduction of pyrazine (10^{-3} M) in aqueous solutions by (a) e_{aq}^- (in presence of 1.0 M t-BuOH, 1 atm of Ar) at pH 4.5, □, and pH 12.8, ⊡. Total dose ~10 krads/pulse. Insert shows change in absorbance at 290 nm with pH; (b) $(CH_3)_2\dot{C}OH$ radicals (in presence of 1.0 M i-PrOH, 1 atm of Ar) in 2.0 M HClO₄, ▲, and 70% HClO₄, △. Total dose ~2.4 krads/pulse.

laser photolysis of pyrazine in the presence of H-atom donors. This species appears to decay by first-order kinetics (to give a species T₂, see more below) with k ~3.0 × 10⁴ sec⁻¹, which is not affected by pH or [t-BuOH]. At pH 12.8, the transient spectrum is blue shifted with maxima at 290 and 242 nm and extinction coefficients of 5.9 × 10³ and 4.8 × 10³ M^{-1} cm⁻¹, respectively. On monitoring the change in absorbance of these species at 290 nm with pH, a

titration curve is obtained (see insert Figure 1) from which a pK_a (radical) = 10.5 ± 0.2 can be obtained. The increase in absorbance at 290 nm above pH ~11.5 is due to the conversion of the H atoms produced in the radiolysis of water into e_{aq}^-, according to the competition between
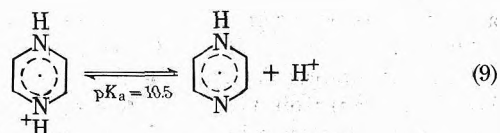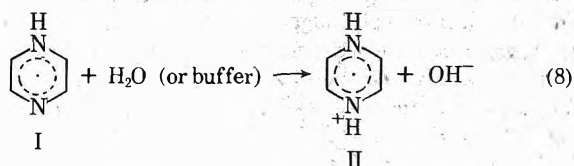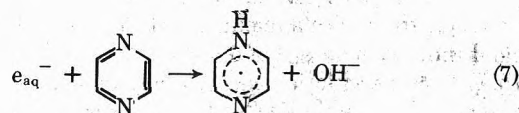
$$H + OH^- \longrightarrow e_{aq}^- \tag{5}$$

and

$$H + pyrazine \longrightarrow H \text{ atom adduct} \tag{6}$$
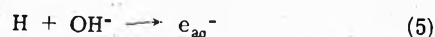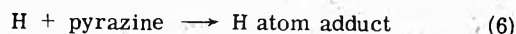
with $k_5 = 2 \times 10^7$ M^{-1} sec⁻¹ and $k_6 = 3.3 \times 10^8$ M^{-1} sec⁻¹ (ref 27). In support of reactions 5 and 6, the titration curve was found to level off at pH ~11.5 when high concentrations of pyrazine were used.

Reactions 7-9 are suggested to account for these obser-

$$e_{aq}^- + \text{[structure]} \longrightarrow \text{[structure]} + OH^- \tag{7}$$

$$\text{[structure]} + H_2O \text{ (or buffer)} \longrightarrow \text{[structure]} + OH^- \tag{8}$$

$$\text{[structure]} \underset{pK_a = 10.5}{\rightleftharpoons} \text{[structure]} + H^+ \tag{9}$$

vations. Rapid protonation follows the addition of e_{aq}^- to pyrazine to form the neutral monohydro radical (I). In neutral solutions the addition of a *second* proton follows immediately with the formation of the dihydro radical cation

TABLE II: Absorption Maxima, Extinction Coefficients, Decay Kinetics, and Ionization Constants of Radicals Produced by One-Electron Reduction of Nitrogen Heterocyclic Compounds in Water
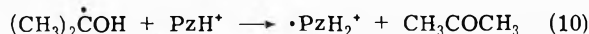
Compd[a]	pH	λ_{max}, nm	ϵ, mM^{-1} cm^{-1}	$2k$, M^{-1} sec^{-1}	pK_a(radical)	Suggested radical
Pyrazine, Pz	4.5	242,[b] 315	4.5,[b] 6.9	c		·PzH$_2$$^+$
	12.8	242,[b] 290	4.8,[b] 5.9	1.3×10^7[d,e]	10.5 ± 0.2	·PzH
	2.0 M HClO$_4$	242, 315	6.9	f		·PzH$_2$$^+$
	70% HClO$_4$	<315, ~380		g		·PzH$_3$$^{2+}$ (?)
	h	340	~3.0[i]			·Pz$^-$
Pyrimidine, Pm	4.5	240, ~325	3.5; 0.55	j		·PmH$_2$$^+$
	13.3	<235, ~325	4.6; 0.9	j	7.6 ± 0.1	·PmH
Pyridazine, Pd	4.5	~265	~3.8	j		·PdH$_2$$^+$
	13.3	~270	~4.4	j	7.6 ± 0.3	·PdH
Quinoxaline, Qx	0, 4.5	363	12.4			·QxH$_2$$^+$
	13.5	347, 425	8.8, 1.6	1.7×10^9[e]	8.8 ± 0.1	·QxH
	70% HClO$_4$	<375, ~450	−, 1.24	k		·QxH$_3$$^{2+}$ (?)
Phthalazine, Pl	5.5, 10.5	345	4.4			
Acridine, Ad	4.2–13.7	~500	4.1			·AdH

[a] Experiments carried out in 1.0 M t-BuOH solutions. [b] From ref 25. [c] Radical decays by first-order kinetics, $k = 3.0 \times 10^{-4}$ sec^{-1}. [d] At pH 13.6. [e] 1.0 M isopropyl alcohol used instead of t-BuOH. [f] Decays to give at 40 μsec after the pulse an intermediate with a band λ_{max} 370 nm and the 315-nm band (now with an ϵ_{315} 6.5 $\times$ 10^3 M^{-1} cm^{-1}); the 370-nm band decays with $k \sim 0.2$ sec^{-1}. [g] Initially decays with $2k/\epsilon = 5 \times 10^6$ sec^{-1} to an intermediate which decays with $t > 20$ sec. [h] In acetonitrile as solvent. [i] Estimated, based on $G(e_{solv}^-) = 2.0$. [j] Mixed decay kinetics. [k] Initially decays with $2k/\epsilon = 3 \times 10^6$ sec^{-1} to an intermediate which decays with $t > 20$ sec.

(II), with maxima at 315 and 242 nm. The rate of reaction 8 was observed[24] under laser photolysis conditions to be k_8 ~ 7.0 $\times$ 10^6 sec^{-1} (in 0.5 M aqueous isopropyl alcohol solutions at pH 7.1).

Support for the assignment of the bands in Figure 1a to radicals I and II was derived from (a) the observation that the absorption spectrum of the pyrazine radical anion has a maximum at 340 nm in neat acetonitrile solutions and (b) esr studies[8-13] of this system: Zeldes and Livingston[11] and Fessenden and Neta[12] observed the dihydropyrazine radical cation in aqueous solutions. At pH >9.0, no esr spectrum was observed[12] due to line broadening by fast proton exchange. Radical I decays, however, relatively slowly with $2k = 1.3 \times 10^7$ M^{-1} sec^{-1} (Table II); support was also derived from a recent study of the electrochemical reduction of pyrazine in water.[28]

On reaction of (CH$_3$)$_2$ĊOH radicals with pyrazine (PzH$^+$) in 2.0 M HClO$_4$ aqueous solutions containing 1.0 M i-PrOH, a spectrum identical with that of radical II is observed

$$(CH_3)_2\dot{C}OH + PzH^+ \longrightarrow \cdot PzH_2^+ + CH_3COCH_3 \quad (10)$$

· PzH$_2$$^+$ decays to give, at 40 μsec after the pulse, a transient spectrum with a maximum at 370 nm and the 315-nm band (now with an ϵ_{315} of 6.5 $\times$ 10^3 M^{-1} cm^{-1}), see Figure 1b. In 70% perchloric acid, a totally different spectrum is observed (see Table II). No firm assignment can be made, and it is tentatively suggested that it may be · PzH$_3$$^{2+}$. However, further work is needed to clarify this observation.

In 2.0 M HClO$_4$, the · PzH$_2$$^+$ cation radical formed was found to be unreactive toward oxygen in solutions containing 10^{-3} M Pz, 1.0 M i-PrOH, 2 $\times$ 10^{-2} M N$_2$O, 5 $\times$ 10^{-5} M O$_2$ and [· PzH$_2$$^+$] = 2.5 $\times$ 10^{-6} M. At pH 13.6, (under otherwise similar experimental conditions), k(· PzH + O$_2$) = 1.9 $\times$ 10^9 M^{-1} sec^{-1}. It would seem that, in general, cation radicals are much more stable toward reaction with O$_2$ than the neutral radical (see more below).

Following the formation of · PzH$_2$$^+$ and · PzH radicals, other transient species are produced at a later time (~100 μsec) in aqueous t-BuOH solution of pyrazine (and also with pyrimidine and pyridazine). The newly formed absorption bands are strongly pH dependent and have differ-
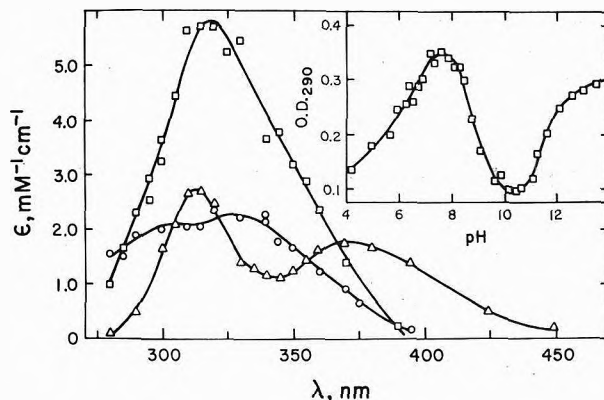

Figure 2. Secondary transient species produced from the reaction of e_{aq}^- with pyrazine (10^{-3} M) in presence of 1.0 M t-BuOH at pH 4.5, △, pH 8.2, □, and pH 12.8, ⊙. OD read at ~100 μsec after the pulse and extrapolated to "zero" time. Total dose ~10 krads/pulse. Insert shows change in absorbance at 290 nm with pH.

ent maxima and extinction coefficients (see Figure 2). Their rate of formation appears to be independent of pH and t-BuOH concentration. Similar transients are produced when i-PrOH is used as an OH radical scavenger, under conditions when (CH$_3$)$_2$ĊOH radicals do not transfer quantitatively to Pz. These bands appear to be produced from the reaction of the alcohol radicals with the diazine radicals.

The hydroxyl radical can add to pyrazine and give a transient absorption spectrum at pH 10.9 (5 $\times$ 10^{-4} M Pz, 1 atm of N$_2$O) with a maximum at ~305 nm and ϵ_{305} of 1.6 $\times$ 10^3 M^{-1} cm^{-1}.

Pyrimidine. The reaction of e_{aq}^- with pyrimidine (Pm) produces transient optical absorptions with lower extinction coefficients (see Figure 3) compared to Pz. At pH 4.5, maxima at ~325 and 240 nm are observed with ϵ values of 550 M^{-1} cm^{-1} and 3.5 $\times$ 10^3 M^{-1} cm^{-1}, respectively. At pH 13.6, the bands are blue shifted with maxima at ~315 and <235 nm. On monitoring the change in absorbance with pH, a pK_a(radical) = 7.6$\pm$ 0.1 can be derived from the titration curve. The following reactions are suggested
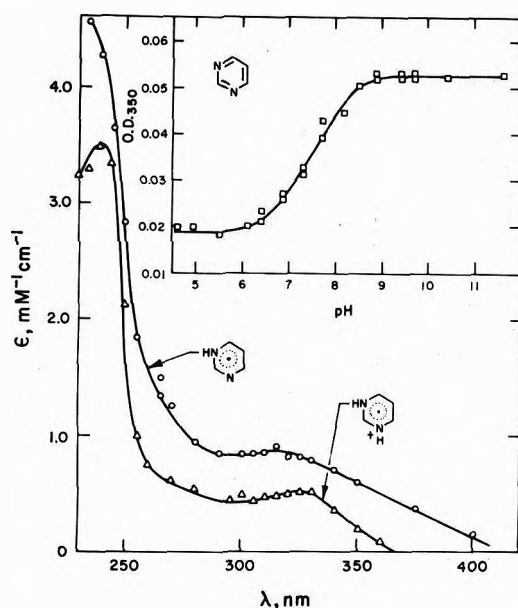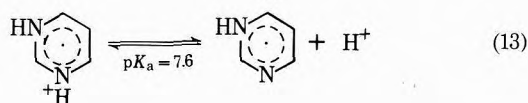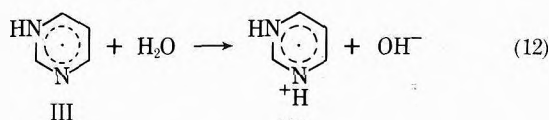
Figure 3. Optical spectra of intermediates produced from the one-electron reduction of pyrimidine (10^{-3} M) by e_{aq}^- (in presence of 1.0 M t-BuOH, 1 atm of Ar) at pH 4.5, $\triangle$, and pH 13.6, $\odot$. Total dose ~20 krads/pulse. Insert shows change in absorbance at 350 nm with pH.

As mentioned above for pyrazine, the radical anions of these nitrogen heterocyclic compounds protonate very rapidly in water. The 1,3-dihydropyrimidine radical cation is rapidly produced at pH 4.5–6.0, while at higher pH the neutral monohydro radical only is formed. It is interesting to point out that the $\cdot$PmH$_2^+$ radical is a stronger acid than the $\cdot$PzH$_2^+$ radical.

The pyrimidine radicals decay with mixed kinetics probably due to reaction with the radical produced from t-BuOH, as mentioned above for pyrazine.

Pyridazine. The intermediates produced from the one-electron reduction of pyridazine (Pd) by e_{aq}^- give poorly defined absorption spectra (Figure 4). Qualitatively, the spectral features are characteristically the same as those observed for the other azyl radicals and radical anions. The following species are produced
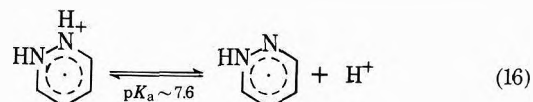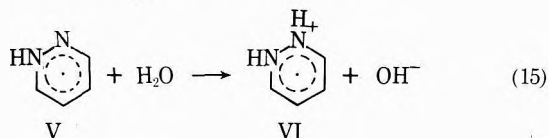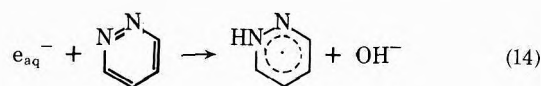
The pK_a of the $\cdot$PdH$_2^+$ radical is close to that of the $\cdot$PmH$_2^+$ radical.

As was found for Pz and Pm, protonation of the pyridazine molecule (pK_a = 2.96) increases the redox potential (*i.e.*, more positive) of PdH$^+$ with respect to Pd, and makes the transfer of an electron from (CH$_3$)$_2$ĊOH possible, see Table I. The insert in Figure 4b shows the pH dependence of the rate constant and the efficiency of

$$(CH_3)_2\overset{\cdot}{C}OH + PmH^+ \longrightarrow \cdot PmH_2^+ + CH_3COCH_3 \quad (17)$$
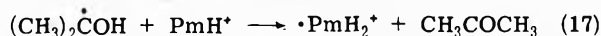
From the curves shown in Figure 4b, a pK_a ~ 2.5–3.0 can be derived in close agreement with the pK_a' = 2.96 of pyridazine.

Quinoxaline. Quinoxaline (Qx) has a pK_a' = 0.56 and a redox potential in neutral solution which is more positive than that of the above-mentioned diazabenzenes. Consequently, (CH$_3$)$_2$ĊOH radicals react with Qx at pH 6.5 with k = 1.6 × 10^8 M^{-1} sec^{-1}, see Table I.

Figure 5a shows the transient optical spectra observed at pH 4.5 and 13.6 produced from the reaction of e_{aq}^- with quinoxaline. These have higher extinction coefficients compared to the transient species from Pz, Pm, and Pd. From the change in absorbance at 370 nm, a pK_a = 8.8 ± 0.1 was obtained. Reactions 18–20 are suggested.
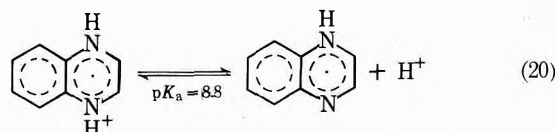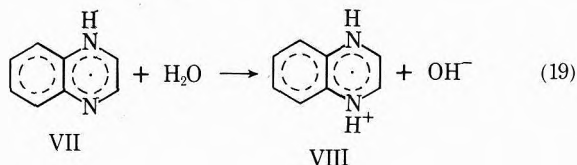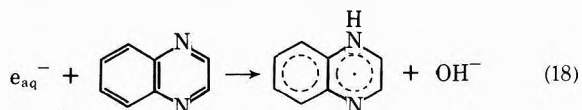
In 2.0 M HClO$_4$, the transient spectrum produced from the reaction of QxH$^+$ with (CH$_3$)$_2$ĊOH is identical with that produced at pH 4.5 by reaction of Qx with e_{aq}^-. This result supports the assignment given for radicals VII and VIII. In 70% HClO$_4$, the spectrum observed is somewhat different (see Figure 5b), and its assignment is not clear. It should be mentioned, though, that at this high acidity quinoxaline is doubly protonated and the intermediate produced is tentatively suggested to be $\cdot$QxH$_3^{2+}$.

The second-order decay kinetics of $\cdot$QxH is given in Table II. The $\cdot$QxH$_2^+$ radical cation is relatively stable, τ > 20 sec. As was found for $\cdot$PzH$_2^+$, the $\cdot$QxH$_2^+$ radical is apparently unreactive toward oxygen (at least over a period of tens of seconds), while the neutral $\cdot$QxH radical reacts with O$_2$ at pH 10.9 and 13.6 with k ($\cdot$QxH + O$_2$) = 3.7 × 10^8 M^{-1} sec^{-1}.

Phthalazine. The reaction of e_{aq}^- with phthalazine produces an intermediate with λ_{max} ~345 nm and another stronger absorption band at lower wavelength (see Tables I and II).

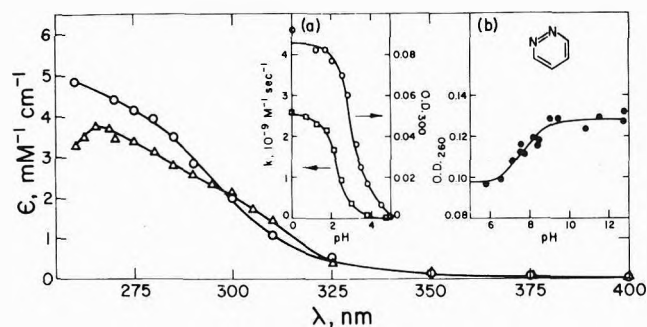*Acridine.* In addition to e_{aq}^-, α-hydroxyalkyl radicals

Figure 4. Optical spectra of intermediates produced from the one-electron reduction of pyridazine (10^{-3} M) by e_{aq}^- (in presence of 1.0 M t-BuOH, 1 atm of Ar) at pH 4.5, $\triangle$, and pH 13.3, $\odot$. Total dose ~15 krads/pulse. Insert shows (a) change in absorbance at 260 nm with pH; (b) absorbance at 300 nm of intermediate produced by reaction with $(CH_3)_2\dot{C}OH$ radicals (1 mM pyridazine, 1.0 M i-PrOH, 1 atm of N_2O) as a function of pH, and k [$(CH_3)_2\dot{C}OH$ + pyridazine] as f(pH).
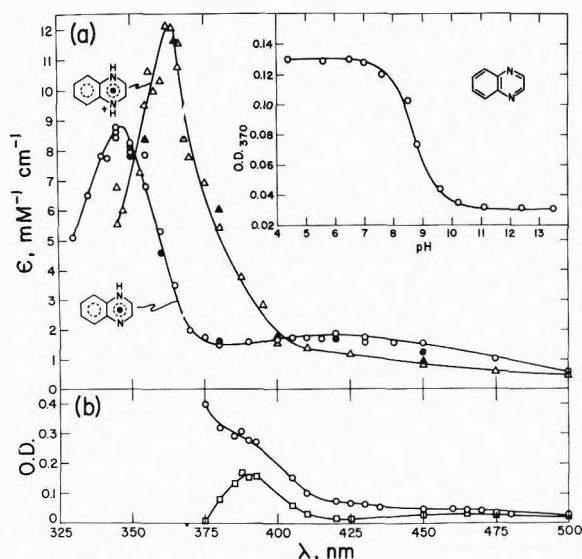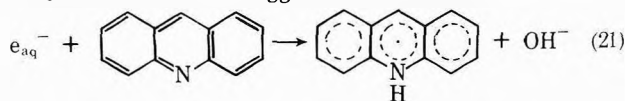

Figure 5. Optical spectra of intermediates produced from the one-electron reduction of quinoxaline (10^{-3} M) by (a) e_{aq}^- (in presence of 1.0 M t-BuOH, 1 atm of Ar) at pH 4.5, $\triangle$, pH 10.1 , $\bullet$, and pH 13.6, O; and by $(CH_3)_2\dot{C}OH$ radicals (in presence of 1.0 M i-PrOH) in 2.0 M $HClO_4$, $\blacktriangle$. Insert shows change in absorbance at 370 nm with pH; (b) $(CH_3)_2\dot{C}OH$ radicals in 70% $HClO_4$, OD as observed, $\square$, and OD corrected for depletion of quinoxaline based on 30% of radiation energy absorbed by water, $\odot$. Total dose 3-7 krads/pulse.

also react with acridine (pK_a = 5.6) in neutral solutions, see Table I, albeit with different efficiency. A transient spectrum is obtained with λ_{max} ~500 nm and ϵ_{500} of 4.1 × 10^3 M^{-1} cm^{-1}, which is independent of pH in the range 4.2-13.7 Reaction 21 is suggested. Ionization of the neutral

$$e_{aq}^- + \text{(quinoline/acridine structure)} \longrightarrow \text{(acridine radical anion structure)} + OH^- \quad (21)$$

acridine radical presumably occurs in very alkaline solutions.

Conclusion

The spectral characteristics and the acid-base properties of the dihydro radical cations and the neutral monohydro radicals of pyrazine, pyrimidine, pyridazine, and quinoxaline have been determined in aqueous solution. The uv spectra of the diazyl monohydro neutral radicals are blue shifted compared to those of the radical cations. The very strong proton affinity of these radical intermediates has been demonstrated. The radical cations are relatively stable toward O_2 whereas the neutral radicals are reactive with $k > 10^8$ M^{-1} sec^{-1}. A reasonably good correlation was found[29] between the ionization constants of these radicals and the redox potentials of the parent diaza compounds. Included in this correlation are the ionization constants of the radicals from phenazine (pK_a = 5.6 ± 0.2 and 9.2 ± 0.2) and from N-methylphenazinium sulfate (pK_a = 6.8 ± 0.2).

References and Notes

(1) Visiting scientist from Bhabha Atomic Research Center, Chemistry Division, Trombay, Bombay 400085, India.
(2) P. Zuman, "Substituent Effects in Organic Polarography," Plenum Press, New York, N.Y., 1967.
(3) J. E. O'Reilly and P. J. Elving, *J. Amer. Chem. Soc.*, **93**, 1871 (1971); **94**, 7941 (1972).
(4) K. B. Wiberg and T. P. Lewis, *J. Amer. Chem. Soc.*, **92**, 7154 (1970).
(5) D. Van der Meer and D. Feil, *Recl. Trav. Chim. Pays-Bas*, **87**, 746 (1968); **88**, 1361 (1969); **89**, 51 (1970).
(6) M. Takagi, R. Hosogaki, and S. Ono, *Rev. Polarogr.*, **14**, 367 (1967).
(7) J. Volke, D. Dumanović, and V. Volková, *Collect. Czech. Chem. Commun.*, **30**, 246 (1965).
(8) J. R. Bolton, A. Carrington, and J. dos Santos-Veiga, *Mol. Phys.*, **5**, 465 (1962).
(9) B. L. Barton and G. K. Fraenkel. *J. Chem. Phys.*, **41**, 1455 (1964).
(10) C. A. McDowell, K. F. Paulus, and J. R. Rowlands, *J. Chem. Soc., Chem. Commun.*, 60 (1962).
(11) H. Zeldes and R. Livingston, *J. Phys. Chem.*, **76**, 3348 (1972); *Mol. Phys.*, **27**, 261 (1974).
(12) R. W. Fessenden and P. Neta, *Chem. Phys. Lett.*, **18**, 14 (1973).
(13) P. Neta, *Radiat. Res.*, **52**, 471 (1972).
(14) See, *e.g.*, W. M. Schwarz, E. M. Kosower, and I. Shain, *J. Amer. Chem. Soc.*, **83**, 3164 (1961); E. M. Kosower, A. Teuerstein, and A. J. Swallow, *ibid.*, **95**, 6127 (1973); U. Brühlman and E. Hayon, *ibid.*, **96**, 6169 (1974).
(15) J. W. Dodd, F. J. Hopton, and N. S. Hush, *J. Chem. Soc., Chem. Commun.*, 61 (1972).
(16) A. Grimison, G. A. Simpson, M. T. Sanchez, and J. Jhaveri, *J. Phys. Chem.*, **73**, 4064 (1969).
(17) M. Simic, P. Neta, and E. Hayon, *J. Phys. Chem.*, **73**, 3794 (1969).
(18) J. P. Keene, E. D. Black, and E. Hayon, *Rev. Sci. Instrum.*, **40**, 1199 (1969).
(19) M. Anbar, M. Bambenek, and A. B. Ross, *Nat. Ref. Data Ser., Nat. Bur. Stand.*, **No.** 43 (1973).
(20) E. Hayon and M. Simic, *Accounts Chem. Res.*, **7**, 114 (1974).
(21) K. D. Asmus, A. Henglein, A. Wigner, and G. Beck, *Ber. Bunsenges. Phys. Chem.*, **70**, 756 (1966).
(22) P. S. Rao and E. Hayon, *J. Phys. Chem.*, **78**, 1193 (1974).
(23) It should be pointed out that the pyrazinyl (and other) radicals observed[11] by esr could not have been produced by reaction with $(CH_3)_2\dot{C}OH$ radicals as suggested, but were instead formed[24,25] by direct photolysis of the diazines and subsequent quenching of the triplet states by H-atom donors.
(24) D. V. Bent, E. Hayon, and P. N. Moorthy, *Chem. Phys. Lett.*, **27**, 544 (1974).
(25) D. V. Bent, E. Hayon, and P. N. Moorthy, *J. Amer. Chem. Soc.*, submitted for publication.
(26) P. S. Rao and E. Hayon, *J. Amer. Chem. Soc.*, **96**, 1287 (1974); submitted for publication.
(27) P. Neta, *Chem. Rev.*, **72**, 533 (1972).
(28) L. N. Klatt and R. L. Rousseff, *J. Amer. Chem. Soc.*, **94**, 7295 (1972).
(29) P. S. Rao and E. Hayon, *J. Phys. Chem.*, to be submitted for publication.

Growth Mechanism of Hydrous Chromium(III) Oxide Spherical Particles of Narrow Size Distribution[1]

Alexander Bell[2] and Egon Matijević*

Institute of Colloid and Surface Science and Department of Chemistry, Clarkson College of Technology, Potsdam, New York 13676
(Received June 3, 1974)

The change in size of spherical hydrous chromium(III) oxide particles of narrow size distribution with time from solutions of chrome alum was followed. Nielsen's chronomal analyses were used to characterize the growth mechanism and to obtain rate constants. Growth is thought to occur *via* surface reaction. Processes related to the formation of such particles are discussed.

Introduction

Nucleation and growth of solids have been subjects of extensive investigations, both theoretical and experimental.[3-11] The vast majority of these studies have dealt with crystalline materials. Nucleation may take place homogeneously (within the parent phase) or heterogeneously (generally at low degrees of supersaturation). Rate-determining growth processes treated in detail include diffusion, surface reaction (or nucleation), and spiral step (screw dislocation).

Quantitative data on nucleation and growth of hydrous metal oxides or hydroxides are rather limited.[12-14] The reason is that during precipitation of the solids, which are frequently amorphous, competing reactions such as hydrolysis, condensation, and anion coordination take place concurrently. The elucidation of the processes is even more difficult when, as a result of the reactions in solution, several solute complexes become involved in solid phase formation.

Recently, an amorphous hydrous oxide was produced consisting of colloidal spherical particles extremely uniform in size. The sols are prepared by heating dilute solutions of chromium(III) salts in the presence of sulfate or phosphate ions, and without the addition of base.[15,16] Significantly, no such sols could be obtained when chromium(III) nitrate, chloride, or perchlorate alone were used. Formation and growth of the sol particles are quite reproducible and light scattering techniques may be employed to obtain the size distribution parameters *in situ* as a function of time. Consequently, growth mechanisms may be postulated.[17]

In addition, the electrolyte environment from which the particles are formed and in which they are suspended is sufficiently inert (kinetically), enabling the complex soluble species to be separated and characterized using suitable analytical techniques.[18,19] Hence, these sols appear to represent model systems as convenient as one could hope to develop for the purpose of elucidating the mechanism of formation of hydrous metal oxide particles.

This investigation is concerned with the period of heating where nucleation and growth occur, *i.e.*, until a condition referred to as the steady state of growth is established. After much longer periods of heating, a second solid phase of different morphology appears (presumably crystalline) indicating that considerable time is required to reach true equilibrium.[20,21]

In order to distinguish between different possible growth mechanisms, Nielsen's chronomal analysis was applied.[3] This requires that the system consist of uniform particles of constant number concentration, the size distribution of which does not change appreciably with time. The hydrous chromium(III) oxide sols with particles of narrow size distribution used in this work meet these conditions.

Experimental Section

The methods for sol preparation, analysis, and characterization have been described in detail elsewhere and, for reasons of brevity, will not be repeated here.[15,17,18] The filtered solutions of 4.0×10^{-4} F chrome alum were heated (without stirring) at 75 or 90° (±0.5°) in capped 0.5-l. vessels of Pyrex or polypropylene. The reaction vessels as received were rinsed with distilled water, steam cleaned, and dried at 100°. Use of smaller vessels was avoided, as it led to significant loss of particles to container walls. Also, initial heating rates (from room to elevated temperatures) depended upon the vessel materials, resulting in variable particle number concentrations when small tubes were used.[22] Cleaning the reaction vessels with chromic acid solution should be avoided.

After heating at the desired temperature for a definite period of time, a 25-ml sample was removed, cooled rapidly to room temperature, and analyzed either by light scattering or microelectrophoresis or both.[23,24]

The remaining sample was filtered to remove sol particles and the total chromium concentration in the filtrate (electrolyte medium) was determined by atomic absorption spectrophotometry.[17]

pH measurements were performed using a combination electrode.[17,18]

Particle size distribution parameters were obtained from light scattering using the polarization ratio method.[25,26] The applicability of this procedure to the characterization of hydrous chromium(III) oxide sols was described in detail previously.[15,27] It is essential that the suspension be diluted (in this case with filtered 0.001 M HNO_3) to minimize multiple scattering. Furthermore, reflection corrections must be made,[28] otherwise erroneous values of α_m and σ_o, defined below, may be obtained.[29]

Results

Figure 1 is a plot of the modal diameter,[30,31] obtained from light scattering measurements, of particles formed from 4.0×10^{-4} F chrome alum solutions as a function of time. The solutions were heated in 0.5-l. reaction vessels of Pyrex and polypropylene, respectively, at 75 and 90°. The
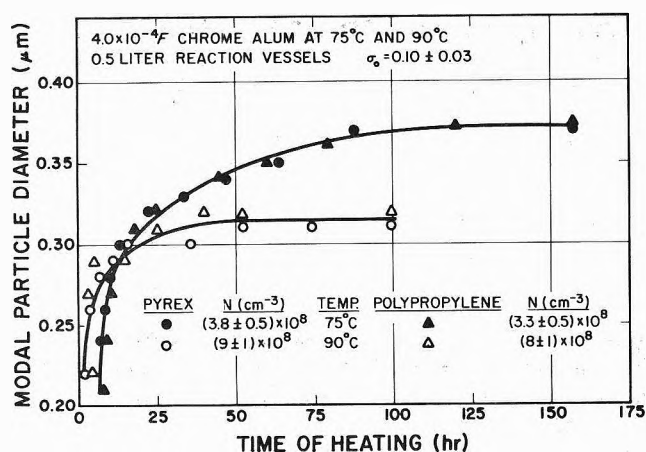
Figure 1. Plot of modal diameter of particles formed from 4.0 × 10⁻⁴ F chrome alum solutions vs. time of heating in 0.5-l. reaction vessels: at 75° Pyrex (●), polypropylene (▲); at 90° Pyrex (O), polypropylene (△). Values of N were obtained using eq 1.

Figure 2. Plot of total chromium concentration in the electrolyte medium (after removal of particles) vs. time of heating in 0.5-l. reaction vessels of solutions initially 4.0 × 10⁻⁴ F in chrome alum: at 75° Pyrex (●), polypropylene (▲); at 90° Pyrex (O), polypropylene (△).

particles eventually reached a limiting size, and the time to reach the steady state, the particle number concentration, N, and the limiting diameter were strongly influenced by temperature. Furthermore, the onset of precipitation, as indicated by the appearance of a Tyndall beam, in the solutions placed in the constant temperature bath, occurred after ∼4 hr at 75° and ∼0.5 hr at 90°. The particle diameter was sufficiently large such that the polarization ratio method of light scattering could be applied after ∼7 hr at 75° and ∼2 hr at 90°.[30]

Figure 2 shows the total concentration of chromium remaining in solution as a function of time of heating for the same sols, after removal of the particles by filtration. There is a small difference in concentration at any given time which is apparently influenced by the reaction vessel material employed; however, since the particle number concentration also varies, the growth rate constants calculated for these systems do not differ appreciably, as will be shown later.

Figure 3 shows the pH at 75 and 90° of unfiltered sols formed from 4.0 × 10⁻⁴ F chrome alum solutions in 50-ml Pyrex tubes in the early stages of heating. Obviously, at the higher temperature, the hydrolytic reactions proceed much faster. It was shown elsewhere[19] that all hydrolyzed species including those containing sulfato groups form more rapidly at 90°. Consequently, the nucleation and growth rates of the sol particles are expected to be greater at the higher temperature. Significantly, the final pH appears to be independent of temperature.

Averaged values of N, the particle number concentration (particles/cm³ shown in Figure 1), were obtained from data given in Figures 1 and 2 using the expression[17]

$$N = \frac{6\pi^2 w}{\rho\lambda^3}\left[\int_{\alpha_m \exp(-3\sigma_0)}^{\alpha_m \exp(3\sigma_0)} \alpha^3 p(\alpha)\,d\alpha\right]^{-1} \quad (1)$$

where w is the mass of particles per cm³ of suspension, ρ the particle density (2.42 g/cm³), λ the wavelength of scattered light in the medium (3.25 × 10⁻⁵ cm), α the particle size parameter (α = 2πr/λ, where r is the particle radius), α_m the modal size parameter, σ_0 the distribution width parameter, and p(α) is the zeroth-order log normal distribution function.[31] The calculated values, within experimental error, are constant throughout the growth periods.
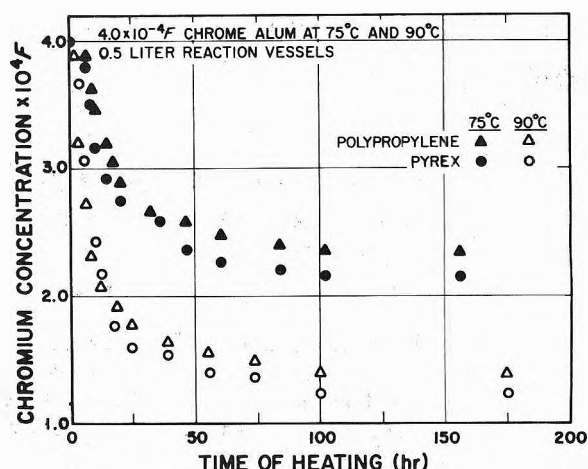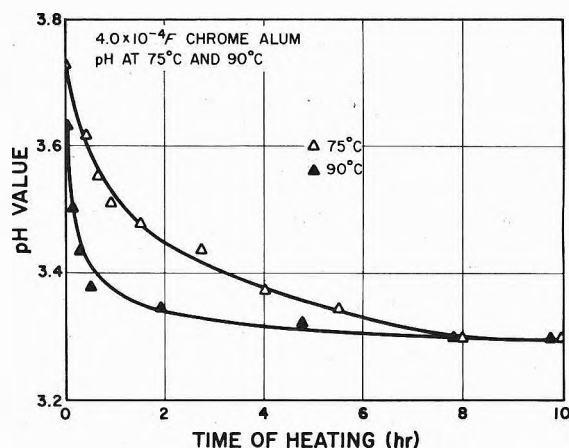
The particle number concentration can also be obtained

Figure 3. pH as a function of time during the early state of heating in Pyrex tubes of unfiltered hydrous chromium(III) oxide sols initially 4.0 × 10⁻⁴ F in chrome alum at 75 (△) and 90° (▲).

from absolute values of the intensity of scattered light.[15,32] This was done for the systems at the early stages of growth, where adsorption onto the container walls and aggregation were not significant, and excellent agreement was found with those values calculated using eq 1.

Another condition to be fulfilled when studying growth kinetics is that the particles must be colloidally stable, i.e., that no appreciable aggregation occurs. Electrophoretic mobilities of the hydrous chromium(III) oxide particles were measured at 75° and again after cooling the systems to room temperature. The ζ potentials calculated using the Henry expression[33] gave a value of ζ ≈ + 25 mV at both temperatures. This value is sufficient to account for colloidal stability on an electrostatic basis alone, not considering solvation effects which further contribute to stability.[34]

Chronomal Analyses

In an attempt to establish the growth mechanism(s) and calculate the growth constants, use was made of Nielsen's "chronomal" (dimensionless time parameter) analyses.[3] This treatment, possibly the most comprehensive in the literature, may distinguish between diffusion controlled, surface reaction (nucleation) controlled, and compound growth mechanisms. As mentioned above, the systems

studied here meet all the prerequisites for these types of analyses.

In the evaluation of data that follows, only surface reaction and diffusion controlled growth processes are considered.

According to Nielsen, surface reaction controlled growth (also referred to as "polynuclear layer" growth) is so rapid that each layer is the result of intergrowth of numerous surface nuclei; consequently, the rates are independent of surface area. However other mechanisms are also possible.[5,7,11]

The rate of surface reaction controlled growth of kinetic order p is given by

$$dr/dt = vk_p c^p \tag{2}$$

where r is the particle radius, t the time, v the molar volume of the precipitate, k_p the rate constant, and c is the concentration of species reacting to form solid, with the underlying assumption that $c \gg s$ where s is the solubility.

The rate constant k_p may be obtained directly from the experimental data using eq 2. Alternatively (and preferably), the equation may be integrated as follows.[3] Let

$$x_p = 1 - (c/c_0) \tag{3}$$

and assume

$$r = r_e x_p^{1/3} \tag{4}$$

where x_p is the degree of reaction and r_e the particle radius at the end of growth (i.e., at the steady state of growth).

Nielsen derived the following relationship

$$t = I_p K_p \tag{5}$$

where I_p, the polynuclear layer chronomal at a defined value of x_p, is given by the integral

$$I_p = \int_0^{x_p} x^{-2/3}(1 - x)^{-p} \, dx \tag{6}$$

and

$$K_p = \frac{r_e}{3vc_0^p k_p} = [(36\pi v^2 N)^{1/3}(c_0^p)^{-1/3}k_p]^{-1} \tag{7}$$

where c_0 is the initial concentration of reacting species and $c \gg s$.

Values of x_p are obtained using eq 3 from analytical data. From tabulated values of I_p (as a function of x_p), a plot of I_p vs. t may be constructed. If, for a given value of p, the plot (or a region thereof) is linear, the values of K_p may be obtained using eq 5 (in the region of linearity), and k_p may be calculated, if N (or r_e), v, and c_0 are known, from eq 7.

For "mononuclear" layer growth, the time that passes between two consecutive nucleations on the surface is much longer than the time to cover all the surface; hence, growth is layer upon layer. Nucleation rates are proportional to the surface area and to a power m of the concentration. Mononuclear layer growth would only be expected to be rate controlling during the very early stages of growth, and then would be superseded by some other mechanism, since the radius would tend to approach infinity at longer periods of time.[8,9]

For diffusion controlled growth, the corresponding expressions are

$$\frac{dr}{dt} = \frac{Dv(c - s)}{r} \tag{8}$$

$$x_D = (c_0 - c)/(c_0 - s) \tag{9}$$

$$r = r_e x_D^{1/3} \tag{10}$$

$$t = I_D K_D \tag{11}$$

$$K_D = r_e^2/3vD(c_0 - s) = [48\pi^2 vN^2(c_0 - s)]^{-1/3}D^{-1} \tag{12}$$

where D is the diffusion coefficient of the reacting species, and I_D, the diffusion chronomal, is

$$I_D = \int_0^{x_D} x^{-1/3}(1 - x)^{-1} \, dx \tag{13}$$

A plot of I_D vs. t should yield a straight line of slope $(K_D)^{-1}$. If N (or r_e), v, and $(c_0 - s)$ are known, D may be calculated and judged whether reasonable ($D \approx 10^{-5}$ cm^2/sec for simple electrolytes in water at 25°).

Selected values of various chronomals (as a function of the degree of reaction) are tabulated by Nielsen;[3,35] more complete tables may be generated by computation. From tabulated values, it is observed that values of I_p in the range $x_p = 0.3$–0.8 should be used to select the most appropriate value of p in a particular experiment, if surface reaction controlled growth is thought to occur.

In the application of chronomal analyses to the growth of hydrous chromium(III) oxide particles, it is necessary to make certain assumptions and approximations, which are based upon consideration of the complex chemistry leading to solid formation. This has been described in detail elsewhere.[19,22] According to the latter, a major particle growth reaction may be represented as

$$\text{Cr(OH)}_3 \cdot \text{(aq)} \longrightarrow \text{Cr(OH)}_3 \text{ (solid, hydrated)} \tag{14}$$
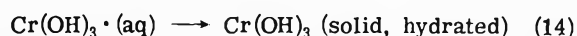
It should be noted that a second basic chromium(III) sulfate species is involved in solid formation, but the resulting particles have been shown to contain no sulfate.

Based upon the above equation, the reacting species is assumed to be monomeric. Analysis of the complex chemistry utilizing radio–paper electrophoresis indicates that the concentration of the neutral solute chromium(III) hydroxide species approaches zero at the steady state of growth.[19,22] This would suggest that the solubility of such species is rather small; therefore, an approximation $(c - s) \approx c$ was used in the calculations. The value of c_0 was obtained by substracting the concentration of Cr(III) at the steady state from the original concentration (4.0×10^{-7} mol/cm^3).

The value of the molar volume which appears in the chronomal equations had to be estimated, because of the amorphous nature of the solid; the value $v \approx 50$ cm^3/mol was chosen which closely approximates that of hydrated chromium(III) hydroxide of density 2.4 g/cm^3.[18]

Plots of chronomal values of the solutions originally 4.0×10^{-4} F in chrome alum vs. times of heating at 75° are shown in Figures 4 and 5 for second- and third-order surface reaction controlled growth. The values of K_p were obtained from least-squares analyses of the data in each plot in the region $x_p = 0.3$–0.8 (shown by the arrows in the figures). Substituting the values of c_0, N, and K_p in eq 7, with $v = 50$ cm^3/mol, one can obtain the growth constant k_p. From k_p values at different temperatures the activation energy of growth, E_a, was calculated by means of the Arrhenius equation, and the results are shown in Table I.

As mentioned previously, mononuclear layer growth would only be expected to occur at very early time periods

TABLE I: Surface Reaction Controlled Growth Constants and Activation Energies

Kinetic order of growth (p)	Vessel material	k_p; $(T_2)^a$ ($\pm 30\%$)	k_p; $(T_1)^a$ ($\pm 30\%$)	E_a, kcal/mol
2	Pyrex	5.2×10^{-14}	2.1×10^{-14}	15 ± 6
2	Polypropylene	4.9×10^{-14}	2.0×10^{-14}	15 ± 6
3	Pyrex	1.3×10^{-15}	3.2×10^{-16}	23 ± 9
3	Polypropylene	1.2×10^{-15}	3.7×10^{-16}	20 ± 8

^{a} $T_2 = 363°K$ (90°), $T_1 = 348°K$ (75°). Units for $p = 2$, $cm^4 mol^{-1} sec^{-1}$; for $p = 3$, $cm^7 mol^{-2} sec^{-1}$.

Figure 4. Plot of second-order polynuclear layer growth chronomal vs. time of heating of solutions initially 4.0×10^{-4} F in chrome alum at 75° in 0.5-l. reaction vessels of Pyrex (●) and polypropylene (▲). Values of c_0, N, and K_2 included were inserted into eq 7 to determine the rate constant k_2. The arrows indicate the region where the degree of reaction $x_p = 0.3$–0.8.
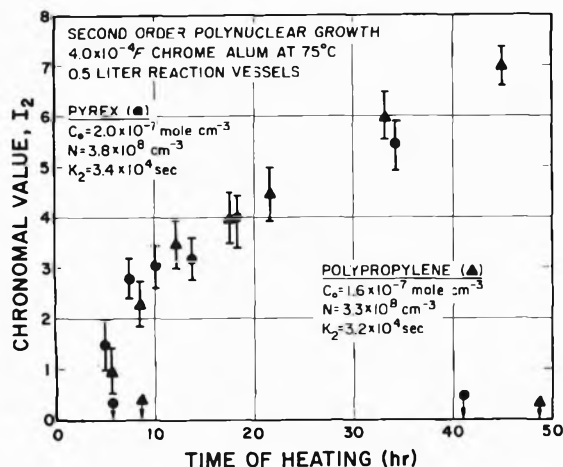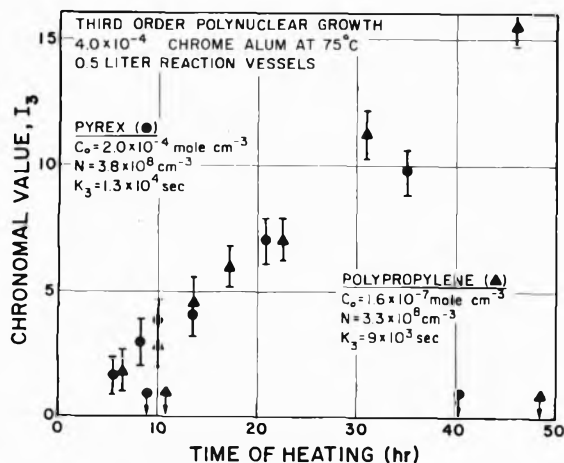

Figure 5. Plot of third-order polynuclear layer growth chronomal vs. time of heating of solutions initially 4.0×10^{-4} F in chrome alum at 75° in 0.5-l. reactions vessels of Pyrex (O) and polypropylene (△). Values of c_0, N, and K_3 included were inserted into eq 7 to determine the rate constant k_3. The arrows indicate the region where the degree of reaction $x_p = 0.3$–0.8.

($x_m \ll 0.3$) if at all. Since the analytical data are not sufficiently reproducible in the early growth stages, no attempt has been made to calculate mononuclear layer growth constants. Nielsen[36] has commented that it would be highly unlikely for mononuclear growth to take place in these systems, involving growth of amorphous material.

Plots of the diffusion chronomals vs. times are not shown since a linear relationship was observed only over a limited region, in the latter stages of growth. From this region values of D calculated using eq 12 are of the order 10^{-10} to 10^{-11} cm²/sec, which are unreasonable for a simple diffusional mechanism.
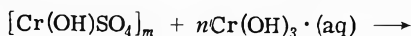
Discussion

Previous studies employing electron microscopy,[22] and particularly utilizing the "wet cell,"[27,37] suggested that prior to the formation of spherical hydrous oxide particles, a strand-like solid (presumably a basic chromium sulfate polymer) is formed. This polymeric material apparently serves as a precursor to or heteronucleating agent for the formation of spherical hydrous chromium(III) oxide particles.

This solid precursor is essential to hydrous chromium(III) oxide formation inasmuch as in its absence no sol is produced, even when the concentration of solute $Cr(OH)_3$ species is high, as shown by aging chromium perchlorate solutions.[19] Obviously, the free energy of nucleation is lowered by the presence of foreign matter which enables the hydrous oxide particles to appear at lower supersaturation levels.[38]

Once the nucleation in the presence of foreign matter has occurred, chronomal analyses suggest that growth proceeds via a surface reaction mechanism of kinetic order 2 or 3. The growth of many inorganic crystals has also been characterized using these values of p.[39,40] The limited amount of data indicates that activation energies for diffusion and polynuclear layer growth of $BaSO_4$ are in the region ~5 kcal/mol.[35]

Table I shows that the activation energies of surface reaction controlled growth are considerably higher; furthermore, the rate constants are significantly lower than those associated with the growth of many inorganic crystals.[39] These findings would indicate that chemical reactions involving chromium(III) species occur at the surface. It is well known that almost all reactions involving Cr(III)— e.g., ligand substitution, hydrolysis, coordinated water exchange with solvent—proceed at rates orders of magnitude smaller than those involving most other metal ions, and at much higher activation energies (20–30 kcal/mol).[41-43] Hence, if growth is indeed surface reaction controlled, on the basis of values of E_a, a third-order mechanism would be favored; this conclusion is further substantiated by the observation that chronomal plots are linear over greater periods of time for $p = 3$, and that they appear to pass through the origin.

Judging from other reactions of Cr(III) species at interfaces, specifically the mercury/solution interface,[44,45] the rate-determining step(s) might include the dissociation or displacement of aquo groups, and subsequent ol- bridge formation.[12] It is also possible that basic chromium sulfate species participate in the growth process by reactions such as

$$[Cr(OH)SO_4]_m + nCr(OH)_3 \cdot (aq) \longrightarrow$$

$$[Cr(OH)_3]_{m+n} \text{ (solid, hydrated)} + mSO_4^{2-} + 2mH^+ \quad (15)$$

giving a solid chromium hydroxide essentially void of sulfate ions. Some evidence for this mechanism was offered elsewhere.[19] Of course, if this reaction were involved, values of k_p (through c_0) would be different from those listed in Table I, although the corresponding values of E_a might remain unchanged.

Even though the above analyses have not fully explained all phenomena associated with the formation and growth of hydrous chromium(III) oxide particles of narrow size distribution, they have certainly provided us with much more insight than was available heretofore.

References and Notes

(1) Supported by the National Science Foundation Grant No. GP 42331X.
(2) Part of a Ph.D. Thesis by A. Bell, Clarkson College of Technology, Potsdam, N.Y., 1974.
(3) A. E. Nielsen, "Kinetics of Precipitation," Pergamon Press, Oxford, 1964, and references therein.
(4) A. G. Walton, "Formation and Properties of Precipitates," Wiley, New York, N.Y., 1967.
(5) E. V. Khamskii, "Crystallization from Solutions," Consultants Bureau, New York, N.Y., 1969.
(6) M. Kahlweit in "Physical Chemistry-An Advanced Treatise," Vol. 10, W. Jost, Ed., Academic Press, New York, N.Y., 1970.
(7) J. W. Mullin, "Crystallisation," The Chemical Rubber Co., Cleveland, Ohio, 1972.
(8) A. E. Nielsen, *Krist. Tech.*, **4**, 17 (1969).
(9) A. E. Nielsen, *Croat. Chem. Acta*, **42**, 319 (1970).
(10) A. G. Walton in "Dispersions of Powders in Liquids," A. L. Smith, Ed., Elsevier, Amsterdam, 1969.
(11) M. O'Hara and R. C. Reid, "Modeling Crystal Growth Rates From Solution," Prentice-Hall, Englewood Cliffs, N.J., 1973.
(12) C. L. Rollinson in "The Chemistry of Coordination Compounds," J. C. Bailar, Ed., Reinhold, New York, N.Y., 1956.
(13) L. Pokras, *J. Chem. Educ.*, **33**, 152 (1956).
(14) K. H. Lieser, *Angew. Chem., Int. Ed. Engl.*, 8, 188 (1969).
(15) R. Demchak and E. Matijević, *J. Colloid Interface Sci.*, **31**, 257 (1969).
(16) E. Matijević, A. D. Lindsay, S. Kratohvil, R. I. Larson, and A. W. Cayey, *J. Colloid Interface Sci.*, **36**, 273 (1971).
(17) E. Matijević, A. Bell, R. Brace, and P. McFadyen, *J. Electrochem. Soc.*, **120**, 893 (1973).
(18) E. Matijević and A. Bell in "Particle Growth in Suspensions," A. L. Smith, Ed., Academic Press, New York, N.Y., 1973, pp 179–193.
(19) A. Bell and E. Matijević, *J. Inorg. Nucl. Chem.*, in press.
(20) P. W. Schindler, *Advan. Chem. Ser.*, **No. 67**, 196 (1967).
(21) W. Stumm and J. J. Morgan, "Aquatic Chemistry," Wiley, New York, N.Y., 1970.
(22) A. Bell, Ph.D. Thesis, Clarkson College of Technology, Potsdam, N.Y., 1974.
(23) J. P. Kratohvil and C. Smart, *J. Colloid Sci.*, **20**, 874 (1965).
(24) R. Brace and E. Matijević, *J. Inorg. Nucl. Chem.*, **35**, 3691 (1973).
(25) M. Kerker, E. Matijević, W. F. Espenscheid, W. A. Farone, and S. Kitani, *J. Colloid Sci.*, **19**, 213 (1964).
(26) R. Jacobsen, M. Kerker, and E. Matijević, *J. Phys. Chem.*, **71**, 514 (1967).
(27) R. I. Larson, E. F. Fullam, A. D. Lindsay, and E. Matijević, *AIChE J.*, **19**, 602 (1973).
(28) J. P. Kratohvil, *J. Colloid Sci.*, **21**, 498 (1966).
(29) In a previous study (ref 18) dilution and reflection corrections were not performed, thus leading to the erroneous conclusion that secondary nucleation was taking place in addition to growth.
(30) M. Kerker, "The Scattering of Light and Other Electromagnetic Radiation," Academic Press, New York, N.Y., 1969.
(31) W. F. Espenscheid, M. Kerker, and E. Matijević, *J. Phys. Chem.*, **68**, 3093 (1964).
(32) R. L. Rowell, T. P. Wallace, and J. P. Kratohvil, *J. Colloid Interface Sci.*, **26**, 494 (1969).
(33) D. C. Henry, *Proc. Roy. Soc., Ser. A*, **133**, 106 (1931).
(34) E. Matijević, *J. Colloid Interface Sci.*, **43**, 217 (1973).
(35) A. E. Nielsen, *Acta Chem. Scand.*, **13**, 784 (1959).
(36) A. E. Nielsen, private communication.
(37) E. F. Fullam, *Rev. Sci. Instrum.*, **43**, 245 (1972).
(38) A. G. Walton in "Nucleation," A. C. Zettlemoyer, Ed., Marcel Dekker, New York, N.Y., 1969.
(39) R. H. Doremus, *J. Phys. Chem.*, **62**, 1068 (1958); **74**, 1405 (1970).
(40) R. H. Doremus, *Croat. Chem. Acta*, **42**, 293 (1970).
(41) M. Eigen and R. G. Wilkins, *Advan. Chem. Ser.*, **No. 49**, 55 (1965).
(42) F. Basolo and R. G. Pearson, "Mechanisms of Inorganic Reactions," 2nd ed, Wiley, New York, N.Y., 1967.
(43) J. P. Hunt, "Metal Ions in Solution," W. A. Benjamin, New York, N.Y., 1963.
(44) R. E. Hamm, R. L. Johnson, R. H. Perkins, and R. E. Davis, *J. Amer. Chem. Soc.*, **80**, 4469 (1958).
(45) H. Yamaoka, *J. Electroanal. Chem.*, **25**, 381 (1970).

Titrimetric Applications of Multiparametric Curve Fitting. III. Evaluation of the Parameters Characterizing Acidimetric Potentiometric Titrations of Laurate Ion

Shiu L. Young, Egon Matijević, and Louis Meites*

Department of Chemistry and the Institute of Colloid and Surface Science, Clarkson College of Technology, Potsdam, New York 13676
(Received June 24, 1974)

The reactions that occur when sodium laurate solutions containing various concentrations of sodium chloride are treated with acid were elucidated by applying a general multi-parametric curve-fitting program to data obtained in acidimetric potentiometric titrations. In some titrations free lauric acid precipitated; in others sodium hydrogen laurate precipitated as well; and in still others micelles formed in addition. It was possible to evaluate the solubility products of both the free acid and the acid soap, as well as the critical micelle concentration, and the resulting values were in excellent agreement with those available in the literature. The procedure described is applicable in principle to the study of the reactions of any fatty acid anion with hydrogen ion and another cation.

Introduction

The wealth of fundamental physicochemical information that can be obtained from potentiometric titration-curve data by nonlinear regression techniques was first demonstrated by Sillén, and he and his collaborators and followers have founded much of the present understanding of the chemistry of metal–hydroxide complexes on this basis.[1] It is odd that there has been so little investigation of the use of these techniques in other titrimetric areas. Anfalt and Jagner[2] suggested that nonlinear regression was a promising approach to end point location, and this was rapidly followed by proofs due to Ingman, et al.[3] and to Barry, Campbell, and Meites.[4,5] Ingman et al., showed that acetic and propionic acids can be determined in their mixtures by titration with standard base even though their pK_a values differ by only 0.12 unit; Barry and Meites[4] were able to determine acetate by titration with standard acid even at dilutions so extreme that the titration curve has no inflection point; and Barry, Meites, and Campbell[5] showed that the concentration of the reagent, as well as that of the solution being titrated, can be obtained from the titration-curve data, so that separate standardization of the reagent is unnecessary. Meanwhile Brand and Rechnitz[6] and Isbell, Pecsok, Davies, and Purnell[7] applied nonlinear regression successfully to analyses by standard addition and titrimetry with ion-selective electrodes.

Acid dissociation constants and other equilibrium constants have been computed in the majority of these applications but have been of primary interest in none. In the present communication we describe the use of nonlinear regression to evaluate the solubility products of the two solid phases that may form, and the critical concentration for micelle formation if a micellar phase separates as well, when a solution of the anion of a long-chain fatty acid is titrated potentiometrically with a strong acid.

The titration curves obtained in such titrations are complex and their form depends on the concentration of soap titrated and also on the identity and concentration of the alkali metal ion M^+ that is present. It has long been known[8,9] that an acid soap having the formula MHL_2 (L^- = laurate ion) can be precipitated on acidifying solutions of sodium or potassium laurate, and this was taken into account by Lucassen,[10] who developed a quantitative description of hydrolysis and precipitation in laurate and other solutions. Rosano, et al.,[11–13] showed that the activity of alkali metal ion varied during an acidimetric titration of a potassium or sodium laurate solution, and Feinstein and Rosano[14] employed values of the equilibrium constants given by Lucassen[10] to account for the differing shapes of the titration curves obtained under different conditions. Their picture, which is accepted here, entails three separate possibilities: that the free acid may precipitate, that the acid soap may precipitate, and that anionic micelles may form.

These three possibilities give rise in principle to eight different cases, but the solubility products of lauric acid and of sodium hydrogen laurate and the critical micelle concentration for laurate ion are such that only three of the eight are conveniently realizable. In very dilute solutions of laurate containing moderate concentrations of sodium ion, free lauric acid separates during a titration. Increasing the initial concentration of laurate leads to the precipitation of acid soap at the start of the titration, and later to the precipitation of free acid as well. A still further increase leads to the presence of laurate micelles during the first portion of the titration. Values of the appropriate equilibrium constants in excellent agreement with those in the literature may be obtained by analyzing curves for any of these cases.

Experimental Section

Stock solutions of sodium laurate were prepared in such a way as to avoid the presence of excess sodium hydroxide, which would have affected both the amounts of acid consumed and the shapes of the initial portions of the curves and would have greatly complicated the calculations. Lauric acid was obtained from Nu-Chek-Prep Inc.; it had been analyzed by gas–liquid chromatography and thin-layer chromatography, and had a stated purity of at least 99.8%. An appropriate amount of the acid was weighed exactly, heated to just above its melting point, and treated with the smallest possible deficiency of concentrated carbonate-free sodium hydroxide solution. Constant stirring was employed during the addition of the sodium hydroxide and for a few minutes thereafter. After dilution with water the solution was transferred quantitatively to a volumetric flask and diluted to the mark. Stock solutions thus prepared were al-

ways clear because they were free from undissolved lauric acid and had laurate concentrations below the cmc; although the cmc was exceeded in some of the titrations, this was the result of subsequent addition of sodium chloride. Care was taken to minimize access of carbon dioxide to the solution during preparation and storage.

Titrations were performed in an atmosphere of nitrogen. Known volumes of distilled water and a solution of sodium chloride were mixed in a 300-ml beaker fitted with a Teflon cover, and a rapid stream of prepurified nitrogen was allowed to flow through a coarse-porosity Corning no. 39533 fritted-glass gas-dispersion cylinder into the mixture for at least 10 min to expel dissolved carbon dioxide. The desired volume of sodium laurate solution was then added and the rate of flow of nitrogen was reduced sufficiently to prevent foaming. Since some of the titrations were very prolonged, the nitrogen was equilibrated with 0.1 F aqueous sodium chloride in an efficient gas-washing bottle before it entered the titration cell, thus obviating gradual changes of composition resulting from evaporation of water from the titration mixture. Continuous magnetic stirring was employed. Titrations were made at room temperature, 24 ± 1°, with appropriate thermal shielding between the titration cell and magnetic stirrer to avoid warming the solution. The solutions of hydrochloric acid used as reagents were prepared by volumetric dilution of a standard stock solution, and often contained known concentrations of sodium chloride so chosen that the ionic strength would remain substantially constant during the titrations. In each titration the reagent was added from a 10-ml buret to 100 ml of the laurate solution.

Measurements of pH were made with a Corning Model 112 pH meter equipped with a Sargent-Welch S-30072-15 combination electrode. Every attempt was made to obtain readings reliable to ±0.002 pH unit. Constant readings were seldom attained in less than 15 min after the addition of an aliquot of acid, and much longer times were required in regions where a new phase was appearing. In a typical titration about a dozen points were obtained in the region, extending from 0.03 to 0.90 mol of acid per mole of soap, on which the computations were based, but there were a few in which the number was as low as 8 or as high as 22.

These conditions differ from those of Feinstein and Rosano[14] in two ways: our solutions did not contain excess alkali-metal hydroxide but usually did contain a swamping excess of sodium chloride. These differences simplified both the titration curves and the calculations based on them.

Computations

A general multi-parametric curve-fitting program described in detail elsewhere[15] was used to compute the equilibrium constants from the data obtained. It was capable of handling each of the three cases that could be realized experimentally, as well as each of the five others that can be imagined but that were not represented in these titrations. Most of the calculations were done in Basic on a Digital Equipment Corp. (Maynard, Mass.) PDP8/1 minicomputer operated in a multiuser configuration that made 4096 words of core memory available as the user area for this work; a few were done in Fortran IV on an IBM 360/44 system.

The coordinates of the data points are entered into the program before execution is begun. We chose to exclude points at which the volume of acid was less than 3%, or

larger than 90%, of that required to contain 1 mol of hydrogen ion for each mole of laurate titrated. The titration mixture is poorly buffered near the start of the titration and near the equivalence point, and the pH values measured in these regions are subject to errors arising from causes such as the slow nucleation of a solid phase, the adsorption of hydrogen or laurate ion by a solid phase, and uncertainties in the purity of the soap or in the concentration of the acid. Moreover, data beyond the equivalence point are nearly useless in these calculations, for the pH values in that region are hardly at all dependent on the parameters of interest. Restricting the width of the region that is included also makes it possible to employ simple titration-curve equations without introducing appreciable errors and thereby greatly decreases the computation time required.

Initial input also includes values of the volume $V_b{}^0$ and concentration $C_b{}^0$ of the laurate solution titrated, of the concentration C_a of the acid used as reagent, of the concentrations C_{MX} of the alkali-metal-ion salt MX in each of these solutions, and of the mean ionic activity coefficients of hydrochloric acid and potassium chloride at the ionic strength employed. The last of these are used to obtain an approximate value of the apparent single-ion activity coefficient of hydrogen ion from the relationship

$$y_{H^+} = \gamma_{\pm,HCl}{}^2/\gamma_{\pm,KCl} \tag{1}$$

This embodies the Guggenheim assumption, neglects the difference between molarity and molality coefficients, and is probably subject to errors of a few per cent even at an ionic strength of 0.1 M. These were deemed to be negligible for the present purpose, especially since other activity coefficients subject to similar uncertainties are involved in interpretations of the concentration constants obtained.

It is tacitly presumed that $C_{MX,b}$ and $C_{MX,a}$ have been so chosen that variations of the ionic strength during the titration are negligible. The liquid-junction potential is also neglected, although it is not certain how far this is justified in the presence of micelles, and the uncertainties arising from this source and from adsorption onto one or both of the solid phases are probably responsible for most of the variations among the values obtained.

The processes believed to have occurred during the titration must also be specified. As has been mentioned above, there are eight possibilities, for micelles may or may not have formed and each of the two possible solid phases may or may not have precipitated. For each process believed to have occurred, an initial estimate of the appropriate parameter is requested. The parameters are defined by

$$K_a = [H^+][L^-]/[HL(aq)] \tag{2a}$$

$$S_{HL} = [HL(aq)] \text{ in a saturated solution} \tag{2b}$$

$$C = \text{cmc} \tag{2c}$$

$$K_{MHL_2} = [M^+][H^+][L^-]^2 \tag{2d}$$

and are thus the concentration or conditional constants appropriate to the ionic strength employed. There is a moderate, but not an extremely large, latitude in these initial estimates. If, for example, that of K_{MHL_2} were several orders of magnitude too low, precipitation of MHL_2 would appear to occur at every point on the curve, and the possibility that MHL_2 was not present at some points might never be tested.

The behavior of laurate in solutions of sodium and potassium salts is well known, and in this work we had the advantage of being able to furnish initial estimates of all the parameters that were fairly close to the truth. In another and less well understood case, it would be advantageous to begin with titrations in which C_b^0 was very small, so that the solubility product $[H^+][A^-] = S_{HA}K_a$ of the free acid HA (or perhaps both S_{HA} and K_a individually, if the acid were sufficiently soluble) could be evaluated alone. In these two-parameter fits the initial estimate $K_a = 1.5 \times 10^{-5}$ would serve, and the initial estimate of S_{HA} could be taken as $C_b^0/2$, which is equivalent to assuming that the free acid precipitates at some points but not at every one. At a higher concentration of soap, where precipitation of the acid soap would accompany that of the free acid, and where the initial estimate of K_{MHA_2} should be such that the acid soap appears to precipitate at some points but not at all, a three-parameter fit would be required. The initial estimate of S_{HA} here should be either the average value of S_{HA} or one obtained from the average value of the product $S_{HA}K_a$ in the preceding two-parameter fits.

Using these initial estimates, a pH value is computed for each experimental point. To do this it is first assumed that neither micelle formation nor precipitation of either solid phase occurs at the point under consideration. According to this assumption

$$[L^-] = (V_b^0 C_b^0 - V_a C_a)/(V_b^0 + V_a) \qquad (3a)$$

$$[HL] = V_a C_a/(V_b^0 + V_a) \qquad (3b)$$

and

$$[H^+] = [HL]K_a'/[L^-] \qquad (3c)$$

while

$$[M^+] = [V_b^0(C_b^0 + C_{MX,b}) + V_a C_{MX,a}]/(V_b^0 + V_a) \qquad (3d)$$

A quantity P8, which is initially set to zero for each successive point, is then increased by 1 if this value of $[L^-]$ exceeds the currently assumed value[16] C' of the cmc, by 2 if $[HL]$ exceeds S_{HL}', and by 4 if $[M^+][H^+][L^-]^2$ exceeds K_{MHL_2}'. The following list of possibilities results

P8	Processes that appear to occur
0	simple homogeneous neutralization
1	micelle formation
2	precipitation of HL
3	micelle formation and precipitation of HL
4	precipitation of MHL₂
5	micelle formation and precipitation of MHL₂
6	precipitation of both MHL₂ and HL
7	micelle formation and precipitation of both MHL₂ and HL

If P8 = 0 the value of $[H^+]$ obtained from eq 3c is accepted. If P8 = 1 the value of $[L^-]$ obtained from eq 3a is replaced by C', while if P8 = 2 that of $[HL]$ obtained from eq 3b is replaced by S_{HL}', and in either case eq 3c is employed to calculate the corresponding value of $[H^+]$. If P8 = 4 all of the prior values are discarded and replaced by others obtained from the appropriate one of the following sets of equations: (1) if $V_a C_a < V_b^0 C_b^0/2$ (before the MHL₂ equivalence point)

$$[L^-] = (V_b^0 C_b^0 - 2V_a C_a)/(V_b^0 + V_a) \qquad (4a)$$

$$[H^+] = K_{MHL_2}'/[M^+][L^-]^2 \qquad (4b)$$

(2) if $V_a C_a = V_b^0 C_b^0/2$ (at the MHL₂ equivalence point)

$$[H^+] = \sqrt[3]{K_{MHL_2}'/4[M^+]} \qquad (4c)$$

$$[L^-] = 2[H^+] \qquad (4d)$$

(3) if $V_a C_a > V_b^0 C_b^0/2$ (beyond the MHL₂ equivalence point)

$$[H^+] = (V_a C_a - V_b^0 C_b^0/2)/(V_b^0 + V_a) \qquad (4e)$$

$$[L^-] = \sqrt{K_{MHL_2}'/[M^+][H^+]} \qquad (4f)$$

together with

$$[HL] = [H^+][L^-]/K_a' \qquad (4g)$$

The values of P8 = 3, 5, and 6 represent situations in which two different phases appear to be in equilibrium with the aqueous phase. That in which P8 = 3 is the simplest of the three, for while the formation of micelles decreases $[L^-]$ below the value initially calculated on the basis of simple homogeneous neutralization it does not affect $[HL]$, and conversely the precipitation of free acid lowers $[HL]$ but does not alter $[L^-]$. Hence one need only replace $[L^-]$ by C' and $[HL]$ by S_{HL}' and solve eq 3c once more for $[H^+]$. The cases for which P8 = 5 or 6 are more complex, because the precipitation of MHL₂ may have removed so much laurate (and hydrogen ion) from the solution that the cmc or the solubility product of the free acid is actually not exceeded. The case in which P8 = 5 will be discussed for illustration. Assuming only homogeneous neutralization, eq 3 gave values of $[L^-]$ and $[H^+]$ that caused both C' and K_{MHL_2}' to be exceeded. These values are replaced by others obtained from eq 4, which represent the assumption that the acid soap is present but that micelles are not. If the resulting value of $[L^-]$ is smaller than C', one possible conclusion is that MHL₂ did precipitate, and in doing so decreased $[L^-]$ so much that micelles did not form. Another possibility is that micelles did form, and in doing so decreased $[L^-]$ so much that MHL₂ did not precipitate. This second possibility is tested by combining $[L^-] = C'$ with eq 3b, 3c, and 3d to compute $[M^+][H^+][L^-]^2$. If this product is less than K_{MHL_2}', so that the acid soap appears to precipitate whether micelle formation is assumed or not, the first possibility above is accepted and the value of $[H^+]$ obtained from eq 4 is accepted. The final possibility is that eq 4 yield a value of $[L^-]$ that exceeds C' while eq 3b–d, with $[L^-] = C'$, yield one of $[M^+][H^+][L^-]^2$ that exceeds K_{MHL_2}'. Here the currently assumed values of the parameters require both micelle formation and precipitation of the acid soap, so that

$$[H^+] = K_{MHL_2}'/[M^+](C')^2 \qquad (5)$$

Exactly similar reasoning is involved for P8 = 6; when neither precipitation of MHL₂ nor that of HL can be rejected the final result is

$$[H^+] = [M^+](K_a'S_{HL}')^2/K_{MHL_2}' \qquad (6)$$

Figure 1 shows the logical structure of the program up to this point.

The final case is that in which P8 = 7. By an argument generally similar to that just outlined, this is sorted out into five possibilities: (1) MHL₂ precipitates, decreasing $[H^+]$ and $[L^-]$ so much that neither the solubility product of HL nor the CMC is exceeded; (2) both MHL₂ and HL
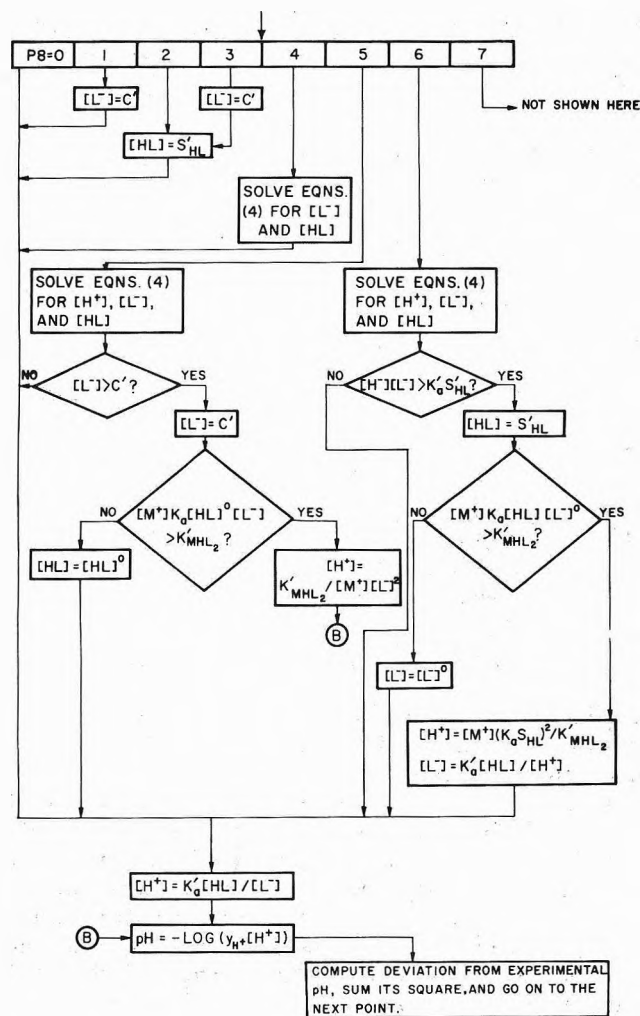
Figure 1. Logical structure of the body of the program.

precipitate; (3) MHL_2 precipitates and micelles are formed; (4) HL precipitates and micelles are formed; (5) the values of C', K_{MHL_2}', and S_{HL}' do appear to correspond to the separation of all three phases at the point under consideration.

The possibility that no phase separation occurs may be dismissed out of hand, and neither micelle formation nor precipitation of HL could cause P8 to equal 7 if it occurred alone. The first four of the listed possibilities correspond to eq 4, 6, 5, and

$$[H^+] = S_{HL}' K_a' / C' \qquad (7)$$

respectively. The fifth possibility, however, contravenes the phase rule and corresponds to an indeterminate hydrogen-ion concentration. If, with $[HL] = S_{HL}'$ and $[L^-] = C'$, the product $[M^+][H^+][L^-]^2$ $(= [M^+]K_a'S_{HL}'C')$ exceeds K_{MHL_2}', the hydrogen-ion concentration obtained from eq 7 is used to compute a pH value to which a deliberate error equal to $0.2(-1)^N$ is added. Here N is the ordinal number of the point in question, and the effect is to punish the apparent violation of the phase rule without systematically displacing the portion of the curve in which it occurs. This provides a stimulus for adjusting the values of S', C', and K_{MHL_2}' so as to prevent violating the phase rule at any point.

This sequence of operations, which has been described at some length because least-squares curve fitting to discontinuous functions is rarely attempted and would present grave difficulties in standard regression procedures, yields a pH value whose deviation from the measured one at the same point is squared and summed over all the points. Each of the parameters in turn is then incremented and decremented, and the corresponding sums of the squares of the deviations are used to guide adjustments of the values in successive cycles of computation.

The situation is so complex chemically that equilibrium is often only slowly reached and adsorption and occlusion by the precipitates are dangerous sources of possible errors. To avoid errors resulting from the inclusion of widely deviant points, provision is made for rejecting, on every fifteenth cycle of computation, any point for which the calculated and measured pH values differ by more than 2.5 times the standard deviation of a single point in that cycle. In about a tenth of the titrations this led to the rejection of one point, which was always the one closest to the equivalence point.

Execution is arbitrarily terminated when the sum of the squares of the deviations has changed by no more than 0.2% over ten cycles of computation. A more stringent condition for termination would prolong execution without changing the value of any parameter more than about 2%, and better accuracy than this is hardly to be expected. Total execution time on a PDP8/I minicomputer operated in Polybasic or an equally efficient interpretive language varies from about 30 sec in the simplest case (P8 = 0) to as much as 10 min in the worst one (P8 = 7).[17]

Results and Discussion

Table I summarizes the results obtained and shows several prominent trends. The most striking is an increase of the standard error of a single pH measurement (the standard deviation from regression) as the chemical complexity of the titration increases. In seven titrations in which solid lauric acid was the only phase that separated, the mean standard deviation from regression was 0.07 pH unit; in seven others in which both the free acid and the acid soap precipitated, it was 0.19 unit; in four in which micelle formation also occurred, it was 0.33 unit. There was clear evidence of systematic errors that could not be taken into account in the calculations and that were responsible for the imperfection of these fits: for example, the pH values at and very near the MHL_2 equivalence points in titrations where the acid soap did precipitate were always above the calculated ones, which suggests that adsorption or occlusion of hydrogen ion by the acid soap is significant. Similarly, the measured pH values always fell below the calculated ones as the HL equivalence point was approached. When the free acid alone precipitated during the titration, the discrepancies in this region were fairly small, suggesting but not proving that laurate ion is coprecipitated to some extent by the free acid, but when precipitation of the acid soap had occurred they were so much larger as to make it seem certain that the overall stoichiometry is affected by the inclusion of some acid soap in the free acid. For these reasons, and in view of the differences between the values obtained in replicate titrations, it does not appear that any of these results should be assigned a reliability better than perhaps ±15%, or roughly 0.05 pK unit.

The solubility of lauric acid in water is so small that it would be exceeded within the first 10% of the titration of

TABLE I: Results of Titrations of Sodium Laurate with Hydrochloric Acid

C_b^0, M	$C_{MX,b}$, M	C_a, M	$C_{MX,a}$, M	Approximate ionic strength, M	$10^{10}K_{HL}$, M^2	$10^{14}K_{MHL_2}$, M^4	10^3cmc, M	Standard error of a single pH measurement
2.5 × 10⁻⁴	4.75 × 10⁻³	0.005	0	0.005	1.37			0.018
					1.75			0.011
5 × 10⁻⁴	0.01	0.01	0	0.01	1.58			0.167
					2.10			0.061
7 × 10⁻⁴	0.043	0.01	0.04	0.044	2.56			0.139
					2.09			0.046
1 × 10⁻³	0.1	0.02	0.08	0.1	2.29	1.14		0.116
1.5 × 10⁻³	0.0985	0.03	0.07	0.1	2.49	1.25		0.215
2.5 × 10⁻³	0.0975	0.05	0.05	0.1	2.34	1.51		0.212
					2.66	1.70		0.197
					2.10	1.34		0.140
5 × 10⁻³	0.1	0.1	0	0.1	3.25	2.46		0.248
					2.40	1.78		0.220
7 × 10⁻³	0	0.1	0	0.007	3.43			0.037
1.25 × 10⁻²	0.1875	0.2	0	0.2	2.02	2.18	5.44	0.341
1.5 × 10⁻²	0.135	0.15	0	0.15	2.20	1.65	5.32	0.245
2 × 10⁻²	0.13	0.15	0	0.15	1.74	1.94	6.35	0.327
5 × 10⁻²	0	1	0	0.05	2.29	2.38	14.1	0.410

even a 2.5×10^{-4} M solution of laurate, which was the highest dilution at which we attempted a titration. Barry and Meites[4] performed successful potentiometric titrations of acetate with hydrochloric acid at somewhat higher dilutions, but we were deterred from following their lead by the fact that our sodium laurate solutions must have contained small concentrations of free lauric acid because of the way in which they were prepared. It is therefore not possible to separate K_a and S_{HL} from the results obtained, and Table I gives only the solubility product K_{HL}, which is equal to the product $K_a S_{HL}$. On plotting the logarithm of this product against the square root of the ionic strength, a straight line with the theoretical Debye–Hückel limiting slope is found to account for the data, obtained from titrations in which the free acid alone separated from the titration mixtures, within an average uncertainty of about 0.02 pK unit. From the intercept of this line the thermodynamic solubility product of lauric acid may be taken as $10^{-(9.86\pm0.05)} = (1.4 \pm 0.2) \times 10^{-10}$ M^2. Lucassen[10] computed $S_{HL} = 1.05 \times 10^{-5}$ M (at 20°) by assuming $K_a = 1.25 \times 10^{-5}$ M; the product of these, $1.3_1 \times 10^{-10}$, is in almost exact agreement with our value.

Our values for the solubility product of the acid soap were constrained to ionic strengths too high to permit equally straightforward treatment; in the absence of a fairly high concentration of sodium ion the acid soap does not form, as witness the single titration of a 7×10^{-3} M laurate solution. A rough estimate of the thermodynamic value may be obtained by assuming that the mean ionic activity coefficient of the acid soap and the square of the mean ionic activity coefficient of the free acid vary identically with the ionic strength. This is equivalent to assuming that the activity coefficients of hydrogen and sodium ions depend on ionic strength in the same way. Although this cannot be exactly so, it suggests the approximation

$$pK_{MHL_2}{}^0 = pK_{MHL_2}{}^{0.1} + 2(pK_{HL}{}^0 - pK_{HL}{}^{0.1})$$

where K^0 denotes a thermodynamic solubility product and $K^{0.1}$ denotes the corresponding conditional constant at $\mu = 0.1$ M. With the average values of the two conditional

constants obtained from titrations involving the formation of both precipitates, and with $pK_{HL}{}^0 = 9.86$, obtained as described in the preceding paragraph, this gives $pK_{MHL_2}{}^0 = 14.14$ or $K_{MHL_2}{}^0 = 7.2 \times 10^{-15}$, to which a relative uncertainty of ±20% may reasonably be attached. Lucassen[10] gave 6.3×10^{-15} for the potassium salt. There appears to be no value in the prior literature for the sodium salt, but Feinstein and Rosano[14] found titration curves for sodium and potassium laurate to be identical within experimental error, and since this would not have been true if the solubility products of the sodium and potassium salts were significantly different it is reasonable to regard 6×10^{-15} as the literature value for the sodium salt as well.

It is more difficult to assess the values given in Table I for the cmc, which may be summarized as 0.014 M at $\mu = 0.05$, 0.0058 M at $\mu = 0.15$, and 0.0054 M at $\mu = 0.20$ M. The values given by Merrill and Getty[18] for the critical micelle concentrations of laurate in sodium chloride solutions at 25° unfortunately extend only to 0.1 M sodium chloride but include 0.014 M at $\mu = 0.042$ M and 0.0115 M at $\mu = 0.069$ M. Linear interpolation between these gives 0.0133 M at $\mu = 0.05$ M. Our value is within 6% of this, and our values at the higher ionic strengths are smaller by about the expected amounts.

From the generally satisfactory agreement between our values and those in the prior literature, it seems fair to conclude that the interpretation of titrimetric data in this way may be of great value in future studies of the behaviors of fatty acid anions and other basic soaps under other conditions. Thus, the method seems to be exceedingly useful in the explanation of complex phenomena related to detergency, soap formation, and to the properties of surfactants in general.

References and Notes

(1) Cf., for example, D. Dryssen, D. Jagner, and F. Wengelin, "Computer Calculation of Ionic Equilibria and Titration Procedures," Almqvist and Wiksell, Stockholm, 1968.

(2) T. Anfalt and D. Jagner, Anal. Chim. Acta, **57**, 165 (1971).

(3) F. Ingman, A. Johansson, S. Johansson, and R. Karlsson, Anal. Chim. Acta, **64**, 113 (1973).

(4) D. M. Barry and L. Meites, Anal. Chim. Acta, **68**, 435 (1974).

(5) D. M. Barry, L. Meites, and B. H. Campbell, Anal. Chim. Acta, **69**, 143 (1974).

(6) M. J. D. Brand and G. A. Rechnitz, Anal. Chem., **42**, 1172 (1970).

(7) A. F. Isbell, Jr., R. L. Pecsok, R. H. Davies, and J. H. Purnell, Anal. Chem., **45**, 2363 (1973).

(8) S. H. Piper, Trans. Faraday Soc., **25**, 348 (1929).

(9) F. V. Ryer, Oil Soap, **25**, 310 (1946).

(10) J. Lucassen, J. Phys. Chem., **70**, 1824 (1966).

(11) H. L. Rosano, K. Breindel, J. H. Schulman, and A. J. Eydt, J. Colloid Interface Sci., **22**, 58 (1966).

(12) H. L. Rosano and M. E. Feinstein, Rev. Franc. Corps Gras, **13**, 661 (1966).

(13) M. E. Feinstein and H. L. Rosano, J. Colloid Interface Sci., **24**, 73 (1967).

(14) M. E. Feinstein and H. L. Rosano, J. Phys. Chem., **73**, 601 (1969).

(15) L. Meites, "The General Multiparametric Curve-Fitting Program CFT3," 2nd ed, Computing Laboratory, Department of Chemistry, Clarkson College of Technology, Potsdam, N.Y., 1974.

(16) Primes denote assumed values, which are at first equal to the initial estimates and are then adjusted by the operation of the basic curve-fitting program.

(17) Listings, in both Basic and Fortran IV, of the program SOAP, with brief directions for use, may be obtained by remitting $25.00, to defray the costs of duplication and postage, to the Computing Laboratory of the Department of Chemistry, Clarkson College of Technology, Potsdam, N.Y. 13676. A copy of the parent curve-fitting program CFT3, accompanied by a 150-page manual of explanation and instruction, and with hard-copy listings in Basic, Polybasic, and Fortran IV, may be obtained at the same time for a total remittance of $45.00.

(18) R. C. Merrill and R. Getty, J. Phys. Colloid Chem., **52**, 774 (1948).

Optical Absorption Spectrum of the Solvated Electron in Some Liquid Amides and Amines[1]

James F. Gavlas, F. Y. Jou, and Leon M. Dorfman*

Department of Chemistry, The Ohio State University, Columbus, Ohio 43210   (Received July 1, 1974)

The optical absorption spectrum of the solvated electron has been determined, at room temperature, in several amides and amines. The absorption maxima are found to be as follows: N,N-dimethylformamide, 1680 nm; N,N-dimethylacetamide, 1800 nm; N,N-diethylformamide, 1775 nm; dimethylamine, 1950 nm; 1,2-propanediamine, 1500 nm. The results for these amides are not in accord with an empirical correlation of such data recently proposed by Freeman. The general spectral grouping of the absorption of e_s^- in a variety of liquids with type of compound is discussed. Rate constants have been determined for reactions of e_s^- in ethanol with formamide, N-methylformamide, and N,N-dimethylformamide. The values are respectively 1.8×10^8, 2.2×10^8, and $1.1 \times 10^9 \ M^{-1} \ sec^{-1}$.

Introduction

Experimental surveys of the spectrum of the solvated electron in various types of liquid have indicated[2,3] a marked spectral grouping of the absorption maxima with type of compound. Although there is considerable overlap of these spectral groupings, the maxima for the aliphatic alcohols[4] are found mostly in the visible to near-infrared;[5] the maxima for the ethers[6] are in the region from 1800 to 2300 nm; several amines which have been reported[3,7] are in the region from about 1300 to 2000 nm. These observations seem to indicate that molecular structure, in terms of functional groups in the molecule, is indeed an important factor[8] (along with the dielectric behavior of the liquid) contributing to the optical properties.

This paper contains results for the spectrum in three amides, two of which have been the subject of a recent report[9] with which our results are sharply at variance. These reported spectra in the amides have a special bearing on the matter of spectral grouping. Spectra have also been determined in two amines and in a hydroxy ether. Kinetics of reactions of the solvated electron in ethanol with several of these compounds have been investigated and rate constants determined.

Experimental Section

As in earlier work,[10] a Varian V-7715A electron linear accelerator was the source of the 4-MeV electrons. This accelerator is capable of generating either pulses of from 10- to 80-nsec duration, with a beam current of 600 mA, or pulses of from 100- to 1400-nsec duration, with a beam current of 325 mA. In general, the shorter, higher intensity pulses were used when the species under observation had lifetimes of less than about 1 μsec. The 200-nsec 325-mA pulse delivers a dose of approximately 1.2×10^{17} eV/g in water. All experiments were conducted at ambient room temperature $(23 \pm 2°)$.

The radiolysis cells were made of fused quartz, with optical windows of high-purity silica. Cells of three different sizes were employed in this work. Liquids which absorbed the analyzing light only weakly in the wavelength region of interest were irradiated in cells having optical paths of 20.0 mm. When stronger optical absorption by the liquid was

encountered, cells having optical paths of either 5.0 or 3.0 mm were needed. These cells were connected to Pyrex storage bulbs, which were equipped with Teflon stopcocks and Teflon-seal joints to allow connection to a vacuum system.

A 500-W flashed xenon arc lamp was the source of the analyzing light beam. Appropriate Corning glass filters were placed in the optical path before the cell to prevent photolysis of the sample, and in front of the monochromator to eliminate second-order diffraction and scattered light effects. Fast optical absorption spectrophotometry was used both to monitor the kinetics and to map the spectra of the transient species. Transient absorptions could be monitored in the wavelength region 230–2300 nm with submicrosecond time resolution. Five-nanosecond time resolution was possible at wavelengths below 1000 nm. The optical detection systems employed in this laboratory have been described in detail elsewhere.[6,11]

Formamide and N,N-dimethylformamide were both reagent grade from Fisher Scientific Co. N-Methylformamide, N,N-diethylformamide, N-methylacetamide, N,N-dimethylacetamide, N-methylpropionamide, dimethylamine, and 1,2-propanediamine were obtained from Eastman Kodak Co. Absolute ethyl alcohol, USP, was from Commercial Solvents Corp.; the 2-methoxyethanol was from Union Carbide Corp.

Each of the amides was dried with Linde (Union Carbide) molecular sieve and distilled at reduced pressure under argon. The 2-methoxyethanol was distilled at 1 atm first from an acidic 2,4-dinitrophenylhydrazine solution and then from sodium. The ethanol was distilled from a sodium ethoxide solution under an argon atmosphere. The 1,2-propanediamine was refluxed for several hours with potassium under a nitrogen atmosphere and then distilled. The dimethylamine was purified by means of two vacuum distillations. All of these liquids, except for dimethylamine, were degassed immediately after distillation by subjection to at least two freeze–pump–thaw cycles and were stored under vacuum in the dark until needed. The dimethylamine was degassed before the vacuum distillations were carried out. Both the dimethylamine and the 1,2-propanediamine were vacuum distilled into Pyrex storage flasks containing mirrors of triply distilled potassium at least 24 hr, but not more than 48 hr, before they were to undergo irradiation. All samples to be irradiated were introduced under vacuum into the Pyrex reservoirs to which the radiolysis cells were connected.

For a typical experiment with ethanol, 2-methoxyethanol, or the amines, approximately 35–45 ml of liquid were used. After each electron pulse, the irradiated liquid was mixed with that in the reservoir to dilute any stable radiolysis products that may have been formed. The dilutions were always at least 15-fold or greater, since the approximate volumes of the cells having 20.0, 5.0, and 3.0-mm optical paths were 2, 1, and 0.6 ml, respectively. No reservoir sample was ever subjected to a total of more than about 60 pulses, and over the course of any experiment no change was perceptible in either the yield or the decay kinetics of the optically absorbing transient species in these liquids.

Experiments with the amides were more difficult to conduct because of the relative ease with which the amides decompose upon irradiation. The decomposition products were found to affect the yields of the transient species, as well as their rates of decay, both in formamide and in N,N-dimethylformamide. Therefore, each sample of amide was irradiated only once, after which it was discarded. The

cell in which a liquid amide was irradiated was always connected to two 100-ml Pyrex bulbs. One of these served as a reservoir for liquid which had not yet been irradiated; the other was used to contain liquid after it had been irradiated. Following each electron pulse, the contents of the radiolysis cell were emptied into the waste bulb, and the cell was refilled from the reservoir bulb. This procedure was followed until all of the liquid initially contained in the reservoir had been irradiated.

Results and Discussion

Spectrum of e_s^- in Liquid Amides. The optical absorption spectrum of the solvated electron has been determined in each of three amides: N,N-dimethylformamide (DMF), N,N-dimethylacetamide (DMAd), and N,N-diethylformamide (DEF). Shown in Figure 1 are the room temperature spectra in these amides over the range 800–2100 nm. The wavelengths at which the absorption maxima occur are DMF, 1680 ± 30 nm; DMAd, 1800 ± 50 nm; DEF, 1775 ± 150 nm.

Data from which our optical absorption spectrum of e_s^- in DMF have been determined are presented in Figure 2, extending from 550 to 2100 nm. As indicated in Figure 2, this spectrum is a composite of results obtained in three separate experiments. This absorption band, having a maximum at 1680 nm, can be eliminated by saturation of the DMF with N_2O at a pressure of 1 atm. In the presence of anthracene (10^{-2} M) the 1680-nm band is also eliminated and the spectrum of the anthracene radical anion is observed instead. Both high reactivity toward N_2O and reaction with aromatic hydrocarbons such as anthracene to form aromatic radical anions are, of course, typical of the solvated electron.

Low signal-to-noise ratios in DEF, primarily the result of low optical densities due to decay of the short-lived e_s^- during the electron pulse, were responsible for the large uncertainty in the location of the optical absorption maximum for the spectrum of e_s^- in that amide.

In an earlier publication, Hayashi, et al.,[9] have reported the observation of e_s^- in both DMF and DMAd. They[9] identified bands with maxima at 650 and 625 nm in DMF and DMAd, respectively, with the solvated electron. As the spectrum in Figure 2 shows, there is no indication, in our work, of any optical absorption maximum at or near 650 nm in DMF, the location of λ_{max} reported by Hayashi, et al.[9] Our determination of these absorption maxima differs from the values which they[9] reported by about 1000 nm.

Our new spectral data suggest that in the amides, as in the alcohols, ethers, and amines, grouping of e_s^- optical absorption bands by class of compound may occur. The range of λ_{max} values in the amides, including the estimated uncertainties, is from 1650 to 1925 nm. The locations of the absorption maxima for e_s^- in numerous polar liquids, including the amides, are illustrated in Figure 3.

The e_s^- spectra in the amides give some indication of the relative importance of the structural class of the molecules of the solvating liquid, compared to its bulk dielectric properties, in determining the location of λ_{max}. From Figure 3 the absorption maxima of the e_s^- spectra in the amides can be seen to be located entirely within the spectral region characteristic of e_s^- in the amines. The optical properties of e_s^- in the amides thus appear to be similar to those in the amines, despite the much higher static dielectric constants of the amides. The hydroxy compounds, which have dielectric constants closer to those of the am-
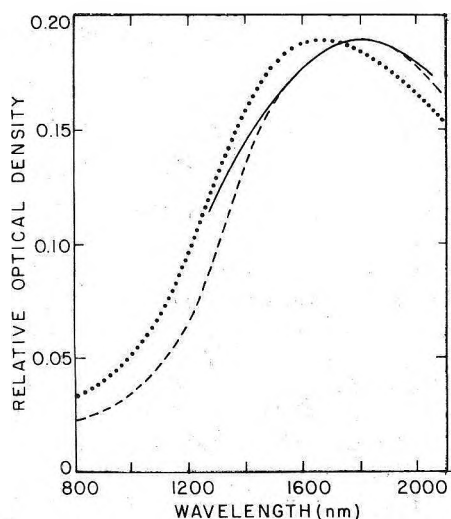
Figure 1. Optical absorption spectra at room temperature of the solvated electron in liquid amides: DMF (·····), DMAd (- - -), DEF (—).
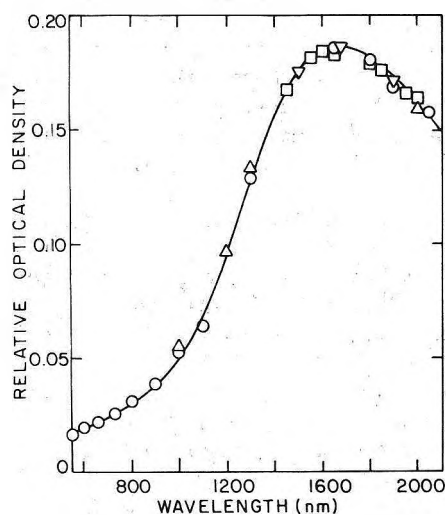

Figure 2. Optical absorption spectrum at room temperature of the solvated electron in DMF showing individual data points. Each separate point represents individual experiments with separate samples; ∇ represents a superposition of such separate experiments.
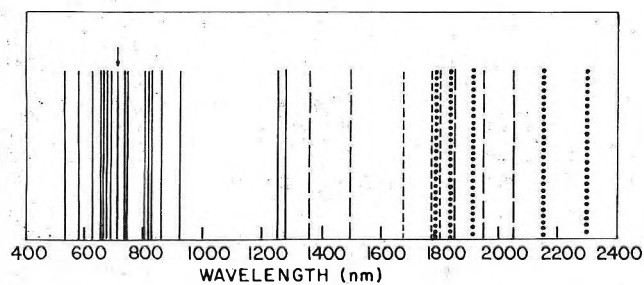

Figure 3. Optical absorption maxima for the solvated electron in various liquids at room temperature: (—) hydroxy compounds [(— ◄—) is for water and 2-methoxyethanol]; (– –) ammonia and amines; (- - -) amides; (····) ethers.

ides, have e_s^- spectra in an entirely different region (see Figure 3). In DMAd, which has a room temperature static dielectric constant[12] of 40.2, λ_{max} is located at 1800 nm; in 1,2-ethanediol, which has a similar dielectric constant (37.7 at 25°),[13] λ_{max} is at 580 nm.[4]

TABLE I: Solvated Electron Transition Energies and Solvent Properties at Room Temperature

	DMF	DMAd	DEF
E_{max}, eV	0.738	0.689	0.698
D_s	36.7[a]	40.2[b]	29.6[b]
d, g/cm³	0.9445[a]	0.9366[c]	0.9030[c,d]
μ, D[b]	4.13	4.60	4.30
$10^{24}\alpha$, cm³[e]	7.844	9.691	11.538
g_K	1.73	1.84	1.84

[a] J. W. Vaughn in "The Chemistry of Non-Aqueous Solvents," Vol. 2, J. J. Lagowski, Ed., Academic Press, New York, N.Y., 1967, Chapter 5. [b] Reference 12. [c] R. C. Weast, Ed., "Handbook of Chemistry and Physics," 52nd ed, The Chemical Rubber Company, Cleveland, Ohio, 1971. [d] R. Gopal and S. A. Rizvi, *J. Indian Chem. Soc.*, **43**, 179 (1966). [e] Calculated from bond refractions given in N. E. Hill, W. E. Vaughan, A. H. Price, and M. Davies, "Dielectric Properties and Molecular Behaviour," Van Nostrand-Reinhold, London, 1969, p 238.
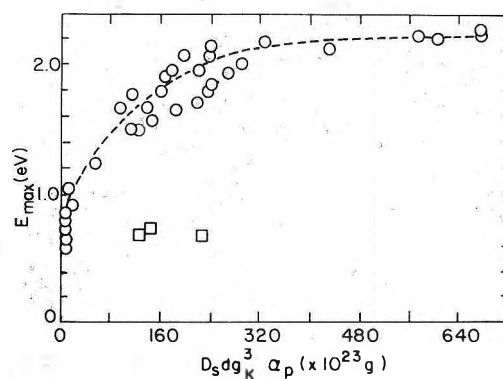

Figure 4. Correlation of Freeman for transition energy for spectrum of e_s^- with liquid properties. E_{max} is plotted against $D_s dg_K^3\alpha_p$: O, various liquids at different temperatures; □, amides.

Recently, Freeman[13] has proposed an empirical correlation of the optical absorption maximum of e_s^- (expressed as a transition energy, E_{max}) with a term which involves the Kirkwood correlation parameter[13,14] and the dielectric constant. A basic premise of this correlation is that short-range interactions are of considerable importance in determining the value of E_{max}. The empirical correlation was developed to fit spectral data for e_s^- in a number of amines, ethers, and alcohols, as well as in ammonia and water. Our data for E_{max} in the foregoing amides are not at all in accord with this correlation.

The parameter which Freeman[13] has used to reflect the structure in liquids is the Kirkwood correlation parameter, g_K, from the equation[13,14]

$$[(D_s - 1)(2D_s + 1)/9D_s](M/d) = (4\pi N/3)[\alpha + (g_K\mu^2/3kT)]$$

where D_s is the static dielectric constant of the liquid, M is the molecular weight, d is the density, N is Avogadro's number, α is the optical polarizability, μ is the molecular dipole moment, k is Boltzmann's constant, and T is the absolute temperature. A value of g_K greater than unity indicates a greater polarity in microscopic regions of the liquid than would be expected from the molecular dipole moment. Freeman has suggested[13] that this enhanced polarity should increase E_{max}.
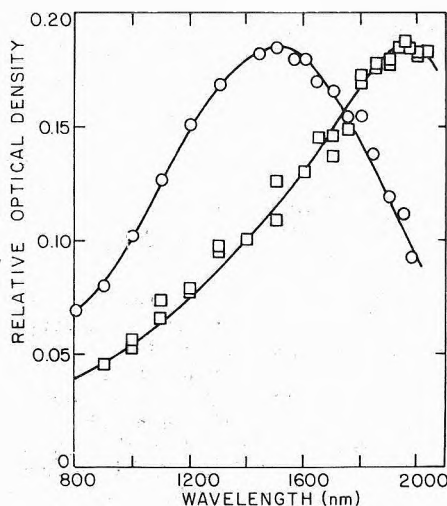
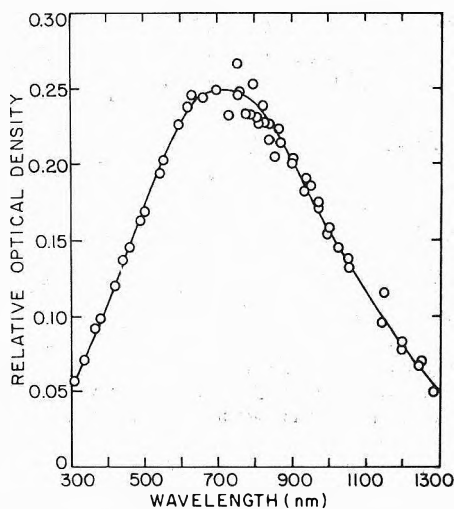**Figure 5.** Optical absorption spectra at room temperature of the solvated electron in amines: O, 1,2-PDA; □, DMA.

Figure 6. Optical absorption spectrum at room temperature of the solvated electron in 2-methoxyethanol. The width at half-height is 14,200 cm^{-1}.

The term with which Freeman has correlated E_{max} is $D_s dg \kappa^3 \alpha_p$, where α_p is the polarizability of the polar group in the solvent molecule. Figure 4 shows a plot[13] of E_{max} vs. $D_s dg \kappa^3 \alpha_p$ for the various liquids which Freeman has considered. Values of E_{max} for the solvated electron in DMF, DMAd, and DEF, together with various physical properties of these liquids, are collected in Table I. Clearly, the correlation fails in the case of the amides.

The primary problem with the correlation term seems to be that the values of D_s are considerably larger for the amides than for other liquids having similar E_{max} values, and no other parameters compensate for this difference. For the amides, therefore, the importance of short-range interactions associated with the functional group relative to long-range ones dependent upon D_s is not correctly represented in the correlation term.

Spectrum of e_s^- in Amines. Shown in Figure 5 are the optical absorption spectra of e_s^- both in dimethylamine (DMA) and in 1,2-propanediamine (1,2-PDA) at room temperature. The optical absorption maxima are at 1950 ± 50 nm in DMA and at 1500 ± 50 nm in 1,2-PDA. Both of these

λ_{max} values are within the spectral region characteristic of e_s^- in other amines. As in the other diamines for which e_s^- absorption maxima have been reported (ethylenediamine,[7] 1360 nm; 1,3-propanediamine,[3] 1500 nm), λ_{max} in 1,2-PDA occurs at a somewhat shorter wavelength than in the monoamines (diethylamine,[3] 2050 nm; DMA, 1950 nm; ethylamine,[15] 1800 nm).

Spectrum of e_s^- in 2-Methoxyethanol. The absorption spectrum of e_s^- in 2-methoxyethanol at 23°, over the range 350–1300 nm, is presented in Figure 6. The location of λ_{max} is 715 ± 30 nm. Hentz and Kenney-Wallace[5] have reported the maximum of the e_s^- absorption band in this liquid at 30° to be 740 nm. Our result is thus in agreement.

The width at half-height of the band is found to be 14,200 cm^{-1}, rather more like the bands of e_s^- in the alcohols than the ethers,[6] where the width at half-height is on the order of 4000 cm^{-1}. The molar extinction coefficient at the maximum, determined from dosimetry and formation of anthracenide ion, is estimated to be 1.3×10^4 M^{-1} cm^{-1}. The location of λ_{max} at 715 nm, well within the alcohol range, indicates that the spectral properties of e_s^- in 2-methoxyethanol are strongly dominated by the alcohol functional group.

Reactions of e_s^- in Ethanol with Amides. Our attempts to generate observable concentrations of e_s^- in several amides other than those already mentioned, namely, formamide, N-methylacetamide (NMAd), and N-methylpropionamide (NMP), have not been successful. The observability of the solvated electron will depend upon its lifetime in a particular liquid and the time resolution of the experiments. Fel', Dolin, and Zolotarevskii[16] have suggested that some guidance as to the lifetime might be gained from the value of the rate constant for reaction of e_{aq}^- with the particular compound. Rate constants[16,17] of about 4×10^7, 1.5 $\times 10^7$, and 5×10^7 M^{-1} sec^{-1} have been reported for reaction with formamide, NMF, and DMF, respectively.

The bimolecular rate constants which we have determined for reactions of the electron solvated by ethanol with the same amides are 1.8×10^8, 2.2×10^8, and 1.1×10^9 M^{-1} sec^{-1} for formamide, NMF, and DMF, respectively. Our bimolecular rate constants were obtained from the slopes of plots of the observed pseudo-first-order rate constants for the decay of e_s^-, monitored at 700 nm, vs. concentration of added amide. The amide concentrations ranged from 3×10^{-3} to not more than 3×10^{-2} M.

The rate constants which we have determined for these reactions of e_s^- in ethanol are all considerably larger than those for reactions of e_{aq}^- with the same amides. For NMF and DMF the differences are greater than an order of magnitude. This dependence of reactivity on the solvating liquid is further illustrated by the lifetime of e_s^- in pure DMF. If the electron were to react with the DMF in which it is solvated with the same rate constant as did the electron solvated by ethanol, then its half-life would be less than 50 psec. However, the experimentally observed half-life for e_s^- in DMF was approximately 1 μsec. These results indicate that the rate with which the electron will react with an amide depends upon the liquid in which the electron is solvated, and may therefore not be useful as a guide toward estimating the lifetime in the pure liquid.

References and Notes

(1) This work was supported by the U.S. Atomic Energy Commission under Contract No. AT(11-1)-1763.
(2) L. M. Dorfman, F. Y. Jou, and R. Wageman, *Ber. Bunsenges. Phys. Chem.*, **75**, 681 (1971).
(3) L. M. Dorfman and F. Y. Jou in "Electrons in Fluids," J. Jortner and N. R. Kestner, Ed., Springer-Verlag, Berlin, 1973, p 447.
(4) M. C. Sauer, Jr., S. Arai, and L. M. Dorfman, *J. Chem. Phys.*, **42**, 708 (1965).
(5) R. R. Hentz and G. A. Kenney-Wallace, *J. Phys. Chem.*, **78**, 514 (1974).
(6) F. Y. Jou and L. M. Dorfman, *J. Chem. Phys.*, **58**, 4715 (1973).
(7) J. L. Dye, M. G. DeBacker, and L. M. Dorfman, *J. Chem. Phys.*, **52**, 6251 (1970).

(8) D. A. Copeland, N. R. Kestner, and J. Jortner, *J. Chem. Phys.*, **53**, 1189 (1970).
(9) N. Hayashi, E. Hayon, T. Ibata, N. N. Lichtin, and A. Matsumoto, *J. Phys. Chem.*, **75**, 2267 (1971).
(10) W. D. Felix, B. L. Gall, and L. M. Dorfman, *J. Phys. Chem.*, **71**, 384 (1967).
(11) E. A. Shaede, H. Kurihara, and L. M. Dorfman, *Int. J. Radiat. Phys. Chem.*, **6**, 47 (1974).
(12) M. Steffen, *Ber. Bunsenges. Phys. Chem.*, **74**, 505 (1970).
(13) G. R. Freeman, *J. Phys. Chem.*, **77**, 7 (1973).
(14) G. Oster and G. J. Kirkwood, *J. Chem. Phys.*, **11**, 175 (1943).
(15) J. B. Weinstein and R. F. Firestone, unpublished results.
(16) N. S. Fel', P. I. Dolin, and V. I Zolotarevskii, *Khim. Vys. Energ.*, **1**, 154 (1967).
(17) E. J. Hart, E. M. Fielden, and M. Anbar, *J. Phys. Chem.*, **71**, 3993 (1967).

COMMUNICATIONS TO THE EDITOR

Solubility Measurements of Aromatic Hydrocarbons and Carbon Disulfide in Liquid Sulfur by Gas Chromatography

Sir: The study of liquid solutions of elemental sulfur with various solvents has been undertaken by several investigators during the past 75 years. This research has been collected and interpreted by Scott[2a] in an excellent review. Still, there remains a paucity of thermodynamic studies involving sulfur with nonelectrolyte solutes. Such data are of extreme importance in the devolatilization of hydrocarbons from molten sulfur and the reclamation of sulfur as a commercial by-product from petroleum feedstocks.

Such thermodynamic data may be conveniently determined by using gas chromatography and employing liquid sulfur as the column solvent. Here the mole fraction-based activity coefficient of the solute in the stationary phase is given as

$$\ln \gamma_f^\infty = \ln \frac{RT}{M p_2^0 V_g^0} - \frac{B_{22} p_2^0}{RT} \tag{1}$$

where γ_f^∞ = fugacity corrected activity coefficient of the solute at infinite dilution in the stationary phase, R = gas constant, T = column temperature in °K, M = molecular weight of the stationary phase, p_2^0 = saturated vapor pressure of the solute, V_g^0 = specific retention volume of the solute in the stationary phase, and B_{22} = second virial coefficient of the pure solute.

Although the use of the mole fraction based γ_f^∞ may be questioned on the grounds that sulfur in the temperature range of these experiments (between the melting point of sulfur [~118°] and the floor temperature [159°]) consists of

several distinct molecular species, conversion to another concentration-activity scale may be readily accomplished.[2b] In this work, we have retained the above convention for theoretical convenience as noted and used by Scott.[3]

A modified Varian Model 1520 gas chromatograph equipped with a flame ionization detector was used to obtain the data in this study. The temperature of the column oven was ascertained by employing an array of copper–constantan thermocouples placed spatially in the volume of the oven occupied by the column. The average short term temperature fluctuation was found to be ±0.1° while the variance from thermocouple to thermocouple was ±0.3°. Helium was used as the carrier gas and its flow rate measured by a soap bubble flow meter. Columns were constructed of 0.25-in. o.d. stainless steel tubing, 4 ft. in length. The stationary phases were supported on 45–60 mesh Chromasorb G.

The sulfur was purified by the method of Bacon and Fanelli[4] and deposited on the support by the method of Urone and Parcher.[5] Tumbling of the coated support material in a stream of dry nitrogen improved the coating uniformity and helped to remove traces of objectable CS_2, H_2S, and SO_2. The coated support was then packed into the stainless steel tubing and purged in the chromatograph for a period of 48 hr with helium. Differential thermal analysis of the sulfur at all stages of the above described operation and on the column support showed identical thermograms.

The degree of stationary phase bleed was checked by measuring the specific retention volume of ethylbenzene at the highest temperature used in this study (153°) and was found not to vary more than 0.5% over a 72-hr period. Reagent grade solutes were employed in all cases and used without further purification. All solutes were injected in

TABLE I: Fugacity Corrected Activity Coefficients at Infinite Dilution and Heats of Solution of Solutes in Molten Sulfur

Solute Temp, °C	γ_f^∞			$\Delta H_s{}^a$
	129.5	142.4	152.9	
Benzene	7.45	7.89	7.14	−7.0
Toluene	9.67	8.62	8.27	−6.2
Ethylbenzene	19.0	16.4	10.6	−8.6
o-Xylene	10.9	9.24	9.28	−7.2
m-Xylene	12.0	10.5	10.3	−8.8
p-Xylene	11.2	10.9	10.8	−8.8
CS₂	1.70	1.64	1.60	−5.6

^{a} In kcal/mole.

triplicate, the mean of the retention volumes employed for subsequent calculations. Data were taken at approximately 10° intervals starting at 130°.

The saturated solute vapor pressures were calculated using the Antoine equation employing the regression contants from Dreisbach.[6] Virial coefficients, B_{22}, were computed in the case of the aromatic solutes, from the modified corresponding states equation of McGlashan and Potter[7] using critical constants obtained from the compendia of Dreisbach[6] and Kudchadker, et al.[8] The viral coefficient for CS₂ was interpolated from the smoothed data in Dymond and Smith.[9]

Table I lists the activity coefficients for six aromatic solutes and CS₂ in molten sulfur at three different temperatures. In all cases, the activity coefficients are greater than unity, indicating positive deviation from Raoult's law. Of the seven solutes, CS₂ exhibits the most ideal solution with sulfur, a result that is not surprising in view of the high solubility of sulfur in CS₂. For the aromatic solutes, there is an increase in γ_f^∞ with alkylation of the benzene ring, implying that an increase in aliphatic character of the solute will increase its positive deviation from Raoult's law.

The above trends are also verified by the large activity coefficients recorded for the n-alkanes (approximately 80 for n-decane to 100 for n-dodecane at 129.5°) with molten sulfur. These results have not been recorded in Table I since they are probably 20–30% in error due to our failure to correct for solute adsorption at the gas–liquid interface.[10] Still, the γ_f^∞ would be larger for the n-alkanes than for the aromatic hydrocarbons on the basis of their respective cohesive energy densities.[11] Research is presently under way to determine γ_f^∞ for the aliphatic hydrocarbons corrected for interfacial adsorption effects.

The temperature dependence of γ_f^∞ is difficult to discern. In most cases γ_f^∞ decreases with temperature, the exception being benzene which shows a high value for γ_f^∞ at 142.4°. This anomolous result may be due to experimental error or more probably due to the strong dependence of the activity coefficient on the second virial coefficient and its temperature derivative.[12,13] The latter statement also probably applies to the slight variation in γ_f^∞ recorded for the xylene isomers as a function of temperature; which com-

pares in magnitude with the results obtained by Newman and Prausnitz[13] for solvent–polymer systems over a similar 20–30° temperature range.

The last column in Table I lists the heats of solution for the various solutes dissolving in molten sulfur. These were calculated from

$$d \ln V_g^0 / dT = \Delta H_s' / RT^2 \qquad (2)$$

where $\Delta H_s'$ is equal to the heat of solution of the solute at 0°. To correct $\Delta H_s'$ to the enthalpy of solution at the column temperature, ΔH_s, requires use of

$$\Delta H_s = \Delta H_s' - RT + RT^2\eta \qquad (3)$$

where η is the thermal expansion coefficient of the solvent. Values of η were obtained from the Critical Tables.[14]

The average standard deviation of the enthalpy values in Table I is 11% making comparison on an absolute basis of limited value. However, in all cases ΔH_s for the solute–sulfur interactions is exothermic and less negative than the corresponding heats of vaporization for the respective solutes. As such, the excess heats of solution are all positive, indicating the absence of any strong interaction between the solutes and sulfur. Unfortunately, there are few data with which to compare our results to. Touro and Wiewiorowski[15] have computed a ΔH_s for CS₂ in molten sulfur of −6.42 kcal/mol. This compares favorably with our result of −5.6 kcal/mol.

Presently, we are continuing these studies to include a larger number of solutes which differ in their electron-donating capacity. From this research we hope to obtain evidence to examine the acid–base theory of liquid sulfur proposed by Wiewiorowski and Touro.[16]

References and Notes

(1) Address correspondence to the Department of Chemistry, Virginia Commonwealth University, Richmond, Va. 23284.
(2) (a) B. Meyer, "Elemental Sulphur Chemistry and Physics," Wiley, New York, N.Y., 1965, p 337; (b) F. H. Covitz and J. W. King, J. Polym. Sci., Part A-1, **10**, 689 (1972).
(3) Reference 2a, p 344.
(4) R. F. Bacon and R. Fanelli, J. Amer. Chem. Soc., **65**, 639 (1943).
(5) J. F. Parcher and P. Urone, J. Gas Chromatogr., **2**, 184 (1964).
(6) R. R. Dreisbach, Advan. Chem. Ser., No. 15 (1955).
(7) M. L. McGlashan and D. J. B. Potter, Proc. Roy. Soc., **60**, 646 (1964).
(8) A. P. Kudchadker, G. H. Alani, and B. J. Zwolinski, Chem. Rev., **68**, 659 (1968).
(9) J. H. Dymond and E. B. Smith, "The Virial Coefficients of Gases," Clarendon Press, Oxford, 1969.
(10) D. E. Martire, Anal. Chem., **38**, 244 (1966).
(11) J. M. Prausnitz, "Molecular Thermodynamics of Fluid-Phase Equilibria," Prentice-Hall, Englewood Cliffs, N.J., 1969, p 273.
(12) D. Patterson, Y. B. Tewari, H. P. Schreiber, and J. E. Guillet, Macromolecules, **4**, 356 (1971).
(13) R. D. Newman and J. M. Prausnitz, J. Paint Technol., **45**, 33 (1973).
(14) E. W. Washburn, "International Critical Tables," Vol. III, McGraw-Hill, New York, N.Y., 1928, p 21.
(15) F. J. Touro and T. K. Wiewiorowski, J. Phys. Chem., **70**, 3534 (1966).
(16) T. K. Wiewiorowski and F. J. Touro, J. Phys. Chem., **70**, 3528 (1966).

Butler University   **Jerry W. King*[1]**
Department of Chemistry   **Paul R. Quinney**
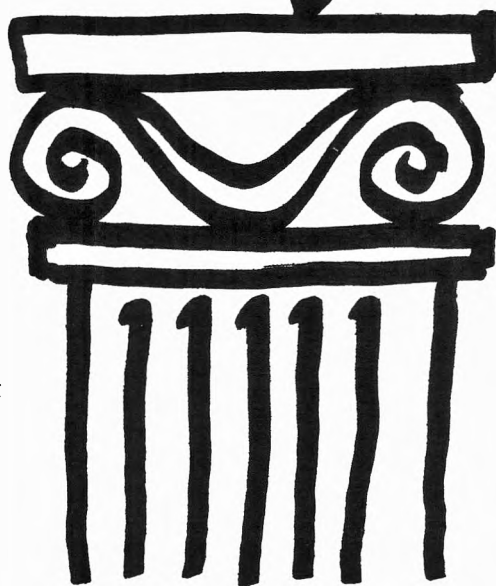*Indianapolis, Indiana 46208*
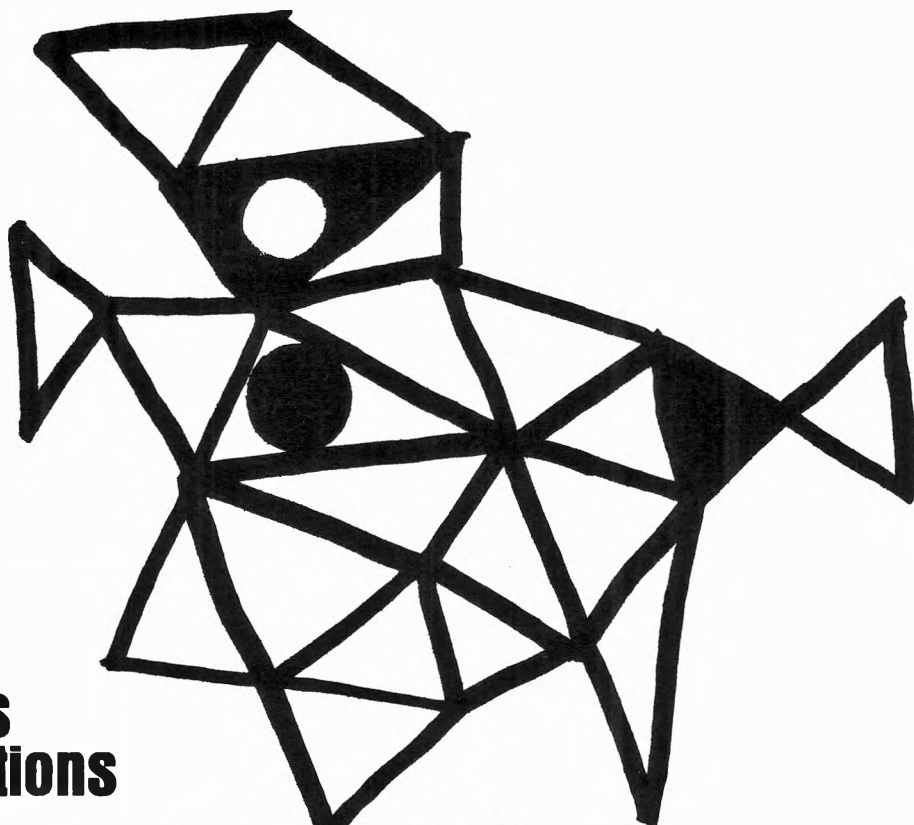
New concepts
new techniques
new interpretations

**. . . together
with valuable reports
on classical areas**

They are all waiting for you between
the covers of our well-balanced
JOURNAL OF PHYSICAL CHEMIS-
TRY. Whatever your particular interest
in physical chemistry, you'll find
the JOURNAL's broad range of
experimental and theoretical research
reports are relevant and beneficial
to your work. Each biweekly issue
brings you an average of 30 authori-
tative, comprehensive reports on
fundamental aspects of atomic and
molecular phenomena, as well as
timely notes, communications and
reports plus the proceedings of
selected symposia.

Join your fellow physical chemists
who rely on JPC as an excellent
biweekly source of data in both new
and classical areas. Just complete
and return the form to start
your own subscription.

... another ACS service

Journal of
Physical
Chemistry

SYMMETRY OF MANY-ELECTRON SYSTEMS

by I. G. KAPLAN
translated by J. GARRAT

TENTATIVE CONTENTS: Mathematical Apparatus. Basic Concepts and Theorems of Group Theory. The Permutation Group. Groups of Linear Transformations. Tensor Representations and Tensor Operators. Principles of the Application of Group Theory to Quantum Mechanics. Classification of States. The Method of Coefficients of Fractional Parentage. Calculation of Electronic States of Molecular Systems.

January 1975, 384 pp., $34.50/£16.50

REACTIVE FREE RADICALS

by J. M. HAY

In this work the author has aimed to relate the reactivity of organic free radicals to their structure, and in particular to the type of orbitals occupied by their unpaired electron or electrons. The treatment is more systematic than in previous publications. An attempt is made to explain certain of the phenomena of free radical reactions, particularly those in the gas phase, on the basis of a simple model in which the shape of a radical—and therefore its reactivity—varies with its energy content. The treatment is extended to show how reactivity patterns might assist in radical structure determination and to provide information about the thermodynamics of organic species and polar effects in their radical reactions.

1974, 170 pp., $11.50/£4.40

DIFFUSION AND SORPTION IN FIBRES AND FILMS, Volume 1

An Introduction with Particular Reference to Dyes

by R. McGREGOR

CONTENTS: MASS TRANSPORT IN CONTINUOUS MEDIA: The Simple Transport Lows. The Brownian Motion and the Continuum Approximation. The Field Quantities. Conservation Equations for Continuous Systems. Systems of a Single Component. Multicomponent Systems. THE FORMALISM OF NONEQUILIBRIUM THERMODYNAMICS: Thermodynamic Flows and Forces. Discontinuous Systems. Continuous Multicomponent Systems. Phenomenological Equations for Continuous Multi-Component Systems. MASS TRANSPORT IN AND BETWEEN PHASES: Thermodynamic Diffusion Equations. Systems of Two Uniformly Accessible Phases. Membrane Processes. Convective Diffusion to a Solid Surface. Some Mechanistic Considerations.

1974, 258 pp., $16.00/£6.20

HIGHER EXCITED STATES OF POLYATOMIC MOLECULES

by M. B. ROBIN

This two-volume monograph presents an encyclopedic description of the vacuum-ultraviolet spectra of all basic classes of molecules, and a unified interpretation of them. Volume 1 begins with a brief introduction to the theories used in later chapters, a synopsis of methods for calculating the properties of the higher states of polyatomic molecules, and a brief section on recent experimental advances. The remainder of the volume considers the experimental spectra of sixteen classes of saturated polyatomic molecules, their relationship to their photoelectron spectra, and their interpretation. Volume 2 applies this unified approach to twenty-two classes of molecules bearing pi-electrons, and to biological and inorganic systems.

Volume 1/1974, 382 pp., $31.00/£14.90
Volume 2/January 1975, 432 pp., $39.50/£18.95

LASER LIGHT SCATTERING

by BENJAMIN CHU

A Volume in the QUANTUM ELECTRONICS Series

This book, intended to serve as an introduction to the interdisciplinary area of laser light scattering, concentrates almost exclusively upon quasielastic laser scattering techniques. The book begins with a review of classical electricity and magnetism, along with the general scattering theory, and then continues with such topics as the basic theoretical concepts related to light mixing spectroscopy, photon-counting fluctuations, Fabry-Perot interferometry, experimental methods, and many others.

1974, 336 pp., $31.50/£15.10

THE PHYSICAL CHEMISTRY OF DYE ADSORPTION

by I. D. RATTEE and M. M. BREUER

CONTENTS: Binding Forces. The Adsorption of Dyes and Adsorption Equilibria. Kinetics of Dyeing. Dyes in Solution. The Adsorption of Dyes by Proteins and Polyamides. The Adsorption of Dyes by Cellulosic Substrates. The Adsorption of Non-Ionic Disperse Dyes. Fibre-Reactive Dyes. Problems of Dyeing Kinetics—Specific Situations. Relating Theory and Practice.

1974, 338 pp., $22.25/£8.60

Prices subject to change without notice.

ACADEMIC PRESS

A Subsidiary of Harcourt Brace Jovanovich, Publishers

111 Fifth Avenue, New York, N. Y. 10003
24–28 Oval Road, London NW1 7DX